

2

Document released under the
Freedom of Information Act
DMA Case No. 89040

AUG 07 1991

OPR

HOUSE

NUCLEAR
EXPLOSIONS

THE

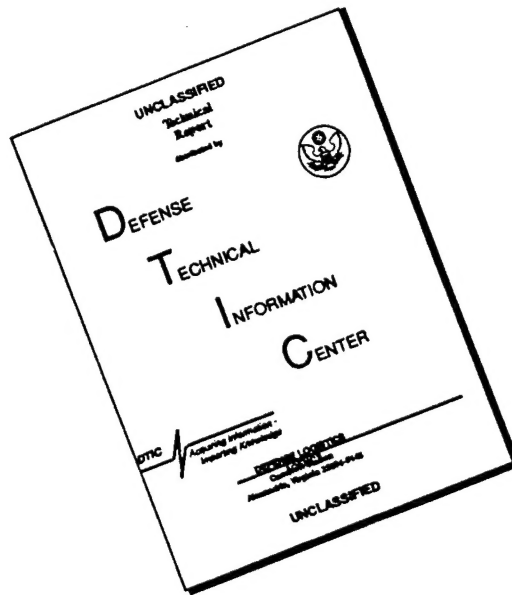
CONFIDENTIAL FORMERLY RESTRICTED DATA

This document has been approved
for public release and sale; its
distribution is unlimited.

19970903 161

01 2 06 021

DISCLAIMER NOTICE



THIS DOCUMENT IS BEST QUALITY AVAILABLE. THE COPY FURNISHED TO DTIC CONTAINED A SIGNIFICANT NUMBER OF PAGES WHICH DO NOT REPRODUCE LEGIBLY.

~~CONFIDENTIAL~~

TRW SYSTEMS GROUP

LAOPS

~~FORMERLY RESTRICTED DATA~~

Handle As Restricted Data In Foreign
Dissemination Section 144B, Atomic
Energy Act, 1954

13865

(2)

This document consists of 240 plus 4 pages
(counting preliminary pages)

No. 2 of 150 copies, Series A

* WT-64

DTIC
SELECTED
AUG 07 1991
S D D

Scientific Director's Report of Atomic Weapon Tests at Eniwetok, 1951

~~GROUP 1~~
Excluded from automatic downgrading
and declassification

Annex 1.6

Blast Measurements
Part I—Summary Report

This document contains information affecting the national
defense of the United States within the meaning of the
Espionage Laws, Title 18, Sections 793 and 794. Its
transmission or the disclosure of its contents in any
manner to an unauthorized person is prohibited by law.

~~FORMERLY RESTRICTED DATA~~
Handle As Restricted Data In Foreign
Dissemination Section 144B, Atomic
Energy Act, 1954

This document has been approved
for public release and sale; its
distribution is unlimited.

~~CONFIDENTIAL~~

~~This document contains information that is defined
as restricted data in the meaning of the
Espionage Laws, Title 18, Sections 793 and 794. Its
transmission or the disclosure of its contents in any
manner to an unauthorized person is prohibited by law.~~

~~CONFIDENTIAL~~

~~SECRET~~
~~RESTRICTED DATA~~

FA 0559 1004

REVIEWED IN ACCORDANCE WITH THE
BRL SECRETARY'S GUIDE

~~SIGNATURE~~

3/15/90
DATE



BLAST MEASUREMENTS

Part I—Summary Report

by

G. K. HARTMANN

C. W. LAMPSON

C. J. ARONSON

Approved by: **FREDERICK REINES**
Director, Program 1

Approved by: **ALVIN C. GRAVES**
Scientific Director

Accession For	
NTIS CRASH	
DTIC Tech	
Unannounced	
Justification	
By <i>per lti</i>	
Distribution	
Availability Code	
Dist	Availability Code
A-1	



DTIC QUALITY INSPECTED 8

Naval Ordnance Laboratory
White Oak, Maryland
Ballistic Research Laboratories
Aberdeen Proving Ground, Maryland

May 1952

UNANNOUNCED





Acknowledgments

The Blast Program was planned with the advice and approval of F. Reines and E. J. Zadina of J-Division, Los Alamos Scientific Laboratory. The Naval Proving Ground, Dahlgren, Va., and the Aberdeen Proving Ground, Aberdeen, Md., provided valuable test facilities. The cooperation of Edgerton, Germeshausen & Grier, Inc., and of C. W. Wyckoff was helpful in attaining desired photographic results. The assignment by Armed Forces Special Weapons Project (AFSWP) and Los Alamos of many able officers to the project was of immeasurable help. The work of H. P. Feldman, Explosives Research Department, Naval Ordnance Laboratory (NOL), was extremely valuable in engineering the field installations in coordination with Holmes and Narver. A major share of the burden of coordinating the program through its many changes was ably borne by C. J. Aronson, Explosives Research Department, NOL. J. R. Mitchell of NOL rendered great assistance in meeting all logistic requirements. Rita B. Granet, NOL, was responsible for typing all NOL reports.

CONTENTS

	Page
ACKNOWLEDGMENTS	v
ABSTRACT	1
CHAPTER 1 INTRODUCTION	3
1.1 Objectives	3
1.2 Plan of the Experiments	3
1.2.1 Free-air Peak Pressure	3
1.2.2 Mach-region Peak Pressure	3
1.2.3 Pressure vs Time	4
1.2.4 Pressures Very Close to the Bomb	4
1.2.5 Asymmetry	4
1.2.6 Effect of Proximity of the Gauge to the Ground	4
1.2.7 Ground Shock	4
1.3 New Developments	4
1.4 Instrument Performance	4
1.5 Instrument Locations	12
1.6 List of Individual Reports	12
CHAPTER 2 PRELIMINARY EXPERIMENTS AND CALCULATIONS	13
2.1 Free-air Curve for TNT	13
2.1.1 Arrival-time Data	13
2.2 Reflection Experiments	14
2.2.1 Discussion of Reflection Coefficients	14
2.2.2 Data on Reflections	14
2.2.3 Bikini Able Model Experiment	20
2.2.4 Summary of Values of R_F as a Function of Reduced Height	20
2.3 Conversion of Shock Velocity into Shock Pressure	20
2.4 Discussion of Errors in the Velocity Method for Shock Waves	20
2.5 Normal Reflection of a Strong Shock in Real Air	33
2.5.1 Hugoniot Equation for Air Taking into Account the Nonideality of the Gas and the Variation in Specific Heats	33
2.5.2 Fundamental Shock Equations	37
2.5.3 Normal Reflection from a Rigid Wall	37
2.5.4 Calculation for Reflected Pressure	40
2.5.5 Reflected-pressure Ratio for Infinite Incident Shock Strength	40
2.6 Flow as Affecting Measurements of Pressure	43
2.6.1 General Remarks on the Problem	43
2.6.2 Simple Theory for a Two-dimensional Wall	43
2.6.3 Compressible Subsonic Steady Two-dimensional Irrotational Isentropic Flow	45

CONTENTS (Continued)

	Page
2.6.4 Experiments with Subsonic Transient Flow: Blast	48
2.6.5 Experiments on Wall Models in the Princeton Shock Tube	48
2.6.6 Experimental Results for Steady Supersonic Flow	51
2.6.7 Disturbance in the Flow Due to Viscous Effects	51
2.6.8 Conclusion regarding Flow Error	54
 CHAPTER 3 PRESENTATION OF RESULTS	 55
3.1 Results for Shot Dog, Mach Region	55
3.2 Results for Shot Easy, Long Line, Engebi, E1, Mach Region	69
3.3 Results for Shot Easy, Short Line, Engebi, E2, Mach Region	69
3.4 Results for Pressures on the Ground near Explosion, Shot Easy	95
3.5 Results for Free-air Measurements, Shot Easy	98
3.6 Results for Shot George	98
3.7 Comparisons of Pressure-time Curves Obtained by Various Instruments	98
 CHAPTER 4 ANALYSIS OF RESULTS	 117
4.1 Assignment of Tonnages from Blast Measurements on Atomic Bombs	117
4.1.1 Assignment of Radiochemical Tonnages from Blast Measurements	117
4.1.2 Method of Determining Blast Tonnage from Pressure Measure- ments	119
4.1.3 Trinity Blast Data Reduced to Sea Level	124
4.1.4 Shot Able Water-intersection Data in the Regular Region	124
4.2 Free-air-pressure-Distance Curve for Shot Easy	124
4.2.1 Comparison of Shots Dog and Easy, Free Air	126
4.3 Comparisons among Various Shots	129
4.3.1 Pressure	129
4.3.2 Impulse	129
4.3.3 Positive Duration	129
4.3.4 Reduced Negative Quantities	129
4.3.5 Decay Parameter for Pressure-time Curves	137
4.3.6 Comparison of Measured θ^* with Theory	137
4.3.7 Calculation of Decay Parameter for Free-air Atomic Blast	137
4.3.8 Reduced Arrival Time	141
4.4 Discussion of Blast Anomalies	141
4.4.1 Asymmetry	141
4.4.2 Pressure near a Jet	141
4.4.3 Discussion of Rise Times	144
4.4.4 Effect of Height of Gauge above Ground	149
4.4.5 Adiabatic Wave	149
 CHAPTER 5 EVALUATION AND CONCLUSIONS CONCERNING BLAST	 157
5.1 Remarks and Recommendations Concerning the Various Experiments	157
5.2 Principal New Results and Conclusions	158
 CHAPTER 6 GROUND-SHOCK MEASUREMENTS	 161
6.1 Introduction	161

CONTENTS (Continued)

	Page
6.2 Scope of the Measurements	161
6.3 Terrain Problems	164
6.4 Results of the Measurements	164
6.5 Summary	172
 CHAPTER 7 ADMINISTRATIVE AND GENERAL TECHNICAL DETAILS	 173
7.1 Scope	173
7.1.1 Authorization	173
7.1.2 Chronological Summary	173
7.2 Administrative Data	173
7.2.1 Division of Responsibilities	173
7.2.2 Personnel	174
7.3 Costs	175
7.3.1 Total Costs	175
7.3.2 NOL Cost Breakdown	176
7.4 Supplies and Shipping	176
7.4.1 Supply Arrangements at the NOL	176
7.4.2 Special Supplies	176
7.4.3 Shipping Arrangements	176
7.4.4 Return Shipping	176
7.4.5 Amount of Shipping	177
7.5 Construction Details	177
7.5.1 Blast Huts	177
7.5.2 Instrument Walls	177
7.5.3 Results of Use of Walls	178
7.5.4 Pylons and Pylon Ground Auxiliary	178
7.5.5 Other Instrument Stations	181
7.6 Timing Signals	185
7.7 General Conditions on Blast Islands	185
7.8 Recommendations	185
 APPENDIX A ACTIVITIES OF THE NOBL ADVANCE PARTY	 211
A.1 Introduction	211
A.1.1 Objectives	211
A.1.2 Personnel	211
A.1.3 Preparation and Planning	211
A.2 Operations at Test Site	211
A.2.1 Preparation for Cable Laying	211
A.2.2 Cable-laying Procedure	211
A.2.3 Disposition of Equipment	217
A.2.4 Miscellaneous	217
A.3 Comments and Recommendations	217
A.3.1 Comments	217
A.3.2 Recommendations	218

CONTENTS (Continued)

	Page
APPENDIX B DETERMINATION OF DESIGN CRITERIA FOR CONSTRUCTION OF A PYLON FOR BLAST INSTRUMENTATION	219
B.1 Problem	219
B.2 Method	219
B.3 Calculations	219
B.4 Stability	221
B.5 Example	223

ILLUSTRATIONS

CHAPTER 1 INTRODUCTION

1.1 Code for Instrumentation Charts of Blast Measurements, Tables 1.2 to 1.4	6
--	---

CHAPTER 2 PRELIMINARY EXPERIMENTS AND CALCULATIONS

2.1 Free-air-pressure vs Distance Curve for Spherical TNT	15
2.2 Reflection Coefficients	16
2.3 Reflection Data for TNT Spheres; $\mu = 2.14$	18
2.4 Reflection Data for TNT Spheres; $\mu = 0.615$	19
2.5 Summary of Image Reflection Experiments, TNT	21
2.6 Summary of Clay Reflection Experiments, TNT	22
2.7 Water Reflection, Approximately $\frac{1}{500}$ Scale of Bikini Able	23
2.8 Reflection Coefficient R_F vs μ , Reduced Height	25
2.9 Shock Strength vs U/C_1 for Various Ambient Temperatures	26
2.10 Shock Strength vs Shock Velocity for Dry and Moist Air	27
2.11 Shock Strength P/P_1 vs U/C_1 ; Range of P/P_1 , 1 to 10	28
2.12 Shock Strength P/P_1 vs U/C_1 ; Range of P/P_1 , 10 to 100	29
2.13 Shock Strength P/P_1 vs U/C_1 ; Range of P/P_1 , 100 to 1,000	30
2.14 Relative Errors in P_s Arising in the Velocity Method	35
2.15 Values of K for a Single Shock of Strength ξ	36
2.16 K as a Function of T/T_0 or of $P/P_0 \times v/v_0$	38
2.17 Normal Reflection from a Rigid Wall	39
2.18 Sample Calculation for P_r	41
2.19 Reflected-pressure Ratio vs Incident Pressure for Real Air	42
2.20 Flow Past a Wall	44
2.21 Variation of the Pressure Coefficient with Distance along a Wall	46
2.22 Arrangement for Interferograms of Wall Models	49
2.23 Isopyknals (Obtained from Interferograms) for Round-nosed Wall	50
2.24 Pressure Coefficient along a Cylindrical Body	52
2.25 Estimated Percentage Error Due to Flow Disturbance Produced by a Wall, $x = 14$	53

CHAPTER 3 PRESENTATION OF RESULTS

3.1 Pressure-time Curves, Shot Dog, Lagoon Side	60
3.2 Pressure-time Curves, Shot Dog, Ocean Side	61

ILLUSTRATIONS (Continued)

	Page
3.3 Maximum Pressure vs Distance	62
3.4 Positive Impulse vs Distance	63
3.5 Positive Duration vs Distance	64
3.6 Negative Pressure vs Distance	65
3.7 Negative Impulse vs Distance	66
3.8 Negative Duration vs Distance	67
3.9 Times of Arrival	68
3.10 Pressure-time Curves, Shot Easy, Lagoon Line, Lagoon Side	78
3.11 Pressure-time Curves, Shot Easy, Lagoon Line, Land Side	79
3.12 Maximum Pressure vs Distance	80
3.13 Positive Impulse vs Distance	81
3.14 Positive Duration vs Distance	82
3.15 Negative Pressure vs Distance	83
3.16 Negative Impulse vs Distance	84
3.17 Negative Duration vs Distance	85
3.18 Times of Arrival vs Distance	86
3.19 Maximum Pressure vs Distance	87
3.20 Positive Impulse vs Distance	88
3.21 Positive Duration vs Distance	89
3.22 Negative Pressure vs Distance	90
3.23 Negative Impulse vs Distance	91
3.24 Negative Duration vs Distance	92
3.25 Times of Arrival vs Distance	93
3.26 Pressure-time Curves, Shot Easy, Ocean Side	94
3.27 Pressure on the Ground, Shot Easy, Mach Region	96
3.28 Pressure on the Ground, Shot Easy	97
3.29 Free-air Time of Arrival of Incident Wave vs Distance, Shot Easy	99
3.30 Free-air Pressure vs Distance, Shot Easy	100
3.31 Time of Arrival of Mach Stem near Triple Point vs Distance, Shot Easy	101
3.32 Pressure of Mach Stem near Triple Point vs Distance from Ground Zero, Shot Easy	102
3.33 Relation between Free-air and Mach-stem Radii at the Triple Point	103
3.34 Path of Triple Point, Shot Easy	104
3.35 Maximum Pressure vs Distance, Shot George	105
3.36 Time of Arrival of Initial Disturbance, Shot George	106
3.37 Inductance Gauge; Interferometer Gauge; Shot Dog, 1,450 yd	108
3.38 Inductance Gauge; Interferometer Gauge; Shot Dog, 1,250 yd	109
3.39 Inductance Gauge; Interferometer Gauge; Shot Dog, 950 yd	110
3.40 Inductance Gauge; Interferometer Gauge; Shot Easy, 1,430 yd	111
3.41 Inductance Gauge; Spring-piston Gauge; Shot Easy, Ocean Line, 900 yd	112
3.42 Inductance Gauge; Spring-piston Gauge; Shot Easy, Ocean Line, 1,250 yd	113
3.43 Inductance Gauge; Spring-piston Gauge; Shot Easy, Lagoon Line, 900 yd	114
3.44 Inductance Gauge; Spring-piston Gauge; Shot Easy, Lagoon Line, 1,550 yd	115

CHAPTER 4 ANALYSIS OF RESULTS

4.1 Reduced Height vs Reduced Distance for Pressure Level of 10 Psi for All Atomic Explosions in Which Blast Was Measured	118
---	-----

ILLUSTRATIONS (Continued)

	Page
4.2 Relation between Reduced Height and Reduced Distance at 10-psi Level for TNT	121
4.3 Blast Efficiencies of Atomic Bombs	123
4.4 Trinity Data	125
4.5 Free-air Pressure vs Reduced Distance; Atomic Bomb and TNT Compared	127
4.6 Free-air Pressure vs Reduced Distance; Shots Dog and Easy Compared	128
4.7 Peak Pressure by the Velocity Method vs Reduced Distance	130
4.8 Mass of Fireball vs Radius for Shots George and Easy	131
4.9 Reduced Positive Impulse vs λ	132
4.10 Reduced Positive Duration vs λ	133
4.11 Reduced Negative Pressure vs λ	134
4.12 Reduced Negative Impulse vs λ	135
4.13 Reduced Negative Duration vs λ	136
4.14 Reduced θ^* vs λ for Free-air Pentolite	138
4.15 Reduced Decay Parameter vs λ ; Theory and Experiment Compared	139
4.16 Calculated Values of Decay Parameters vs Free-air Pressure for Atomic Bomb	140
4.17 Reduced Arrival Time vs Reduced Distance for All Shots	142
4.18 Times of Arrival of Initial Disturbance, Shot Easy	143
4.19 Crusher-gauge Locations, Shot Easy	145
4.20 Deformation vs Horizontal Distance for Ball-crusher Gauges on Shots Dog and Easy	146
4.21 Pressure-time Curves, Shot Easy, Pylon 37a	151
4.22 Pressure-time Curves, Shot Easy, Pylon 37b	152
4.23 Pressure-time Curves, Shot Easy, Pylon 37c	153
4.24 Pylon Data, Shot Easy, Maximum Overpressure vs Height above Ground at Various Distances	154
4.25 Ratio of the Velocities of the Peak to the Velocity of Sound for Shock and Adiabatic Waves as a Function of Pressure	155
CHAPTER 6 GROUND-SHOCK MEASUREMENTS	
6.1 Blast Line, Easy Shot	162
6.2 Blast Line, George Shot	163
6.3 First Peak Horizontal Acceleration as a Function of λ_{RC} , Easy Shot	165
6.4 First Peak Vertical Acceleration as a Function of λ_{RC} , Easy Shot	166
6.5 Maximum Horizontal Velocity as a Function of λ_{RC} , Easy Shot	167
6.6 Maximum Vertical Velocity as a Function of λ_{RC} , Easy Shot	168
6.7 Maximum Displacement as a Function of λ_{RC} , Easy Shot	169
6.8 Time-travel Curves for First Ground Motion, Easy Shot	170
6.9 First Peak Acceleration as a Function of λ_{RC} , George Shot	171
CHAPTER 7 ADMINISTRATIVE AND GENERAL TECHNICAL DETAILS	
7.1 Main Group of NOBL Personnel	175
7.2 Blast-hut Structures (Stations 23a, 23b)	179
7.3 Blast-hut Structures (Station 25)	180
7.4 Exterior of Station 23a, Runit	181
7.5 Interior of Station 23a, Runit	182

ILLUSTRATIONS (Continued)

	Page
7.6 Interior of Station 23a, Runit	182
7.7 Interior of Station 23a, Engebi	183
7.8 Interior of Station 23b, Engebi	184
7.9 Field Panel for Wall	184
7.10 Wall (Stations 20 and 21)	185
7.11 Structure of Wall Field Panel	186
7.12 Looking South along Blast Line near Station 20c, Runit	187
7.13 Tipped-over Wall, Runit (Station 20b)	188
7.14 Tipped-over Wall, Engebi (Station 20b)	188
7.15 Inclined Wall and Foundation, Runit (Station 20c)	189
7.16 Inclined Wall and Foundation, Runit (Station 20c)	189
7.17 Pylon Structure	190
7.18 Ground Pylon Auxiliary Structure	191
7.19 Pylon (Station 37b)	192
7.20 Pylon (Station 37b) and Ground Auxiliary (Station 37e)	192
7.21 End View of Pylon (Station 37b)	193
7.22 Tipped Pylon and Foundation (Station 37b)	194
7.23 Pylon Which Was Blown Away (Station 37a)	195
7.24 Pylon (Blown Away) Showing Original Location (Station 37a)	195
7.25 Sketch of Pylon Misalignments	196
7.26 Blast-velocity Post (Structure)	197
7.27 Blast-velocity Post, Runit (Station 28b)	198
7.28 Ground-shock Station, Engebi (Station 36c)	198
7.29 Ground-shock Station (Structure)	199
7.30 Concrete Mount for Crushers (Structure)	200
7.31 Concrete and Stake Crusher Gauges, Runit (Stations 33, 34)	201
7.32 Stake Mount for Crushers (Structure)	202
7.33 Timing Relay Rack (Rear)	203
7.34 Timing Relay Rack (Front)	203
7.35 Engebi Long Line from Zero Tower Showing Mound of Earth Crossing Blast Line between Stations 28b and 28c	204
7.36 Engebi Long-line Station 28c (See also Fig. 7.35)	205
7.37 Engebi Short Line from Zero Tower, Showing Guy Wire	206
7.38 Engebi Long-line Station 20c, Showing Piles of Dirt near Wall	207
7.39 Runit, Station 20d, Showing How Close Wall Was to Drop-off of Island toward the Beach	207
7.40 Runit, Stations 20a and 20b, Showing Blast Line, Zero Tower, and Telemetering Balloon	208
7.41 Runit Blast Hut (Station 23a) after Shot, Showing Sand Forced through Cable Inlet by Blast	209
7.42 Engebi (Concrete and Stake Gauges) after the Shot (Stations 27b and 33b)	209

APPENDIX A ACTIVITIES OF THE NOBL ADVANCE PARTY

A.1 Cable Laying	212
A.2 Cable Laying (Close-up)	212

ILLUSTRATIONS (Continued)

	Page
APPENDIX B DETERMINATION OF DESIGN CRITERIA FOR CONSTRUCTION OF A PYLON FOR BLAST INSTRUMENTATION	
B.1 Overpressure vs Drag Pressure	220
B.2 Overpressure and Drag Pressure vs Time	222

TABLES

CHAPTER 1 INTRODUCTION

1.1 Range and Performance for Each Instrument as Observed under Test Con- ditions	5
1.2 Blast Measurements Instrumentation Chart for Dog Shot, Runit Island	7
1.3 Blast Measurements Instrumentation Chart for Easy Shot, Engebi Island	8
1.4 Blast Measurements Instrumentation Chart for George Shot, Eberiru, Aomon, Bijiri, and Rojoa Islands	10
1.5 Report Titles for Greenhouse Report, Annex 1.6, Blast Measurements	11

CHAPTER 2 PRELIMINARY EXPERIMENTS AND CALCULATIONS

2.1 Reflection Data for Spherical Charges, $\mu = 2.14$	17
2.2 Reflection Coefficients for $\mu = 2.14$	17
2.3 Reflection Data for Spherical Charges, $\mu = 0.615$	17
2.4 Reflection Coefficients for $\mu = 0.615$	17
2.5 Water Reflection Data	20
2.6 Values of R_F	24
2.7 Initial Conditions for Hirschfelder and Curtiss Tables	24
2.8 Relative Errors in P_s Arising in the Velocity Method	34
2.9 Calculated Reflected-pressure Ratios	41
2.10 Calculated Error Using Incompressible Theory	45
2.11 Calculated Error Using the Compressible Theory	47

CHAPTER 3 PRESENTATION OF RESULTS

3.1 Summary of Results, Shot Dog	56
3.2 Summary of Results, Shot Easy	70
3.3 Data Summary for Shot George	107

CHAPTER 4 ANALYSIS OF RESULTS

4.1 Radiochemical Tonnages, Heights of Bomb, Radius of 10-psi Level, and Reduced Values for Various Atomic Explosions	119
4.2 Radiochemical Kilotonnages Deduced from Pressure Measurements and Previous Atomic Bomb Experiments	120
4.3 Results for Operation Greenhouse Shots	120
4.4 Relation between μ and λ_r at 10-psi Level for TNT	120
4.5 Tonnages for All Bombs	122
4.6 Analysis of Shot Able in the Region of Regular Reflection	126
4.7 Pressures in the Vicinity of a Jet	147

TABLES (Continued)



	Page
4.8 Rise Times in the Low-pressure Region	148
4.9 Pylon Data for Shot Easy	150
CHAPTER 5 EVALUATION AND CONCLUSIONS CONCERNING BLAST	
5.1 Total Yields Determined from Blast	160
CHAPTER 7 ADMINISTRATIVE AND GENERAL TECHNICAL DETAILS	
7.1 Holmes and Narver Drawings Prepared for the Blast-measurements Program .	178
APPENDIX A ACTIVITIES OF THE NOBL ADVANCE PARTY	
A.1 Cable Schedule, E1, Long Line	213*
A.2 Cable Schedule, E2, Short Line	214
A.3 Cable Schedule, Site C	215
A.4 Cable Schedule, Site D-V	216
A.5 Total Cable Requirements	217



Abstract

Measurements of the blast pressures in Shots Dog, Easy, and George, together with earth-shock measurements on Shots Easy and George, gave new and important information concerning the magnitude and character of the blast wave near an atomic bomb. These experiments showed that secondary phenomena due presumably to thermal radiation and ion combination affect the pressure wave rather markedly near the source by introducing a large secondary pulse into the pressure-time curve and by causing the pressure wave near the ground to be nonshock in character. Both of these perturbations coalesce into a shock front at greater distances producing a blast wave of conventional shape.

New techniques of measurement involving smoke-trail rockets, balloons, telemetering, and high-speed photography allowed the peak blast pressures in free air near the bomb to be obtained from which the explosive equivalent of one bomb (Easy) was determined. The equivalent blast energy was found to be approximately 50 per cent of the radiochemical energy for this case. By this is meant that only half the energy is required to produce the same blast wave at a great distance if released by a TNT explosion.

Evaluation of the radiochemical kilotonnages from blast measurements was made by comparison with previous shots, giving kilotonnages of  58,  for Shots Dog, Easy, and George, respectively.

Asymmetry of the explosion was investigated by measuring pressures on the ground along two radii. The results indicated a great asymmetry in the case investigated (Easy), which may be due to the presence of jets along the guy cables from the tower.

Earth-shock measurements showed that the accelerations and frequencies of the motion were higher by a factor of 10 than predicted from small-scale experiments in soil and that the displacements were correspondingly smaller than predicted by a factor of 10.

Page 2 is blank.

Chapter 1

Introduction

1.1 OBJECTIVES

The Blast Measurement Project of Operation Greenhouse was undertaken with the object of obtaining accurate basic information on the blast produced by atomic bombs. For this reason, pressure measurements were made along the ground in both the regular and the Mach regions as well as in free air. A secondary objective was to learn more about the methods by means of which the blast could be accurately and reliably measured. Many new instruments and methods were used with reasonable success, and a considerable amount of new information was obtained concerning the free-air-pressure vs distance curve and the pressure-time curve at high pressure, as well as blast asymmetry and perturbations due to the presence of the ground. Certain measurements were also made of the accelerations and displacements produced in the ground. This report presents and interprets all these results and also gives the results of some preliminary work occasioned mainly by the Greenhouse program. Details of the individual instruments and measurements will be found in the appropriate reports which are referenced in Sec. 1.6.

1.2 PLAN OF THE EXPERIMENTS

The choice of methods and the design of the experiments were dictated by considerations of accuracy, reliability, precision, and economy and by experience gained in previous atomic bomb experiments. It was also considered essential to provide at least two ways of measuring a quantity not only to increase the chance of success but also to confirm any unusual re-

sult which might otherwise be attributed to the idiosyncrasies of a particular instrument.

1.2.1 Free-air Peak Pressure

The free-air measurements, which were actually measurements of the time of arrival of the shock front at a succession of known distances, were of two kinds. In the first method the arrival times indicated by blast switches on a balloon cable were telemetered to a distant receiving station. Distances to the switches were determined by triangulation of data from photographs of flash bulbs on the balloon cable.

Small explosive charges fired a few seconds before the bomb explosion provided sound pulses, the arrival times of which at microphones on the balloon cable were also telemetered. This provided either a measure of sound velocity or a calibration of the relative distances, whichever proved to be the more accurate.

The second free-air method consisted in making the position of the shock front visible by allowing it to refract light from a series of rocket trails. This method proved to be very fruitful in that information concerning the path of the triple point was obtained, as well as pressure in the free-air region and pressure in the Mach region. The shape of the Mach stem itself in the early stages was displayed on many of the pictures.

1.2.2 Mach-region Peak Pressure

In the Mach region along the ground, shock and sound velocities were measured by recording on magnetic tape the times of arrival at a series of known positions. From these arrival times, subject to certain assumptions, values

[REDACTED]

of the initial pressure in the wave may be calculated. In addition, indenter gauges and foil meters were used to give peak-pressure readings.

1.2.3 Pressure vs Time

With regard to pressure as a function of time, the primary method relied on the use of diaphragm gauges which, when subjected to pressure, caused a change of inductance in a Hartley oscillator. The resulting frequency-modulated signal was stored on magnetic tape after amplification and heterodyning. This method represented a simplification over the Sandstone pressure-time system which telemetered the information and discriminated out the signal at the time of reception. The second method for measuring pressure as a function of time consisted in the use of a mechanical piston which was driven by the pressure against a spring restoring force and properly damped by means of silicone oil of a suitable viscosity. The record was scratched directly on a rotating lucite drum coated with aquadag.

1.2.4 Pressures Very Close to the Bomb

In the regular region and near Mach region a number of ball-crusher gauges were used (1) to obtain actual pressures on the ground, (2) to distinguish between ground and steel backed with concrete as reflecting surfaces, (3) to discover any changes in pressure at or near the inception of the Mach stem, and (4) to adduce evidence for the existence of extraordinary pressures at the footings of the tower guy wires. In this sense the ball-crusher data were to contribute to the information on blast asymmetry. No secondary or backup method was used to supplement the ball-crusher measurements.

1.2.5 Asymmetry

Two blast lines leading from the E-tower including an angle of about 60° were used in order to study asymmetry in detail if it should occur. Many of the instrumented structures of Program 3 were located between these two lines.

Aerial photography both from drones nearly overhead and from manned aircraft was undertaken with indifferent success in an attempt to

obtain further information on jets and their contribution to shock asymmetry.

1.2.6 Effect of Proximity of the Gauge to the Ground

In order to study the variation of the blast behavior with height above ground and to determine the effect of the ground on measurements made at ground level, pylons were constructed at various distances to hold inductance gauges, and pressure-time records were obtained at ground level and up to 14 ft above ground.

1.2.7 Ground Shock

Ground-shock measurements were made on Shots Easy and George, using both Calidyne and Engineering Research Associates self-recording accelerometers and using free-piston seismic devices to record displacements. Vertical and radial accelerations were measured, and all quantities were recorded as a function of time.

1.3 NEW DEVELOPMENTS

No attempt is made here to catalogue all new developments which were made in order to carry out the program briefly described above. These are described in the detailed reports. However, a few should be mentioned such as (1) the development of a new smoke-trail rocket whose trail persists for many seconds, reaches an altitude of 6,500 ft, and can be seen and photographed from a distance of several miles; (2) the development of a new spring-piston pressure-time gauge and particularly its recording system of high resolution and great simplicity; (3) the development of a magnetic-tape recording system for pressure-time records of high reliability and of over-all frequency response that is flat from 0 to 600 cps, capable of operation over cables 1 mile in length; and (4) the development of thermal-radiation-resistant lightweight cable.

1.4 INSTRUMENT PERFORMANCE

Table 1.1 lists the various instruments and methods used and gives an idea as to their performance. By range is meant the interval of

**TABLE 1.1 RANGE AND PERFORMANCE FOR EACH
INSTRUMENT AS OBSERVED UNDER TEST CONDITIONS**

Method or Instrument	Approximate Range	Reliability
Balloon telemetering	30-100 psi	Fair
Rocket-trail photography	30-10 ⁴ psi	Fair
Aerial photography	30-1000 psi	Poor
Shock velocity	5-200 psi	Very good
Indenter gauges	1-150 psi	Very good
Flush-mounted foils	5-120 psi	Very good
Inductance gauges	5-120 psi	Very good
Spring-piston gauges	5-125 psi	Very good
Crusher gauges	200-3 × 10 ⁴ psi	Fair
Calidyne accelerometers	0-50 g	Fair
ERA accelerometers	0-100 g	Good
Free-piston displacement	4 in.	Good

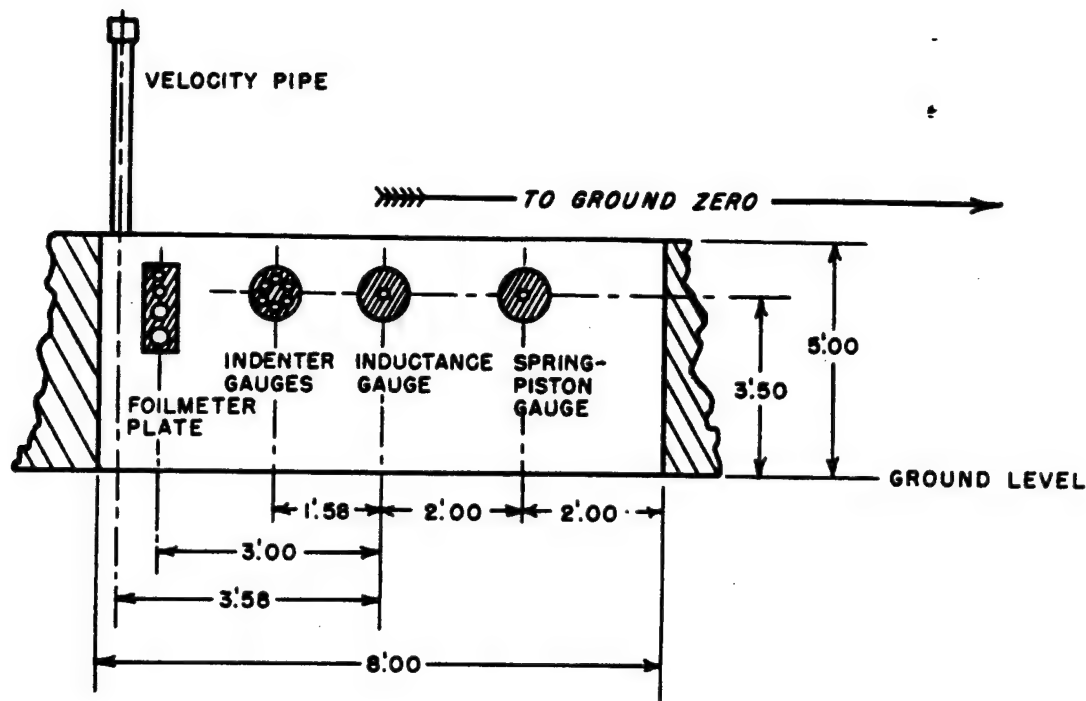


Fig. 1.1 Code for Instrumentation Charts of Blast Measurements, Tables 1.2 to 1.4.

- | | |
|---|--|
| <p>(1) Wall, as sketched, containing two inductance gauges for pressure-time measurements, two spring-piston gauges for pressure-time measurements, twelve indenter gauges, two foil-meter plates, and velocity pipes as indicated by items 2 and 3.</p> <p>(2) Velocity pipe containing blast-velocity switches.</p> <p>(3) Velocity pipe containing blast-velocity switches and sound-velocity pickups.</p> <p>(4) Ground-shock station with Calidyne and ERA accelerometers.</p> <p>(5) Ground-shock station with Calidyne accelerometer and free-piston-displacement gauge.</p> <p>(6) Firing location of dynamite charge for sound-velocity measurement.</p> | <p>(7) Four ball-crusher gauges in concrete-block mount.</p> <p>(8) Group of three steel-stake-mounted ball-crusher gauges.</p> <p>(9) Underwater mount for seven ball-crusher gauges.</p> <p>(10) Blast hut with wind-speed and wind-direction gauges.</p> <p>(11) Ground mounts for six indenter gauges.</p> <p>(12) Blast hut.</p> <p>(13) Pylon with inductance gauges at 3.50, 7, 10, and 14 ft above ground level.</p> <p>(14) Ground mount with two inductance gauges.</p> <p>(15) Ground mount with three indenter gauges.</p> <p>(16) Telemetering balloon anchorage.</p> <p>(17) Group of three steel-stake-mounted ball-crusher gauges off end of guy wire.</p> |
|---|--|

TABLE 1.2 BLAST MEASUREMENTS INSTRUMENTATION CHART FOR DOG SHOT, RUNIT ISLAND†

Distance from Ground Zero		Station No.	Bearing from Ground Zero				Walls	Velocity Gauges	Rocket Launchers	Ball Crushers	Indenters (Ground)	Blast Hut	Teleme- tering
Nominal (yd)	Measured (ft)		N/S	°	'	"	E/W						
4	12.01	27a	S	83	50	02	W			7			
5	15.00	33a	S	81	31	03	W			8			
23	68.98	27b	S	83	50	02	W			7			
23	69.00	33b	S	81	31	03	W			8			
57	170.95	27c	S	83	50	02	W			7			
57	171.00	33c	S	81	31	03	W			8			
80	240.00	33d	S	81	31	03	W			8			
80	240.01	27d	S	83	50	02	W			7			
93	279.01	33e	S	81	31	03	W			8			
93½	280.05	34a	N	81	31	03	E			17			
103	309.01	33f	S	81	31	03	W			8			
103	309.06	34b	N	81	31	03	E			17			
113	338.99	33g	S	81	31	03	W			8			
113	339.08	34c	N	81	31	03	E			17			
123	368.96	33h	S	81	31	03	W			8			
123	369.11	34d	N	81	31	03	E			17			
133½	399.97	33i	S	81	31	03	W			8			
200		26c	S	8	48	38	E						16
450			S	36			E	6					
550	1,649.96	28a	S	36	29	06	E	3			15		
650	1,950.01	20a	S	36	29	05	E	1			15		
651	1,953.59	20a	S	36	29		E	3					
750	2,249.95	20b	S	36	29	03	E	1			15		
751	2,253.53	20b	S	36	29		E	3					
850	2,550.00	28b	S	36	29	05	E	3					
950	2,850.03	20c	S	36	29	04	E	1			15		
951	2,853.61	20c	S	36	29		E	2					
1,050	3,150.02	28c	S	36	37	47	E	2					
1,070			S	36			E	6					
1,150	3,450.02	28d	S	36	29	03	E	2					
1,250	3,750.04	20d	S	36	29	06	E	1			15		
1,251	3,753.62	20d	S	36	29		E	2					
1,350	4,050.01	28e	S	36	29	04	E	2					
1,450	4,349.95	20e	S	36	29	07	E	1			15		
1,451	4,353.53	20e	S	36	29		E	2					
1,550	4,649.87	28f	S	36	29	10	E	2					
1,650	4,949.91	28g	S	36	38	09	E	2					
1,750	5,250.01	28h	S	36	29	07	E	2			15		
1,779	5,337.95	23a	S	36	53	23	E						
1,793	5,378.90	32d	S	40	41	14	E				10		
2,000	5,999.97	20f	S	34	18	25	E	1		X			
2,001	6,003.55	20f	S	34	18		E	2			15		
2,250	6,749.99	28i	S	34	29	22	E	2					
2,500	7,499.99	28j	S	33	53	11	E	2			15		
2,552	7,655.49	32a	S	38	41	47	E			X			
2,737	8,209.79	32c	S	34	25	09	E			X			
4,890		†	N	27			W				15		
4,910		‡	N	27			W				15		
7,200		¶	N	14			W				11		

†For identification of code used in entries in columns 9 through 15, see Fig. 1.1.

‡Piiraa1.

§Piiraa2.

¶Rojoa.

TABLE 1.3 BLAST MEASUREMENTS INSTRUMENTATION CHART FOR EASY SHOT, ENGEBI ISLAND†

Distance from Ground Zero		Station No.	Bearing from Ground Zero				Walls	Velocity Gauges	Rocket Launchers	Ball Crushers	Indenters (Ground)	Blast Hut	Teleme- tering	Ground Shock	Pylons
Nominal (yd)	Measured (ft)		N/S	°	'	"	E/W								
4		35	S	45			E	6							
4	12.03	27a	N	11	36	32	E			7					
5	14.97	33a	N	22	15	49	E			8					
23	68.86	27b	N	89	59	00	W			7					
23	69.00	33b	N	86	50	15	W			8					
57	171.00	27c	S	73	39	12	W			7					
57	171.00	33c	S	76	00	00	W			8					
80	240.00	27d	S	73	39	12	W			7					
80	240.00	33d	S	76	00	00	W			8					
93	279.00	33e	S	76	00	00	W			8					
100	299.90	29a	N	77	59	12	E	3							
100	300.00	28a	S	45	01	18	E	3							
103	309.00	33f	S	76	00	00	W			8					
103	309.00	34a	S	13	39	12	W			17					
107	320.00	u/w 3	N	2			E			9					
113	339.00	33g	S	76	00	00	W			8					
113	339.00	34b	S	13	39	12	W			17					
123	369.00	33h	S	76	00	00	W			8					
123	369.00	34c	S	13	39	12	W			17					
133		26b	S	90	00	00	W						16		
143	429.00	33i	S	76	00	00	W			8					
143	429.00	34d	S	13	39	12	W			17					
180	540.00	28b	S	43	57	38	E	2							
180	540.00	29b	N	77	59	27	E	2							
188	564.00	u/w 2	S	62	30		W			9					
233		26a	S	30	00	00	E						16		
248	737.00	u/w 1	S	45			W			9					
260	780.00	28c	S	45	01	18	E	3							
260	780.00	29c	N	77	59	27	E	3							
360	1,080.00	29d	N	77	59	27	E	3							
360	1,080.00	28d	S	45	01	18	E	3							
360	1,080.00	36a	S	45	33	08	E							4	
460	1,380.00	29e	N	77	59	27	E	3							
460	1,380.06	20a	S	45	01	27	E	1			15				
461	1,383.64	20a	S	45	01		E	3							
560	1,680.00	29f	N	77	59	27	E	2							
560	1,680.00	20b	S	45	01	18	E	1			15				
561	1,683.58	20b	S	45	01		E	2							
560			S	45	01		E	6							
560			N	77	59		E	6							
620	1,860.00	29g	N	77	59	27	E	2							
620	1,860.00	28e	S	45	01	18	E	2							
700	2,100.00	20c	S	45	01	18	E	1			15				
700	2,100.00	29h	N	77	59	27	E	2							
700	2,100.00	37d	N	77	18	31	E								14
700	2,100.11	36b	S	45	17	49	E							4	
700	2,100.13	37a	N	76	37	32	E								13
701	2,103.58	20c	S	45	01		E	2							
800	2,399.92	28f	S	45	01	15	E	2							
800	2,400.00	29i	N	77	59	27	E	2							

† For identification of code used in entries in columns 9 through 17, see Fig. 1.1.

TABLE 1.3 (Continued)

Distance from Ground Zero		Station No.	Bearing from Ground Zero				Walls	Velocity Gauges	Rocket Launchers	Ball Crushers	Indenters (Ground)	Blast Hut	Teleme- tering	Ground Shock	Pylons
Nominal (yd)	Measured (ft)		N/S	°	'	"	E/W								
900	2,700.00	21a	N	77	59	27	E	1			15				
900	2,700.00	20d	S	45	01	18	E	1			15				
901	2,703.58	21a	N	77	59		E	2							
901	2,703.58	20d	S	45	01		E	2							
950	2,850.00	37b	N	76	59	08	E								
950	2,850.00	37e	N	77	29	18	E								13
979	2,936.47	32d	S	89	50	09	E		X						14
981	2,942.52	32c	N	83	48	17	E		X						
985	2,954.69	36f	S	68	59	49	E							4	
1,000	3,000.00	36c	S	45	12	46	E							4	
1,000	3,000.00	28g	S	45	01	18	E	2							
1,000	3,000.00	21b	N	77	59	27	E	1							
1,001	3,003.58	21b	N	77	59		E	2							
1,002	3,005.06	32b	N	77	04	10	E		X						
1,032	3,096.08	32a	N	72	00	07	E		X						
1,100	3,300.00	28h	S	45	01	18	E	2							
1,100	3,300.00	29j	N	77	59	27	E	2							
1,200	3,600.00	29k	N	77	59	27	E	2							
1,200	3,600.09	28i	S	45	01	15	E	2							
1,230	3,690.00	25	N	75	40	00	E					12			
1,232	3,695.83	32e	S	79	31	39	E		X						
1,233	3,700.00	21c	N	77	59	27	E	1			15				
1,234	3,703.58	21c	N	77	59		E	2							
1,269	3,806.76	32f	S	74	16	27	E		X						
1,280	3,840.06	32g	S	69	23	21	E		X						
1,300	3,899.93	36d	S	45	10	16	E								
1,300	3,900.00	20e	S	45	01	18	E	1			15			5	
1,301	3,903.58	20e	S	45	01		E	2							
1,350	4,050.69	32i	S	59	53	41	E		X						
1,369	4,107.22	32h	S	65	03	42	E		X						
1,405	4,216.41	32j	S	55	36	22	E		X						
1,430	4,290.00	37f	S	45	21	19	E								
1,430	4,290.00	37c	S	45	41	22	E								14
1,460	4,380.09	28j	S	45	01	18	E	2							13
1,462	4,385.14	32k	S	51	33	03	E		X						
1,500	4,501.47	36e	S	46	10	42	E								
1,533	4,600.15	32i	S	48	06	22	E		X					5	
1,550	4,650.00	20f	S	45	01	23	E	1			15				
1,551	4,653.58	20f	S	45	01		E	2							
1,590	4,769.68	23a	S	45	17	10	E					10			
2,261		1	S	42			E				11				
3,503		1	S	45			E				11				

1Muzinbaarikku.

2Kirinian.

TABLE 1.4 BLAST MEASUREMENTS INSTRUMENTATION CHART FOR
GEORGE SHOT, EBERIRU, AOMON, BILJIRI, AND ROJOA ISLANDS†

Distance from Ground Zero		Station No.	Bearing from Ground Zero					Velocity Gauges	Rocket Launchers	Blast Hut	Ground Shock
Nominal (yd)	Measured (ft)		N/S	°	'	"	E/W				
620	1,860.00	36a	S	61	03	12	E				4
620	1,860.16	28a	S	56	15	55	E	2			
667			S	56			E	6			
700	2,100.00	36b	S	55	39	23	E				4
700	2,100.00	28b	S	56	28	36	E	3			
800	2,400.00	28c	S	56	40	52	E	3			
900	2,700.00	88d	S	56	50	26	E	3			
1,000	3,000.00	28e	S	56	58	04	E	3			
1,093	3,279.18	36c	S	56	33	27	E				4
1,100	3,300.00	28f	S	57	04	20	E	3			
1,200	3,600.00	28g	S	57	09	32	E	2			
1,220			S	57			E	6			
1,300	3,900.00	28h	S	57	13	56	E	2			
1,300	3,900.00	36d	S	57	32	27	E				5
1,400	4,200.00	28i	S	57	17	43	E	2			
1,650	4,950.00	28j	S	58	48	30	E	2			
1,750	5,250.00	28k	S	57	27	00	E	2			
1,850	5,550.00	28l	S	58	44	00	E	2			
1,950	5,850.00	28m	S	58	42	06	E	2			
1,966	5,896.98	32a	S	69	02	36	E		X		
1,997	5,990.75	32b	S	66	48	41	E		X		
2,031	6,093.55	32c	S	64	39	01	E		X		
2,068	6,204.67	32d	S	62	33	48	E		X		
2,092	6,275.34	32e	S	60	24	28	E		X		
2,142	6,425.47	32e ₁	S	59	31	39	E		X		
2,150	6,450.00	28n	S	58	38	50	E	2			
2,158	6,475.00	36e	S	58	06		E				5
2,162	6,487.38	23a	S	58	06	42	E			10	
2,164	6,493.09	32f	S	58	50	54	E		X		
2,180	6,540.70	32f ₁	S	57	33	11	E		X		
2,195	6,583.99	32g	S	56	45	39	E		X		
2,212	6,645.83	32g ₁	S	55	56	29	E		X		
2,241	6,724.28	32h	S	54	58	44	E		X		
2,600	7,800.00	28o	S	58	33	17	E	2			
2,700	8,099.90	28p	S	58	32	18	E	2			

† For identification of code used in entries in columns 9 through 12, see Fig. 1.1.

**TABLE 1.5 REPORT TITLES FOR GREENHOUSE REPORT
ANNEX 1.6, BLAST MEASUREMENTS**

Part I	Summary Report on Blast Measurements at Eniwetok, 1951
Part II	Free-air Peak-pressure Measurements
Section 1	Peak Pressure vs Distance in the Free-air and Mach Regions Using Smoke-rocket Photography
Section 2	The Measurement of Free-air Peak Pressure by Telemetering from Moored Balloons
Part III	Pressure near Ground Level
Section 1	Determination of Mach-region Peak Blast Pressures from Shock-velocity Measurement
Section 2	Determination of Mach-region Peak Blast Pressures with Foil Meters
Section 3	Positive Peak Pressure Measurements in the Mach-stem Region by Means of Copper-indenter Gauges
Section 4	Blast Asymmetry from Aerial Photographs
Section 5	Ball-crusher-gauge Measurements of Peak Pressure on the Ground in the Area beneath the Explosion
Part IV	Pressure-time Measurements in the Mach Region
Section 1	With Variable-inductance Diaphragm Gauge
Section 2	With Spring-piston Gauge
Part VI	Ground-shock Measurements
Section 1	Measurements of Ground Motion
Section 2	Crater Survey

[REDACTED]

space, time, or other quantity over which the other remarks apply. By reliability is meant an estimate of the chance that a given instrument or method will work as it is expected to, taking into account the likelihood of the occurrence of all extraneous factors which might affect the performance.

1.5 INSTRUMENT LOCATIONS

Tables 1.2 to 1.4 show the locations of instruments on Shots Dog, Easy, and George, respectively.

1.6 LIST OF INDIVIDUAL REPORTS

Table 1.5 lists the titles of the detailed reports on the various measurements. In these reports, which form additional volumes in this series, are given design information, details of calibration, field use, analysis and theory of the instrument, preoperation experiments, and a detailed presentation of all results obtained with an evaluation and interpretation of same, together with recommendations for improvements in the future.

Chapter 2

Preliminary Experiments and Calculations

2.1 FREE-AIR CURVE FOR TNT

It has become customary to describe the total yield of an atomic explosion in terms of kilotons of TNT with the understanding that the kiloton is really an energy unit such that 1 kt is equal to 4.20×10^{18} ergs. This is equal to the energy released on the detonation of 1,000 short tons of TNT, taking the energy of detonation as equal to 1,100 cal/g and ignoring any after-burning.

Good experimental information on the pressure-distance curve for TNT in free air is now available. The experimental points of Fisher¹ and of Weibull² lie almost exactly on the theoretical curve calculated by Kirkwood and Brinkley.³ This calculation starts with 1,060 cal/g as the energy of detonation. A similar calculation for Pentolite,⁴ although leading to a curve below 100 psi in fair agreement with experiment, starts with an energy release of 1,450 cal/g, which is considerably more than the detonation energy of Pentolite. Because of these reasons and because the calculated TNT and Pentolite curves below 100 psi are practically identical in shape, it has been decided to use the TNT curve as tabulated³ in Report OSRD-5481 as a standard blast curve. At the time of writing of Sandstone Report, Annex 5, Vol. 20, Blast Measurement Summary Report, 1948, sufficient information was not available to make this seem a reasonable choice.

2.1.1 Arrival-time Data

Weibull² has conducted at the Physical Research Department at Bofors, Ltd., a series of very accurate measurements on the times of arrival t of the shock wave from centrally

detonated spherical TNT charges at various distances R . λ is defined as $R \text{ (ft)}/[W \text{ (lb)}]^{1/3}$. The data were fitted out to $\lambda = 4$ to an equation of the form

$$t = b_0(R - R_0) + b_1(R - R_0)^2 + b_2(R - R_0)^3,$$

where R_0 is the radius of the charge and b_0 , b_1 , and b_2 are fitting coefficients. The shock velocity $U = dR/dt$ was found analytically from this, and the values of U/C_0 were converted to pressures using the tables of Hirschfelder and Curtiss.⁵ Velocities for large values of λ were given by Weibull using the following graphical method. Let Δ be the difference between the travel times of a sound wave and the shock wave over the same path; then

$$\Delta = \frac{R - R_0}{C_0} - t.$$

Differentiating,

$$\frac{d\Delta}{dR} = \frac{1}{C_0} - \frac{1}{U}.$$

Hence

$$U = \frac{C_0}{1 - C_0 \frac{d\Delta}{dR}}.$$

The values of $d\Delta/dR$ are obtained by graphical smoothing of a graph of Δ vs R .

The second source of information on the free-air curve consists in some careful experiments on arrival times made by Fisher⁶ using spherical 8-lb TNT charges. The calculated mean pressures from this work have a

standard deviation of less than 1 per cent. The experimental points and the theoretical curve are shown in Fig. 2.1.

2.2 REFLECTION EXPERIMENTS

Since the Greenhouse bombs were to be fired on towers and since many measurements were being made on the ground, it was felt to be advisable to make some model reflection experiments with spherical blast waves.¹ The experiments were made using 8-lb spheres of TNT and 1-lb spheres of Pentolite, centrally detonated. The time of arrival of the blast wave at a series of known positions was measured. The precision of all measurements was such that the standard deviation of the mean of all pressures quoted was less than 1.5 per cent. The reflecting media were (1) hard-packed clay and (2) water.

2.2.1 Discussion of Reflection Coefficients

There are at least two different ways of looking at the phenomena of blast reflection. Suppose that a spherical charge of weight W is fired in free air. Values of the excess pressure P_s at various values of $\lambda = R/W^{1/2}$ are obtained. If a flat horizontal reflecting medium such as clay, water, or steel plate is brought up so that the charge is a distance h from it and if pressures are measured along the surface of the medium, it is found that the pressures are larger than they were before at the same distance (slant range). The charge weight in free air W_F necessary to give the same pressure at the same distance can easily be found from the free-air curve. The "reflection coefficient" may be defined as W_F/W , and it represents a measure of the amount of blast energy prevented by the reflecting medium from spreading out into space and becoming lost. As so defined, the reflection coefficient is a function of the reflecting medium, the pressure level, and also the geometry. There is nothing in this definition to say, for example, that the reflection coefficient must be less than 2. If, for example, consideration is given the head-on reflection of an incident excess pressure of 50 psi and if the reflecting medium is perfectly rigid, the reflected excess pressure is 198 psi. The free-air λ for 198 psi is 1.90 using TNT (see Fig. 2.1). Hence

$$\frac{R}{W_F^{1/2}} = 1.90,$$

and

$$\frac{R}{W^{1/2}} = 4.05.$$

It is therefore seen that for this particular case the reflection coefficient W_F/W as defined above is equal to 9.7. If the effect of the reflection is observed at distances which are large compared with the distance at which the Mach stem begins to form, then it is observed that the reflected-pressure curves are very closely parallel to the free-air curves and that therefore the reflection coefficient is independent of distance in this region. Thus it is a useful concept when applied to measurements in the far Mach region.

There is, however, another way to define a reflection coefficient so that its value is bounded between 1 and 2 and so that its definition holds throughout the regions of both Mach and regular reflection. If two spherical charges of equal weight are fired simultaneously, then it will be said that pressures measured in the plane which perpendicularly bisects the line joining their centers are identical with those which would be obtained at a perfectly rigid reflector. The simultaneous firing of a charge and its image in free air are thus equivalent to firing a single charge over a perfect reflector. Let the single charge be of weight W and the equivalent pair of charges in free air be each of weight $W'/2$. Define the reflection coefficient as W'/W . If the surface is a perfect reflector, then in order to get the same pressure levels at the same (horizontal) distances it is evident that $W = W'/2$. Therefore the reflection coefficient, defined in this manner, is equal to 2 at all distances. If the reflecting medium is not perfect, then W' may be made smaller, and therefore the reflection coefficient is less than 2. Figure 2.2 illustrates the two concepts under discussion.

2.2.2 Data on Reflections

The data available are barely sufficient to illustrate the differences in the two reflection coefficients. In plotting the data the following conventions are used: $\lambda_F = R/W_F^{1/2}$ for free air; $\lambda_r = R/W^{1/2}$ for the case of reflection, geometry

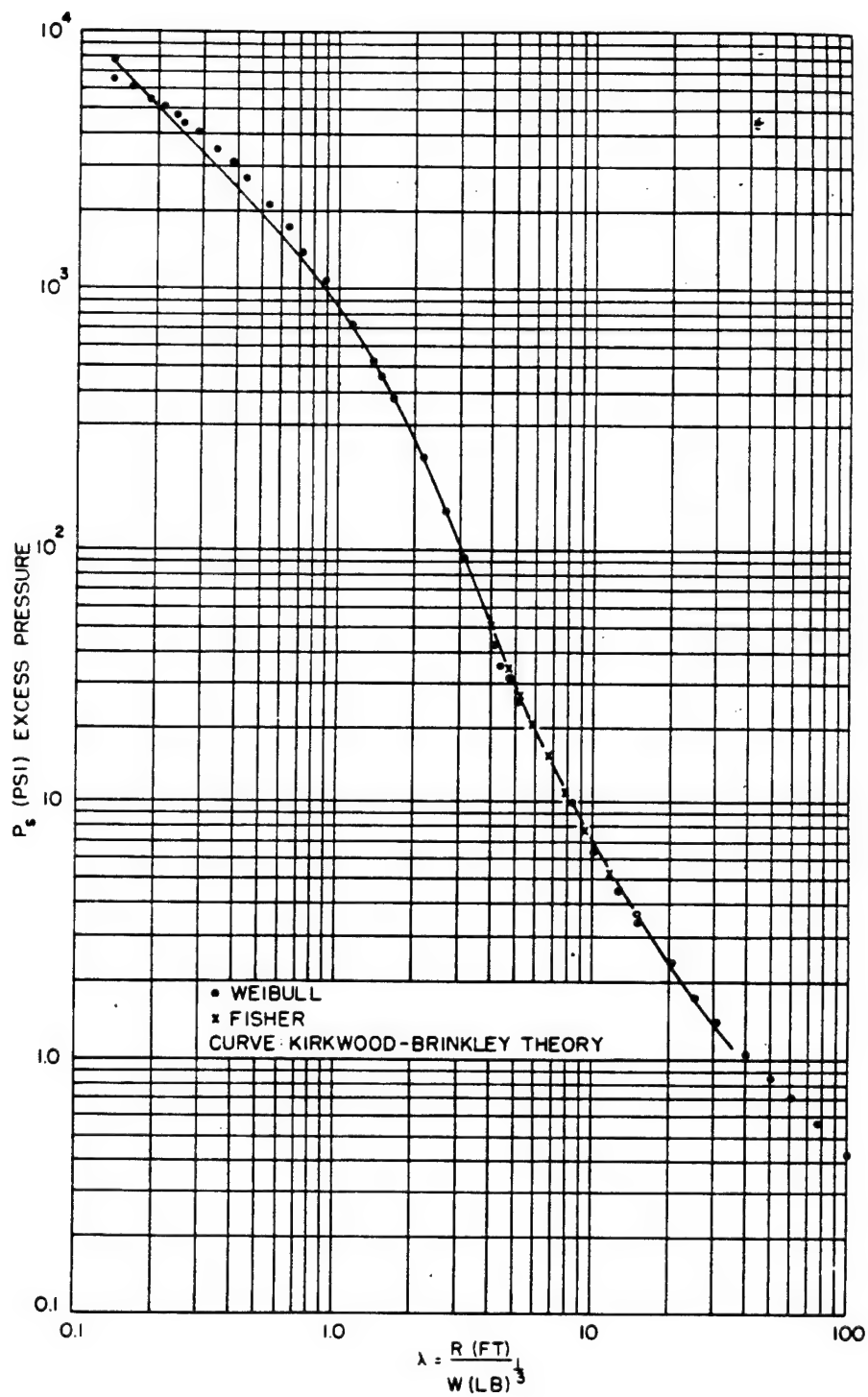
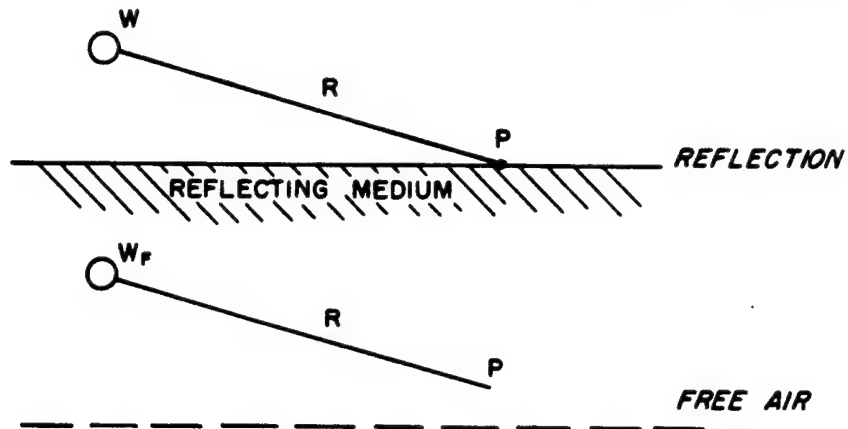


Fig. 2.1 Free-air-pressure vs Distance Curve for Spherical TNT

A. USING FREE-AIR CURVE, REFLECTION COEFFICIENT, $R_r = \frac{W_r}{W}$



B. USING IMAGES, REFLECTION COEFFICIENT, $R_z = \frac{W'}{W}$

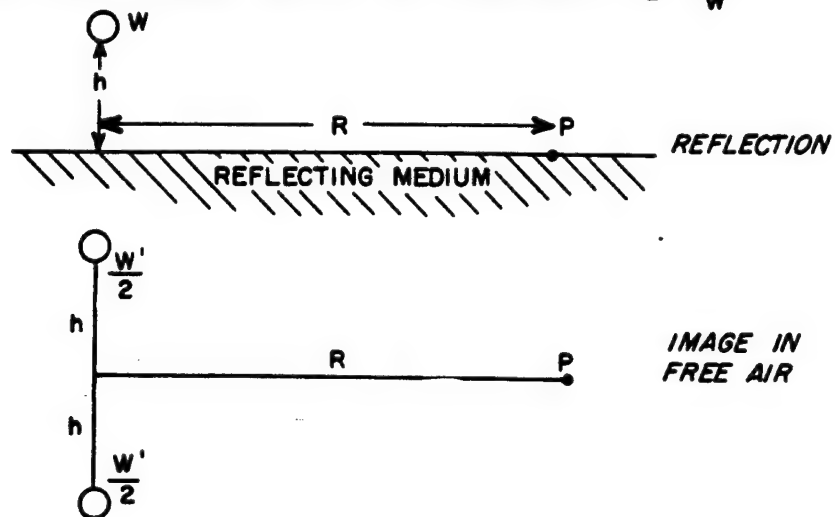


Fig. 2.2 Reflection Coefficients

of Fig. 2.2A; and $\lambda' = R/(W/2)^{1/2}$ for the case of image reflection, geometry of Fig. 2.2B.

Table 2.1 contains data plotted in Fig. 2.3. For free-air data see Sec. 2.1. The symbol

TABLE 2.1 REFLECTION DATA FOR SPHERICAL CHARGES
 $\mu = 2.14$

Single Charge†		Two Charges‡	
λ_r	P_s	λ'	P_s
4.63	54.02	4.58	59.11
5.08	44.70	5.00	47.66
5.55	39.88	5.48	40.95
6.14	29.74	6.05	32.54
6.96	22.04	6.90	24.82
8.05	16.56	7.95	18.18
9.65	11.44	9.55	12.79
11.85	7.55	11.75	8.88

†Charge height, 4.28 ft above ground; charge weight, 8 lb of TNT; values are averages of six shots.

‡Charge weight, each, 8 lb of TNT; charge separation, 8.56 ft; values are averages of four shots.

TABLE 2.2 REFLECTION COEFFICIENTS FOR $\mu = 2.14$

P_s	λ'	λ_r	λ_F	R_I	R_F	$(\lambda'/\lambda_F)^3$
10	10.9	10.35	8.35	1.71	1.91	2.24
15	8.82	8.45	6.82	1.76	1.90	2.16
30	6.25	6.10	5.00	1.86	1.81	1.95
50	4.90	4.84	4.05	1.93	1.70	1.78
		Av.	1.82	1.83	2.03	

μ is defined as reduced height $h/W^{1/2}$; also $\mu' = h/(W'/2)^{1/2}$. The ratio of μ to λ is so small for the data quoted that slant range and horizontal range differ by less than 1 per cent at the near points. It is because of this that the free-air curve can be shown on the same graph, Fig. 2.3.

It is easy to show that $R_F = (\lambda_r/\lambda_F)^3$ and that $R_I = 2(\lambda_r/\lambda')^3$.

From Fig. 2.3, values are obtained for these coefficients at different pressure levels as

shown in Table 2.2. An R_F for a perfect reflector can also be found, as shown in the last column. The increase in the value with de-

TABLE 2.3 REFLECTION DATA FOR SPHERICAL CHARGES
 $\mu = 0.615$

Single Charge†		Two Charges‡	
λ_r	P_s	λ'	P_s
4.30	79.37	4.10	87.70
4.40	68.27	4.60	62.79
4.80	58.23	5.10	47.60
4.90	51.01	5.70	36.40
5.30	43.62	6.60	26.35
5.40	39.41	7.70	18.58
5.90	30.20	9.30	12.00
6.00	28.97	11.50	8.50
6.80	22.78		
6.90	21.47		
7.90	16.30		
8.00	16.09		
9.50	10.91		
9.70	10.51		
11.80	7.63		
11.90	7.33		

†Charge height, 1.23 ft above ground; charge weight, 8 lb of TNT; values are averages of 14 shots.

‡Charge weight, each, 8 lb of TNT; charge separation, 2.46 ft; values are averages of six shots.

TABLE 2.4 REFLECTION COEFFICIENTS FOR $\mu = 0.615$

P_s	λ'	λ_r	λ_F	R_I	R_F	$(\lambda'/\lambda_F)^3$
10	10.35	10.0	8.35	1.80	1.71	1.90
15	8.41	8.15	6.82	1.82	1.70	1.88
30	6.20	6.03	5.00	1.84	1.75	1.90
50	5.05	4.96	4.05	1.90	1.84	1.94
		Av.	1.84	1.75	1.90	

creasing pressure is curious but may be real. Similar data are shown in Tables 2.3 and 2.4 and Fig. 2.4 for a smaller reduced height.

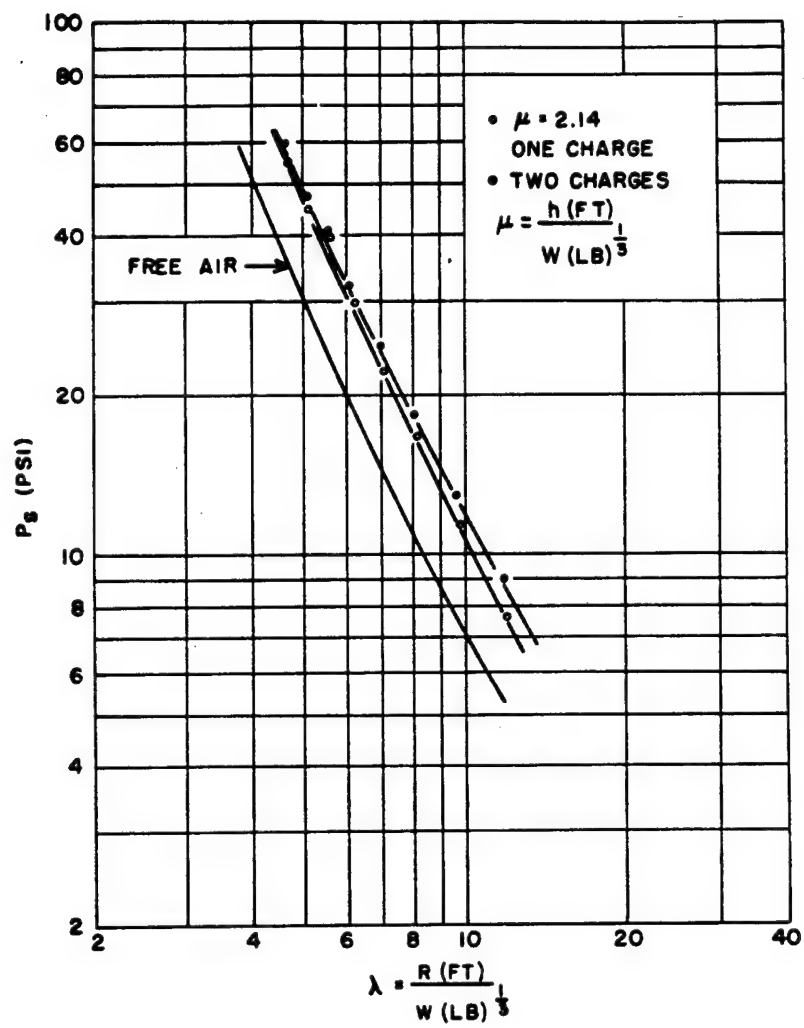


Fig. 2.3 Reflection Data for TNT Spheres, $\mu = 2.14$

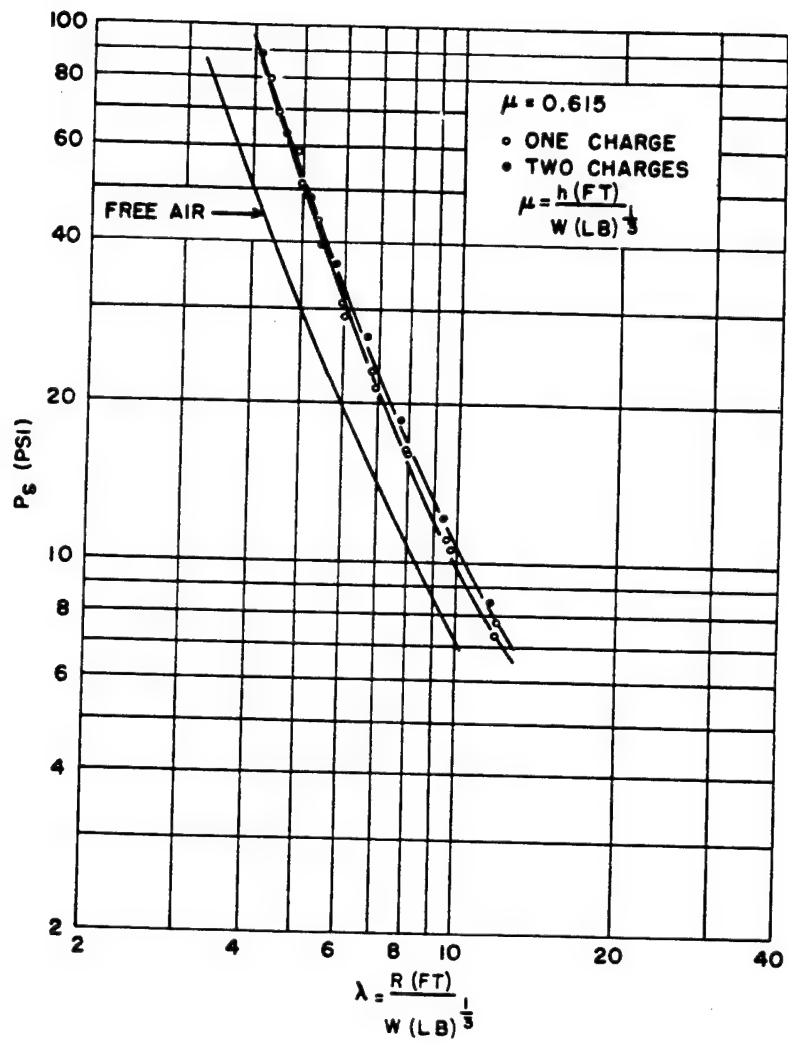


Fig. 2.4 Reflection Data for TNT Spheres, $\mu = 0.615$

A summary of image and clay reflection experiments is shown in Figs. 2.5 and 2.6. Further details may be found⁸ in Report NavOrd 2123.

2.2.3 Bikini Able Model Experiment

In order to determine R_F for the situation of the Able explosion, a model experiment was set up using 1-lb spherical charges of Pentolite placed with center 1.5 ft above the water surface. The water depth was 0.5 ft. The linear scale of the experiment was thus approximately 1:350. The results were as shown in Table 2.5. The value of R_F obtained from these data

TABLE 2.5 WATER REFLECTION DATA[†]

λ_r	P_s
5.11	51.3
6.07	33.6
7.03	24.6
8.24	16.4
9.94	11.6
12.15	8.22
15.33	5.50
19.77	3.50

[†]The standard deviation of the pressure quoted is 3 per cent.

and plotted in Fig. 2.7 is 1.90 ± 0.06 within the excess pressure range 5 to 50 psi.

2.2.4 Summary of Values of R_F as a Function of Reduced Height

Table 2.6 summarizes the values of R_F obtained to date from the experiments in Sec. 2.2.2 and others. The values of R_F are plotted in Fig. 2.8.

2.3 CONVERSION OF SHOCK VELOCITY INTO SHOCK PRESSURE

Hirschfelder and Curtiss⁹ have tabulated the properties of air along the Hugoniot curve for a variety of initial conditions as shown in Table 2.7. If shock strength P/P_1 is plotted against the Mach number U/C_1 , taking values of P and U from the tables for various ambient

temperatures, it turns out that all points fall on a single curve as shown in Fig. 2.9. Furthermore, the influence of water content can be accounted for in the same manner. Figure 2.10 shows shock strength vs shock velocity for dry air and for air containing 5 mole % water vapor. By replotting these values against U/C_1 , the two curves can be made to coincide. The velocity of sound may be calculated for moist air within 0.03 per cent of the Hirschfelder and Curtiss values using

$$C = C_{\text{dry}} \left(1 + 0.149 \frac{p_w}{p - p_w} \right),$$

where C_{dry} is the velocity of sound in dry air at the ambient temperature, p_w is the partial pressure of water vapor, and p is the total ambient pressure. The mole percentage of water f_w is equal to $100p_w/p$. If p_{sw} is the water-vapor pressure of saturated air at temperature T , then the mole percentage and the relative humidity are related by

$$f_w p = p_{sw} \text{ (relative humidity).}$$

Thus, if the temperature is 300°K, then $p_{sw} = 27$ mm Hg; and if the relative humidity is 80, then $f_w = 2.84$ mole %. This shows that the water-vapor content encountered at Eniwetok is well within the range covered in the Hirschfelder and Curtiss tables.

Kirkwood, Brinkley, and Richardson¹⁰ have given the properties of air along the Hugoniot curve up to about 15,000°K. The values of shock strength and velocity have been used to extend the Hirschfelder and Curtiss values up to a shock strength of 1,000. The values are plotted in Figs. 2.11 to 2.13, which then afford a means of determining shock strength in any region of the atmosphere with any water content, any ambient temperature, or any density provided only that the shock velocity and sound velocity are known over the interval in question. It is, of course, necessary that the shock velocity be measured in a direction at right angles to the shock-wave front.

2.4 DISCUSSION OF ERRORS IN THE VELOCITY METHOD FOR SHOCK WAVES

The problem of measuring an arbitrary velocity is, of course, far more general than the

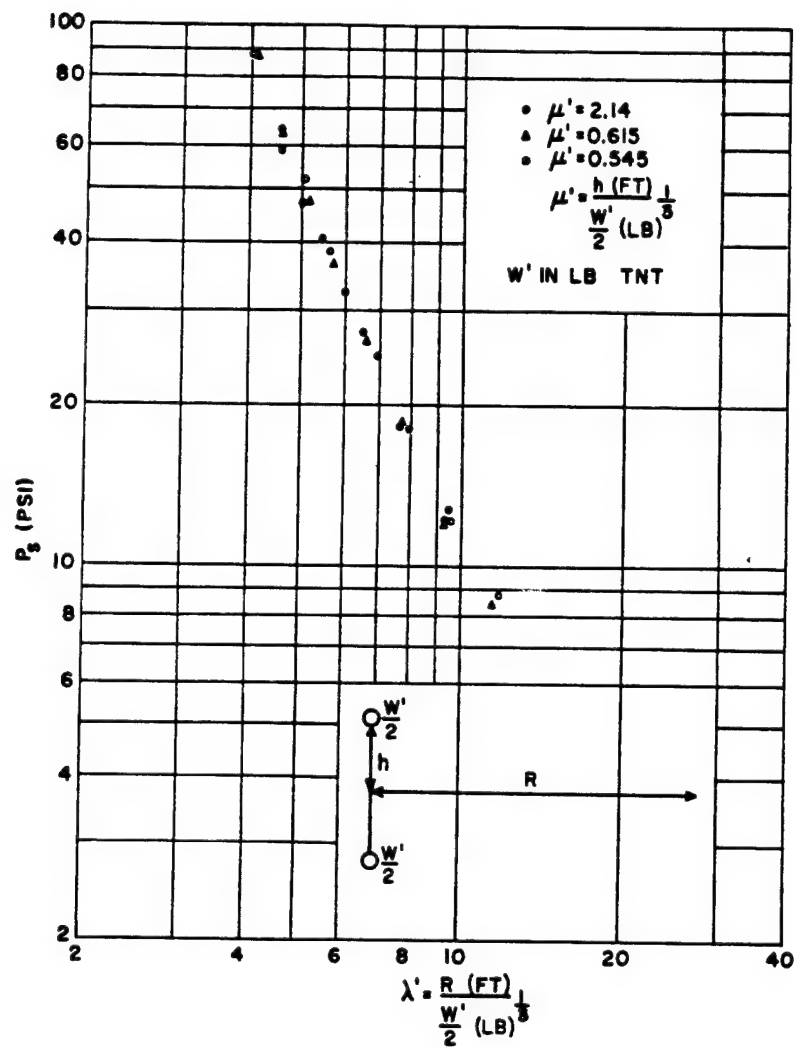


Fig. 2.5 Summary of Image Reflection Experiments, TNT

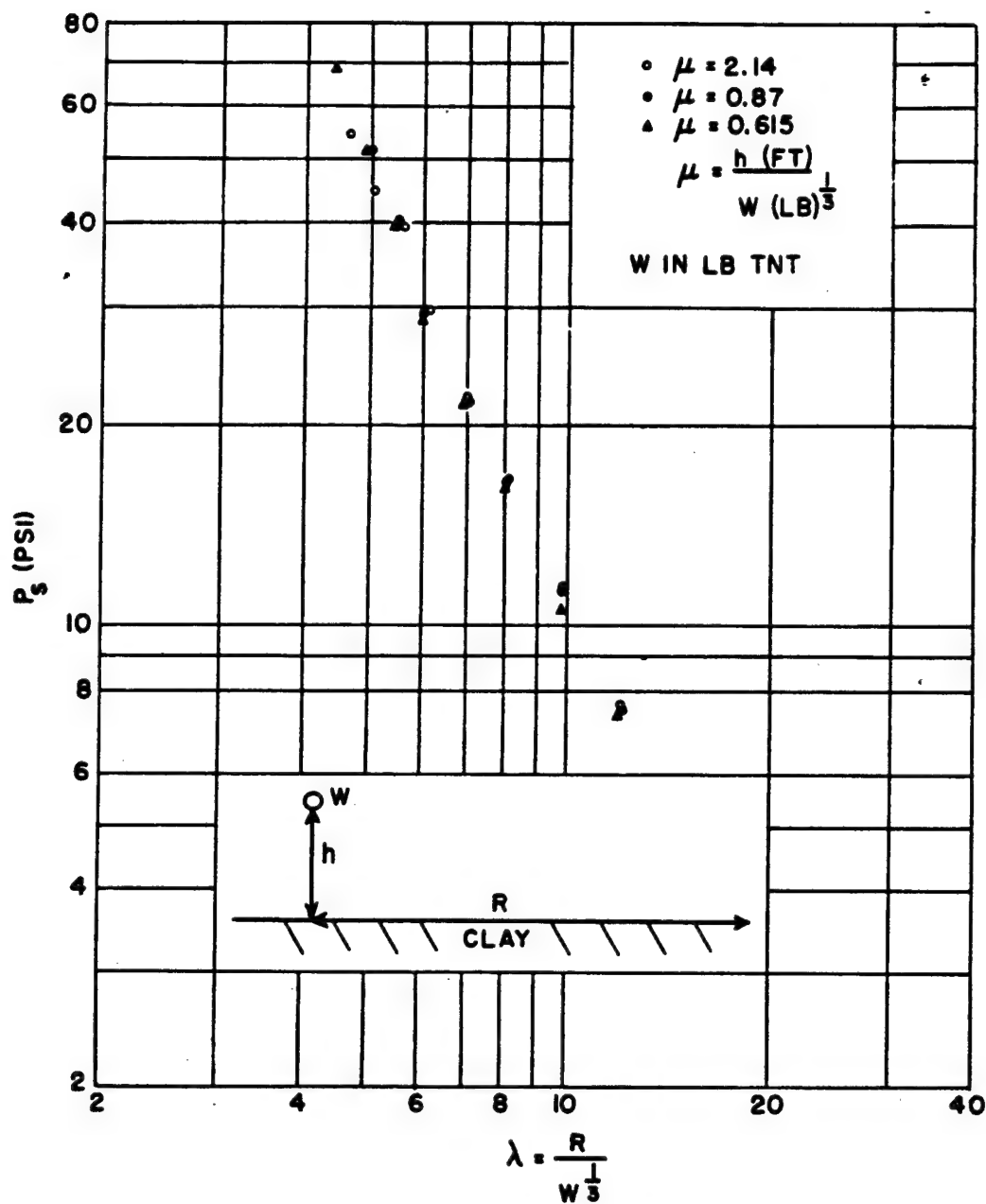


Fig. 2.6 Summary of Clay Reflection Experiments, TNT

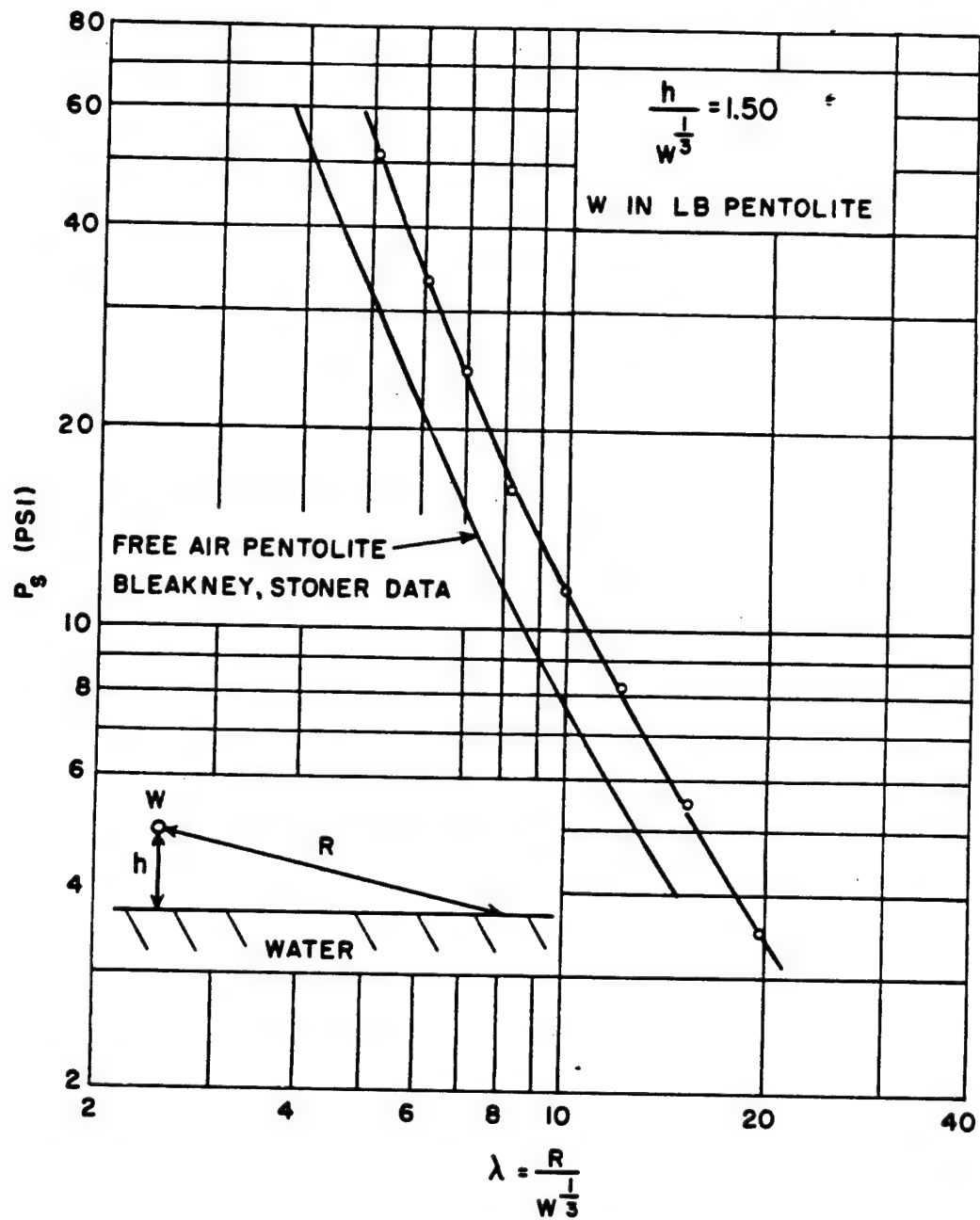


Fig. 2.7 Water Reflection, Approximately 1/350 Scale of Bikini Able

TABLE 2.6 VALUES OF R_F

W (lb of Pentolite)	h (ft)	$h/W^{1/2}$	R_F (Av.)	Reflecting Medium	Pressure Range within Which Results Were Obtained (psi)
1.0	0.125	0.125	1.28	Hard clay	10-50
1.0	0.25	0.25	1.50	Hard clay	16-63
6.85	1.23	0.65	1.75	Hard clay	8-50
6.85	1.75	0.92	1.80	Hard clay	10-50
6.85	4.28	2.25	1.85	Hard clay	10-38
6.85	1.10	0.58	1.91	Image	9-50
6.85	1.23	0.65	1.90	Image	9-50
6.85	4.27	2.25	2.04	Image	9-50
1.0	1.50	1.50	1.90	Water	5-50

TABLE 2.7 INITIAL CONDITIONS FOR HIRSCHFELDER AND CURTISS TABLES

P_1 (atm)	T_1 (°K)	Water Content (mole %)	Ambient Sound Velocity (meters/sec)	ρ_1
0.64	175	0	266.0	0.001293
1.00	273.2	0	332.6	0.001293
1.833	500	0	446.5	0.001293
1.00	273.2	0.5	332.9	0.001291
1.00	273.2	1	333.2	0.001288
1.00	273.2	5	336.1	0.001269

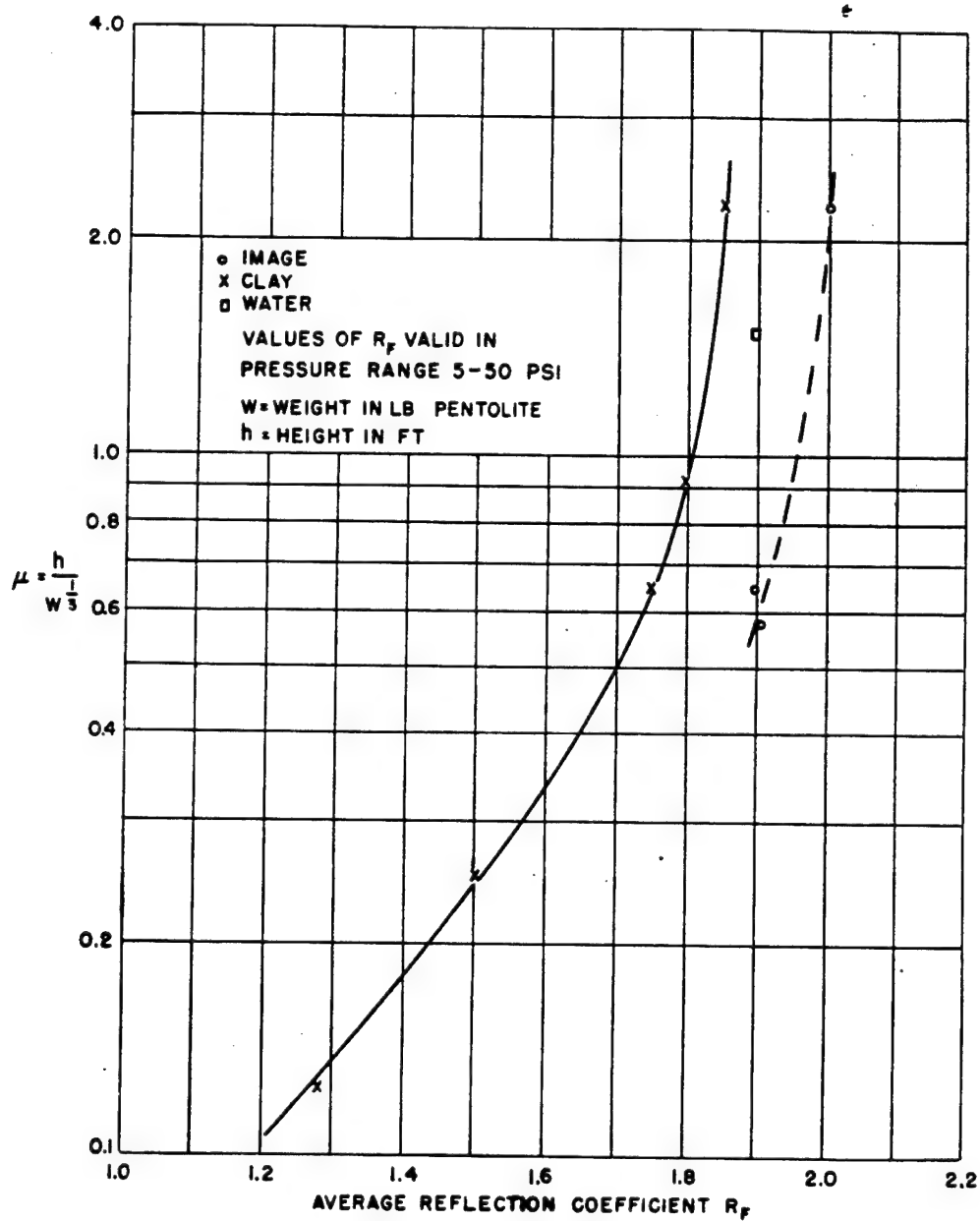


Fig. 2.8 Reflection Coefficient R_F vs μ , Reduced Height

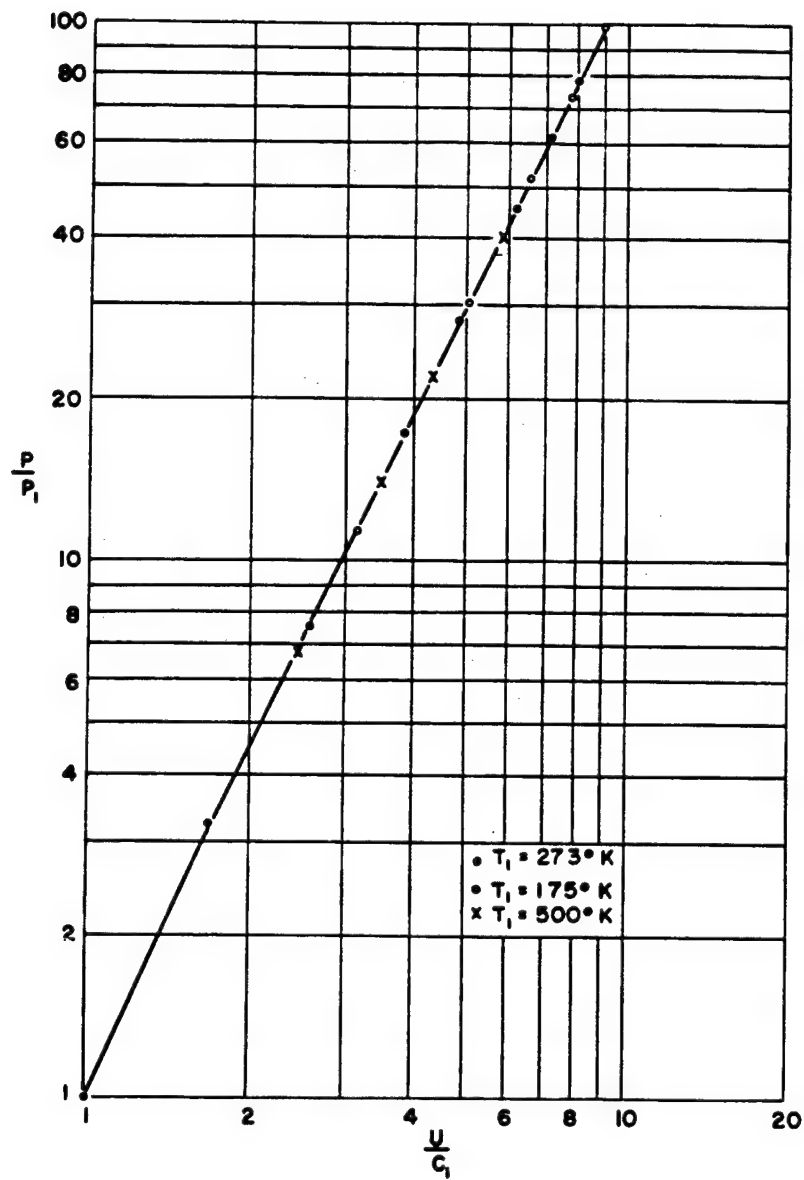


Fig. 2.9 Shock Strength vs U/C_1 for Various Ambient Temperatures

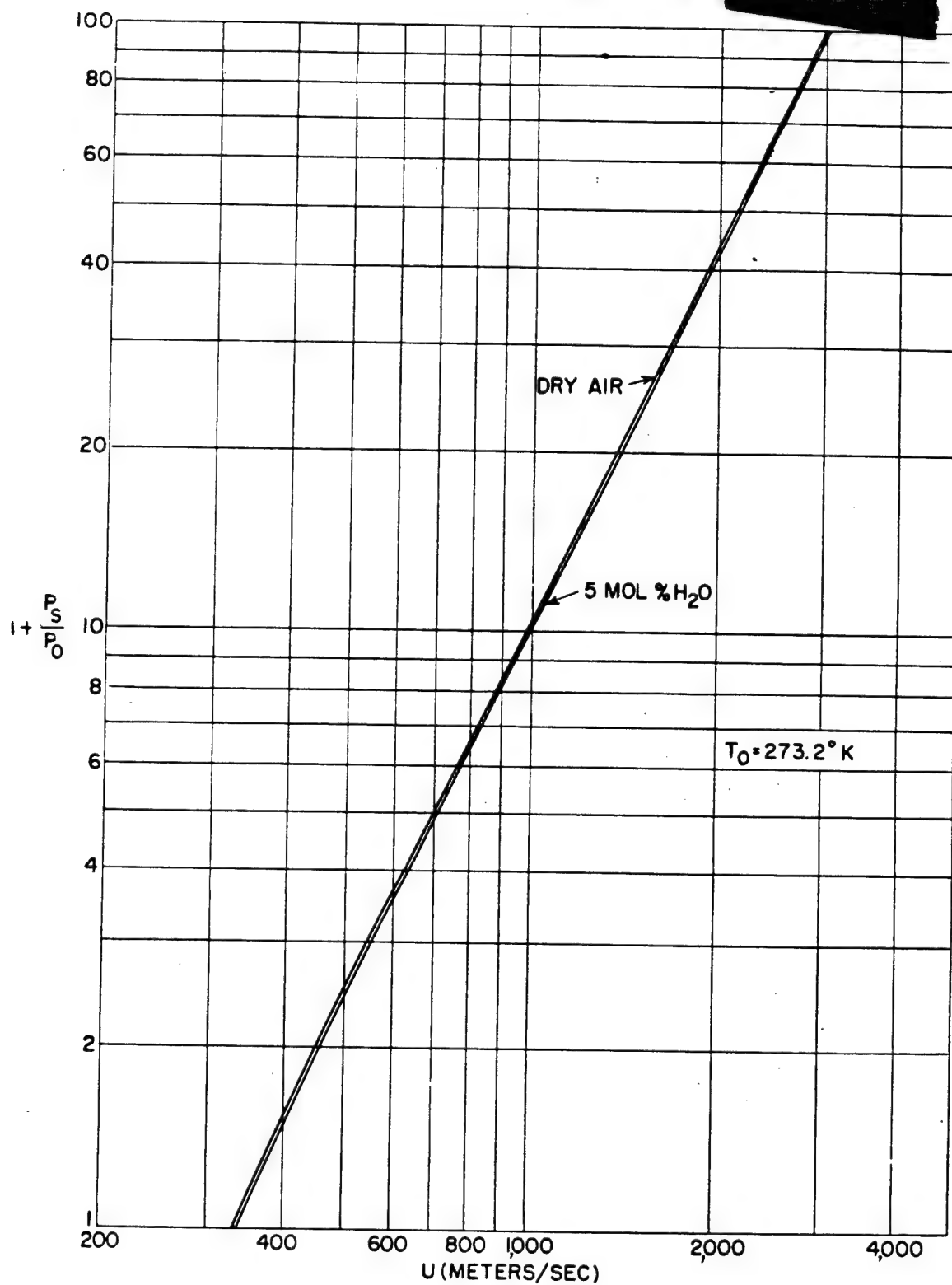


Fig. 2.10 Shock Strength vs Shock Velocity for Dry and Moist Air

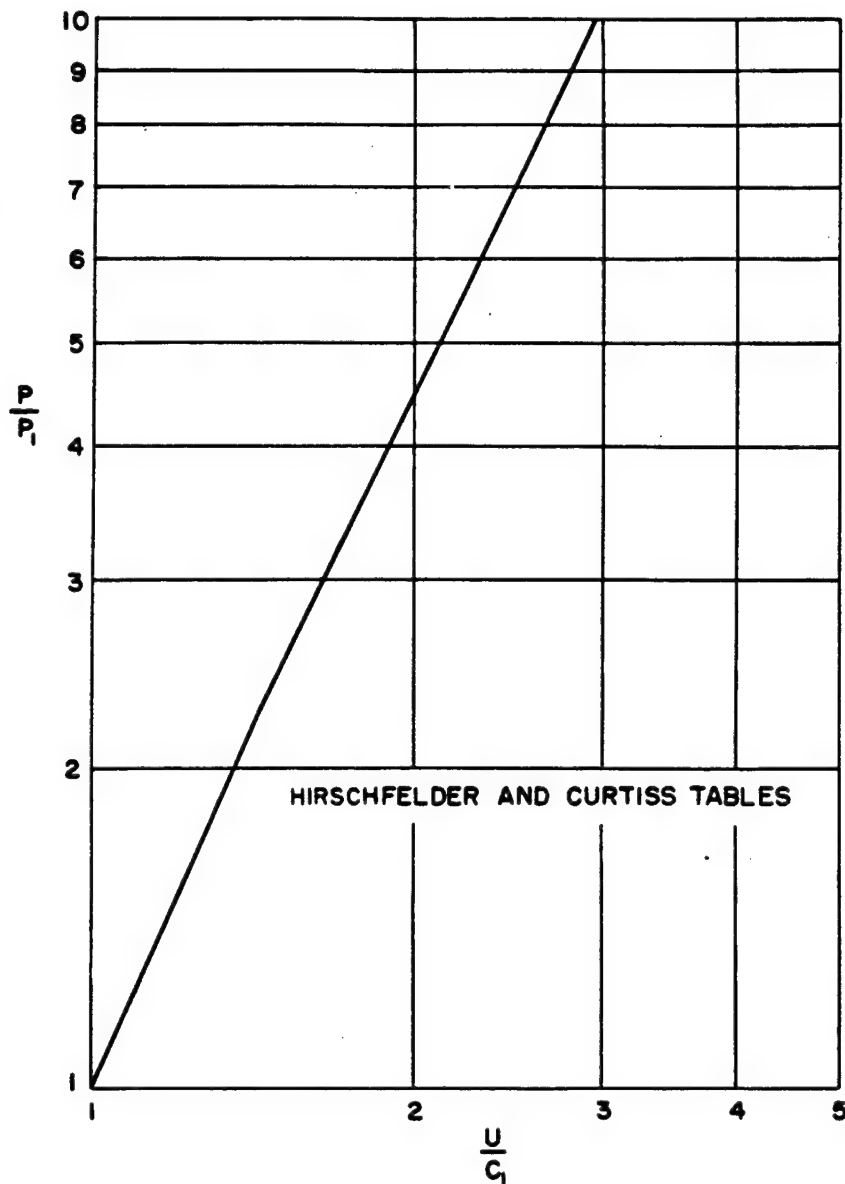


Fig. 2.11 Shock Strength P/P_1 vs U/C_1 ; Range of P/P_1 , 1 to 10

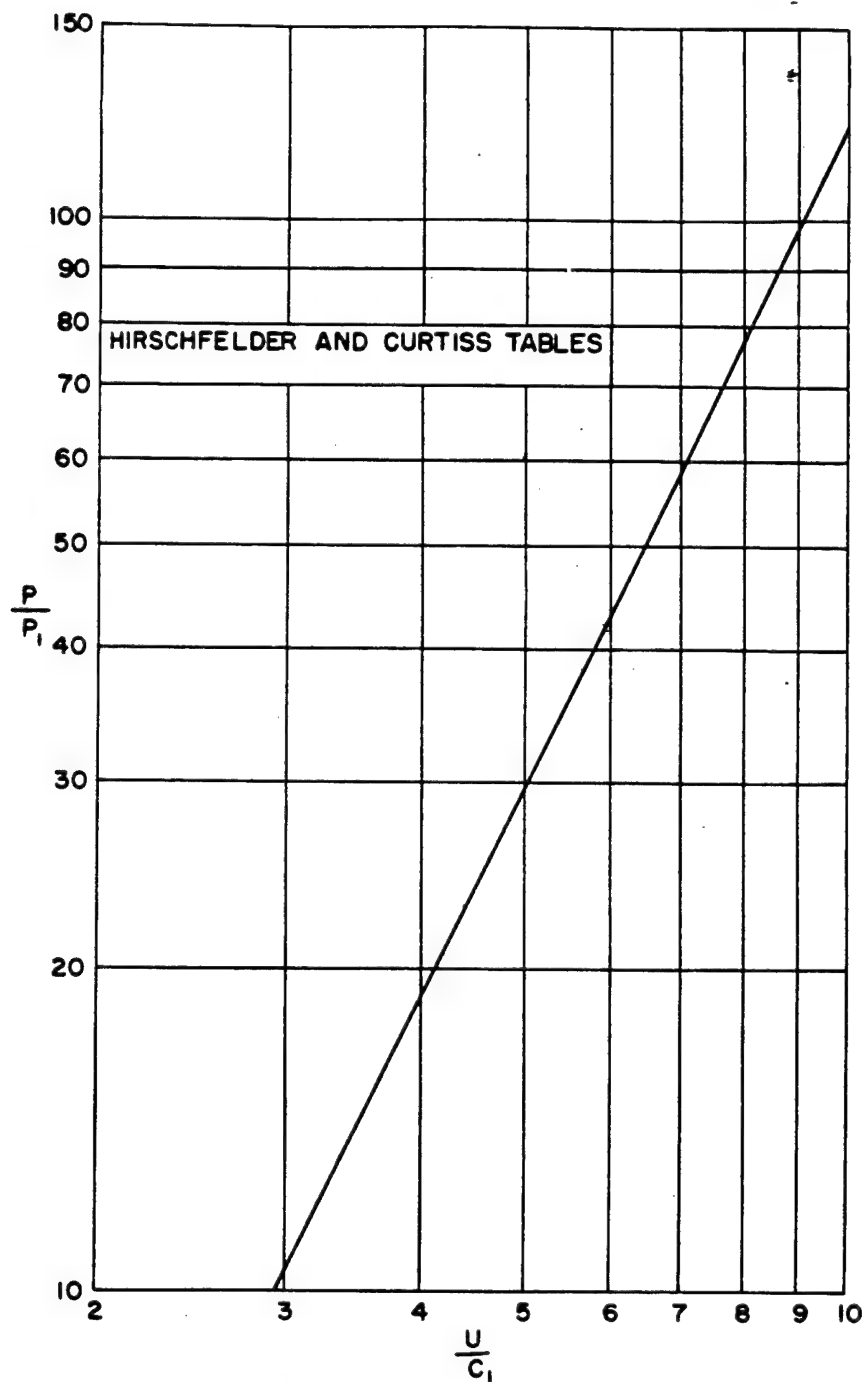


Fig. 2.12 Shock Strength P/P_1 vs U/C_1 ; Range of P/P_1 , 10 to 100

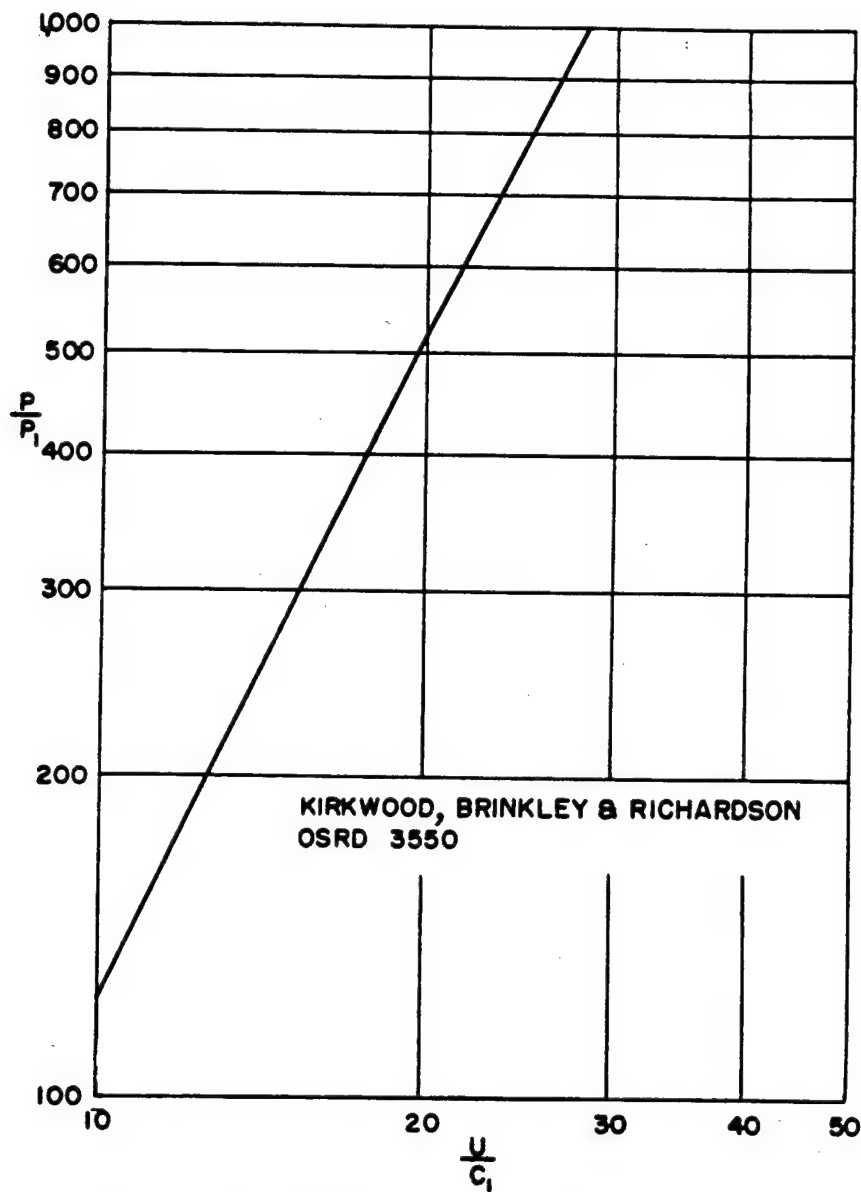


Fig. 2.13 Shock Strength P/P_1 vs U/C_1 ; Range of P/P_1 , 100 to 1,000

problem of measuring the velocity of a shock wave that is assumed to be spherical and monotonically decreasing. This section discusses the accuracy required in shock-velocity measurements in air in order to attain a given accuracy in shock pressure. Measurements of the times of arrival of the shock front at various distances are made. The uncertainty in time is denoted by Δt and the uncertainty in distance by ΔR . It will be supposed for ease of discussion that the measurements are made at low enough pressures, i.e., outside the fireball, so that γ may be considered constant and so that the relation between velocity and pressure is

$$\frac{P_s}{P_0} = \frac{2\gamma}{\gamma+1} \left[\left(\frac{U}{C_0} \right)^2 - 1 \right], \quad (2.1)$$

in which U and C_0 are the velocities of the shock wave and of the sound wave, respectively, in still air. Assume for the moment that C_0 is known without error. Then the error in P_s (ΔP_s) is related to the error in U (ΔU) by the equation

$$\frac{\Delta P_s}{P_s} = \frac{2 \frac{\Delta U}{U}}{1 - \left(\frac{C_0}{U} \right)^2}.$$

If an attempt is made to determine U at a point by using arrival times at two neighboring points, then an average value of U associated with this point will be given by $(R_2 - R_1)/(t_2 - t_1)$, and consequently the error in U will be equal to the sum of the errors associated with these intervals. If $R_2 - R_1$ is taken as small, then the relative error in its determination, namely, $\Delta R/(R_2 - R_1)$, will be large. In principle it is therefore impossible to determine U accurately if the distance over which the passage of the shock is observed is made small enough. The conclusion that it is therefore fruitless to attempt accurate measurements by the velocity method is, however, false for two reasons: (1) at low pressures the velocity changes so slowly with distance that it is not necessary to restrict unduly the interval over which the passage of the shock is timed, and (2) in using the velocity method many more than two points are determined, which contributes to the accuracy of the velocity assigned to any given interval.

It has been shown by Fraenkel¹¹ and even more generally by Theilheimer¹² that the average velocity over a fairly wide interval is closely equal to the instantaneous velocity at the mid-point of the interval. In order to demonstrate any such statement, it is necessary to have an idea of the manner in which shock velocity varies with distance. Suppose that for a given shock wave there is a unique continuous monotonic function which relates the arrival time to the distance (the origin of time and distance being the instant and place of explosion) and that the slope of this curve, dR/dt , is equal to the shock velocity U . If an analytical expression were available for this curve, $R = R(t)$, containing a number of parameters, the values of these parameters could be found by fitting sufficient data (R_1, t_1) , (R_2, t_2) , etc., and proceeding thereafter by analytical methods to calculate P_s . In such an expression it appears likely that the number of parameters to be determined would be very small, perhaps limited to one, an effective energy. Since no such expression is available in closed form, however, it is possible to resort to simple fitting functions which are acceptable over a limited pressure range. Several methods may be used to obtain such a function. For example, experimental results over the range $5 < P_s < 50$ may be represented by

$$\frac{P_s}{P_0} = \frac{a}{R} + \frac{b}{R^2} + \frac{c}{R^3}.$$

It is also possible in more limited ranges to represent the pressure by the equation $P_s/P_0 = A\lambda^{-n}$, where A and n are adjusted for each pressure range and $\lambda = R/W^{1/2}$. The entire range between 100 and 5 psi can be fitted with an accuracy of a few per cent by two or three pairs of values of A and n . Using this relation and the equation connecting P_s and U (Eq. 2.1), U can easily be found as a function of λ from Eq. 2.1,

$$U = C_0 \sqrt{\frac{\gamma+1}{2\gamma} A \lambda^{-n} + 1}. \quad (2.2)$$

Differentiation of Eq. 2.2 shows that dU/U , the relative error in shock velocity, decreases as λ (or R) increases. This means that at greater distances the value of shock velocity changes more and more slowly. This conclusion is the result of knowledge concerning the variation of

U with distance, derived from measurements at several distances.

If, on the other hand, the shock velocity is measured at a given place by timing the shock front passing two points, then $U = (R_2 - R_1) / (t_2 - t_1)$. If the error in time is zero and the uncertainty in the interval $R_2 - R_1$ is ΔR , then

$$U + \Delta U = \frac{R_2 - R_1 + \Delta R}{t_2 - t_1}.$$

From this there results

$$\frac{\Delta U}{U} = \frac{\Delta R}{R_2 - R_1}.$$

It will be seen that this requires $\Delta U/U$, the relative error in U, to be constant for a given interval, $R_2 - R_1$, regardless of the distance from the explosion. This result is correct for a single observation of the velocity. On the other hand, as greater distances and hence more slowly varying shock velocity are approached, the interval $R_2 - R_1$ can be increased so that $\Delta U/U$ can decrease in agreement with the previous statement. This means that greater accuracy can be obtained in measuring a slowly varying function by choosing larger intervals.

If a number of arrival times and distances are measured and if these are fitted to some function from which velocity and therefore pressure can be derived, then the closeness of fit or the deviation of the measured points from the fitted curve provides a measure of the accuracy of the derived pressure. In the treatment of actual data it has been found that a cubic of the form $T = a + bR + cR^2 + dR^3$ gives a good fit over a fairly wide range of distance. However, an analysis of error based on this is unnecessarily complicated. Therefore in the following discussion an equivalent expression will be used, namely, $P_s = AP_0 \lambda^{-n}$.

Let w be the component of the wind in the direction of propagation of the shock wave. Any error in estimating the magnitude of this component contributes to the error in the shock velocity.

The transverse wind component under most conditions does not contribute any error worth considering and will be ignored. Values of C_0 and w may be found by independent sound-velocity measurements (in two directions) or

by meteorological observations of temperature, humidity, and wind velocity. The accuracy of each of these methods is limited in principle by random shifts in wind velocity which occur during the time required to make the observations.

Returning to Eq. 2.1, the error in P_s , (ΔP_s) will be due to errors in U and C_0 , denoted by ΔU and ΔC_0 , thus

$$\frac{\Delta P_s}{P_s} = 2 \left(1 + \frac{2\gamma}{\gamma+1} \frac{P_0}{P_s} \right) \left(\frac{\Delta U}{U} - \frac{\Delta C_0}{C_0} \right). \quad (2.3)$$

Now $\Delta C_0/C_0$ is the fractional error in the determination of sound velocity and will be taken as constant over the entire range of distances involved. A decrease in sound velocity of $1/2$ per cent per 1,000 ft of altitude, corresponding to a vertical temperature gradient of -2°C per 1,000 ft, will be omitted from this discussion. It is still necessary to express $\Delta U/U$ in terms of errors in space, time, and wind velocity. If an error occurs in λ , the change in U is $\partial U / \partial \lambda \Delta \lambda$. If an error occurs in t, the change in U is

$$\frac{\partial U}{\partial \lambda} \frac{d\lambda}{dt} \Delta t.$$

If U is the value of shock velocity corrected for wind component, the change in U, including error in wind component, may be written

$$\Delta U = \frac{\partial U}{\partial \lambda} \left[\Delta \lambda + \frac{U \Delta t}{W^{1/2}} \right] + \Delta w, \quad (2.4)$$

where Δw is the error in estimating the wind component in the direction in which the shock propagates.

By the substitution of Eqs. 2.2 and 2.4 into Eq. 2.3,

$$\begin{aligned} \frac{\Delta P_s}{P_s} = 2 \left(1 + \frac{2\gamma}{\gamma+1} \frac{P_0}{P_s} \right) & \left[\left(\frac{\Delta w}{C_0 \sqrt{\frac{\gamma+1}{2\gamma} \frac{P_s}{P_0} + 1}} - \frac{\Delta C_0}{C_0} \right) \right. \\ & \left. - \frac{\left(n C_0 \sqrt{\frac{\gamma+1}{2\gamma} \frac{P_s}{P_0} + 1} \right) \Delta \tau}{\lambda} - \frac{n \Delta \lambda}{\lambda} \right]. \quad (2.5) \end{aligned}$$

It is to be observed that in Eq. 2.5 the values of Δw , ΔC_0 , $\Delta \lambda$, and $\Delta \tau$ severally may be either

positive or negative. The exponent n occurs only in the terms relating to errors in distance and time. The constant A has been absorbed into P_s and does not appear explicitly. In the last term, reduced time $\tau = t/W^{1/2}$ has been employed. This function is tabulated in Table 2.8 and is shown in Fig. 2.14 for certain typical values of Δw , ΔC_0 , $\Delta \lambda$, and $\Delta \tau$.

The values of the various quantities used in the calculations were

$n = 1.8$	$1 < \lambda < 3$
$n = 2.2$	$3 < \lambda < 6$
$n = 1.9$	$6 < \lambda < 15$
$C_0 = 1,139 \text{ ft/sec}$	
$\gamma = 1.4, \text{ const.}$	
$P_0 = 14.7 \text{ psi}$	

The error in P_s can be easily assessed from Fig. 2.14 for other values of Δw , ΔC_0 , and other variables. For example, if the error in wind is 2 ft/sec instead of 1 ft/sec, then the corresponding $\Delta P_s/P_s$ is to be doubled.

In applying this analysis to calculations from motion-picture photography of shock positions, it is concluded that, if an arrival-time curve is fitted to the data and if the mean deviation of data points from the curve is, for example, $\pm 20 \text{ ft}$, at a distance of 1,000 ft, then the error in P_s due to this is $n \Delta x/x$, or not more than $[3x(\pm 20)]/1,000 = \pm 6 \text{ per cent}$. At 2,000 ft the error from this cause is less than 3 per cent since n is less than 3.

2.5 NORMAL REFLECTION OF A STRONG SHOCK IN REAL AIR

As an aid in the interpretation of ball-crusher readings obtained at the base of the tower, the task of computing the reflected pressures was undertaken for the case of normal incidence of a strong shock against a perfectly rigid, plane reflecting surface.

2.5.1 Hugoniot Equation for Air Taking into Account the Nonideality of the Gas and the Variation in Specific Heats

The thermodynamic properties of air have been tabulated by Hirschfelder and Curtiss⁹ up to 5,000°C. The virial form of the equation of state was used, considering only the second virial coefficient. A new parameter K may be defined by the relation $E = pv/(K - 1)$, where E

and v are the specific internal energy and specific volume, respectively, and p is the pressure. Clearly, K is equal to the ratio of specific heats at constant pressure and volume if the values of density and temperature are low. If, on the other hand, the temperature is high and if E is written in the simple form assumed above, then K is no longer exactly equal to the specific-heat ratio. The reason for this is that the expression for E , including the contribution due to vibrational energy and ionization, does not retain the simple form it has for a perfect gas with constant specific heats, or, perhaps more simply, it is known that the expression $E = pv/(\gamma - 1)$ depends on the adiabatic equation of state $pv^\gamma = \text{const.}$, which depends on the constancy of γ throughout the compression. If compression results in a temperature rise which changes the ratio of specific heats, then the simple expression above no longer is valid. In defining the parameter K by $E = pv/(K - 1)$, it is realized that, if the specific-heat ratio is changing, the expression for E is not in the correct form for K to be a specific-heat ratio. Consequently K is not the specific-heat ratio at the final state but is a kind of average taken over the range of values of E during the transition. Furthermore, the parameter K behaves like a slowly varying state variable and therefore is uniquely determined if p and v are given. If air is passed over by a single shock of strength ξ , then all state variables are determined by ξ , and therefore K may be plotted as a function of ξ . This is done in Fig. 2.15, which is similar to Porzel's work in Los Alamos Scientific Laboratory Report LA-1214, using the tables of Hirschfelder and Curtiss in the region up to 180 atm, of Brinkley, Kirkwood, and Richardson (Report OSRD-3550) up to 1,000 atm, and of Los Alamos Scientific Laboratory Report LA-1020, Tables 3.5 and 3.1-6(h), above 1,000 atm. If air is passed over by two shocks, the final state depends on the order of occurrence of the shocks as well as on the shock strengths. In this case it is reasonable to suppose that K depends on the final temperature or on a parameter analogous to temperature.

Consider air in state p_0, v_0, T_0, γ which is raised to state p, v, T, K by the passage of a shock, $\xi = p/p_0$. The Hugoniot equation,

$$E - E_0 = \frac{1}{2} (p + p_0) (v_0 - v),$$

TABLE 2.8 RELATIVE ERRORS IN P_s ARISING IN THE VELOCITY METHOD

λ	$\Delta w =$ 1 ft/sec ($\times 10^{-3}$)	$C_0 = 1.139$ ft/sec	$\Delta \lambda =$ $5.84 \times 10^{-3}\dagger$ ($\times 10^{-3}$)	$\Delta \tau =$ $1.46 \times 10^{-4}\ddagger$ ($\times 10^{-6}$)	Total of Absolute Values ($\times 10^{-2}$)
		Velocity of Sound Error = 0.1% ($\times 10^{-3}$)			
1.00	0.257	2.04	10.5	2083	1.49
1.50	0.366	2.08	7.0	997	1.04
2.00	0.508	2.14	5.3	593	0.85
2.50	0.588	2.20	4.2	394	0.74
3.00	0.703	2.28	3.5	285	0.68
4.00	1.231	2.72	3.2	178	0.73
5.00	1.694	3.17	2.6	121	0.76
6.00	2.300	3.70	2.1	82	0.82
7.00	2.871	4.42	1.6	61	0.89
8.00	3.505	5.12	1.4	51	1.01
9.00	4.210	5.90	1.2	43	1.11
10.00	4.986	6.74	1.1	38	1.29
11.00	5.835	7.72	1.0	33	1.46
12.00	6.726	8.72	0.9	30	1.64
13.00	7.672	9.79	0.8	27	1.83
14.00	8.760	11.03	0.8	25	2.06
15.00	9.702	12.09	0.7	23	2.25

\dagger Corresponds to $\Delta x = 2$ ft for 20 kt or $\Delta x = 0.7$ in. for 1 lb.

\ddagger Corresponds to $\Delta t = 50$ μ sec for 20 kt or $\Delta t = 0.146$ μ sec for 1 lb.

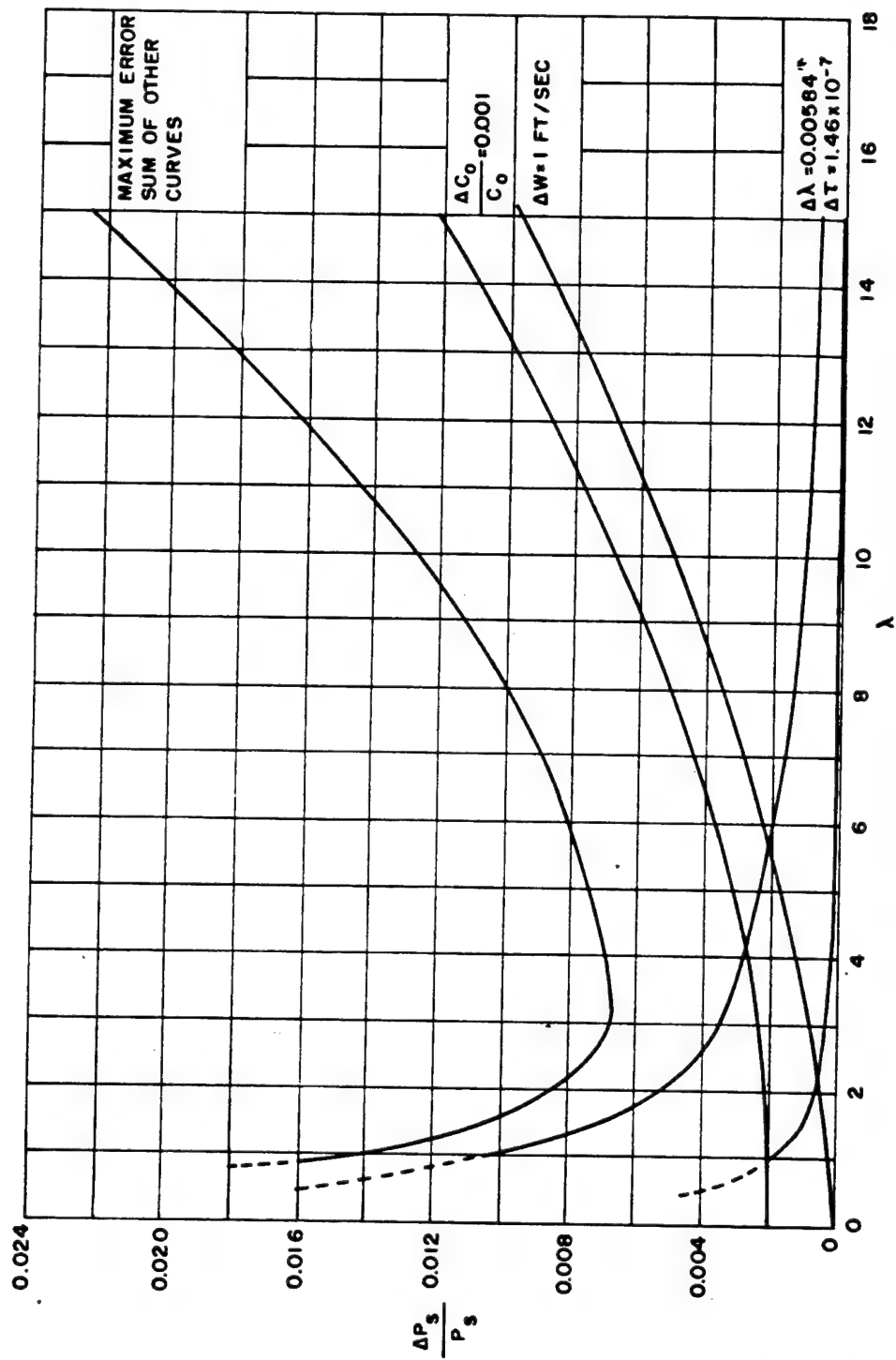


Fig. 2.14 Relative Errors in P_s Arising in the Velocity Method

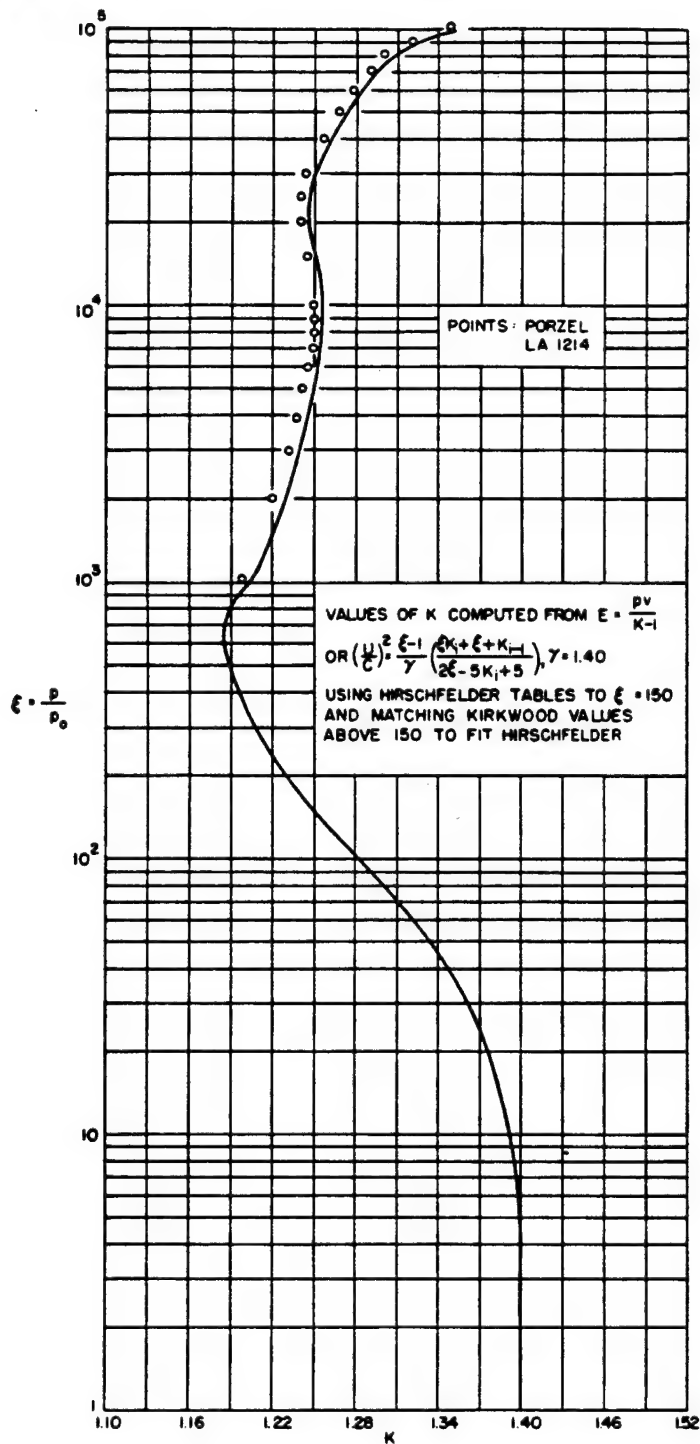


Fig. 2.15 Values of K for a Single Shock of Strength ξ

may be written as

$$\frac{v}{v_0} = \frac{\xi + 6}{\xi A + 1},$$

where $A = (K + 1)/(K - 1)$ and $\gamma = 1.4$. If the perfect gas law, $pv = RT/M$, is assumed, then

$$\frac{T}{T_0} = \frac{\xi(\xi + 6)}{\xi A + 1}$$

may be plotted against K using the dependence between ξ and K displayed in Fig. 2.15. This is shown in Fig. 2.16.

If, on the other hand, K is plotted against the product of $\xi \times v/v_0$ calculated from the tables, the result is indistinguishable from Fig. 2.16. This is an indication that K is dependent primarily on the temperature and that, within the range of density considered, the air behaves very nearly like an ideal gas with variable specific heat. The variation in K with temperature comes about mainly through changes in the specific heat.

2.5.2 Fundamental Shock Equations

In this section the usual shock equations are put into a form convenient for the treatment of reflection.

Let W_1 equal the normal incoming material velocity with respect to a shock, and let W_2 equal the normal receding material velocity with respect to the shock; then conservation of mass requires

$$\frac{W_1}{v_1} = \frac{W_2}{v_2}.$$

Furthermore, conservation of mass and momentum requires

$$W_1 = v_1 \sqrt{\frac{p_2 - p_1}{v_1 - v_2}}.$$

Subscripts 1 and 2 refer to medium in front of and behind the shock, respectively, v refers to volume per unit mass, and p refers to total pressure at a point. These equations together with the Hugoniot equation are sufficient to describe each shock. With the definition of K given previously, the Hugoniot equation can be written

$$\frac{p_2 v_2}{K_2 - 1} - \frac{p_1 v_1}{K_1 - 1} = \frac{1}{2}(p_2 + p_1)(v_1 - v_2).$$

This may be written

$$\frac{v_2}{v_1} = \frac{\frac{p_2}{p_1} + A_1}{\frac{p_2}{p_1} A_2 + 1},$$

where $A_1 = (K_1 + 1)/(K_1 - 1)$ and $A_2 = (K_2 + 1)/(K_2 - 1)$. If a shock is moving into air under usual ambient conditions, then $K_1 = 1.4$ and $A_1 = 6$.

2.5.3 Normal Reflection from a Rigid Wall

Consider a plane shock moving normally toward a rigid wall with velocity U_1 . The situation is as depicted in Fig. 2.17A. Following the definitions of W in Sec. 2.2, it is clear that $W_1 = U_1$ and $W_2 = U_1 - u_1$ or

$$\frac{U_1}{v_0} = \frac{U_1 - u_1}{v_1}$$

and

$$U_1 = v_0 \sqrt{\frac{p_1 - p_0}{v_0 - v_1}}.$$

Also

$$\frac{v_1}{v_0} = \frac{\frac{p_1}{p_0} + 6}{\frac{p_1}{p_0} A_1 + 1}.$$

Eliminating U_1 and v_1 from these three equations gives

$$u_1^2 = \frac{p_0 v_0 (p_1 - 1) [p_1 (A_1 - 1) - 5]}{p_1 A_1 + 1},$$

where $P_1 = p_1/p_0$, $A_1 = (K_1 + 1)/(K_1 - 1)$, and K_1 and P_1 are related by the curve of Fig. 2.15.

After reflection, the reflected shock moves into the medium previously traversed by the incident shock. The situation is now as shown in Fig. 2.17B. The boundary condition imposed by the wall is ensured by requiring u_r to be zero. All velocities shown are with respect to the wall. After the definition of W ,

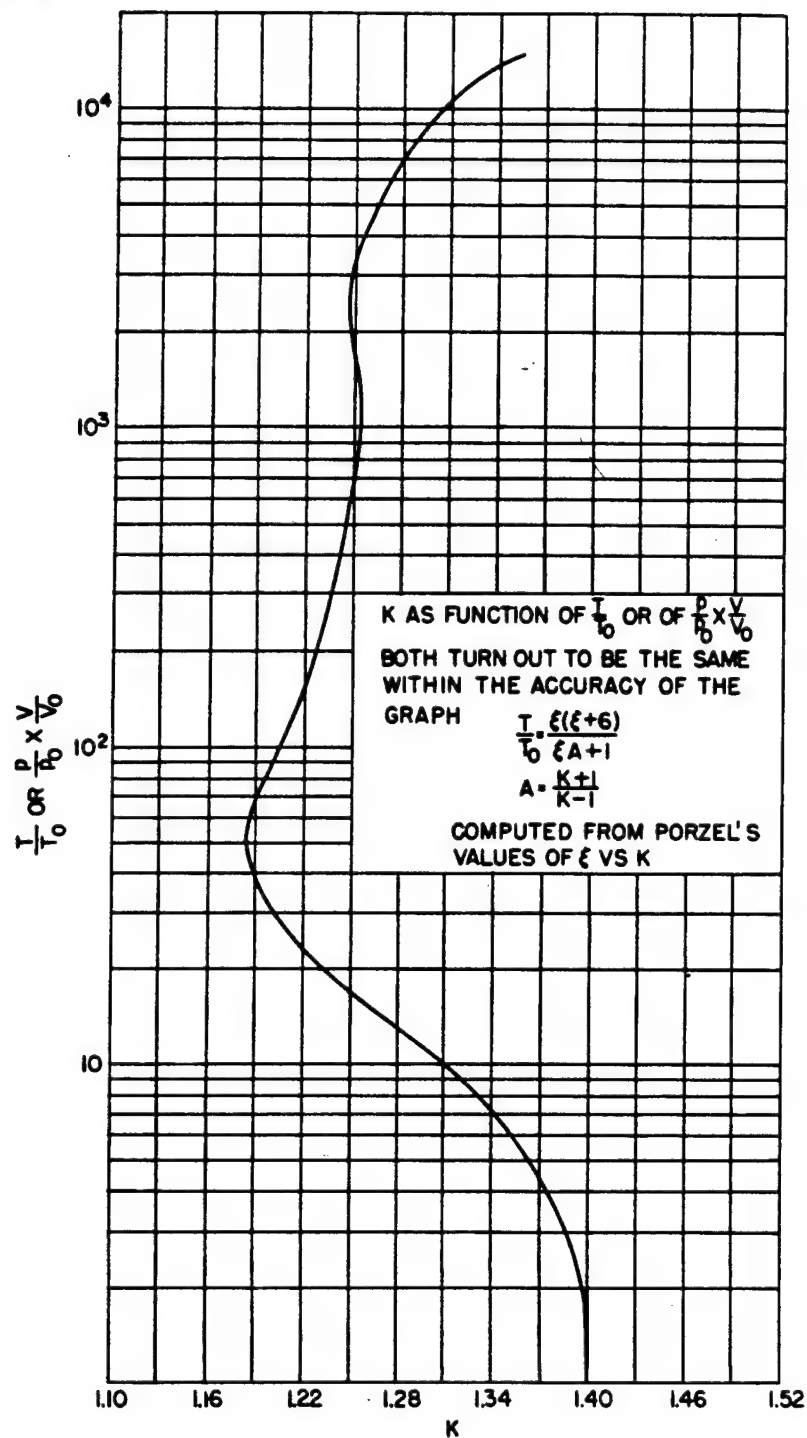
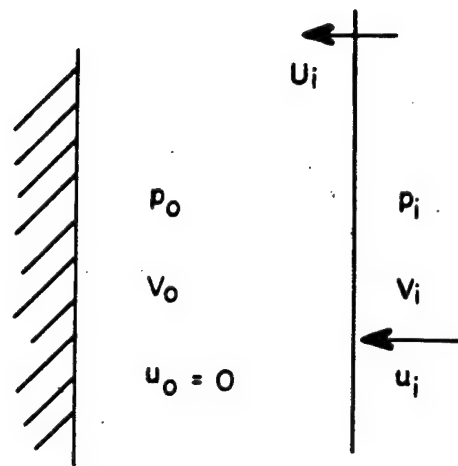
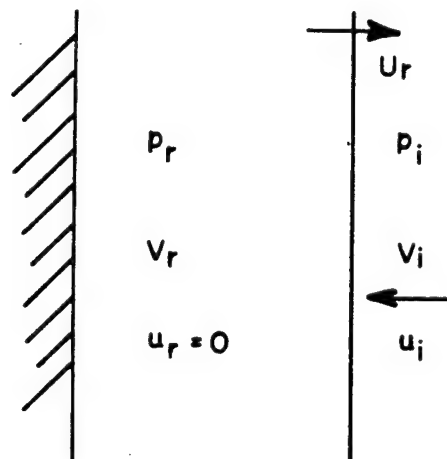


Fig. 2.16 K as a Function of T/T_0 or of $P/P_0 \times v/v_0$



A PLANE SHOCK MOVING TOWARD WALL



B PLANE SHOCK AFTER REFLECTION

Fig. 2.17 Normal Reflection from a Rigid Wall

$$W_1 = U_r + u_1 \quad W_2 = U_r,$$

from which, following a procedure similar to that used for the incident shock, it is easy to show that

$$u_1^2 = \frac{P_1 v_1 (P_r - 1) [P_r (A_r - 1) + 1 - A_1]}{P_r A_r + 1},$$

where $P_r = p_r/p_1$ and A_r is a function of T_r , the final temperature to which the gas is raised. The method of evaluating this will be discussed in the next section. As would be expected, if $A_r = A_1 = 6$, then the relation between P_r and P_1 , found by equating the two expressions for u_1^2 , reduces to the usual expression,

$$P_f = 2P_s \frac{4P_s + 7p_0}{P_s + 7p_0},$$

where P_s is taken as the excess pressure in the incident shock, $P_s = p_1 - p_0 = (P_1 - 1)p_0$, and P_f is the excess pressure in the reflected shock,

$$P_f = p_r - p_0 = (P_r P_1 - 1)p_0.$$

This expression may also be written in terms of P_r and P_1 as

$$P_r = \frac{8P_1 - 1}{P_1 + 6},$$

which is plotted in Fig. 2.18.

2.5.4 Calculation for Reflected Pressure

From Sec. 2.5.3, by elimination of u_1^2 , the following relation is obtained:

$$\begin{aligned} \frac{(P_r - 1) [P_r (A_r - 1) + 1 - A_1]}{P_r A_r + 1} \\ = \frac{(P_1 - 1) [P_1 (A_1 - 1) - 5]}{P_1 (P_1 + 6)}. \end{aligned}$$

Furthermore, since A_r is a function of T_r as given by Fig. 2.16, the argument of this function may be found in terms of the variables in the problem. Thus,

$$\frac{T_r}{T_0} = \frac{p_r v_r}{p_0 v_0} = P_r P_1 \frac{P_r + A_1}{P_r A_r + 1} \frac{P_1 + 6}{P_1 A_1 + 1}, \quad (2.6)$$

using the Hugoniot equation to eliminate the specific volumes.

Therefore there are two equations and two graphs, Figs. 2.15 and 2.16, relating the five quantities P_1 , P_r , T_r/T_0 , A_1 , and A_r . The procedure for solution is to choose a value for P_1 and then to obtain a satisfactory adjustment of the other quantities by graphical interpolation. Note that

$$A_r = \frac{D + (P_r - 1) (P_r + A_1 - 1)}{(P_r - 1 - D)P_r}, \quad (2.7)$$

where

$$D = \frac{(P_1 - 1) P_1 (A_1 - 1) - 5}{P_1 (P_1 + 6)}.$$

For ease in calculation, curves of A vs K and D vs P_1 are plotted. A point is computed as follows: Let $P_1 = 140$. Then $K_1 = 1.255$ from Fig. 2.15, $A_1 = 8.83$, and $D = 7.35$. Under these conditions, if $P_r = 10.0$, $A_r = 10.3$ using Eq. 2.7, and if $P_r = 10.5$, $A_r = 8.04$. Then using Eq. 2.6, T_r/T_0 can be calculated thus,

P_r	A_r	T_r/T_0	K_r^\dagger	or	A_r
9.75	11.8	25.8	1.214		10.32
10.0	10.3	29.9	1.205		10.75
10.5	8.04	39.2	1.193		11.35

These values are plotted in Fig. 2.18. The value of P_r is 9.95, corresponding to $P_1 = 140$. A series of values has been calculated by this procedure. These values are shown in Table 2.9 and Fig. 2.19.

2.5.5 Reflected-pressure Ratio for Infinite Incident Shock Strength

The formulas developed in the preceding sections lead to the following if the incident shock strength is increased without limit. This, of course, does not correspond to any real physical situation since energy transfer passes over into radiative rather than mechanical processes. As $P_1 \rightarrow \infty$, $D \rightarrow A_1 - 1$. As the medium becomes completely ionized, the value of K approaches $\frac{5}{3}$. As $P_1 \rightarrow \infty$, $K_1 \rightarrow \frac{5}{3}$. Therefore

$$A_1 = \frac{\frac{5}{3} + 1}{\frac{5}{3} - 1} = 4$$

[†]From Fig. 2.16.

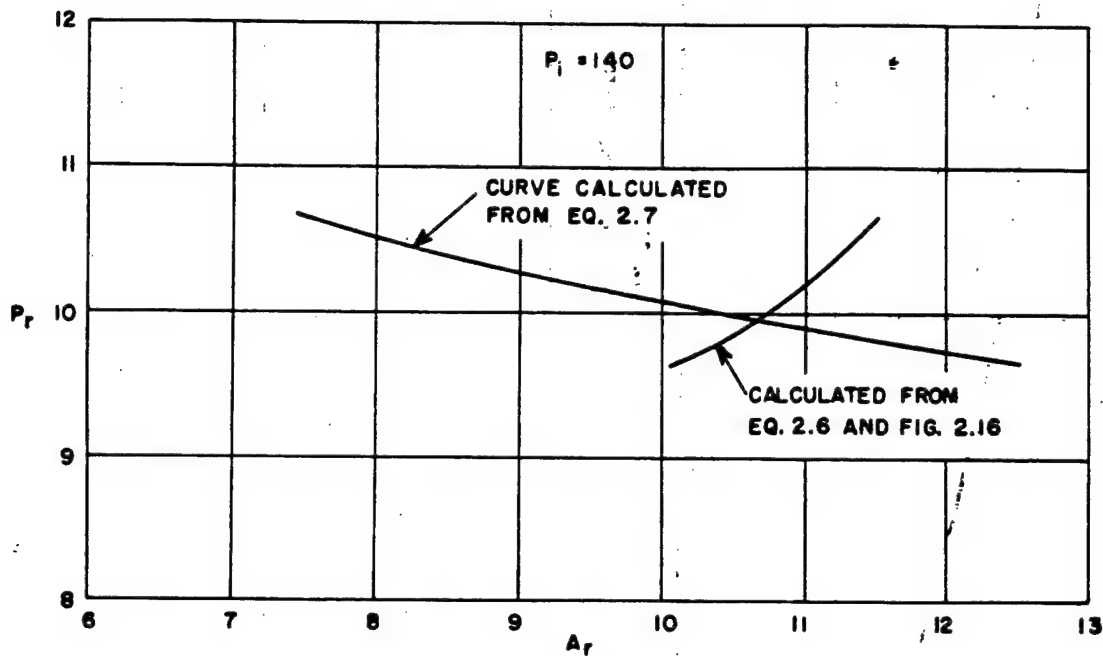


Fig. 2.18 Sample Calculation for P_i

TABLE 2.9 CALCULATED REFLECTED-PRESSURE RATIOS

P_r	P_i
4.9	10.0
5.43	12.8
6.22	20.0
6.50	24.5
6.82	30.5
7.50	46.5
8.5	78.0
9.93	140.0
11.0	200.0
11.95	270.0
12.28	300.0
12.90	400.0

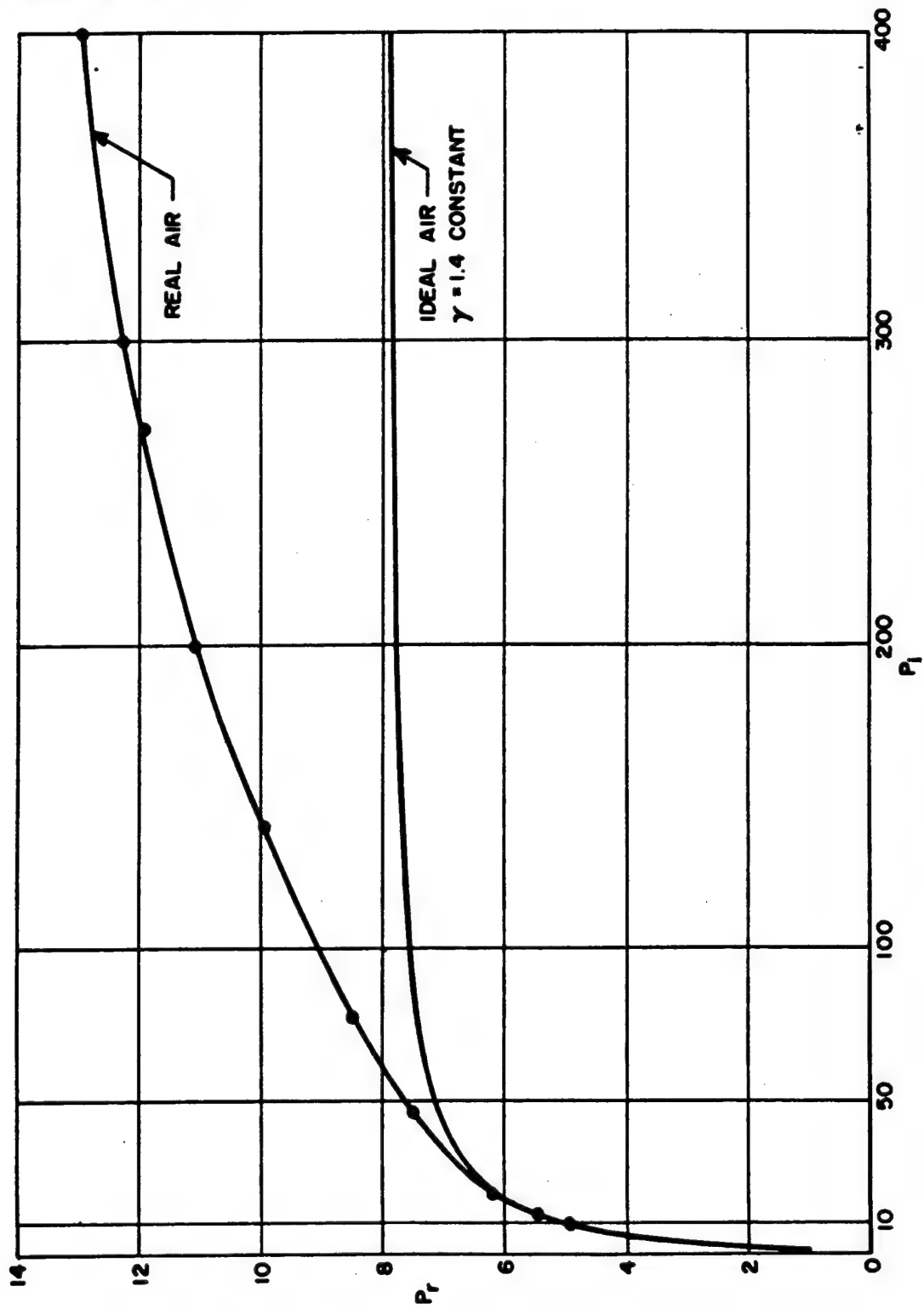


Fig. 2.19 Reflected-pressure Ratio vs Incident Pressure for Real Air

and $D_{\infty} = 3$. Then

$$A_r = \frac{3 + (P_r - 1)(P_r + 3)}{(P_r - 4)P_r}.$$

Now A_r will also equal 4, and consequently $P_r = 6$.

2.6 FLOW AS AFFECTING MEASUREMENTS OF PRESSURE

Certain results obtained on Operation Sandstone indicated that gauges placed at ground level gave pressure values which were significantly lower than values obtained from gauges placed 2 or 3 ft off the ground. In order to avoid this error, which could have been caused by flow perturbations due to small local irregularities or by the fact the ground is not a perfect reflector, it was decided to place all gauges at a level above the ground at least ten times the height of local irregularities in the vicinity. A streamlined wall was designed for the purpose of holding all instruments in position at each location. In this way the ease of field installation was greatly increased. It was also possible to avoid some of the difficulties due to the effects of rain water on gauges. The following sections discuss the flow problem introduced by the wall.

2.6.1 General Remarks on the Problem

The blast from explosions gives rise to a transient flow which, for blast-peak excess pressures of 57 psi and greater, starts as a supersonic flow and rapidly passes through transonic and into subsonic flow as the shock front moves past a given point. If a pressure-sensitive device is placed in this flow, it is necessary to know what perturbations in the pressure measurement are caused by the disturbance in the flow. In the case of blast measurements from high-explosive charges of the order of 1 lb to several hundred pounds in weight, it has been found that the pressures indicated by small piezoelectric gauges are as much as 10 to 20 per cent low at excess pressure levels ranging up to about 30 psi. This deficiency has been largely corrected by inserting the gauges in a baffle which permits the flow to readjust itself toward the undisturbed velocity before the pressure is applied to the

gauge. However, the great majority of successful measurements of the pressure-time curve for air blast have been made at pressures less than about 30 psi where the flow is entirely subsonic and the velocities are relatively slow. The precise relation between the length and shape of the baffle and the disturbance in the pressure as a function of pressure (i.e., velocity) has been calculated under simplifying assumptions for special cases by MacDonald and Schaaf.¹³ The question posed here is more complicated than that posed in aerodynamics by the fact that the flow in a blast is not steady, and consequently even the results of the theoretical calculations which can be made for certain restricted cases may not be more than indicative.

2.6.2 Simple Theory for a Two-dimensional Wall

The first case to be considered is confined to two-dimensional subsonic nonviscous irrotational flow of an incompressible fluid. Consider a rectangular wall of unit thickness and let the free-stream pressure and velocity at a distance remote from the wall be denoted by p_{∞} and u , respectively. It is supposed that the flow velocity along the wall is different from u and may be denoted by uV , where V is a dimensionless number and a function of x , which is the distance downstream from the front face of the wall measured in thickness units. The ordinary Bernoulli equation for incompressible flow then states that

$$p_w - p_{\infty} = \frac{1}{2} \rho_{\infty} u^2 (1 - V^2),$$

where p_w is the static pressure on the wall at the distance x and ρ_{∞} is the free-stream density at a great distance from the wall. The top view of the arrangement described is shown in Fig. 2.20. Letting $q = \frac{1}{2} \rho_{\infty} u^2$, by definition the incompressible pressure coefficient is

$$p = \frac{p_w - p_{\infty}}{q} = 1 - V^2.$$

Note that p is negative since $V > 1$. It is now necessary to find the relation between x and V , which can be done by making use of standard hydrodynamic theory as described by Milne-Thomson.¹⁴ Briefly, the flow is described by a

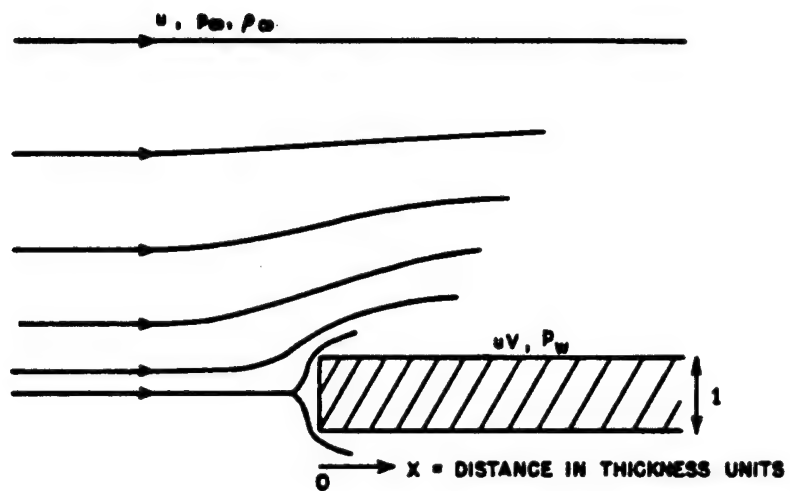


Fig. 2.20 Flow Past a Wall

complex potential function which, to be analytic, satisfies the Cauchy-Riemann conditions and therefore Laplace's equation. This, of course, is also the requirement placed on the potential and stream functions by the equation of continuity for incompressible flow. Consequently a linear flow along a line in the ξ plane may be transformed into the flow over a right-angle step in the Z plane by the Schwarz-Christoffel transformation which transforms the line into the step. Since the actual flow around a wall is symmetrical, the flow around a wall is reproduced by this process. The result after considerable reduction is

$$x = \frac{1}{2\pi} \left[\frac{+2V}{V^2 - 1} - \ln \frac{V + 1}{V - 1} \right].$$

It is therefore possible to construct a table giving V and therefore P as a function of x . This relation is plotted in Fig. 2.21, and it gives the variation in pressure coefficient with x . The difference in excess pressure read at the wall compared with the free-stream excess pressure is of interest, however. The fractional error in pressure is therefore defined as

$$f = \frac{P_w - P_\infty}{P_\infty - P_0}.$$

This will also be a negative number. Consequently $f = pq/(p_\infty - p_0)$, where p_0 is equal to the pressure in the air at rest ahead of the shock and p_∞ is equal to the total pressure in the shock undisturbed by the wall. The velocity u is now the particle velocity in the shock and is related to the shock strength ξ by means of the conservation equations and the Rankine-Hugoniot relation¹⁵

$$\left(\frac{u}{C_0} \right)^2 = \frac{2(\xi - 1)^2}{\gamma(\gamma + 1)\xi + \gamma - 1},$$

where C_0 is the sound velocity in the undisturbed medium, which is equal to the square root of $\gamma p_0/\rho_0$; $\gamma = 7/5$; and $\xi = p_\infty/p_0$. Therefore

$$q = \frac{5}{2} \frac{(p_\infty - p_0)^2}{6p_\infty + p_0} \frac{\rho_\infty}{\rho_0}.$$

Using the Rankine-Hugoniot relation for the density ratio,

$$q = \frac{5}{2} \frac{(p_\infty - p_0)^2}{6p_0 + p_\infty}.$$

Therefore

$$f = \frac{5}{2} P(x) \frac{\xi - 1}{6 + \xi}.$$

Table 2.10 has been compiled, using Fig. 2.21, showing percentage error in peak excess pres-

TABLE 2.10 CALCULATED ERROR USING INCOMPRESSIBLE THEORY

Excess Pressure P_s (psi)	ξ	$x = 5$ (%)	$x = 10$ (%)	$x = 14$ (%)	$x = 20$ (%)
15	2	-1.88	-0.94	-0.69	-0.52
30	3	-3.34	-1.67	-1.22	-0.93
45	4	-4.50	-2.25	-1.65	-1.25

sure calculated from the incompressible approximation.

2.6.3 Compressible Subsonic Steady Two-dimensional Irrotational Isentropic Flow

It is now necessary to see how the percentages in Table 2.10 may be modified if the assumption of incompressibility is removed. The pressure coefficient for compressible flow may be defined by

$$p^1 = \frac{p^1_w - p_\infty}{\frac{1}{2} \rho_\infty u^2},$$

analogous to the definition of the pressure coefficient for incompressible flow. Note that for either compressible or incompressible flow the pressure, density, and velocity at a great distance from the wall are the same. Therefore the relation between p_∞ and ρ_∞ in both cases is the Rankine-Hugoniot relation previously used.

For perturbations of the flow velocity which are small compared with the velocity, the linearized theory leads to the Prandtl-Glauert transformation which shows that

$$p^1 = \frac{P}{\sqrt{1 - M_\infty^2}},$$

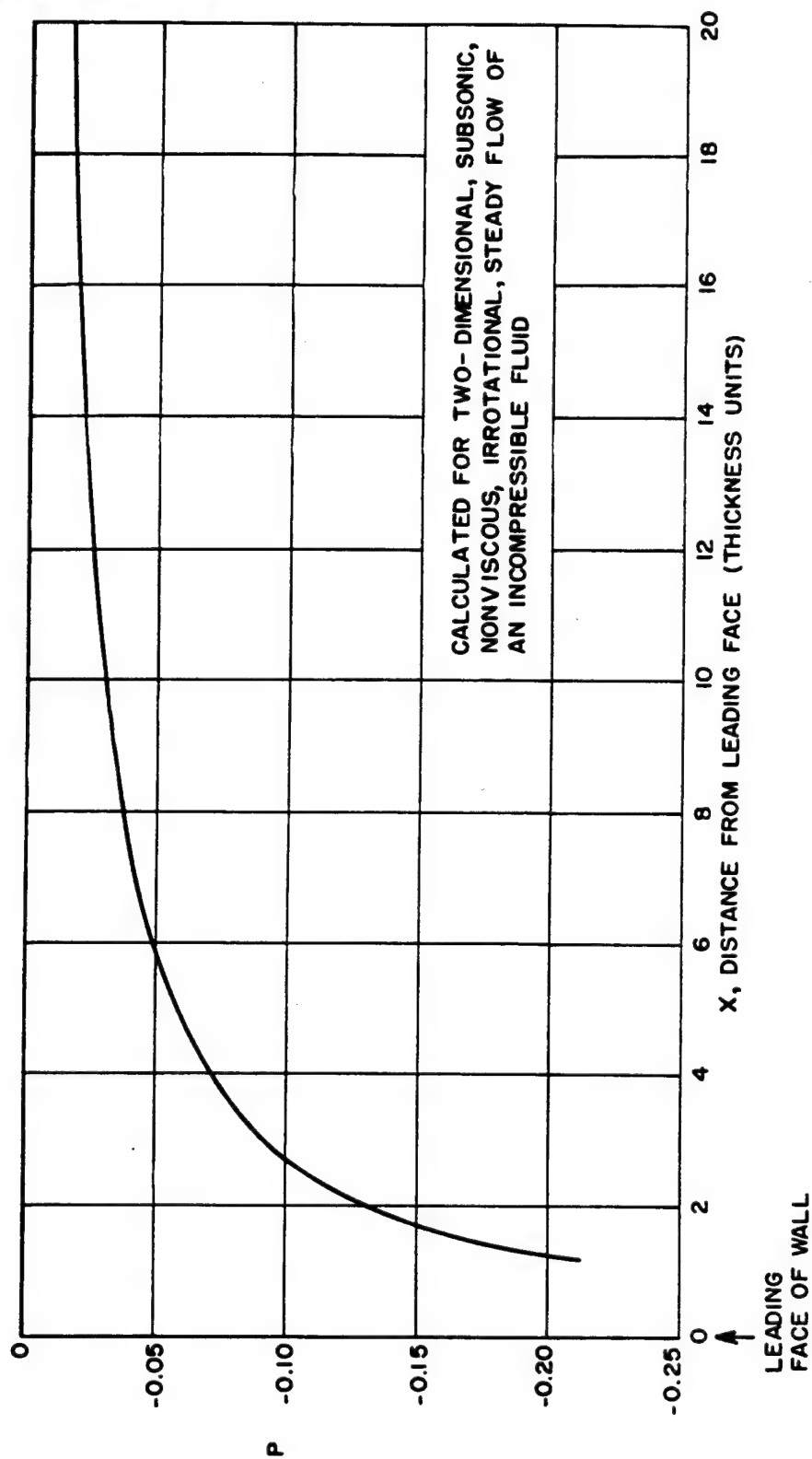


Fig. 2.21 Variation of the Pressure Coefficient with Distance along a Wall

M_∞ being the local Mach number of the flow at infinity.¹⁶ (It is also possible to use the von Karman-Tsien theory here, but there is no particular point to bringing in this refinement for a reason to be mentioned later.)

In the present case, $M_\infty = u/C_\infty$, and C_∞ is the sound velocity in the medium passed over by the shock. Therefore M_∞ may be written as a function of the shock strength ξ . It turns out that if $\xi = p_\infty/p_0$,

$$M_\infty = \frac{\xi - 1}{\sqrt{\frac{\gamma}{2} \xi [(\gamma - 1) \xi + \gamma + 1]}}$$

It will be noted that $M_\infty = 1$ for $\xi = 4.8$ or for an excess pressure in a shock of 57 psi, whereas, in order for the Mach number to reach its maximum value of 1.89 (retaining perfect gas and constant γ), the shock strength must increase without limit. The error in the peak excess pressure for the compressible case is now given as

$$f_s^1 = \frac{p_w^1 - p_\infty}{p_\infty - p_0} = \frac{p^1 q}{p_\infty - p_0}$$

Table 2.11 has been constructed to show the calculated error in excess pressure for the compressible case.

TABLE 2.11 CALCULATED ERROR USING THE COMPRESSIBLE THEORY

P_s	ξ	$x = 5$ (%)	$x = 10$ (%)	$x = 14$ (%)	$x = 20$ (%)
15	2	-2.12	-1.1	-0.78	-0.59
30	3	-4.8	-2.4	-1.76	-1.34
45	4	-9.2	-4.9	-3.60	-2.73

Both Tables 2.10 and 2.11 give calculated errors based on the restriction that the flow is two-dimensional. This means that the wall is infinitely high. In actual fact, of course, this restriction is rather badly violated since the wall is only 5 thickness units in height. Considering the wall as an air foil, the dimension in the direction of flow, which has been denoted by x , corresponds to the chord of the air foil. The wall height h corresponds to the span of the wing, and the "aspect ratio" corresponds

to $2h/x$, the factor of 2 coming from the mirror image of the wall in the ground. In the two-dimensional case considered above, this ratio is infinite. However, for a wall on the ground for $x = 10$, the aspect ratio is reduced to unity. This means that pressure along the sides of the wall can be equalized by contributions from the flow along the top of the wall, whereas this equalization is prevented in the two-dimensional case. Consequently the two-dimensional theory overemphasizes the pressure drop due to the flow disturbance if the aspect ratio is not large. If this ratio is less than 2, it is believed that the two-dimensional incompressible theory is a better estimate of the flow of a compressible fluid than the Prandtl-Glauert theory for compressible flow. MacDonald and Schaaf¹⁷ have shown a decrease in pressure coefficient from 2.1 to 0.16 by comparing elliptic cylinders with ellipsoids, and they consider this to be a measure of the error made in two-dimensionalization. Consequently the errors listed in Table 2.11 should more nearly apply to compressible flow when the aspect ratio is 2 or more, whereas the errors listed in Table 2.10 should apply to compressible flow when the aspect ratio is less than 2. The latter corresponds more nearly to the wall actually used in the experiments.

A further word should be added concerning the influence of the shape of the nose. In the rectangular wall already considered, the nose is a plane at right angles to the flow. It is possible to derive the flow patterns around curved noses by conformal mapping or by the use of a simple source in the uniform stream. In all these cases it turns out that $|P(x)|$ is greater than it is at corresponding locations behind the plane nose. In the subsonic case at steady flow, at least, it is better to introduce all the disturbance in the flow at one place and then to allow the flow to straighten itself out than to introduce the disturbance gradually by a curved or tapered nose which brings changes in the velocity closer to the measuring section where everything is supposed to have reached the undisturbed state. The above applies to the case of steady flow. According to experiments performed by Bleakney, if a shock front impinges on a plane nose, the reflected shock creates a greater disturbance than is created with rounded or tapered noses, and consequently a rounded nose is considered more

desirable in smoothing out the flow following a shock.

2.6.4 Experiments with Subsonic Transient Flow: Blast

The question immediately arises as to what extent the conclusions of the foregoing sections are borne out by experiment. The obvious means of producing transient flow is, of course, to use the blast from small charges of high explosives. The difficulty of making reliable pressure-time measurements using explosions on the scale of 1 to 50 lb in weight is well known. A long series of experiments was carried out at the Naval Ordnance Laboratory (NOL) with the object of finding by trial the proper length-to-thickness ratio for a rectangular baffle, which holds a piezoelectric gauge, in order to reduce the flow error to a given percentage such as, for example, 2 per cent. The correct peak pressure in these experiments was ascertained on the spot at each pressure level by a simultaneous shock-velocity measurement made with a different set of gauges. Baffles used were rectangular, having length-to-thickness ratios of 14.6, 24.6, and 44.8. The baffle height was in all cases 5 thickness units, as were the walls, and the gauges were mounted in the central portion, as in the walls. Experiments were performed in free air and also at ground level. Gauges were calibrated statically by the manufacturer, as well as statically and dynamically by NOL. Dynamic calibrations were of two types, i.e., in the shock tube without baffle, extrapolating to shock of zero strength, and in the field using high-explosive blast with independent velocity measurement. The results may be summarized by the statement that the scatter which was shown to exist either in the performance of the gauges under shock loading or in the experiment as a whole (or in both) was sufficient to mask any flow effects of the order of magnitude predicted by the theory applied to the wall baffles. When gauges were placed unbauffed in the shock tube, a decrease in apparent pressure with increasing flow velocity was found in approximate accordance with the theory of Schaaf.¹⁸ In the field experiments with baffles in the air, there was no indication of any trend due to flow where baffles 24.6 thickness units in length were used. Experiments were made in the overpressure

range from 7 to 67 psi. In the field experiments with baffles on the ground the indications were that all three baffles were sufficiently long to make the readings independent of flow.

Many other experiments performed at NOL and Ballistic Research Laboratories (BRL) (some of the latter are discussed in a report by Marks¹⁹) have shown that the assumption of flow errors in accordance with the theory is not inconsistent with the experimental results. All this work also leads to the conclusion that piezoelectric tourmaline gauges are inconsistent between static and dynamic calibrations and that they are also subject to much uncertainty in their responses, some behaving as if their electrode areas were variable with pressure, others as if their coatings were viscoelastic, others as if they were more subject to pyroelectric effects, etc. Improvements in gauge design, possibly using new principles, would be of great help in the investigation of flow problems.

2.6.5 Experiments on Wall Models in the Princeton Shock Tube

A series of interferograms was made by Walker Bleakney showing the density distribution along two-dimensional models of a wall. Pictures were taken for each of three models having flat, round, and 90°-wedge nose contours at the times and locations shown in Fig. 2.22. These pictures show that (1) the round nose causes less disturbance due to reflected shock than either the flat or pointed noses, (2) all experiments were made with shocks of strength 1.94 or 1.97 corresponding to about 29 psi overpressure at $p_0 = 1$ atm, and (3) in region II, i.e., $5 < x < 14$, when the incident shock may be seen and the fringe shift across it may be determined, this shift is approximately that which is expected for a shock of this strength. No disturbed flow is visible. The departure from uniformity in this region is less than $\frac{1}{4}$ fringe in 8 fringes or $\Delta\rho/\rho_0 \leq 1.2$ per cent, whence $\Delta p/p \leq 1.7$ per cent.

Figure 2.23 shows interferograms for a round-nosed wall in region I at $\Delta t \approx 129 \mu\text{sec}$, $\Delta t \approx 400 \mu\text{sec}$, and $\Delta t \approx 1264 \mu\text{sec}$. This material has been supplied by Bleakney.

From these experiments it can be concluded that there is no reduction of pressures greater than that called for by the theory and that

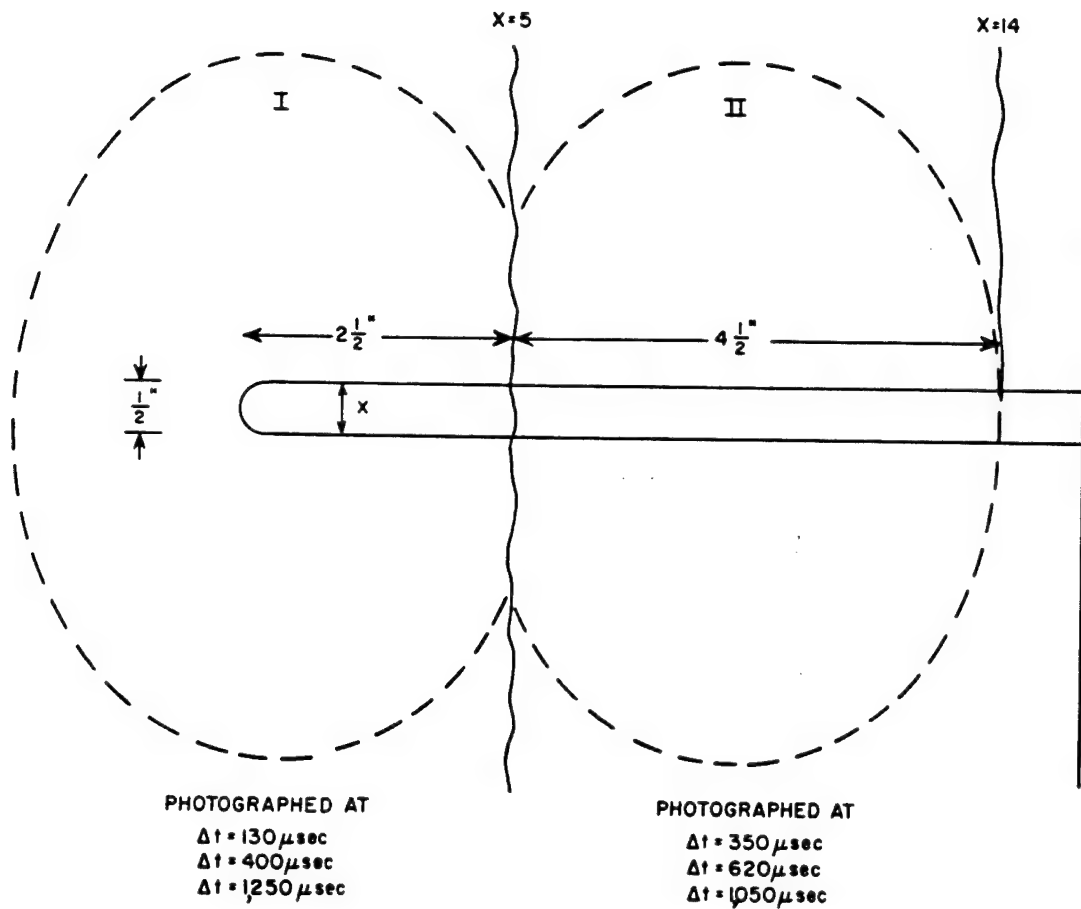


Fig. 2.22 Arrangement for Interferograms of Wall Models

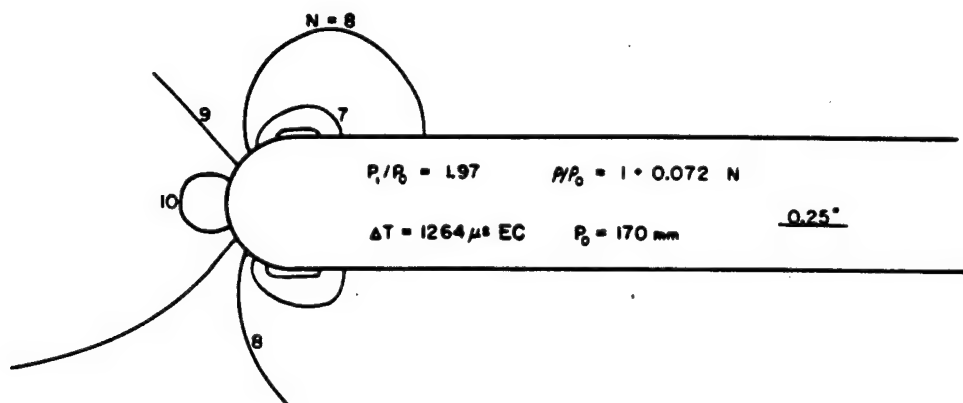
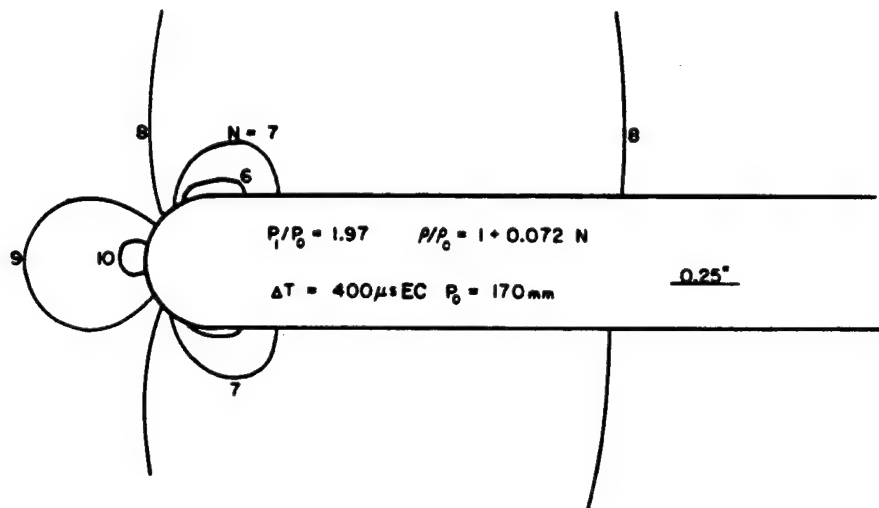
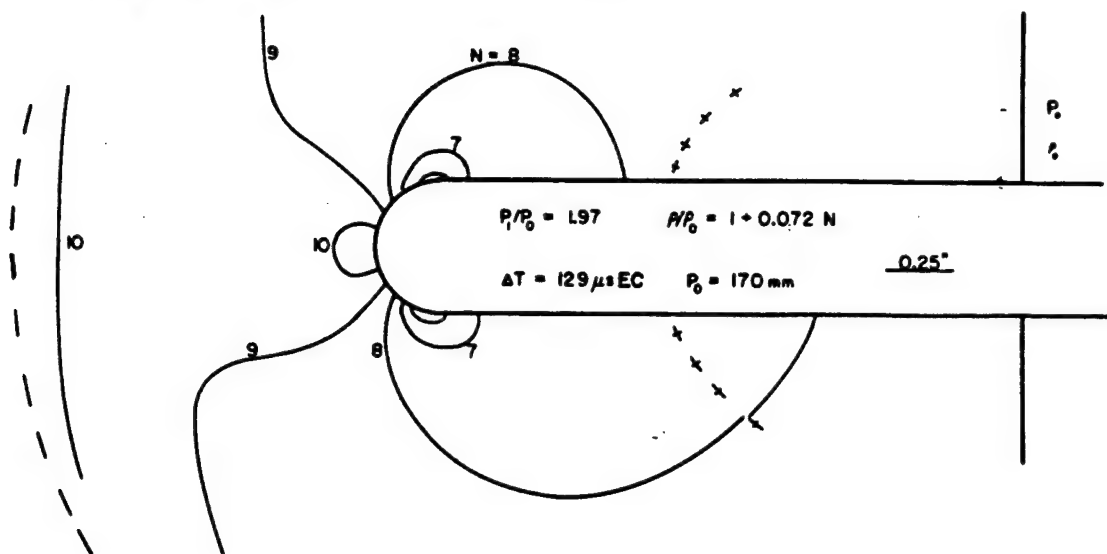


Fig. 2.23 Isopycnals (Obtained from Interferograms) for Round-nosed Wall

therefore the theory is consistent with the experiments, although the experiments do not have sufficient resolution to give quantitative or detailed confirmation of the theory, nor is there any information for stronger shocks.

2.6.6 Experimental Results for Steady Supersonic Flow

The following relevant information is taken from a confidential paper by Hasel²⁰ which was printed in a compilation of papers presented to the NACA Conference on Supersonic Aerodynamics, Ames Aeronautical Laboratory, Moffett Field, Calif., 30-31 August 1948.

The theoretical distribution of pressure on two cylindrical bodies is given schematically in Fig. 2.24. A number of tests have been made to determine some quantitative aspects of these curves for supersonic flow. These may be summarized as follows:

Nose	Mach No.	Value of x from End of Nose Section
Ogival	1.94	4, 8, 12, 16, 20
Conical (14° cone)	1.51	For small angles of attack and for x = 6 the measured static pressures on both tubes were within 1 per cent of the free-stream pressures at both Mach numbers
Spherical	2.19	
Flattened ogive	1.93	Measured static pressures at zero pitch and yaw were 3.5 per cent lower than free-stream static pressure, x = 3.5
	1.62	Measured static pressures at zero pitch and yaw were 1 per cent lower, x = 3.5

Result: $P_{\text{measured}} - P_{\text{true}}$ was 1½ per cent lower at x = 4 than at the other values of x. At all other greater values of x, $P_{\text{measured}} = P_{\text{true}}$.

It will be noted that these experiments were made on cylinders at rather large Mach numbers compared with those pertaining to the shock region of interest. In extending pressure-time measurements from shocks having an excess pressure of 57 to 100 psi, the correspond-

ing peak Mach numbers range from 1.0 to 1.26. In a supersonic flow an obstacle gives rise to a shock, attached or not, depending on the nose shape, which at a great distance from the obstacle becomes a Mach line, i.e., a weak shock. The angle β between this line and the flow direction is given by

$$\sin \beta = \frac{1}{M_{\infty}}.$$

The larger the angle β , the less the disturbance in the flow since the bow wave shock is weaker. For shocks of excess pressure 100 psi, $\beta = 53^\circ$, whereas for Mach number of 1.5, $\beta = 42^\circ$. For the latter case, experiments show that p_w differs from p_{∞} by less than 1 per cent at x = 6. It is consequently concluded that for steady flow the errors are less than 1 per cent at x = 6 for Mach numbers less than 1.5 and greater than 1.0, i.e., as long as the regime is supersonic.

2.6.7 Disturbance in the Flow Due to Viscous Effects

Many standard texts, such as Milne-Thomson's,²¹ show that the thickness of the laminar boundary layer in contact with the wall is given by

$$\delta \approx \sqrt{\frac{\nu l}{u}},$$

where ν is the kinematic viscosity at the wall, u is the velocity of the free stream, and l is the length measured along the wall from the stagnation point or from a leading edge. For the case of air, taking $\nu = 0.15$ cgs, $u = 3.5 \times 10^4$ cm/sec, i.e., transonic flow, and $l = 14$ ft or 420 cm, then $\delta \approx 0.5$ mm. By the same considerations the variation of pressure across this layer is found to be entirely negligible. Consequently the flow pressure is transmitted to the wall or baffle unchanged by the boundary layer along the wall.

There is, however, another effect due to viscosity which may produce appreciable deviations in pressure measurements made near or on various objects, including the ground. Bleakney's interferograms of flow over obstacles have revealed the formation of vortices in the flow following the passage of a shock. These vortices are the result of the torque given the fluid by the boundary layer as the

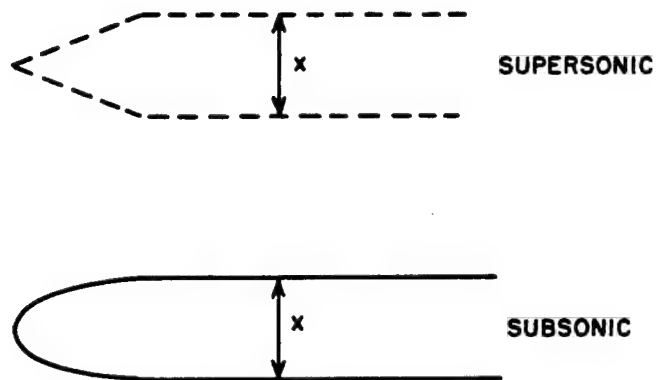
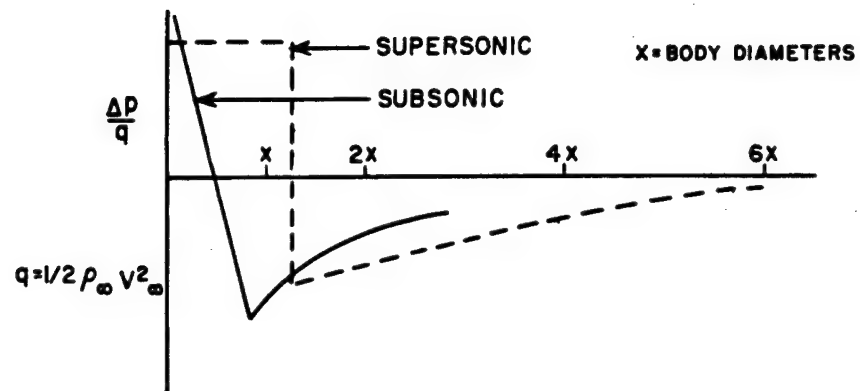


Fig. 2.24 Pressure Coefficient along a Cylindrical Body

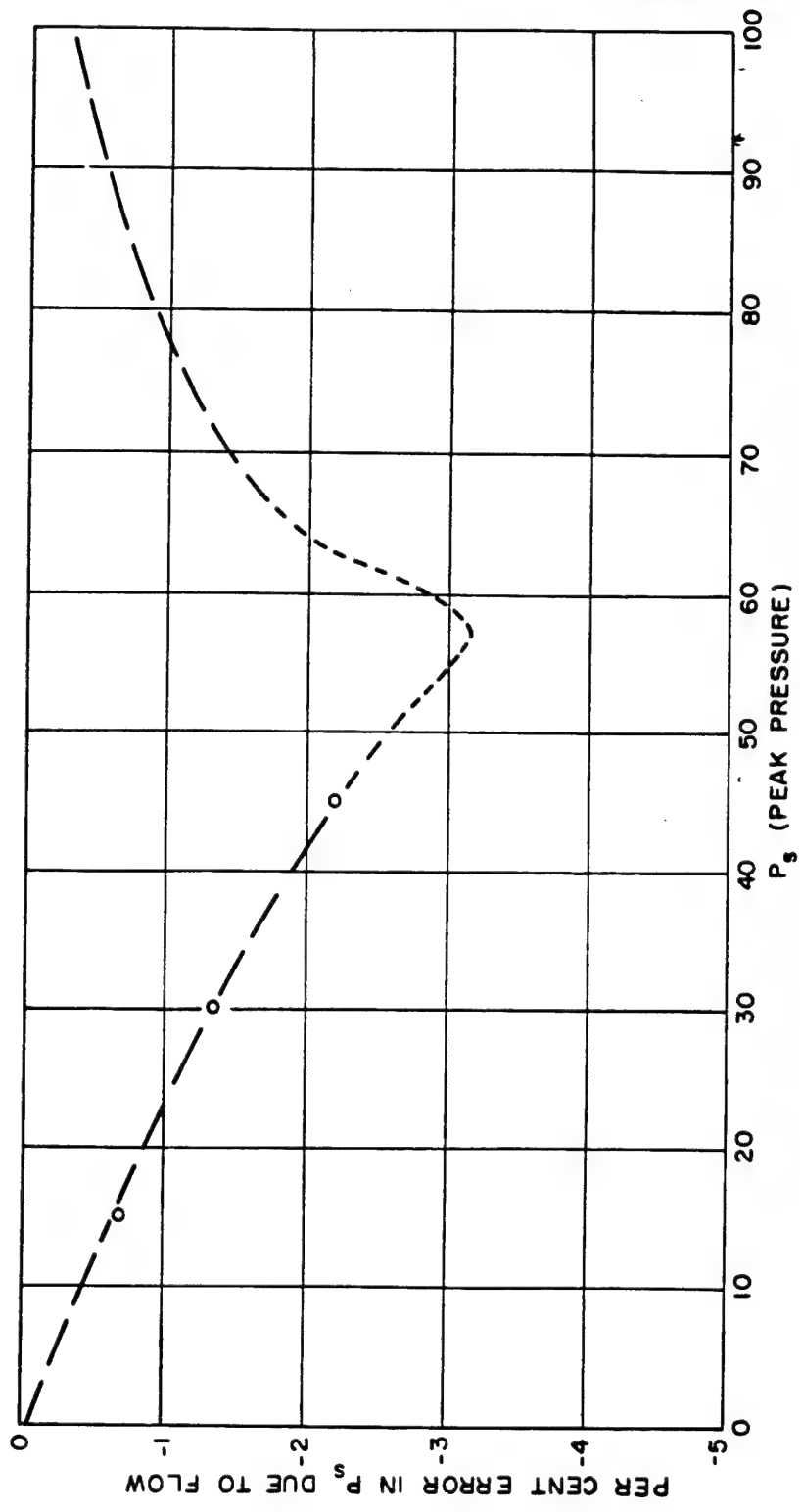


Fig. 2.25 Estimated Percentage Error Due to Flow Disturbance Produced by a Wall, $x = 14$

fluid spills over the obstacle. The vortices are more noticeable for shock fronts than for steady flows of the same velocity because in the former the reflected shock pressure is acting on the fluid, whereas in the latter the much weaker stagnation pressure is acting. The pressure within a vortex is greatly lowered. Consequently any pressure measurements made in the region of vortex disturbances, even those small in area, can be quite misrepresentative of the free field pressures.

2.6.8 Conclusion regarding Flow Error

It is believed on the basis of present knowledge that measurements made in baffles extending 14 thickness units fore and aft of the measuring device will yield pressures correct within 3 per cent at all pressure levels from 0 to 100 psi and that, over the greater part of this range, the accuracy will be between 1 and 2 per cent. The larger errors are to be expected in the fast subsonic region at peak pressures between about 50 and 57 psi. The error will in all cases be on the low side and will be a systematic error. It is therefore proposed to state, until it is proved otherwise, that the percentage error in pressure due to flow disturbance produced by the wall at a distance equal to $x = 14$, the center of the measuring section, is given in Fig. 2.25.

Since the scatter in the pressure data due to many other causes is much larger than 3 per cent, no attempt is made in quoting data or in the analyses of subsequent chapters to correct for wall flow. The pressures quoted are those actually indicated by the gauges in situ.

REFERENCES

1. E. M. Fisher, Spherical Cast TNT Charges; Air Blast Measurements on, Report NOLM-10780, NOL, January 1950.
2. W. Weibull, Explosion of Spherical Charges in Air: Travel Time, Velocity of Front and Duration of Shock Waves, BRL Translation Report X-127, February 1950.
3. Kirkwood and Brinkley, Theoretical Blast-Wave Curves for Cast TNT, Report OSRD-5481, August 1945.
4. Kirkwood and Brinkley, Theory of the Propagation of Shock Waves from Explosive Sources in Air and Water, Report OSRD-4814, March 1945.
5. Hirschfelder and Curtiss, Thermodynamic Properties of Air, II, Report CM-518, University of Wisconsin, Contract NOrd 9983, Task WIS-1-C, December 1948.
6. E. M. Fisher, Spherical Cast TNT Charges; Air Blast Measurements on, Report NOLM-10780, NOL, January 1950, p. 31.
7. E. M. Fisher, Experimental Shock Wave Reflection Studies with Several Different Reflecting Surfaces, Report NavOrd-2123, NOL, September 1951.
8. E. M. Fisher, Experimental Shock Wave Reflection Studies with Several Different Reflecting Surfaces, Report NavOrd-2123, NOL, September 1951, p. 33.
9. Hirschfelder and Curtiss, Thermodynamic Properties of Air, II, Report CM-518, University of Wisconsin, Contract NOrd 9983, Task WIS-1-C, December 1948, p. 32.
10. Kirkwood, Brinkley, and Richardson, Tables of the Properties of Air along the Hugoniot Curve and the Adiabatics Terminating in the Hugoniot Curve, Report OSRD-3550, April 1944.
11. Fraenkel, Apparatus for the Measurement of Air Blast Pressures by Means of Piezoelectric Gauges, Report OSRD-6251.
12. Greenhouse Report, Annex 1.6, Part II, Sec. 2.
13. MacDonald and Schaaf, On the Estimation of Perturbations Due to Flow around Blast Gauges, Report OSRD-5639, September 1945.
14. L. M. Milne-Thomson, "Theoretical Hydrodynamics," 2d ed., The MacMillan Co., New York, 1949.
15. Sandstone Report, Annex 5, Vol. 20, Blast Measurement Summary Report.
16. H. W. Liepmann and A. E. Puckett, "Introduction to Aerodynamics of a Compressible Fluid," John Wiley & Sons, Inc., New York, 1947.
17. MacDonald and Schaaf, On the Estimation of Perturbations Due to Flow around Blast Gauges, Report OSRD-5639, September 1945, p. 80.
18. Schaaf, Estimation of Perturbations Due to Flow around Blast Gauges with Spheroidal Shapes, Report AMG-NYU-144, March 1946.
19. S. T. Marks, Response of Air Blast Gauges of Various Shapes as a Function of Pressure Level, Report BRL-734, August 1950.
20. L. E. Hasel, Use of Pitot-Static Tubes at Transonic and Supersonic Speeds, Langley Aeronautical Laboratory.
21. L. M. Milne-Thomson, "Theoretical Hydrodynamics," 2d ed., p. 81, The MacMillan Co., New York, 1949.

Chapter 3

Presentation of Results

The raw data in the Blast Project have been obtained in various forms, such as indentations in copper, frequency shifts, and arrival times vs distance measurements. These data are presented in the individual detailed reports, and their analysis leads to results in terms of pressures, impulses, and other characteristics of blast waves. It is the purpose of this chapter to present these results in tabular and graphical form.

3.1 RESULTS FOR SHOT DOG, MACH REGION

The results for Shot Dog on Runit Island are shown in Table 3.1. This table contains all the results and numerous footnotes to indicate any special conditions or to qualify the results. The pressure-time curves obtained by the inductance gauges are shown in Figs. 3.1 and 3.2. In Figs. 3.3 to 3.9, only those results which are considered the most accurate are plotted. Where values were obtained on both sides of a wall, the average value has been plotted.

In Fig. 3.3 the best values of maximum pressure are plotted against distance in yards. The lower part of the curve, i.e., below 10 psi, is identical in shape with the standard TNT curve. This shows that a pressure of 10 psi would occur at $R = 1,560$ yd, from which it is deduced by the method outlined in Chap. 4 that the total energy yield [REDACTED]. The remaining part of the curve is drawn by hand through the points and is thought to represent the effect of adiabatic wave propagation before the end of the transition distance is reached, at which point a single peaked shock is formed. These phenomena are discussed in Chap. 4.

In Fig. 3.4 are plotted the best impulse data

for Shot Dog. These are so-called "static impulses" equal to $\int P_s dt$ and do not include the $\int \rho u^2 dt$ contribution due to momentum carried in the mass motion. The integration is to be carried out over the positive phase only. The spring-piston data are omitted because the results on this shot are unreliable due to air leakage into the wall through the underground cable duct. The curve has been fitted by a process explained in Chap. 4 and corresponds to a total energy release [REDACTED]

Figure 3.5 shows positive duration vs distance for Shot Dog.

Figure 3.6 shows maximum negative pressure vs distance for Shot Dog. The symbol P_n designates the maximum underpressure, i.e., the largest difference between pressure measured in the negative phase and atmospheric pressure.

Figure 3.7 shows negative impulse vs distance for Shot Dog. The dotted curve labeled 1 represents the values of negative impulse which would be expected if the negative and positive impulses in the blast wave were equal. The dotted curve 2 represents the best visual fit to the points of a curve of shape similar to curve 1. The positions of these curves would imply that the negative impulse was, on the average, about seven-eighths of the positive impulse.

Figure 3.8 shows duration of negative phase as a function of distance for Shot Dog. It is surprising that these points show so little scatter, since the points at which the pressure-time curve crosses the ambient-pressure axis are difficult to determine.

Figure 3.9 shows arrival time of initial disturbance and of maximum pressure for Shot Dog. This graph shows that the arrival of the

[REDACTED]

first or initial disturbance at the inductance gauge coincides in time with the closure of the velocity switches and that the maximum pressure indicated by the pressure-time records occurs much later, as shown by the dotted curve. For distances equal to and greater than 1,450 yd the maximum pressure occurs at the front of the shock wave and coincides in time with the switch closures. The principal point to be made here is that the shock-velocity switches indicate the time of arrival of the initial disturbance whether this is a low or a high pressure and do not necessarily indicate the arrival time of the pressure maximum.

3.2 RESULTS FOR SHOT EASY, LONG LINE, ENGEBI, E1, MACH REGION

The peak-pressure results for Shot Easy for both long and short lines are shown in Table 3.2a, including all peak-pressure measurements obtained in free air, in the regular region, and in the Mach region by all methods. Table 3.2b contains all pressure-time data obtained on Shot Easy. Figures 3.10 and 3.11 show the pressure-time curves obtained by the inductance gauges in the walls. Figures 3.12 to 3.18 show the best data for the long line.

Figure 3.12 shows the pressure-distance curve for Shot Easy along the long line. The curve which, extrapolated, passes through 1,240 yd at 10 psi has the shape of the TNT blast curve and gives a radiochemical or total tonnage of 47.6 kt. The indenter points are low for various reasons pointed out in the detailed report on indenters. The curve selected passes through the velocity points and has the merit of giving agreement between Shot Easy and the other two shots when reduced arrival times are plotted against reduced distances as is done in Fig. 4.17.

Figure 3.13 shows the positive-impulse data along the long lines. The solid line represents the best fit of the inductance points drawn by hand. The lower part of this curve coincides with the fitting curve used, as described in Sec. 4.3.2. The dotted line is the fitting curve used, taken from values for TNT calculated in Report OSRD-5481. There are two anomalies exhibited by the data, one of them being instrumental in that the spring-piston impulse values in the high range are much higher than

the inductance values. There is at present no explanation for this. The inductance values are considered, in view of the consistent behavior of the inductance system, to be the more reliable. The second anomaly consists in the fact that even these impulses are considerably higher than the fitting curve which was found to agree very well along its entire length with the measured impulses on Shot Dog. Choosing the fitting curve which agrees with the measured values beyond about 1,200 yd, where the blast anomalies have ironed themselves out, permits a kilotonnage to be assigned to the Easy Shot on the basis of impulse measurements.

NOTE: A value of W is found by trial which makes the measured impulse I at a distance R fall on the calculated similarity curve (Report OSRD-5481). This is divided by the reflection coefficient and multiplied by the blast efficiency factor taken as 2.

[REDACTED]

Figure 3.14 shows the variation of positive duration with distance along the long line. The line is simply drawn through the inductance points with no additional significance.

Figures 3.15 to 3.17 show the variation with distance of the three parameters characteristic of the negative phase, namely, negative pressure, negative impulse, and negative duration, respectively.

Figure 3.18 displays the same characteristic as Fig. 3.9, namely, that the velocity switches indicate the time of arrival of the initial disturbance and not necessarily of the maximum pressure. The solid line is obtained from the velocity switches, and the points are obtained from the arrival times at the inductance gauges.

3.3 RESULTS FOR SHOT EASY, SHORT LINE, ENGEBI, E2, MACH REGION

Figures 3.19 to 3.25 give corresponding results for Shot Easy, short line. Figure 3.26 shows the pressure-time curves obtained with inductance gauges in the walls. Since the greatest distance available on this line was

TABLE 3.2a SUMMARY OF RESULTS, SHOT EASY
(Numbers in Parentheses Refer to Footnotes at End of This Table)

Station No.	Distance (yd)(1)	Arrival Time (sec)															
		Blast-velocity Switches(2)		Inductance(3)						Inductance(4)				Inductance(5)			
				Long(6)		Short(6)		Pylon		Long(6)		Short(6)					
		Long(6)	Short(6)	(7)	(8)	(9)	(8)	High	Ground	La- goon	Land	Ocean	Land	Long (6)	Short (6)	High	Ground
27a	4																
33a	5																
27b,33b	23																
27c,33c	57																
	67																
27d,33d	80																
33e	93																
28a,29a	100																
33f,34a	103																
u/w 3	107																
33g,34b	113																
33h,34c	123																
	133																
33i,34d	143																
	167																
28b,29b	180		0.0206														
u/w 2	188																
	200																
	233																
u/w 1	246																
28c,29c	260	0.0824	0.0646														
	267																
	300																
	333																
28d,29d,36a	360	0.1424	0.1217														
	367																
	400																
	434																
20a,29e	460	0.2178	0.1723	0.292	0.288					0.098	0.094			0.194			
	467																
	481																
	500																
	533																
20b,29f	557																
	560	0.3228	0.2551	0.455	0.434					0.143	0.122			0.312			
	567																
	595																
	600																
25e,29g	620	0.3953	0.3224														
	626																
	633																
	656																
	667																
	681																
36b,37a,37d, 30c,29h	700	0.5102	0.4231	0.729	0.740					0.193	0.204			0.536		0.426	0.411
	705																
	733																
28f,29i	800	0.6775	0.5818														
20d,21a	900	0.8620	0.7723	0.917	0.902	0.913	0.961			0.067	0.052	0.168	0.216	0.850	0.745		
37b,37e	950							0.879	0.852							0.879	0.852
36f	985																
36c,21b,28g	1,000	1.0879	1.0021			1.287	1.289					0.301	0.303		0.986		
28h,29j	1,100	1.2922	1.2542														
28i,29k	1,200	1.5003	1.4954														
21c	1,233		1.5737									0.103	0.105				
36d,20e	1,300	1.7149		1.734	1.734									1.734			
37c,37f	1,430							1.995	1.995							1.995	1.995
28j	1,460	2.0572															
36e	1,500																
20f	1,550	2.2596		2.274	2.274									2.274			
Muzin	2,261																
Kirinian	3,503																

TABLE 3.2a (Continued)

Station No.	Distance (yd)(1)	Arrival Time (sec) (Continued)					Positive Pressure (psi)							
		Shock Photography			Balloon Telemeter(10)	Altitude of Triple Point (ft)	Foil Meters(11)		Indenters		Blast-velocity Switches			
		Mach	Mach Stem near T.P.	Rocket Trails(10)			Total Interval				Long(6)		Short(6)	
							Long(6)	Short(6)	Long (6)	Short (6)	Adiabatic $\frac{E}{\rho}$	Shock	Adiabatic	Shock
27a	4													
33a	5													
27b,33b	23													
27c,33c	57													
	67			0.00257										
27d,33d	80													
33e	93													
28a,29a	100			0.00731										
33f,34a	103													
u/w 3	107													
33g,34b	113													
33h,34c	123													
	133	0.030		0.0160		20.5								
33i,34d	143													
	167	0.038		0.0276		51.0								
28b,29b	180													
u/w 2	188													
	200	0.048		0.04257		82.0								
	233			0.06145		122.0								
u/w 1	246													
28c,29c	260										510.0			
	267	0.064		0.08138		158.0								
	300			0.10836		204.0								
	333	0.128	0.132	0.13834		258.0								
28d,29d,36a	360										205.0		446.0	
	367		0.157	0.17090		319.0								
	400	0.186	0.186	0.20609		392.0								
	434		0.216	0.24368		470.0	89.6-90.5							
20a,29e	460								68.4		91.0		192.0	
	467	0.258	0.248	0.28337		575.0								
	481				0.3474									
	500		0.283	0.32507		680.0								
	533	0.346	0.320	0.36858		788.0								
	557				0.4392									
20b,29f	560								46.0		44.0		72.0	
	587		0.359	0.41389		908.0								
	595				0.4948									
28e,29g	600	0.434	0.400	0.46023		1,038.0								
	620										25.5		40.0	
	626				0.5328									
	633		0.443	0.50799		1,192.0								
	656				0.5723									
	667	0.733	0.489	0.55681										
	681				0.6314									
36b,37a,37d, 20c,29h	700		0.537	0.60647			33.2-39.2		19.0		18.5(12)		21.3	
	705				0.6515									
	733	0.587		0.65679										
28f,29i	800	0.695									15.0(12)		13.3(12)	
20d,31a	900						20.3-24.0		14.2	9.0	13.2(12)		10.0(12)	
37b,37e	950													
38f	985													
36c,21b,28g	1,000							13.7-16.4		7.7	11.7(12)		8.0(12)	
28h,29j	1,100											10.7	6.9(12)	
28i,29k	1,200											9.6		6.0
21c	1,233							9.6-11.7		7.4				5.7
36d,20e	1,300						7.8-11.7		8.4			8.7		
37c,37f	1,430													
28j	1,460											7.2		
36e	1,500													
20f	1,550						6.4-7.8		6.3			6.4		
Muzin	2,261								3.57					
Kirinian	3,503								1.62					

TABLE 3.2a (Continued)

Station No.	Distance (yd)(1)	Positive Pressure (psi) (Continued)												
		Shock Photography			Balloon Telemeter (10)	Crushers				Spring Piston				
		Mach (13)	Mach Stem near T.P.	Rocket Trails (10)		Concrete	Stake	Guy-wire Stakes	Under-water	Long(6)		Short(6)		
										Lagoon	Land	Ocean	Land	
27a	4						10,700(14,15)							
33a	5													
27b,33b	23						17,400(18)	19,800(18)						
27c,33c	57						11,200(17)	19,600(17)						
	87			13,060.0										
27d,33d	80						9,600(18)							
33e	93							5,500(19)						
28a,29a	100			3,653.0										
33f,34a	103							3,550(20)	3,050(15,20)					
u/w 3	107									3,660(21)				
33g,34b	113							3,040(22)	3,450(15,22)					
33h,34c	123							2,550(23)	3,210(15,23)					
	133	5,406.0		1,353.0										
33i,34d	143							2,360(24)	1,850(24)					
	167	1,619.0		774.0										
28b,29b	180													
u/w 2	188									1,100(25)				
	200	814.0		459.0										
	233			288.0										
u/w 1	246													
28c,29c	260													
	267	316.0		187.4										
	300			148.8										
	333	167.0	302.0	117.6										
28d,29d,36a	360													
	367		171.0	97.2										
	400	104.0	139.0	81.9										
	434		118.0	71.4										
30a,29e(26)	460													
	487	70.6	100.0	63.2							90.4(27)	83.8(27)		
	481				52.5									
	500		86.2	54.8										
	533	51.7	73.9	49.4										
30b,29f(28)	557				39.7									
	560													
	567		64.1	44.6										
	565				36.2									
28e,29g	600	38.6	55.1	42.6										
	620													
	626				33.2									
	633		48.1	38.6										
	656				27.9									
	667	29.9	41.8	36.5										
	681				25.9									
36b,37a,37d, 20c,29h	700		36.9	34.7										
											37.9(27,29)	26.2(27,29)		
	705				24.8									
	733	23.9	32.2	34.0										
28f,29i	800		34.8											
30d,31a	900													
37b,37e	950										19.4(27)	14.0(27)	8.32	11.35
36f	985													
36c,31b,28g	1,000												9.42	7.96
28h,29j	1,100													
28i,29k	1,200													
21c	1,233												8.26	8.34
36d,30e	1,300													
37c,37f	1,430										9.72(27)	10.1(27)		
28j	1,460													
36e	1,500													
20f	1,550										6.97(27)	6.64(27)		
											7.79(30)	7.48(30)		
Muxin	2,261													
Kirinian	3,503													

TABLE 3.2a (Continued)

Station No.	Distance (yd)(1)	Positive Pressure (psi) (Continued)																			
		Inductance								Inductance											
		Long (6)				Short (6)															
		Lagoon		Land		Ocean		Land		Pylon 0(31)				Pylon 3.5(31)		Pylon 7(31)		Pylon 10(31)		Pylon 14(31)	
		(32)	(33)	(32)	(33)	(32)	(33)	(32)	(33)	(32)	(33)	(32)	(33)	(32)	(33)	(32)	(33)	(32)	(33)	(32)	(33)
27a	4																				
33a	5																				
27b,33b	23																				
27c,33c	57																				
	87																				
27d,33d	80																				
33e	93																				
28a,29a	100																				
33f,34a	103																				
u/w 3	107																				
33g,34b	113																				
33h,34c	123																				
	133																				
33i,34d	143																				
	187																				
28b,29b	180																				
u/w 2	188																				
	200																				
	233																				
u/w 1	248																				
28c,29c	280																				
	287																				
	300																				
	333																				
28d,29d,36a	360																				
	387																				
	400																				
	434																				
20a,29e	460	16.5	66.0	14.0																	
	467																				
	481																				
	500																				
	533																				
	557																				
20b,29f	560	13.5	38.4	14.3	61.8																
	587																				
	595																				
	600																				
28e,29g	620																				
	626																				
	633																				
	656																				
	667																				
	681																				
36b,37a,37d, 30c,29h	700	12.5	23.0	13.0	20.7					14.3	17.3	15.4	17.35		24.6		22.7		22.8		
	705																				
	733																				
28f,29i	800																				
20d,21a	900	7.8	15.1	8.8	15.0	4.55	9.55	4.60	11.90												
37b,37e	950									7.9	10.42	8.2	10.80	10.35	13.80	9.35	12.77	8.82	13.15	9.4	12.32
36f	985																				
36c,21b,22g	1,000					9.15	9.40	4.80	8.04												
28h,29j	1,100																				
28i,29k	1,200																				
21c	1,233					7.30	7.80	7.1	8.0												
36d,20e	1,300	9.51	9.51	9.52	9.53																
37c,37f	1,430									8.51	8.51	8.23	8.23	7.23	7.23	8.71	8.71	8.27	8.27	8.00	8.00
28j	1,460																				
36e	1,500																				
20f	1,550	7.0	7.0	7.9	7.9																
Muzin	2,261																				
Kirinian	3,503																				

TABLE 3.2a (Continued)

Station No.	Distance (yd)(1)	Ground Shock															
		Peak Acceleration (g units)(34)				Frequency(cycles/sec)					Displacement (ft)			Arrival Time (35)(sec)		Peak Velocity (ft/sec)	
		ERA		Calidyne		ERA		Calidyne		Free Piston	Free Piston (36)	Calidyne		Calidyne		Calidyne	
		Rad	Vert	Rad	Vert	Rad	Vert	Rad	Vert			Rad	Vert	Rad	Vert	Rad	Vert
27a	4																
33a	5																
27b, 33b	23																
27c, 33c	57																
	87																
27d, 33d	80																
33e	93																
28a, 29a	100																
33f, 34a	103																
u/w 3	107																
33g, 34b	113																
33h, 34c	123																
	133																
33i, 34d	143																
	187																
28b, 29b	180																
u/w 2	188																
	200																
	233																
u/w 1	248																
28c, 29c	280																
	287																
	300																
	333																
28d, 29d, 36a	360	19.9	14.1	11.2(37)	16.4(38)	50	80	45	50			1.6(39)	0.188	0.177	8.4(37)	10.0(39)	
	387																
	400																
	434																
20a, 29e	480																
	487																
	481																
	500																
	533																
	557																
20b, 29f	560																
	587																
	595																
	600																
28e, 29g	620																
	628																
	633																
	658																
	687																
	681																
36b, 37a, 37d, 20c, 29h	700	1.4	2.7	0.61(37)	0.70(38)	70	70	39	24			0.14(37)	0.44(38)	0.360	0.378	0.45(37)	1.1(38)
	705																
	733																
28f, 29i	800																
20d, 21a	900																
37b, 37e	950																
36f	985	0.71	0.63	0.19(37)		37	46										
36c, 21b, 28g	1,000	0.21	0.29			30	30	21			0.13(40)		0.497		0.34(40)		
28h, 29j	1,100																
28i, 29k	1,200																
21c	1,233																
38d, 20e	1,300			0.44(40)	0.17(38)			32	21	0.85	0.071	0.06(38)	0.697	0.651	1.9(37)	0.14(38)	
37c, 37f	1,430																
28j	1,480																
38e	1,500			0.14(37)	0.14(38)			21	15	0.76	0.053		0.870	0.708			
20f	1,550																
Muxin	2,261																
Kirinian	3,503																

FOOTNOTES TO TABLE 3.2a

- (1) All distances are horizontal distances from ground zero unless otherwise noted by footnote (10).
- (2) Time of switch closure, may not be arrival time of maximum pressure.
- (3) Arrival of maximum peak.
- (4) Arrival of maximum peak after initial signal.
- (5) Arrival of initial disturbance.
- (6) Short and long refer to short and long blast lines. The long line was at an approximate bearing of S45°E from zero. The short line was at the approximate bearing of N78°E from the zero tower and was in the general direction of a tower guy wire.
- (7) Lagoon side.
- (8) Land side.
- (9) Ocean side.
- (10) Distance indicates the radial distance from actual zero.
- (11) Readings for walls 20a, 20c, and 20d are estimated.
- (12) Transition zone.
- (13) Pressure on ground at Mach stem.
- (14) Slant distance 298 ft or 99.3 yd.
- (15) Static calibration.
- (16) Slant distance 306 ft or 102 yd.
- (17) Slant distance 343 ft or 114.3 yd.
- (18) Slant distance 382 ft or 127.3 yd.
- (19) Slant distance 408 ft or 136 yd.
- (20) Slant distance 429 ft or 143 yd.
- (21) Slant distance 441 ft or 147 yd.
- (22) Slant distance 451 ft or 150.3 yd.
- (23) Slant distance 472 ft or 158 yd.
- (24) Slant distance 521 ft or 174 yd.
- (25) Slant distance 641 ft or 213.7 yd.
- (26) Station 20a was tilted.
- (27) Measured peak pressure.
- (28) Wall knocked flat.
- (29) This gauge probably contained air in the oil channel.
- (30) Extrapolated peak pressure.
- (31) Numbers indicate height in feet of gauge in pylon.
- (32) Initial peak pressure.
- (33) Maximum pressure.
- (34) In terms of standard acceleration of gravity (32.174 ft/sec/sec).
- (35) Of peak acceleration.
- (36) Horizontal radial, toward zero.
- (37) Toward zero.
- (38) Up.
- (39) Down.
- (40) Away from zero.

TABLE 3.2b SUMMARY OF RESULTS, SHOT EASY

[illegible]

†Short and long refer to short and long blast lines. The long line was at an approximate bearing of 945°E from zero. The short line was at the approximate bearing of N70°E from the zero tower and was in the general direction of a tower guy wire.

‡This gauge probably contained air in the oil channel.

TABLE 3.2b (Continued)

Station No.	Distance from Ground Zero (yd)	Maximum Negative Pressure (psi)												Negative Impulse (lb sec./in. ²)											
		Inductance												Inductance											
		Spring Platoon						Pylon						Spring Platoon						Pylon					
		Longt			Shortt			Longt			Shortt			Longt			Shortt			Longt			Shortt		
		Lagoon	Land	Ocean	Land	Ocean	Land	Lagoon	Land	Ocean	Land	Ocean	Land	Lagoon	Land	Ocean	Land	Ocean	Land	Lagoon	Land	Ocean	Land	Ocean	Land
20a	460	4.050	2.250											5.180	2.810										
20b	560																								
20c	700	2.230	3.500											3.590	7.870										
37a	700																								
37d	700																								
20d	900	2.500	2.120											6.070	4.180										
21a	900																								
37b	950																								
37e	950																								
21b	1,000																								
21c	1,233																								
20e	1,300	1.830	1.900											4.100	3.180										
37c	1,430																								
37f	1,430																								
20f	1,550	1.300	1.360											2.860	2.860										
		Negative Duration (sec)												Spring Platoon											
20a	460	2.280	1.880											3.788	3.372										
20b	560																								
20c	700	2.270	3.370																						
37a	700																								
37d	700																								
20d	900	4.060	3.840											4.116	3.632										
21a	900																								
37b	950																								
37e	950																								
21b	1,000																								
21c	1,233																								
20e	1,300	4.230	4.210											4.105	4.092										
37c	1,430																								
37f	1,430																								
20f	1,550	4.260	4.290											3.655	3.100										

†Short and long refer to short and long blast lines. The long line was at an approximate bearing of S45°E from zero. The short line was at the approximate bearing of N78°E from the zero tower and was in the general direction of a lower guy wire.

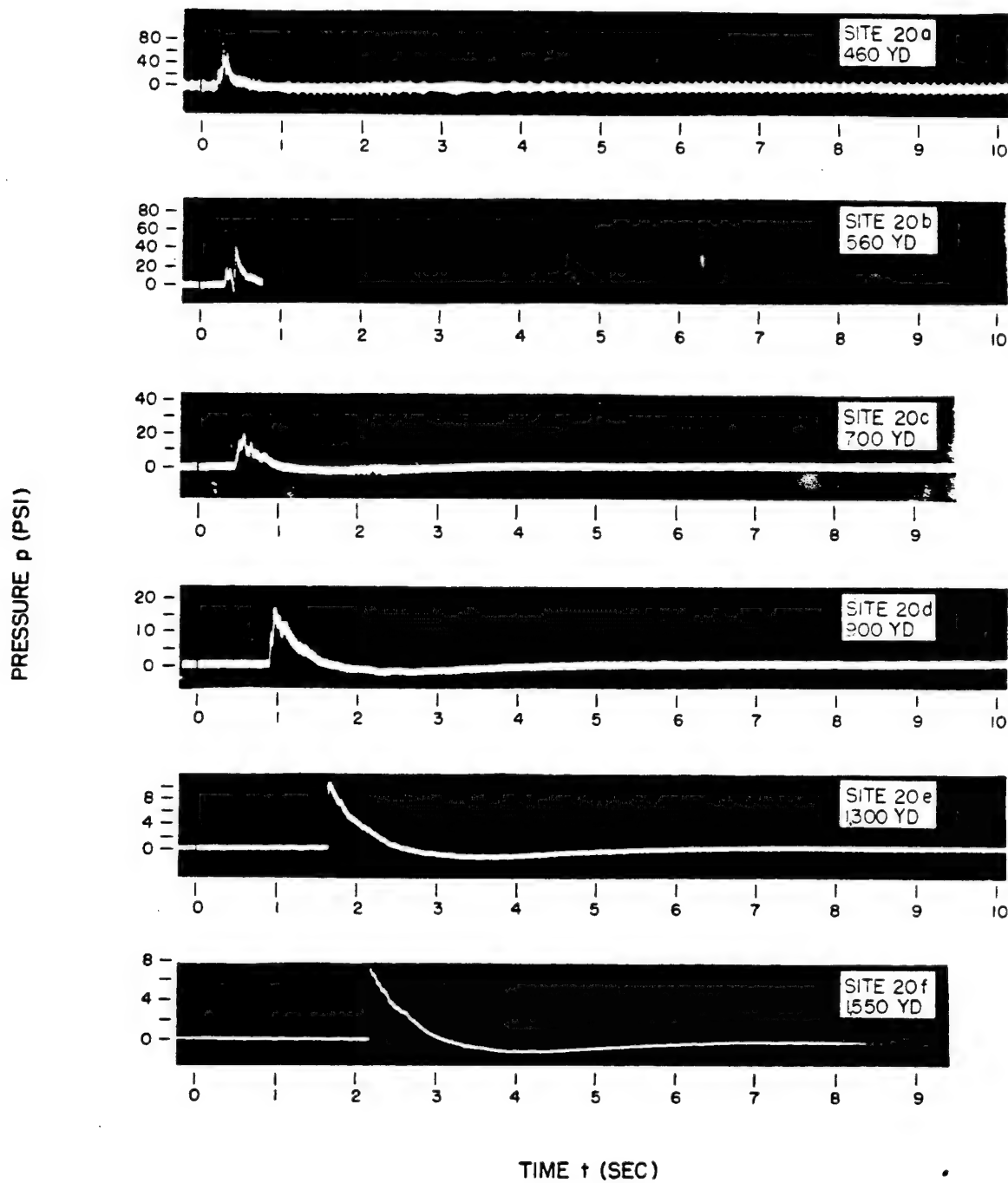


Fig. 3.10 Pressure-time Curves, Shot Easy, Lagoon Line, Lagoon Side

PRESSURE p (PSI)

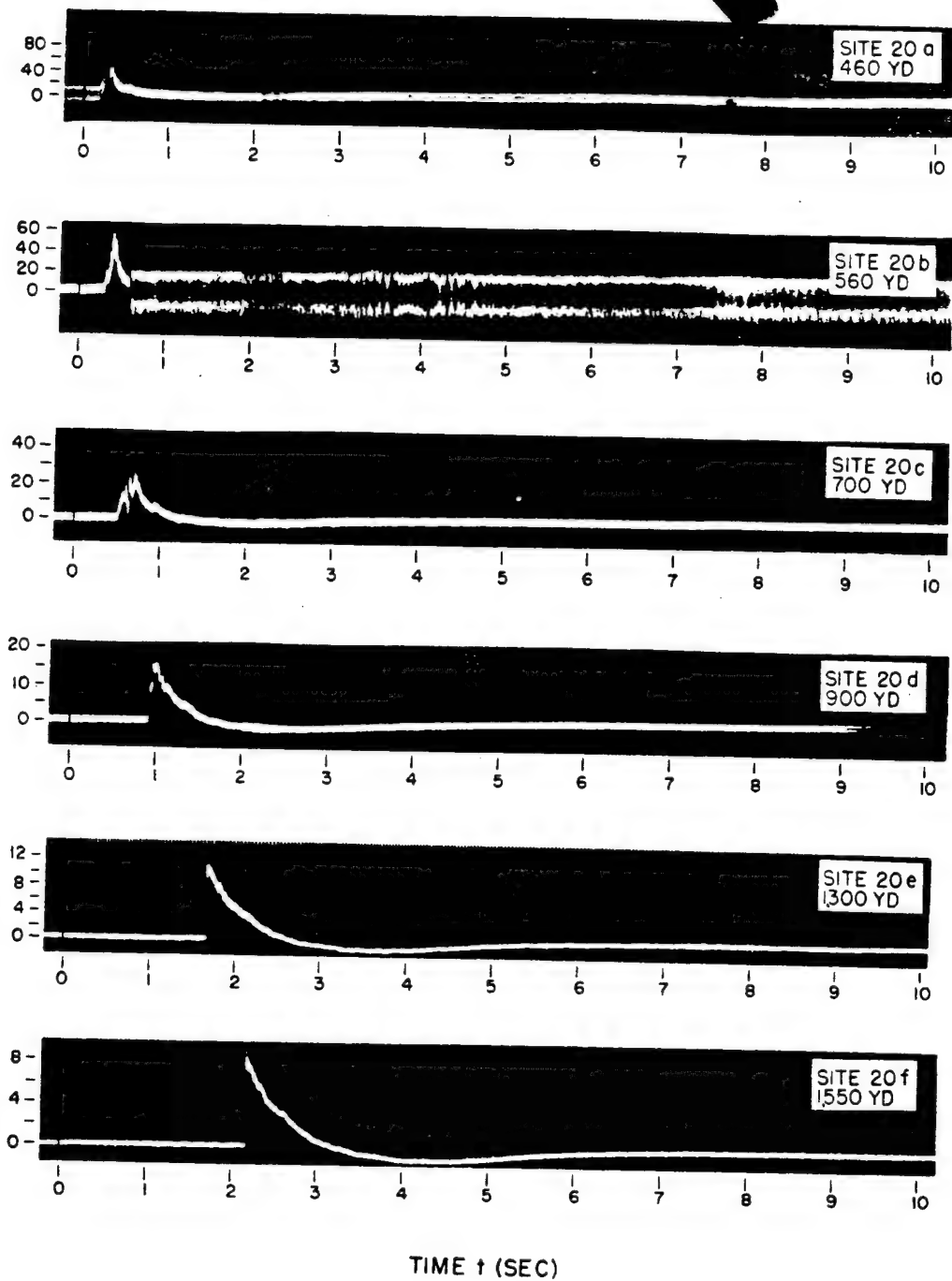


Fig. 3.11 Pressure-time Curves, Shot Easy, Lagoon Line, Land Side

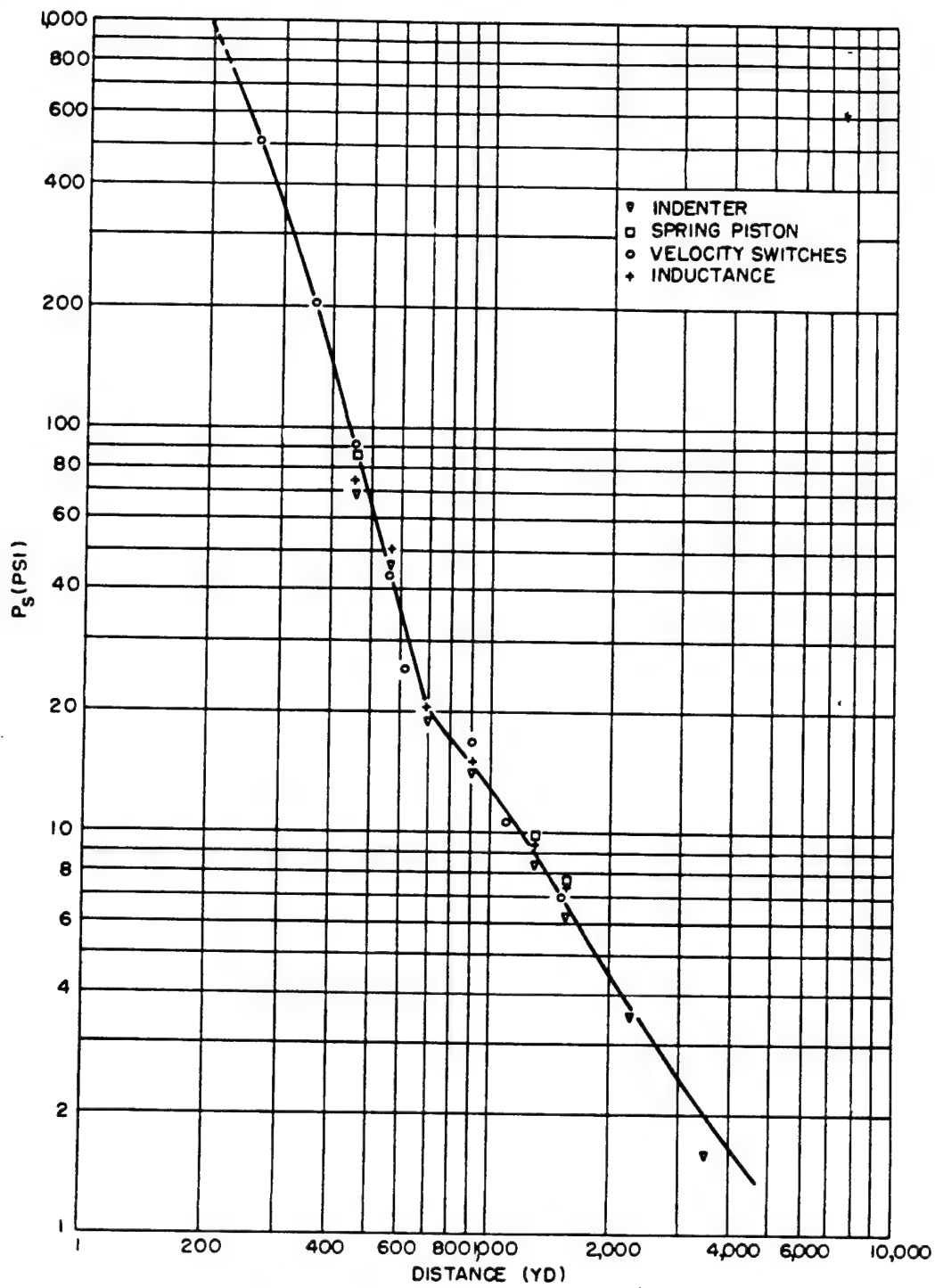


Fig. 3.12 Maximum Pressure vs Distance

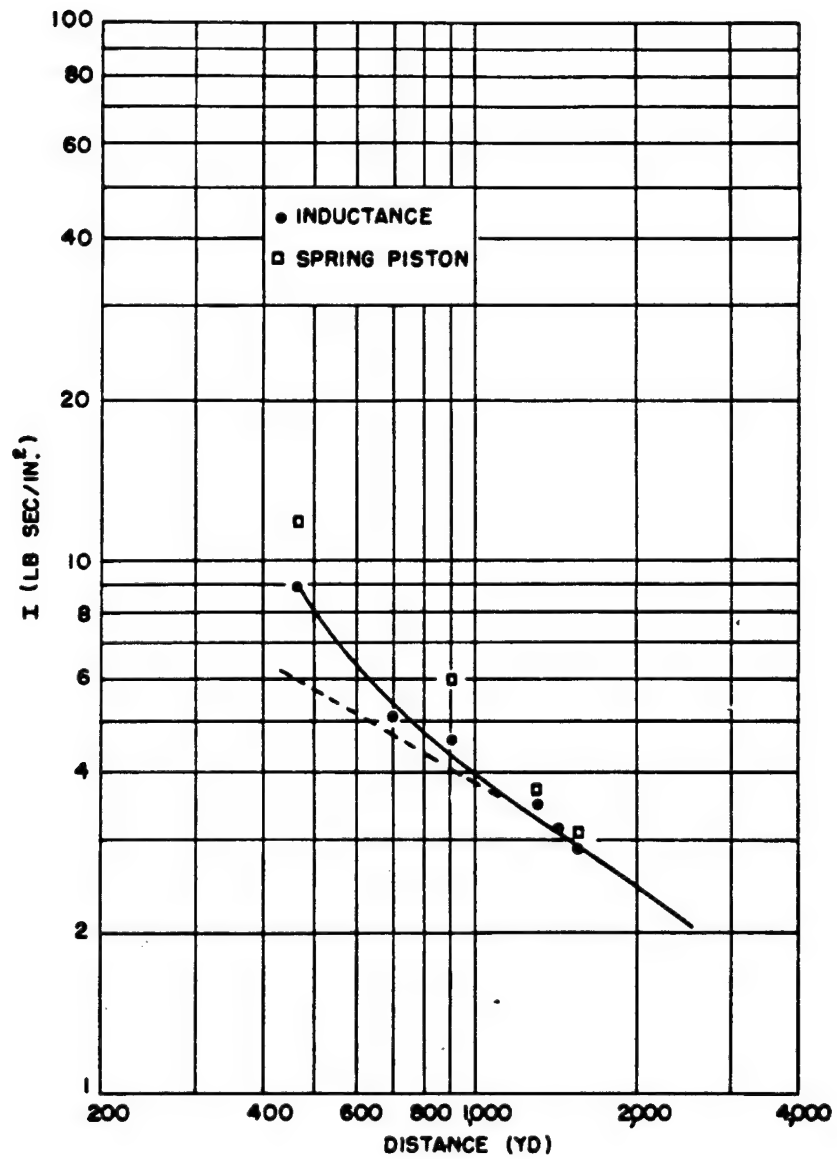


Fig. 3.13 Positive Impulse vs Distance

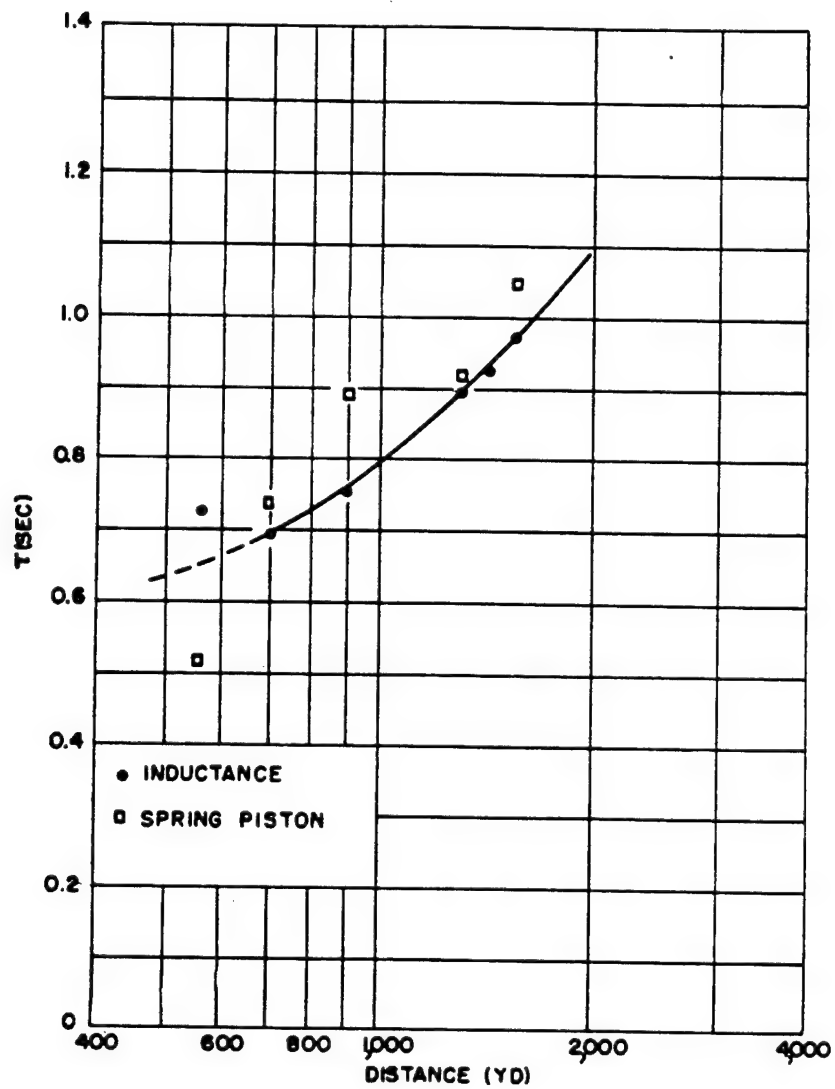


Fig. 3.14 Positive Duration vs Distance

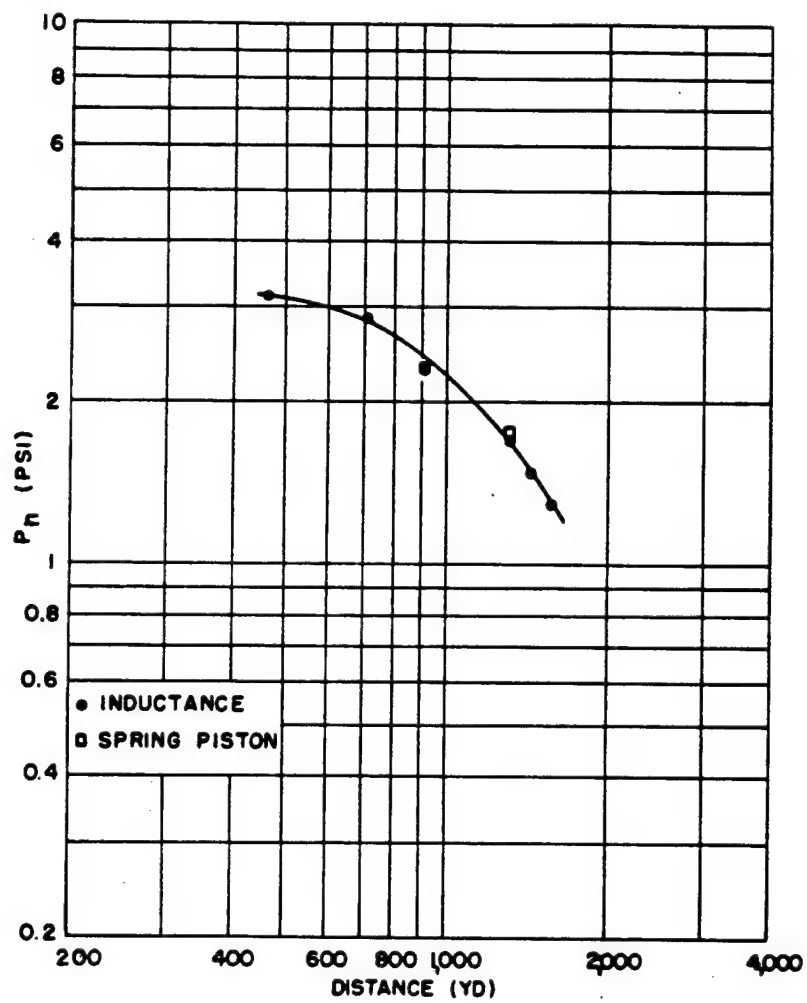


Fig. 3.15 Negative Pressure vs Distance

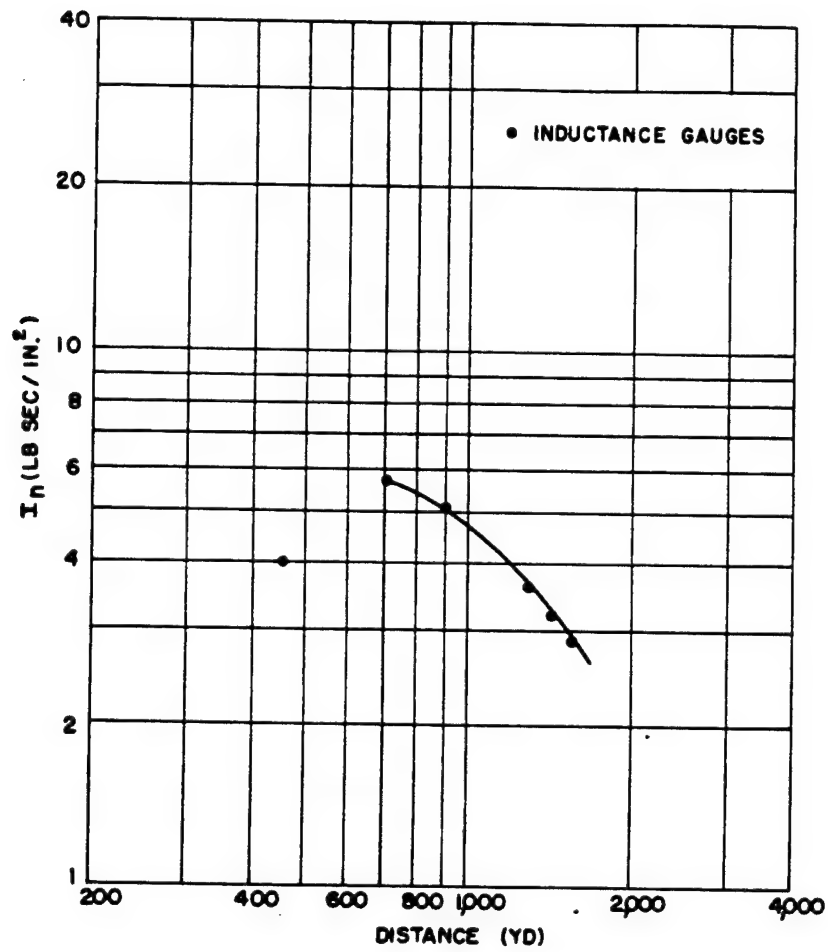


Fig. 3.16 Negative Impulse vs Distance

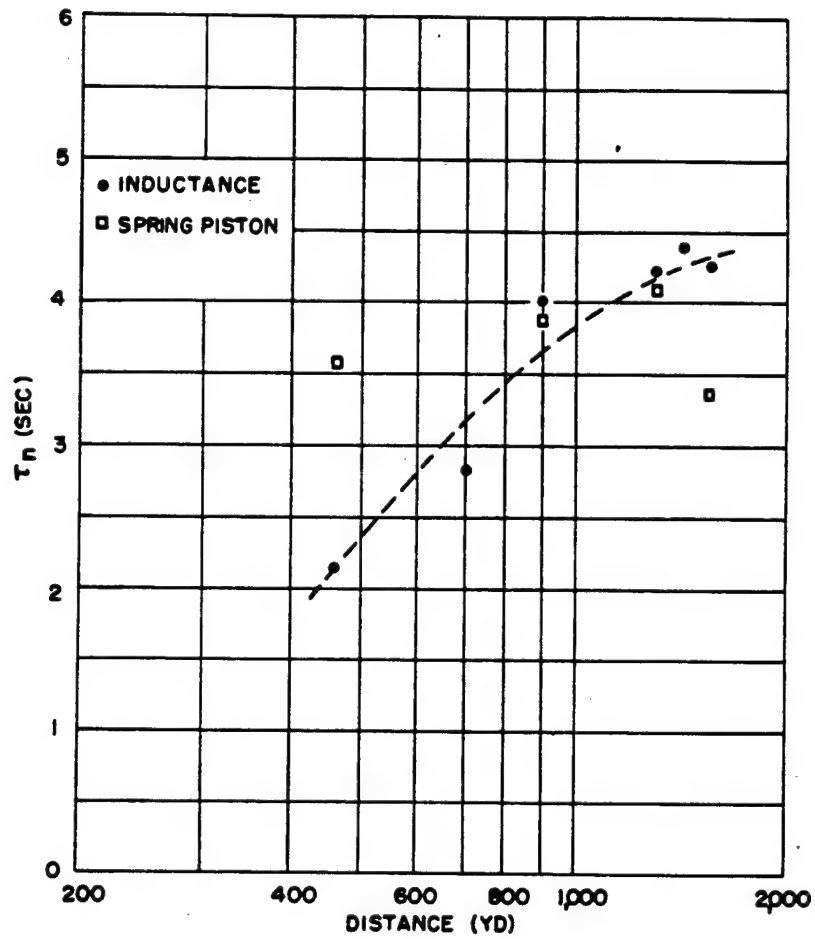


Fig. 3.17 Negative Duration vs Distance

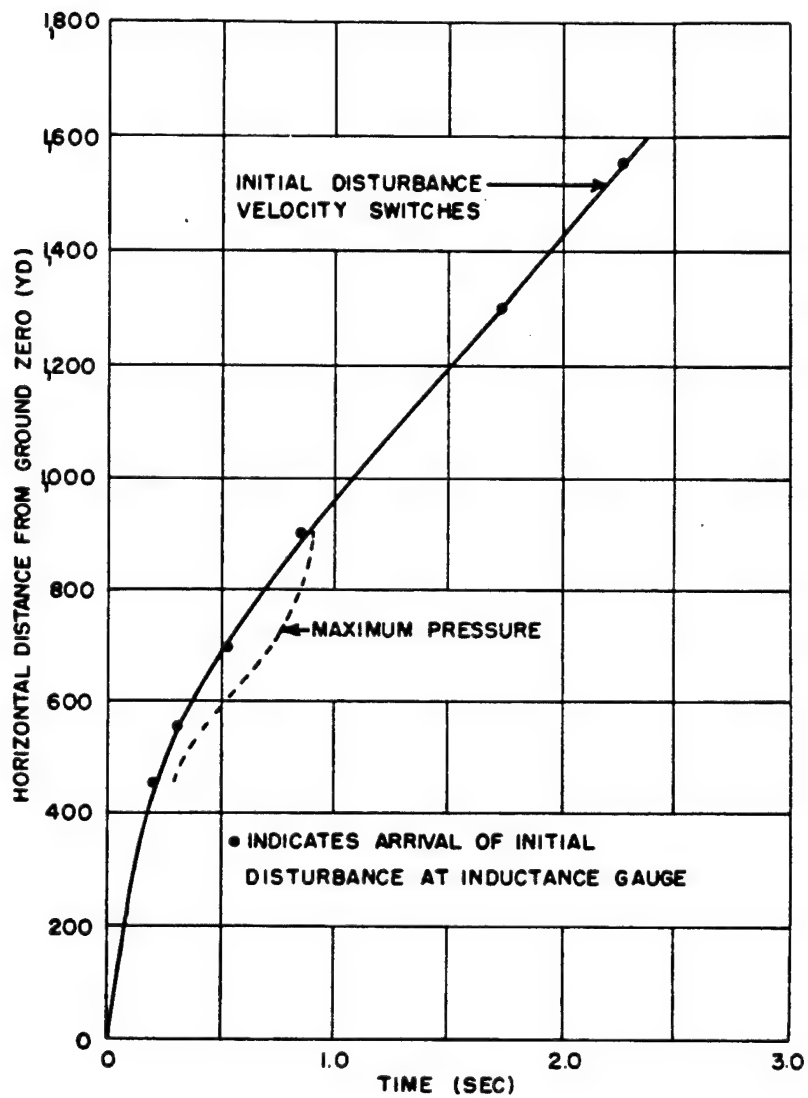


Fig. 3.18 Times of Arrival vs Distance

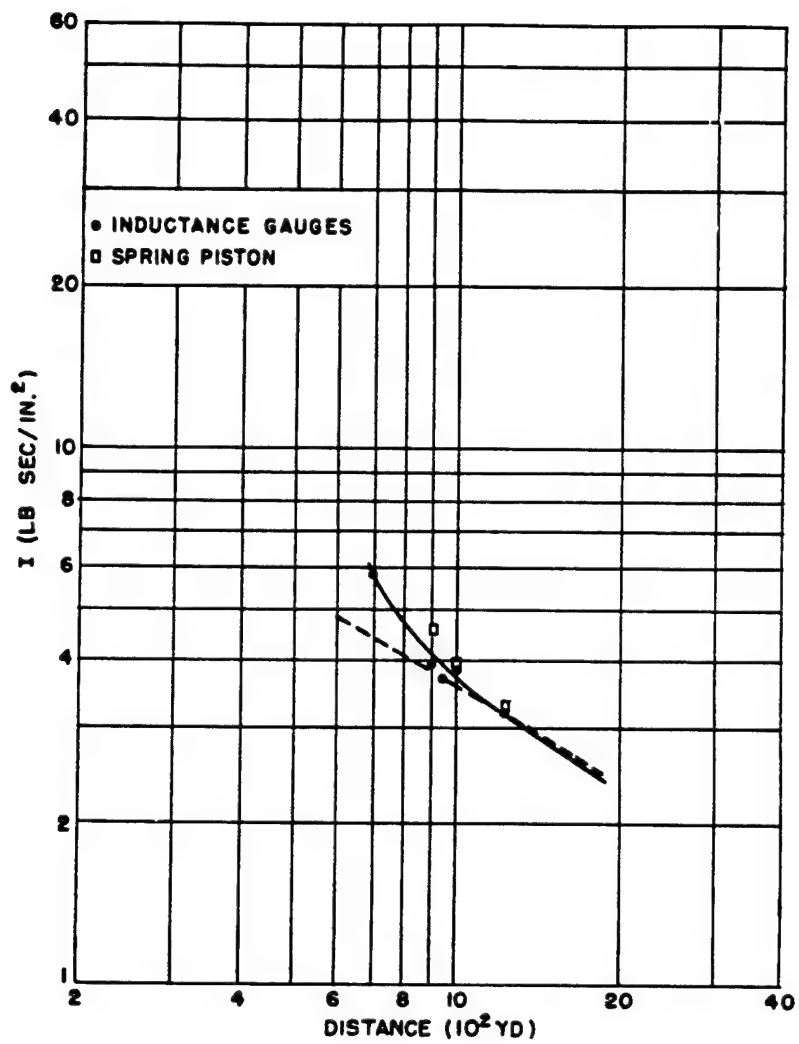


Fig. 3.20 Positive Impulse vs Distance

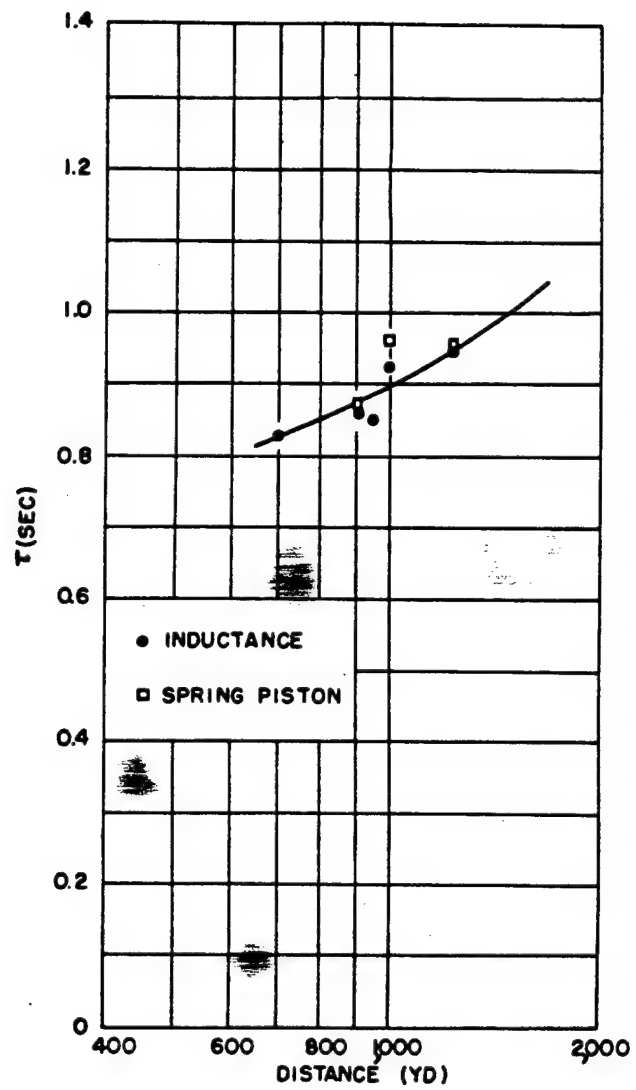


Fig. 3.21 Positive Duration vs Distance

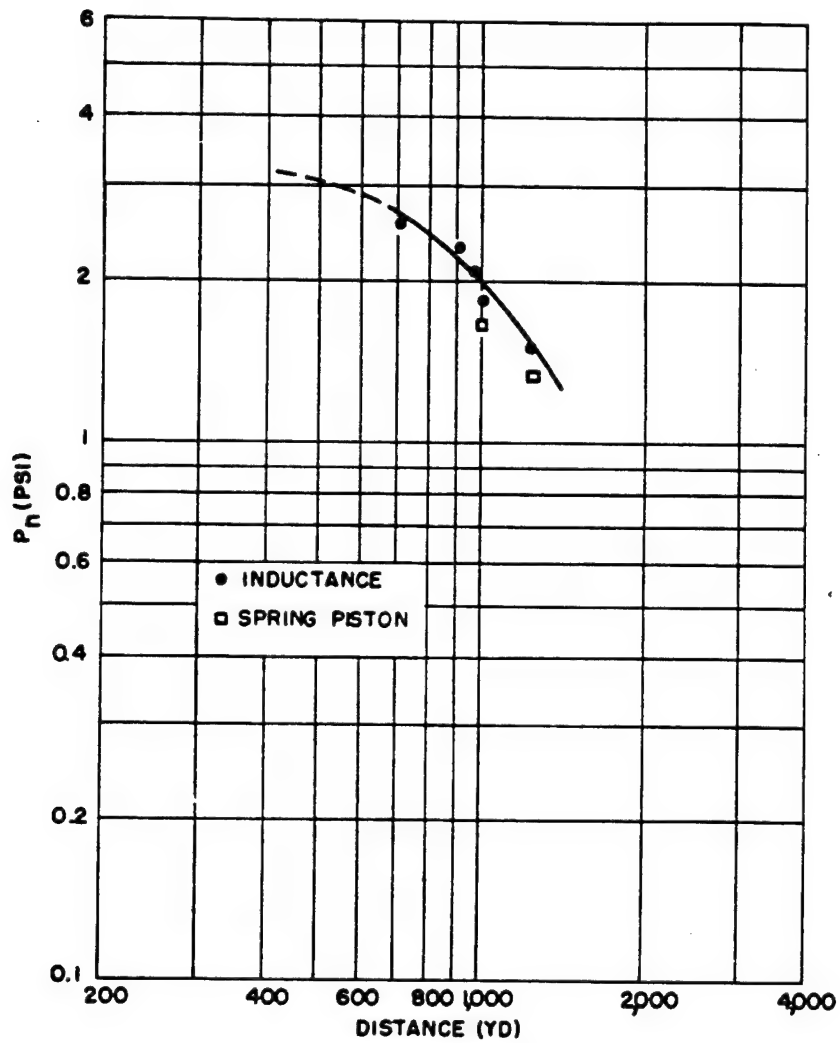


Fig. 3.22 Negative Pressure vs Distance

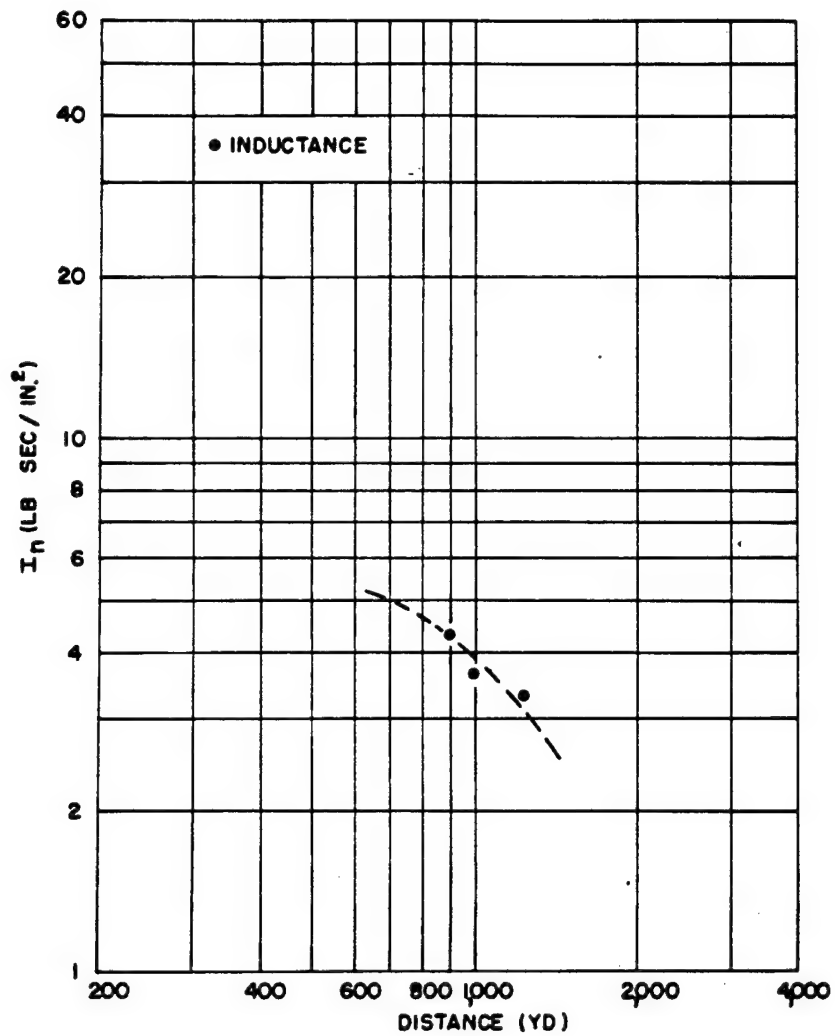


Fig. 3.23 Negative Impulse vs Distance

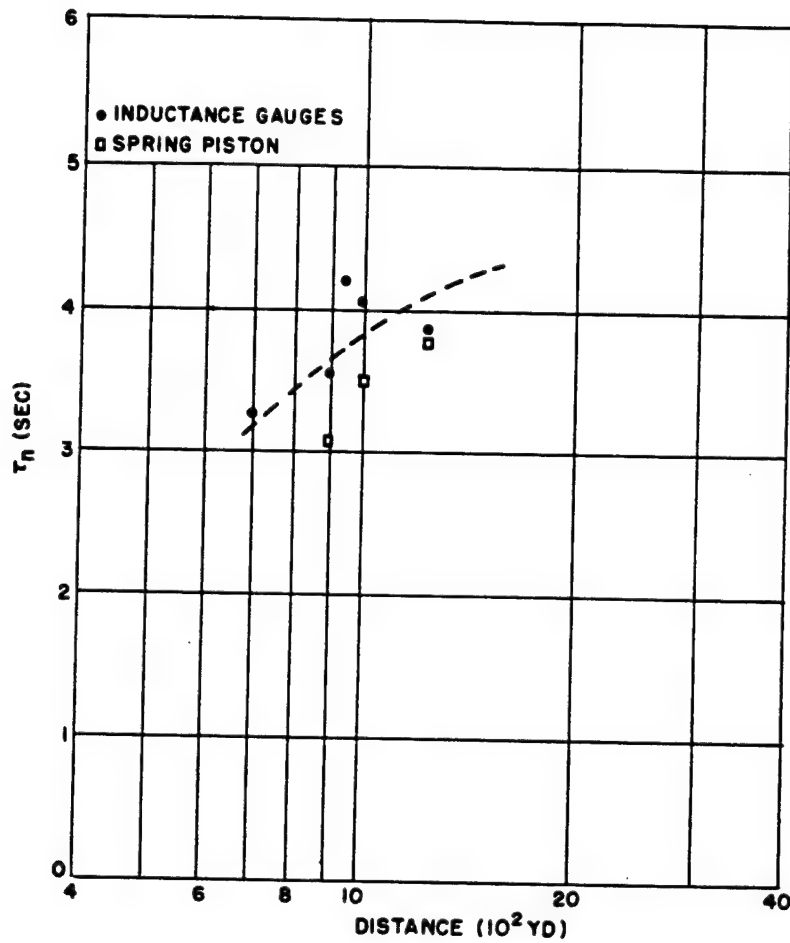


Fig. 3.24 Negative Duration vs Distance

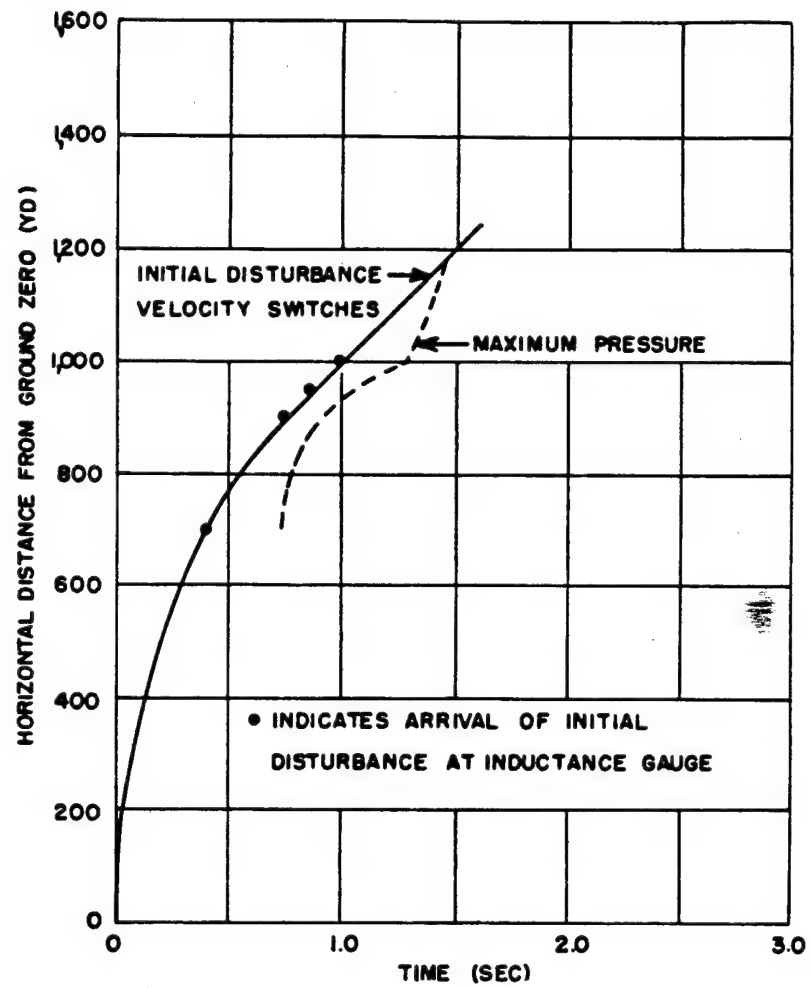


Fig. 3.25 Times of Arrival vs Distance

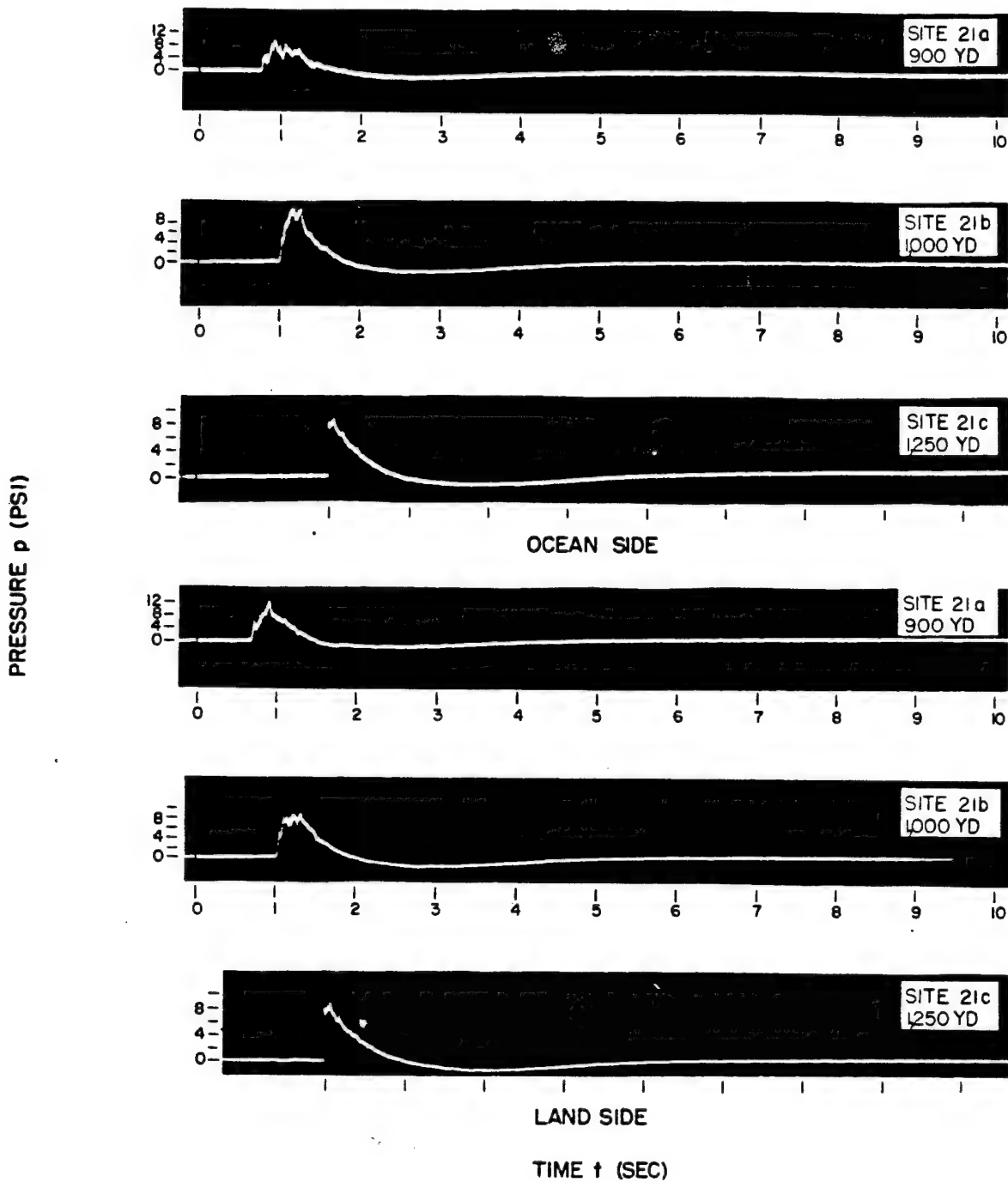


Fig. 3.26 Pressure-time Curves, Shot Easy, Ocean Side

1,230 yd, the blast wave had not reached its stable shape, and any deductions as to tonnage would therefore be misleading. Although the pressures are higher along the short line than along the long line at the nearest distances, they quickly fall below and remain so throughout the remainder of its length. The dotted line in Fig. 3.19 represents the values found for the long line, corresponding to 46.7 kt (radio-chemical). From an inspection of the data on the short line alone it is necessary to conclude that the yield was approximately 34 kt (radio-chemical). The short line, which was set up originally in an effort to obtain data on asymmetry, has certainly yielded some asymmetrical results.

Figure 3.20 shows nearly the same impulse as Fig. 3.13 at the same distances. They are, however, significantly lower, and the tonnage derived from them turns out to be 72 kt (radio-chemical), which is more than would be expected from the low-pressure results. Therefore it is suspected that the positive durations on the short line would be longer than on the long line, and this is indeed the case as a comparison of Fig. 3.21 with Fig. 3.14 will show.

Figures 3.22 to 3.24 show negative pressures, negative impulses, and negative durations, respectively.

Figure 3.25, showing arrival time, displays characteristics already commented on.

3.4 RESULTS FOR PRESSURES ON THE GROUND NEAR EXPLOSION, SHOT EASY

Figure 3.27 shows pressures measured by ball-crusher gauges on the ground in the Mach region near the tower. The points marked U are derived from gauges placed just offshore in the lagoon, about 1 ft under water. They indicate that the pressure transmittal from air to water was accomplished without appreciable loss, at least during the 178 μ sec required for the gauge to register. Points 1 and 2 are obtained from velocity measurements on the long and short line.

There is very good agreement between the crusher results and the long line (which was free of jets) even though they were along a line making an angle of about 120° with the long line. The short-line points are higher, indicating that the disturbance reached the same distance in

less time. It should be pointed out that the pressure is calculated from the arrival times on the assumption that the shock or adiabatic wave is traveling in the direction defined by the line between the pickup switches. Since the jet action may easily vitiate this assumption, the pressures calculated may be fictitious. In fact the ball-crusher deformations at the base of a different guy wire were actually half as much as those at the same distance along the longer line of ball-crusher gauges. If it is assumed that the loading on these gauges was slow compared with 180 μ sec because of the jet action, then the static calibration should be used in deducing the pressures. The results of this are shown in Fig. 3.27, and it is seen that the maximum pressures at the base of the guy wires are in good agreement with maximums elsewhere. In other words, there is no evidence from the crusher gauges that the pressures at and immediately beyond the base of the guy wire are any higher than elsewhere at the same distance.

In Fig. 3.28 are shown the values of pressure along the ground in both the regular and the Mach region. The abscissa chosen is the slant range instead of the horizontal range. The crusher deformations are converted to pressure by assuming that they are struck by a shock wave which does not decay during the deformation of the ball. An estimate of the error made in this assumption based on the probable decay parameter θ and the known deformation time shows that the calculated pressure is only a few per cent lower than that which would be given by an exact calculation using the estimated decay rate. No correction has been made for this minor effect. In Sec. 4.4 is given a more detailed discussion of the readings obtained at the base of the guy wire. These are not shown on Fig. 3.28. A curious fact concerning the observations in the regular region is that the closest set of concrete-mounted gauges, almost directly under the tower, showed very low readings, the deformations being less than half those of the other gauges in this region. Even the assumption that these gauges were subjected to a relatively gradual rise in pressure because of possible jet action down the tower legs gives a pressure which is about 12,000 psi compared with 18,000 psi or so measured a few yards away. It should be noted that in all cases where there were

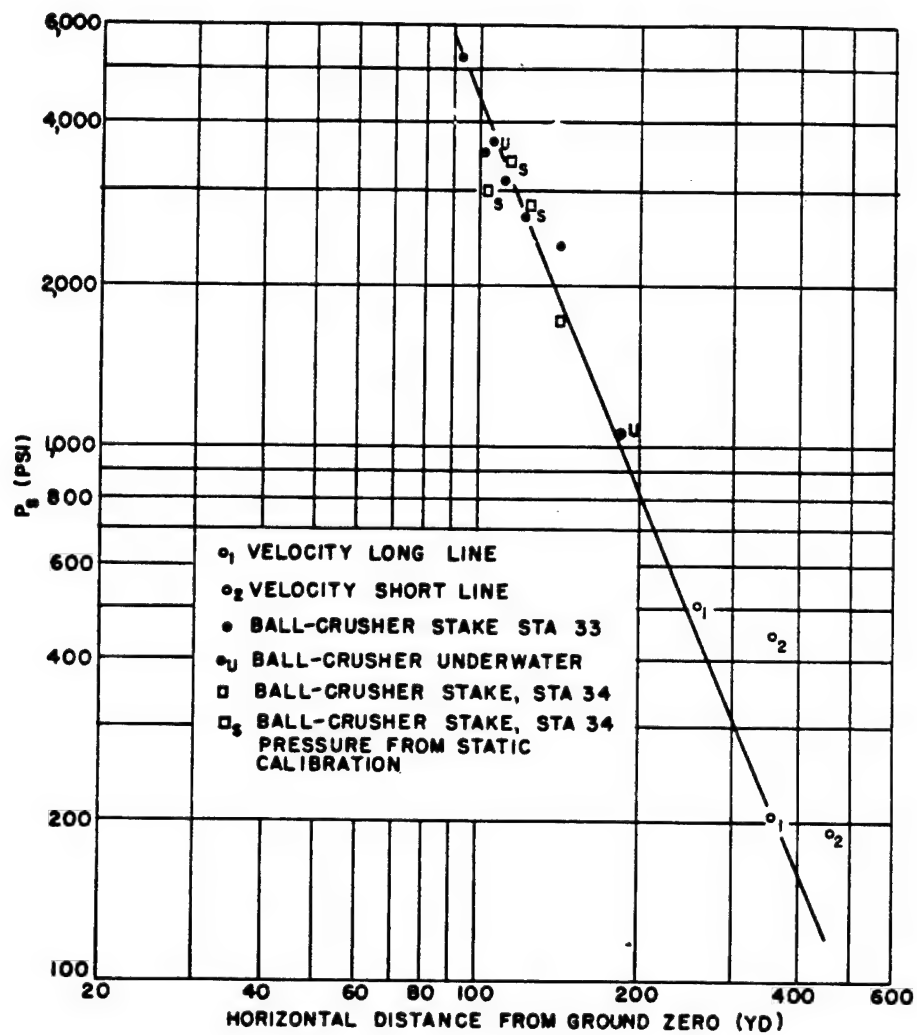


Fig. 3.27 Pressure on the Ground, Shot Easy, Mach Region

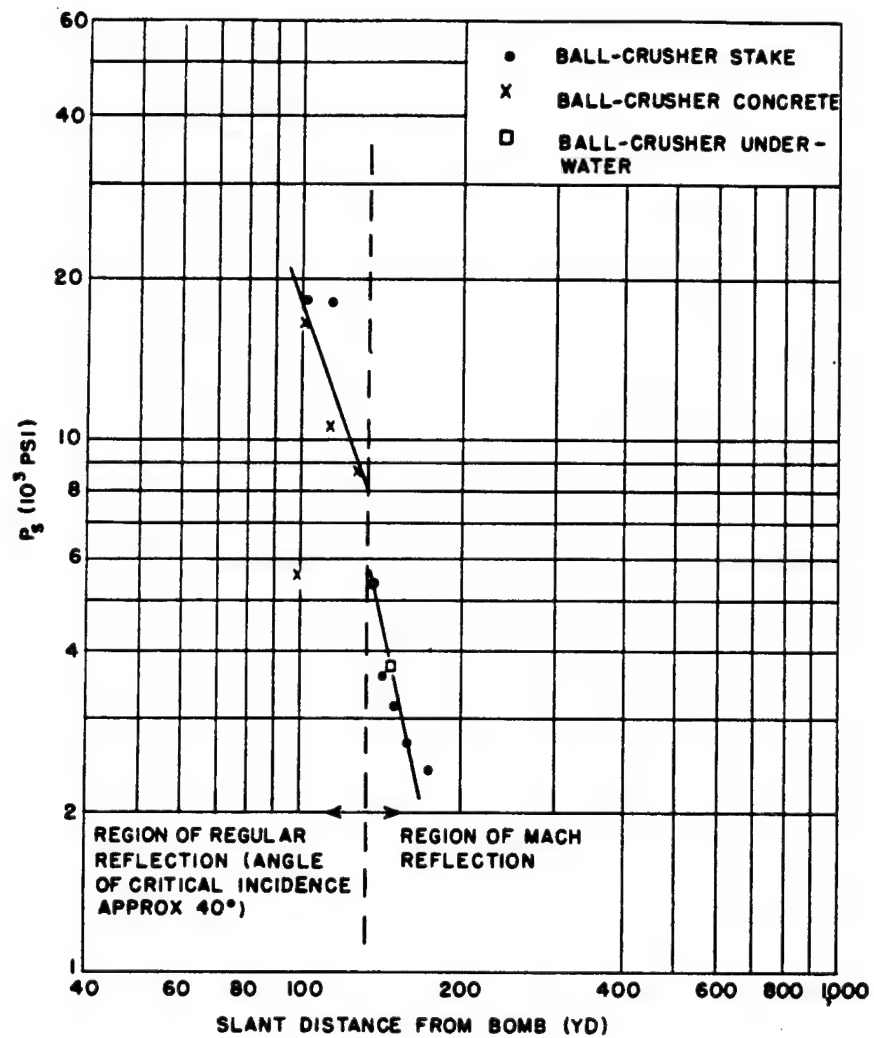


Fig. 3.28 Pressure on the Ground, Shot Easy

several gauges together they read similarly with good reproducibility. It is believed that these gauges responded faithfully to the pressure pulse statically or dynamically applied as the case may have been.

3.5 RESULTS FOR FREE-AIR MEASUREMENTS, SHOT EASY

Figure 3.29 shows the position of the free-air shock wave as a function of time as determined by the rocket smoke-trail-photography measurements on Shot Easy.

Figure 3.30 shows the calculated pressures in free air obtained from both rocket-trail data and the balloon-telemetering experiment. The dotted line is the extension of the high-pressure data using the standard blast curve to give the shape. It is clear that both rocket and telemetering data show a distinct jog in the curve which corresponds to a considerable amount of energy. Further discussion is to be found in Chap. 4.

Figure 3.31 presents some of the data obtained from the rocket-trail photography in the region of the triple point. The distance from ground zero to the Mach stem at a point near the triple point is plotted against time. As well as can be observed, the Mach stem at this point is a shock traveling in a direction determined by the radius from ground zero to the point. As time goes on, the altitude (i.e., angle made with the horizon) of this line changes.

On the supposition that the usual relation between velocity and pressure can be applied in this situation, the velocities were calculated from a least-squares fit of a cubic equation to the data, and the results are shown in Fig. 3.32. Comparison with free-air data shows that the Mach-stem pressures at the triple point are considerably higher than free-air pressures. Thus at $R_2 = 1,800$ yd the free-air pressure is 36 psi. When $R_2 = 1,800$ ft, reference to Fig. 3.33 shows that $R_1 = 1,940$ ft. Therefore, by Fig. 3.32, the Mach-stem pressure is 46 psi. Similarly at $R_2 = 1,100$ ft, $R_1 = 1,180$, and the corresponding free-air and Mach-stem pressures are 97 and 143 psi.

The solid line of Fig. 3.33 is drawn in where data exist and is extrapolated as a dotted line to the point where the theory of regular reflection indicates that the triple point is formed.

The dashed line is drawn at 45° merely to illustrate the difference between perfect spherical symmetry and the case of reflection under consideration.

Figure 3.34 shows the path of the triple point in dimensionless coordinates. The quantity h_0 is the height of the explosion above the reflecting plane, and in this case it is the tower height, 300 ft. Since the path of the triple point depends on the charge size as well as on the charge height, the curve shown may be applied to other explosions, provided only that

$$\frac{h_0 \text{ (ft)}}{[WRC(\text{lb})]^{1/3}} = 0.615.$$

3.6 RESULTS FOR SHOT GEORGE



3.7 COMPARISONS OF PRESSURE-TIME CURVES OBTAINED BY VARIOUS INSTRUMENTS

One of the more comforting features of the blast results was the general agreement among the various methods of measuring the pressure

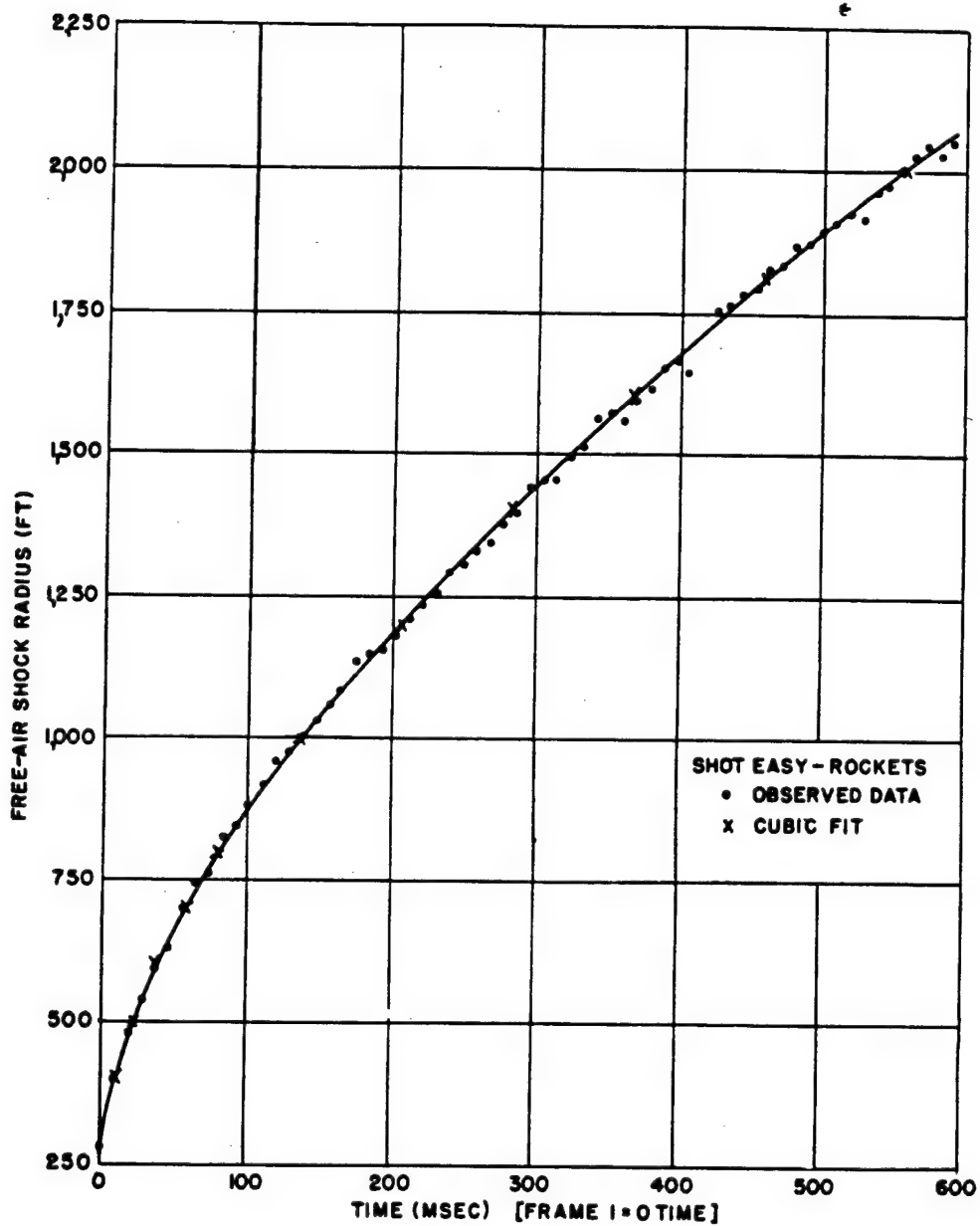
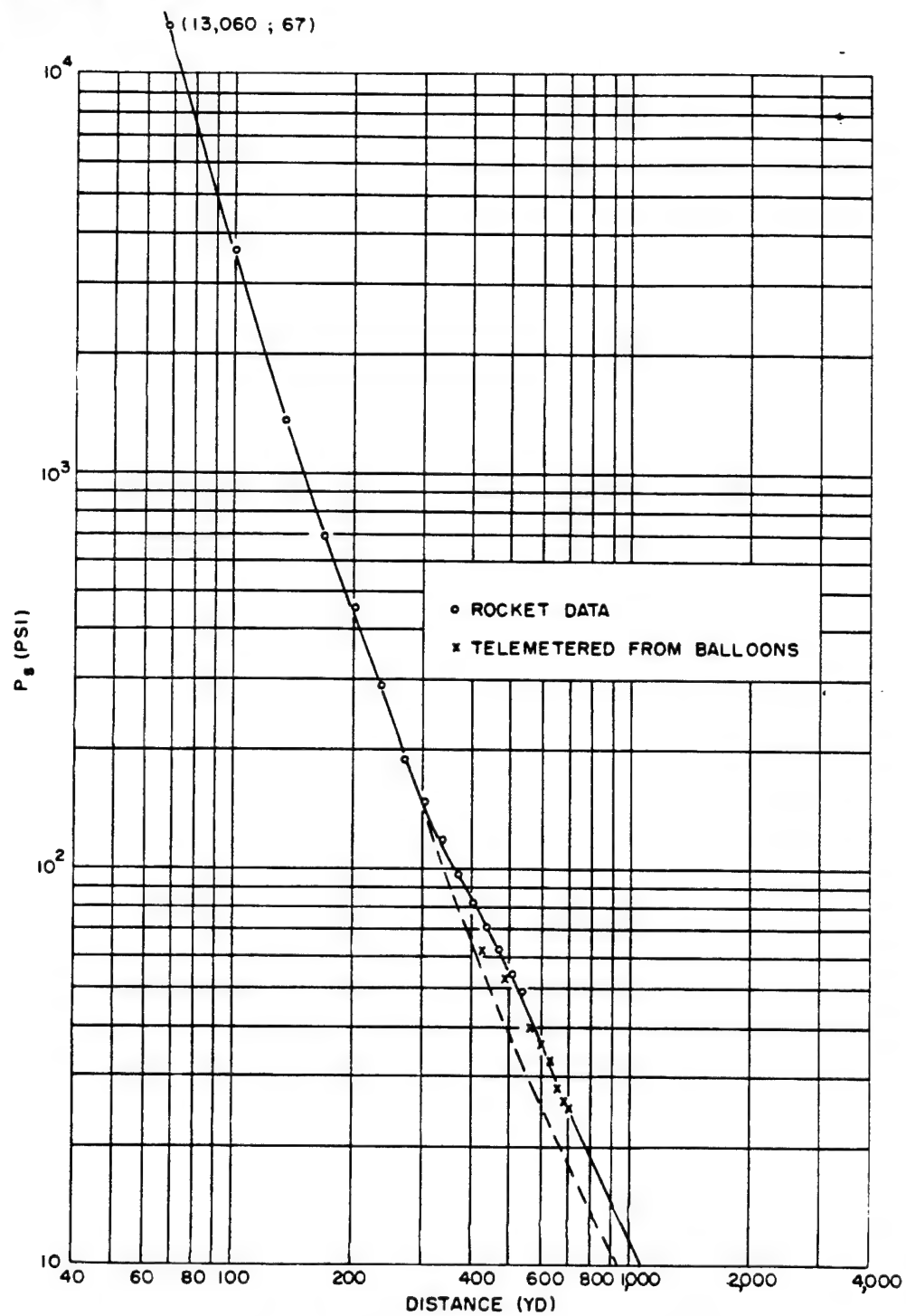


Fig. 3.29 Free-air Time of Arrival of Incident Wave vs Distance, Shot Easy



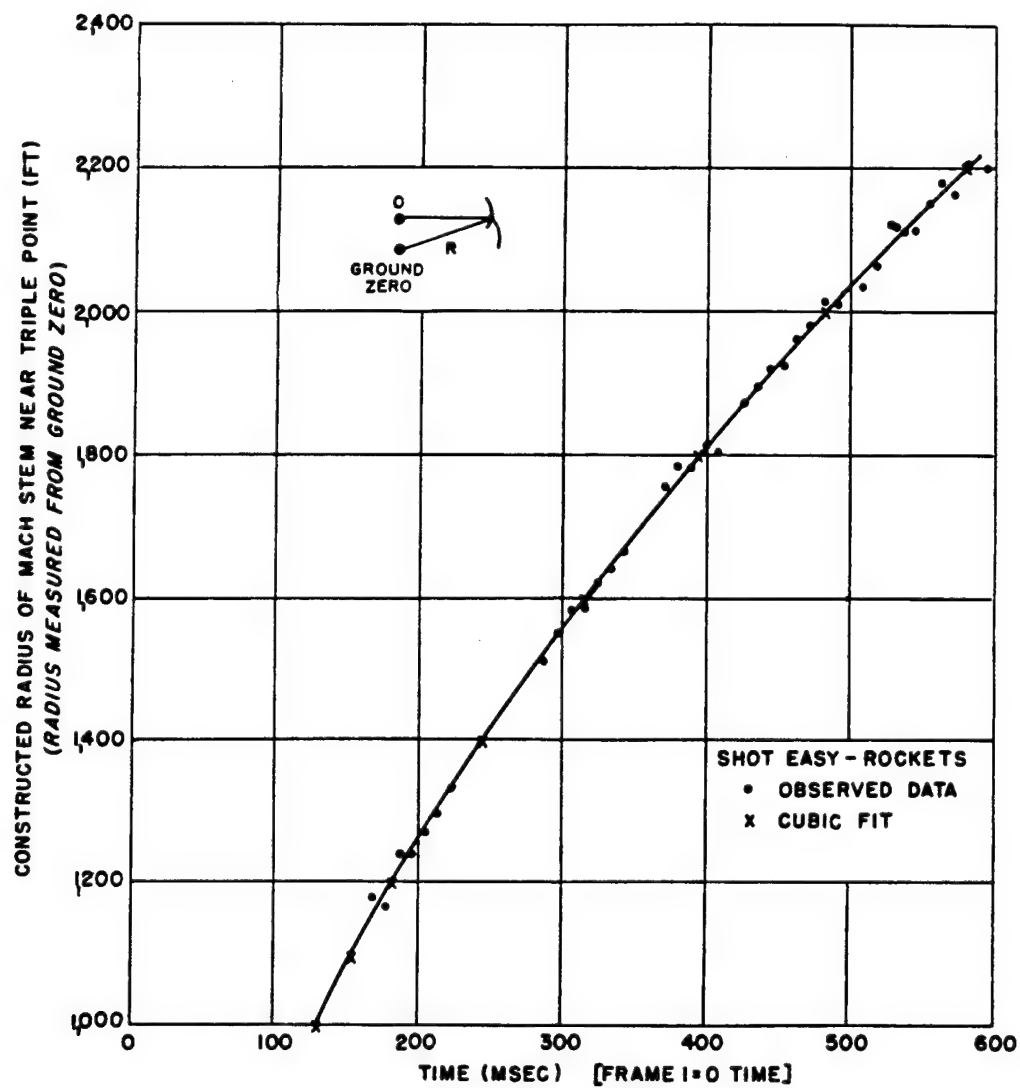


Fig. 3.31 Time of Arrival of Mach Stem near Triple Point vs Distance, Shot Easy

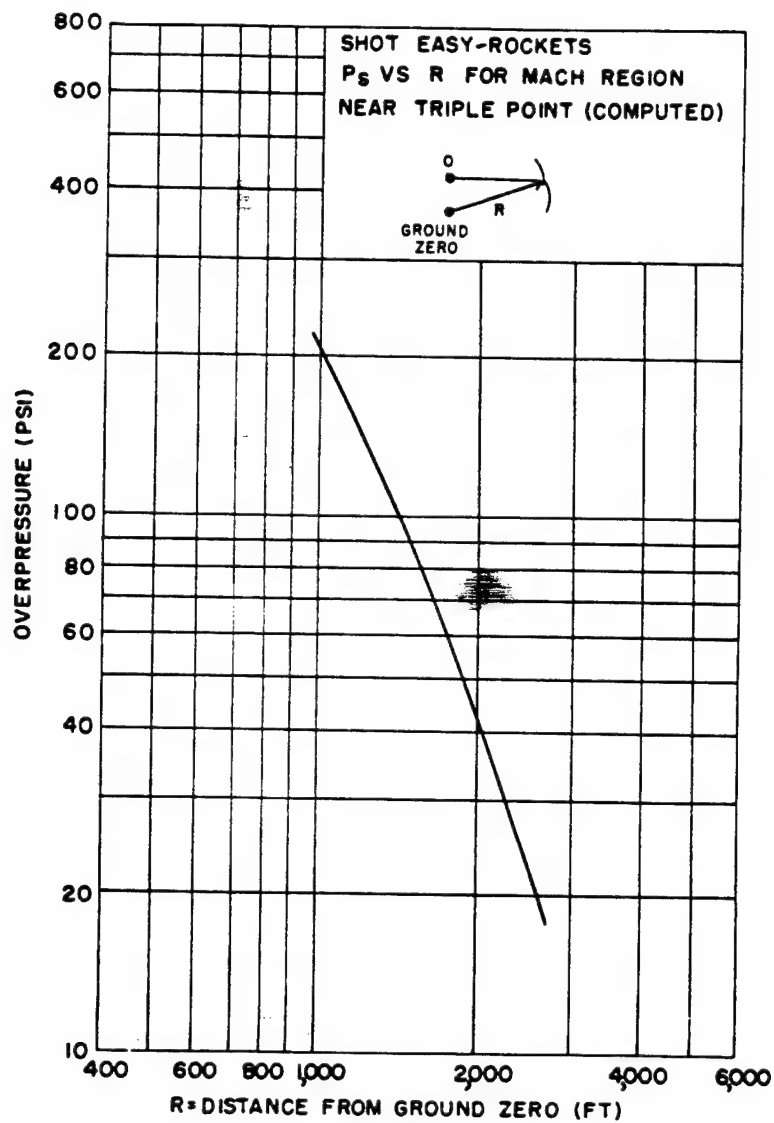


Fig. 3.32 Pressure of Mach Stem near Triple Point vs Distance from Ground Zero, Shot Easy

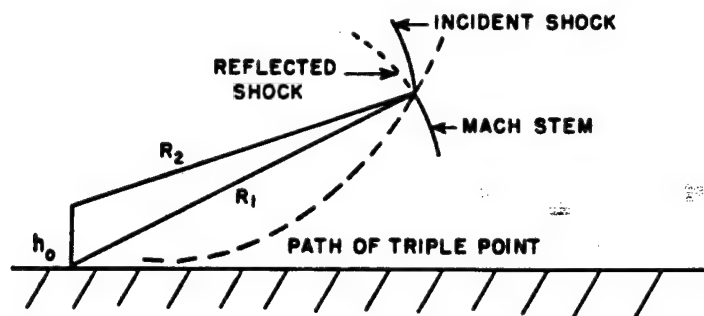
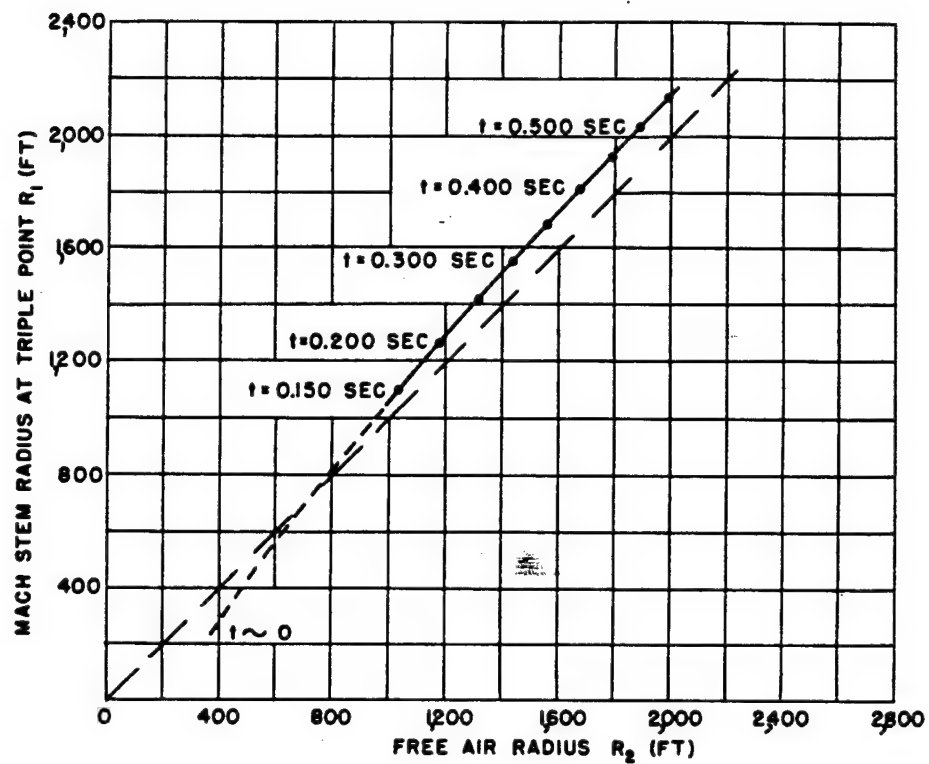


Fig. 3.33 Relation between Free-air and Mach-stem Radii at the Triple Point

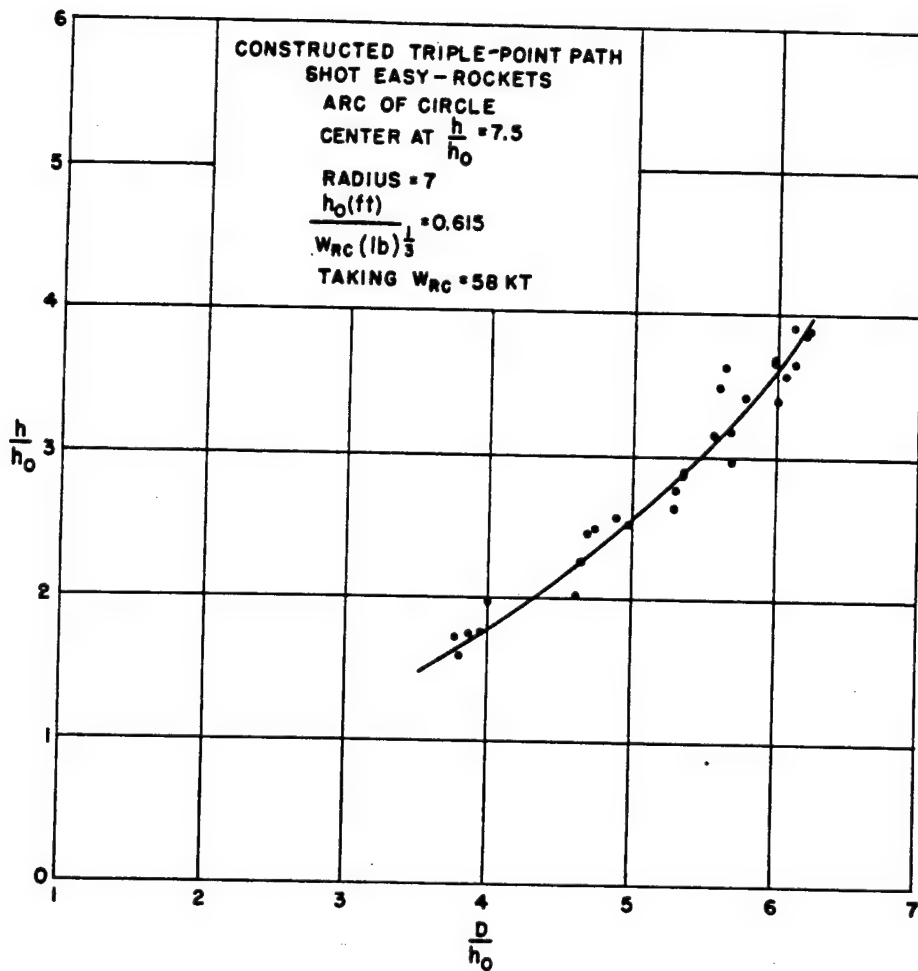


Fig. 3.34 Path of Triple Point, Shot Easy

Pages 105 through 110
 inclusive are deleted.
 DNA (b)(3)

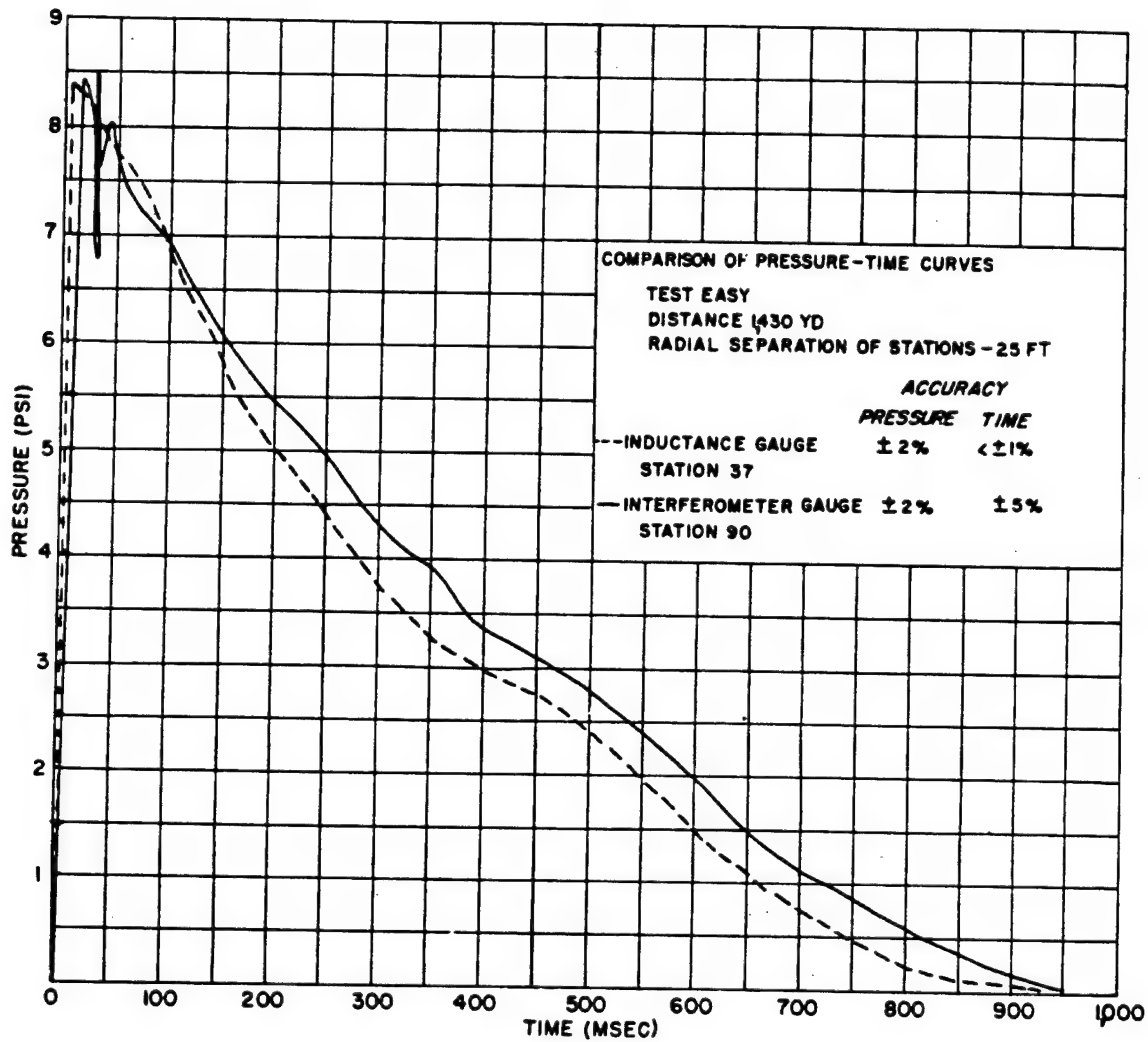


Fig. 3.40 Inductance Gauge; Interferometer Gauge; Shot Easy, 1,430 Yd

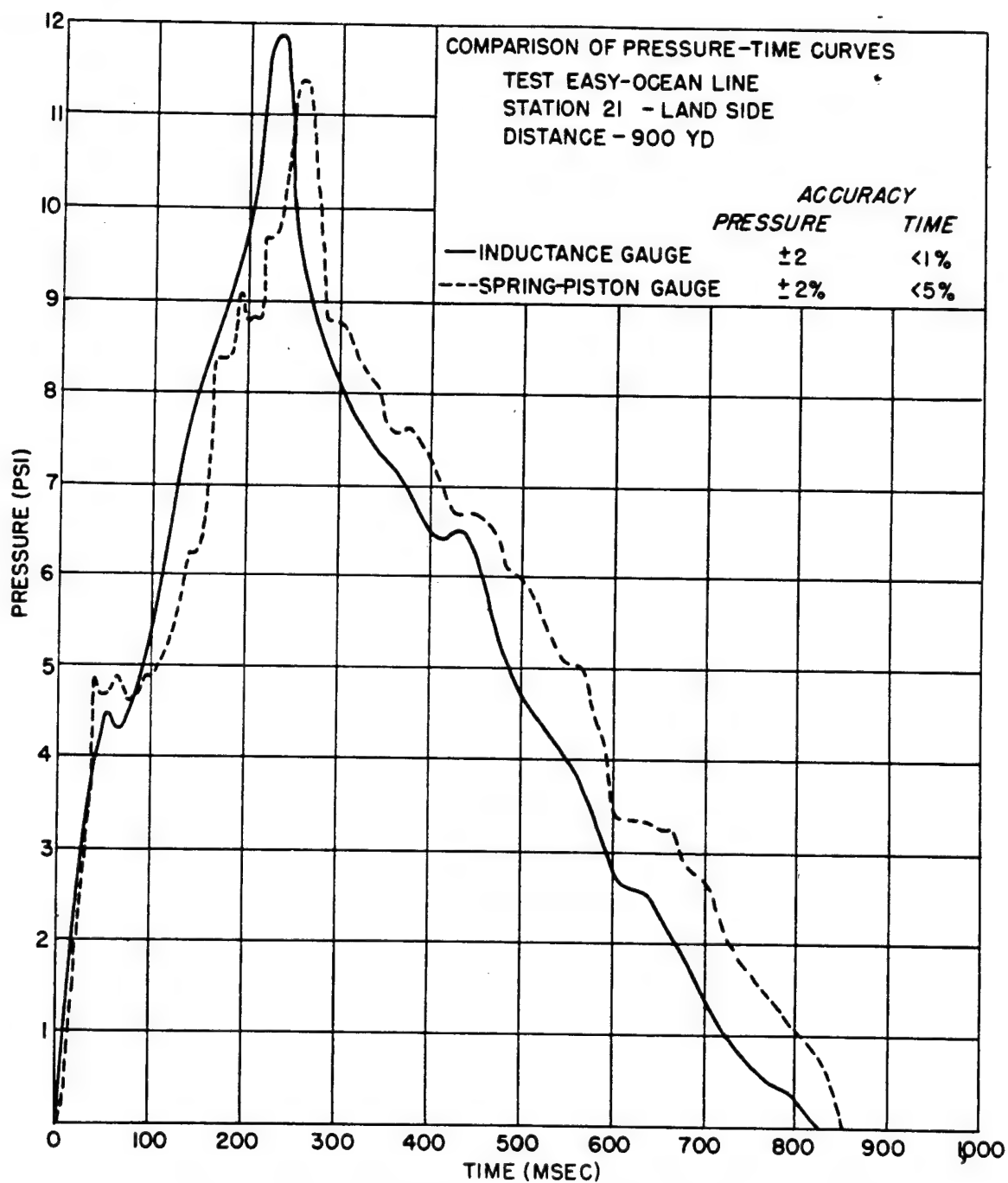


Fig. 3.41 Inductance Gauge; Spring-piston Gauge; Shot Easy, Ocean Line, 900 Yd

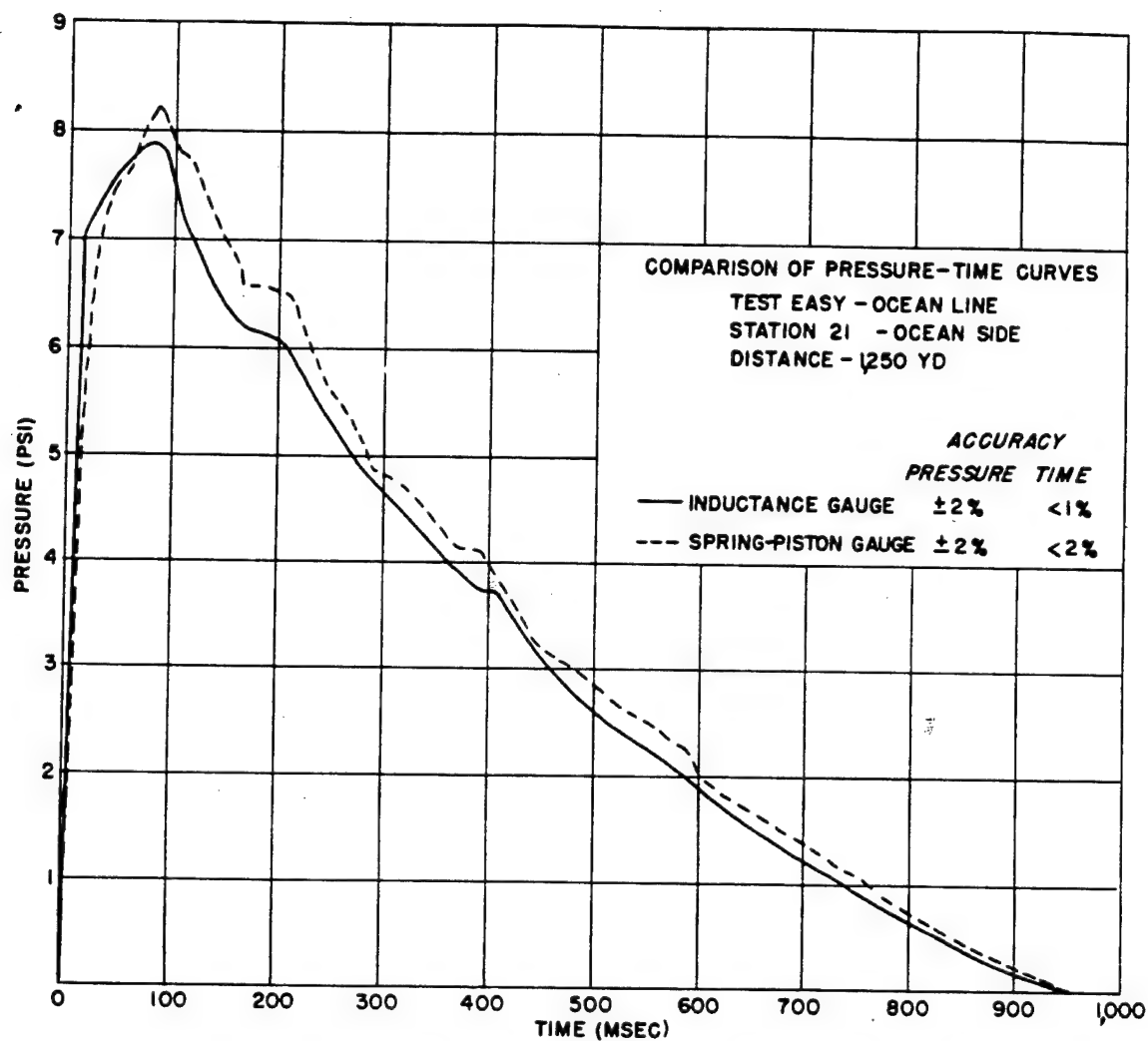


Fig. 3.42 Inductance Gauge; Spring-piston Gauge; Shot Easy, Ocean Line, 1,250 Yd

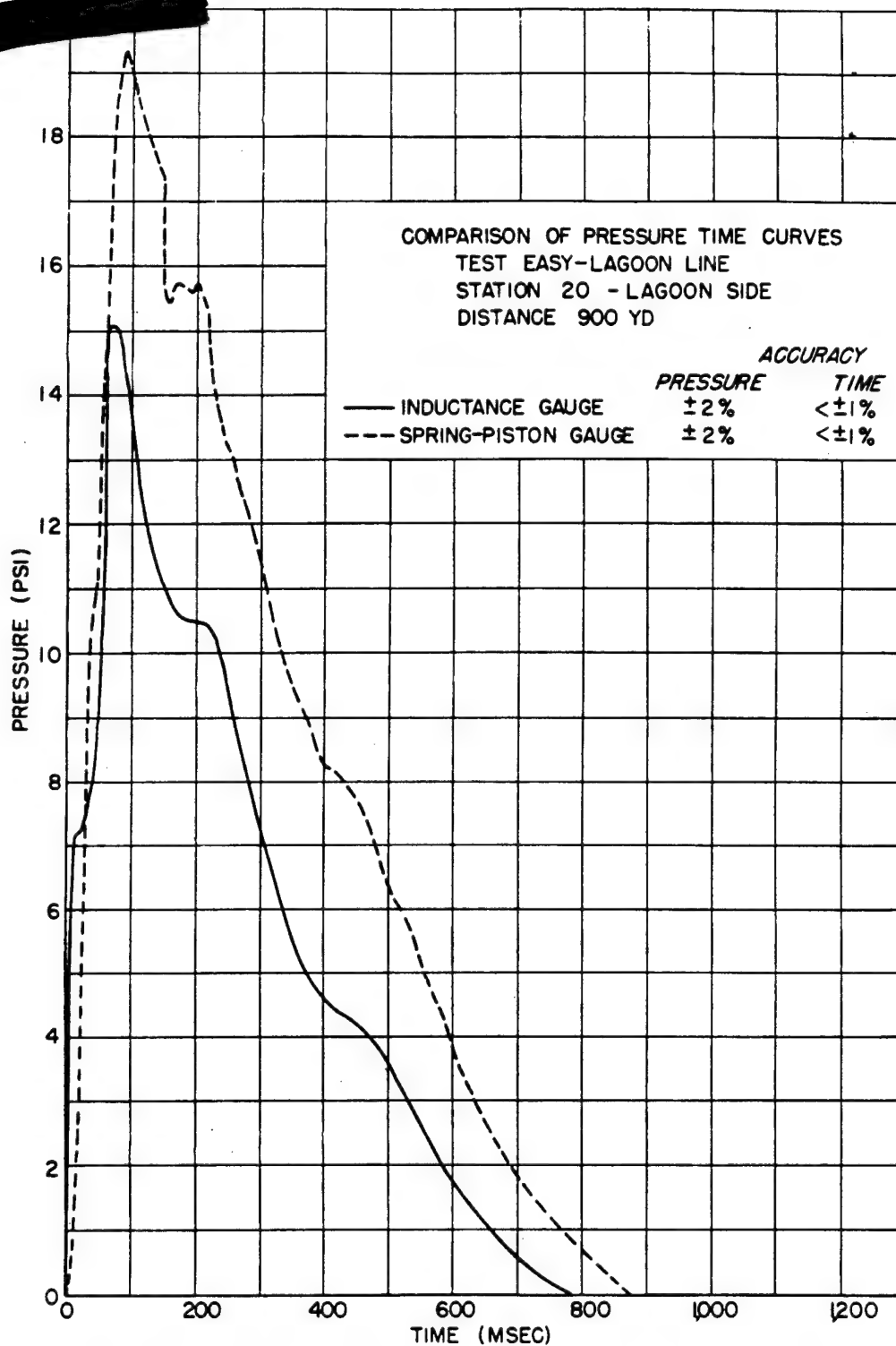


Fig. 3.43 Inductance Gauge; Spring-piston Gauge; Shot Easy, Lagoon Line, 900 Yd

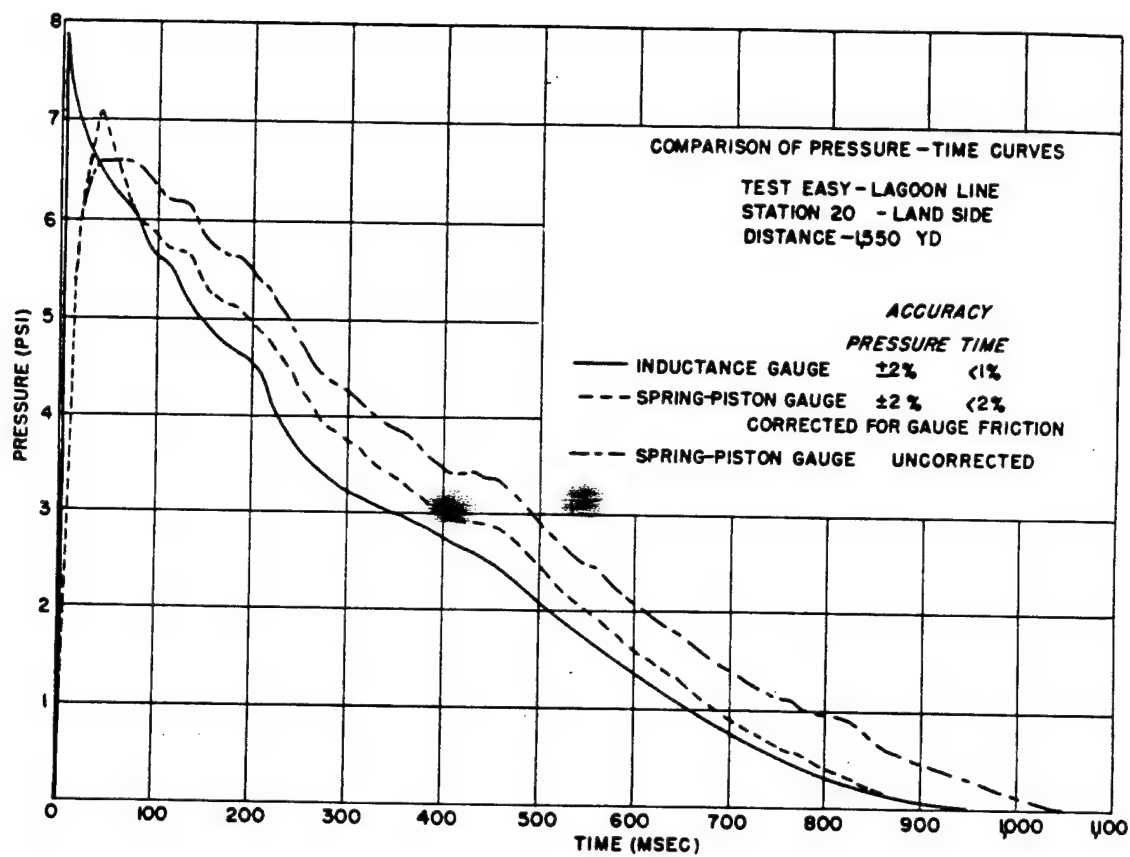


Fig. 3.44 Inductance Gauge; Spring-piston Gauge; Shot Easy, Lagoon Line, 1,550 Yd

[REDACTED]

as a function of time. In spite of the large number of gauges of all types that were used, there were relatively few that were placed closely enough together to make possible a detailed comparison of the records. A few examples of comparable readings have been culled, however, and the records have been re-plotted on the same scale in order to investigate the reality of the more detailed features. Figures 3.37 to 3.39 compare inductance and interferometer gauges at 1,450, 1,250, and 950 yd, respectively, on Shot Dog. The agreement is very good, although it is apparent that something happened to the time scale of one or both gauges at the closest distance. There is, however, little doubt of the finite rise time or of the multiple peak. Figure 3.40 shows similar agreement at 1,430 yd on Shot Easy. Agreement

between inductance gauge and spring-piston gauge is no less striking. Figures 3.41 and 3.42 display the records obtained at 900 and 1,250 yd, respectively, on the ocean line, Shot Easy. This line, along which the blast appeared particularly anomalous, produced the extraordinary pressure-time curve at 900 yd which would have to be confirmed to be believed. Figures 3.43 and 3.44 at 900 and 1,550 yd, respectively, lagoon line, Shot Easy, lend additional confirmation to the unorthodox shapes observed.

The data for the interferometer curves were obtained from John Kirk before publication of Greenhouse Report, Annex 8.2B. The inductance and spring-piston data are presented in Greenhouse Report, Annex 1.6, Part IV, by Price, Sokol, Vader, et al.

Chapter 4

Analysis of Results

4.1 ASSIGNMENT OF TONNAGES FROM BLAST MEASUREMENTS ON ATOMIC BOMBS

In this section all blast measurements made on Operations Greenhouse, Sandstone, and Crossroads are correlated.

4.1.1 Assignment of Radiochemical Tonnages from Blast Measurements

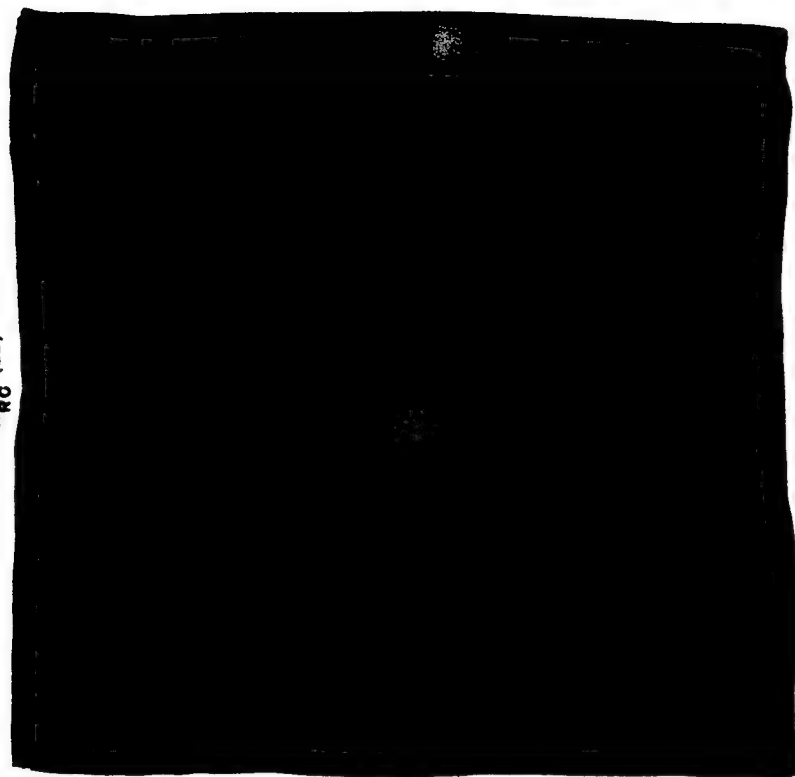
The problem of scaling up the results of high-explosive blast measurements to the equivalent sizes of atomic bombs is one of great difficulty mainly because of three previously undetermined factors: (1) the reflection coefficient, (2) the thermal-energy absorption by the adjacent ground surface, and (3) the explosive equivalence in free air of equal-energy tons of atomic and conventional high explosives. Advances have been made in the current set of experiments toward the evaluation of the third factor, and small-scale experiments have provided information concerning the reflection coefficient of blast waves from high explosives over various types of soil. The second factor must be inferred from field experiments and a knowledge of the other two factors.

It is, however, now possible to by-pass this somewhat involved process by utilizing the information already gained by previous experiments on atomic explosions and to predict directly the radiochemical tonnage by a knowledge of the distance at which an arbitrary pressure level is observed and comparison of this by direct scaling with the distance at which this same pressure level was obtained in previous atomic explosions of known radiochemical tonnages. This simple and straightforward procedure is complicated by the fact that almost all

atomic explosions have been at slightly different scaled heights above the ground and by the recently observed fact that there is a certain apparent variability of pressure wave shape as a function of distance and mass of material about the bomb. It is true, however, that beyond a critical distance and below a rather definite pressure level this variability of wave shape becomes negligible so that if the arbitrary pressure level is placed at or below this value these effects become very small. The effects of scaled height of explosion can be ascertained by plotting, in reduced coordinates as a function of scaled height of bomb, the distances at which this arbitrary pressure level (10 psi) is attained and then passing a curve through these points. These values have been plotted in Fig. 4.1, and a straight line has been drawn through the assembly of points. In this graph the ordinate is the radius in feet from the tower foot divided by the cube root of the radiochemical weight in pounds as defined in Sec. 2.1. The abscissa is the height of the bomb center in feet above the ground surface divided by the cube root of radiochemical weight as above. It is obvious from physical considerations that the curve cannot be a straight line over a large range, but sufficient information at the greater heights of detonation does not exist to warrant anything but a straight line being drawn here.

In order to use this graph for the determination of tonnages a standard TNT pressure-distance curve is passed through the points below about 8 psi and extended to the intersection of the 10-psi level in those cases where the coalescence of the secondary pulse occurs below the 10-psi level. This procedure could be carried out for a lower pressure level if desired, thus eliminating the necessity of extrapolation to the 10-psi level in some cases.

$$\frac{R (FT) (10 PSI)}{W_{RC} (LB)^{\frac{1}{3}}}$$



DNA
(b)(3)

$$\frac{h (FT)}{W_{RC} (LB)^{\frac{1}{3}}}$$

Fig. 4.1 Reduced Height vs Reduced Distance for Pressure Level of 10 Psi for All Atomic Explosions in Which Blast Was Measured

Table 4.1 gives the data from which the graph was produced.

In order to determine a radiochemical tonnage consistent with the data so far obtained for

nage was taken as 1.19 kt.

TABLE 4.1 RADIOCHEMICAL TONNAGES, HEIGHTS OF BOMB, RADIUS OF 10-psi LEVEL, AND REDUCED VALUES FOR VARIOUS ATOMIC EXPLOSIONS

Shot	Radius of 10-psi Level (yd)	Radiochemical Kilotonnage, W_{RC}	$W_{RC}^{1/3}$	Height of Charge, h (ft)	$\frac{h (ft)}{W_{RC}^{1/3}}$	$\left[\frac{R (ft)}{W_{RC}^{1/3}} \right]_{10 \text{ psi}}$
Able	1,066	21.9	352.5	520	1.475	9.072
X ray	1,070	36.7	418.0	200	0.4785	7.68
Yoke	1,260	47.5	455	200	0.439	8.300
Zebra	895	18.8	334	200	0.600	8.05
Trinity	960†	23.8	362	100	0.276	7.71

† Reduced to sea level.

Operations Trinity, Crossroads, and Sandstone the value is adjusted by trial and error until the reduced height and reduced distance at which 10 psi occurs give a point which lies on the line in Fig. 4.1. Values so arrived at are shown in Table 4.2. These values compared more or less favorably with preliminary radiochemical kilotonnages obtained in the field from fireball measurements, namely, Shot Dog, Shot Easy, 50; Shot George

As of approximately December 1951 the following radiochemical values were given to the authors by Maj Knauf of the editorial staff, Los Alamos Scientific Laboratory (LASL), on the edited rough draft copy:

Shot	Radiochemical Kilotonnage
Dog	
Easy	46.7 ± 0.6
George	

These values may be used to augment Fig. 4.1. Table 4.3 gives the additional data.

Point S on Fig. 4.1 represents the Operation Jangle surface shot using preliminary Ballistic Research Laboratories (BRL) velocity data. The 10-psi level occurred at 1,025 ft, the height of burst was 3.5 ft, and the radiochemical ton-

4.1.2 Method of Determining Blast Tonnage from Pressure Measurements

The question may be raised as to what actual weight of TNT placed with its center at the same location as the atomic bomb will produce the same pressure at the same distance. As shown in Sec. 4.2, the TNT and atomic blast curves are essentially parallel at sufficiently low pressure. Therefore a certain pressure level may be chosen, e.g., 10 psi, and the various reduced quantities at this level may be found. By referring to Fig. 2.4, for example, for explosions over clay the values of R_F are found for various reduced heights μ given in Table 4.4. By definition, $\lambda_r = \lambda_F R_F^{1/3}$ and $\lambda_F = 8.35$ for TNT at 10 psi. Therefore λ_r may be found, and the values are shown in the table. Figure 4.2 shows λ_r vs μ for TNT.

By means of Fig. 4.2 a blast tonnage may be assigned by an iterative process. Thus, a value of μ is assumed, and from the figure the value of λ_r is read. This, with the experimental knowledge of the distance at which the pressure was 10 psi, makes it possible to calculate a value

TABLE 4.2 RADIOCHEMICAL KILOTONNAGES DEDUCED FROM PRESSURE MEASUREMENTS AND PREVIOUS ATOMIC BOMB EXPERIMENTS

Shot	Radius of 10-psi Level (yd)	Height (ft)	Radiochemical Kilotonnage Required	Resulting Re- duced Height	Resulting λ_{10} psi
Dog					
Easy	1,240	300	47.6	0.66	8.15
George					

TABLE 4.3 RESULTS FOR OPERATION GREENHOUSE SHOTS

Shot	Radius of 10-psi Level (yd)	Radiochemical Kilotonnage Given	$W_{RC}^{1/2}$	$\frac{h}{W_{RC}^{1/2}}$	λ_{10} psi
Dog					
Easy	1,240	46.7	454	0.661	8.2
George					

TABLE 4.4 RELATION BETWEEN μ AND λ_r AT 10-psi LEVEL FOR TNT

Reflecting Medium	$\mu = \frac{h \text{ (ft)}}{[W_{TNT} \text{ (lb)}]^{1/2}}$	R_F	$\lambda_r = \frac{R}{[W_{TNT} \text{ (lb)}]^{1/2}}$
Clay	2.20	1.85	10.25
Clay	0.92	1.80	10.15
Clay	0.50	1.70	9.95
Clay	0.25	1.50	9.55
Clay	0.125	1.28	9.06
Water	1.50	1.90	10.32

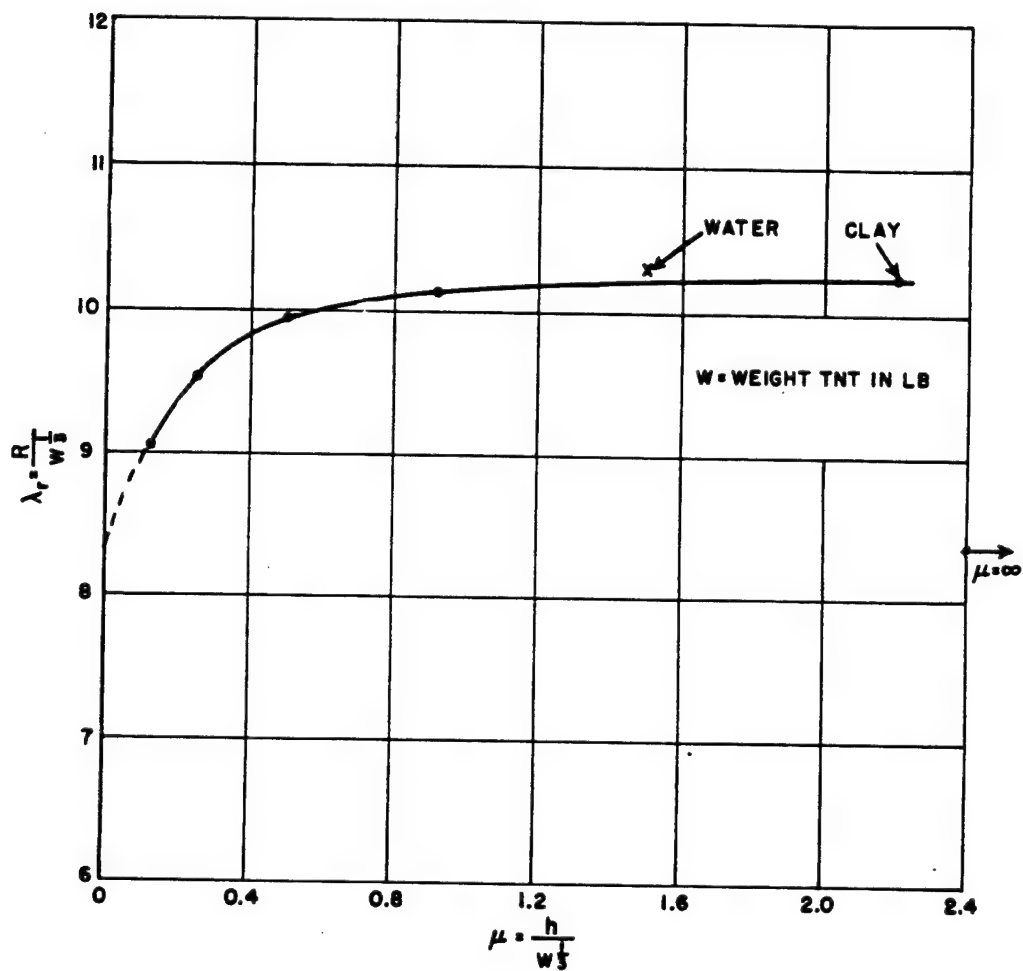


Fig. 4.2 Relation between Reduced Height and Reduced Distance at 10-psi Level for TNT

for W. With this value and the known height of the burst, a value of μ is found. This process may then be repeated until consistency is obtained. Table 4.5 gives the essential data for all instrumented bomb explosions to date and the results of such calculations.

case with high explosives. The G shot is more efficient than the remaining shots perhaps because the temperature of the fireball was lower and relatively less energy was lost by radiation or by the propagation of the shock wave at its most intense stages. The A shot is more effi-

TABLE 4.5 TONNAGES FOR ALL BOMBS

Shot	R (ft) for 10 psi	h (ft)	$\frac{h}{[W_{TNT} (lb)]^{1/3}}$	W_{TNT} (kt)	W_{RC} (kt)	$\frac{W_{TNT}}{W_{RC}}$
Dog						
Easy	3,720	300	0.81	25.0	46.7†	0.53
George						
Able‡	3,198	520	1.67	14.7	21.9	0.67
X ray	3,210	200	0.625	16.4	36.7	0.45
Yoke	3,780	200	0.53	27.3	47.5	0.58
Zebra	2,685	200	0.75	9.5	18.8	0.51
Trinity	2,880§	100	0.34	13.0	23.8	0.55

† Data from radiochemical analysis approximately December 1951.

‡ Using water reflection.

§ Reduced to sea level.

The ratio for W_{TNT} to W_{RC} for Shot Easy as determined along the ground at 10 psi is 25 to 47 or 0.53. The ratio at 10 psi, as determined by free-air measurements and discussed in Sec. 4.2, is 0.61. It appears that the bomb is slightly more efficient as a blast producer if the measurements are made high in the air rather than on the ground.

A blast efficiency defined as

$$Eff = \left(\frac{W_{TNT}}{W_{RC}} \right)_{10 \text{ psi}}$$

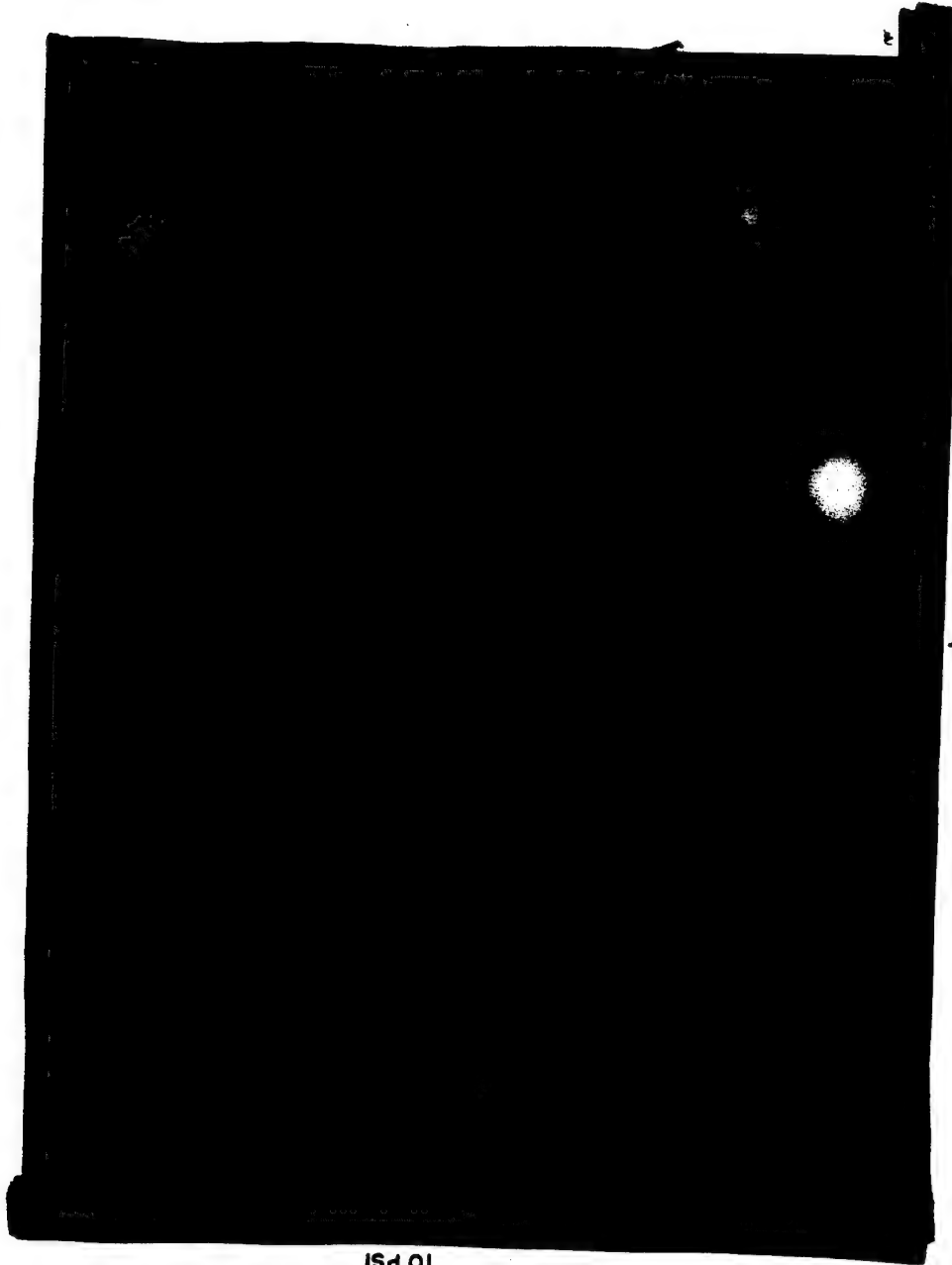
has been plotted for each explosion against reduced height in Fig. 4.3. Point S denotes the surface shot on Operation Jangle. The remaining points exhibit a scatter about a value of 0.58 for blast efficiency. The three shots S, G, and A are each special cases. The S shot is an efficient blast producer compared to high explosive in the same location, perhaps because of the failure of the crater to follow the geometrical scaling law. The nuclear explosion at ground level creates a smaller crater, and relatively more of its energy goes into blast than is the

cient perhaps because the experiment was conducted over water instead of over land so that a thermal layer could not form to the same extent to weaken the blast wave. The foregoing remarks are to be taken as tentative, but they illustrate that the wide variety of conditions represented by the explosions shown in Fig. 4.3 makes it difficult to generalize on the results.

The principal point seems to be that the blast efficiency does not depend on the fraction of the fireball cut off by the ground, Shot George having apparently more blast efficiency than Zebra or X ray.

The Bacher hypothesis advanced in Sandstone Report, Annex 5, Vol. 20, that energy was lost from the fireball into the ground for cases where the fireball was partly cut off and flattened by the ground is apparently incorrect since the blast efficiencies do not depend on reduced height, i.e., on fraction of fireball intercepted by the ground. This hypothesis was advanced in an effort to explain why the Sandstone blast tonnages were lower than the Able blast tonnage. The problem now can be reversed, and an explanation must be provided to

DNA
(6)(3)



$\left(\frac{W_{RC}}{W_{TNT}} \right)$
10 PSI

$\frac{h}{(W_{RC})^{\frac{1}{3}}}$

DNA
(b)(3)

Fig. 4.3 Blast Efficiencies of Atomic Bombs

account for Able being larger than the other bombs. It is conceivable either that Able was actually a more efficient blast producer for some reason or other, or that the blast was channeled owing to propagation over a slightly cooler air layer next to the water surface, or that the foil meters biased the blast curve to a somewhat higher general level since foils have been shown in Greenhouse to read somewhat higher under field conditions than when calibrated in the laboratory.

4.1.3 Trinity Blast Data Reduced to Sea Level

The blast data for Trinity are very sketchy. A few velocity points and a scatter of foil-meter points¹ allow a standard blast curve to be visually fitted. The curve and points are shown in Fig. 4.4. The distance at which 10 psi occurs is approximately 930 yd. In order to compare with other atomic bomb blast data it is necessary to reduce this to sea level. The altitude of Alamogordo, N. Mex., is given² as 4,303 ft. However, in Report LA-1012 the exact location of the Trinity site is given³ as 33°40'31" north latitude and 106°28'29" west longitude. A Geological Survey contour map prepared by M. H. Dardon from 1913 to 1918 data shows the altitude of this spot as 5,100 ft. It is therefore assumed that 5,100 ft is the proper altitude to use. According to the U. S. standard atmosphere the ambient pressure at this altitude is 12.2 psi or 0.83 atm. The relative overpressure at 930 yd is 10.0/12.2 or 0.82. This same relative overpressure will occur at sea level at a $\lambda_{\text{sea}} = (0.83)^{1/2} \lambda = 0.940\lambda$ or at a distance which is about 6 per cent closer. The overpressure at this distance at sea level is 0.82×14.7 or 12.0 psi. It is therefore concluded that the Trinity bomb exploded at sea level would have produced an overpressure of 12.0 psi at a distance of 930×0.940 yd or 874 yd. From this the 10-psi level is found to occur at 960 yd or 2,880 ft. What weight of TNT placed 100 ft above ground at sea level will produce 10 psi overpressure at 2,880 ft? This turns out to be 13.0 kt TNT, using the reflection data of Fig. 4.2. Taking the radiochemical kilotonnage as 23.8, the blast efficiency for Trinity is set at 0.55.

Note: According to information received after the preparation of this report, Manhattan District Report 112/15 gives the altitude for the Trinity explosion (including tower height) as 4,724 ft. The altitude correction for this height is sub-

stantially the same as that for the height used in the text.

4.1.4 Shot Able Water-intersection Data in the Regular Region

Aerial photography on Shot Able gave data on the rate of growth of the horizontal circle of spray under the bomb caused by the intersection of the expanding shock front with the water surface.⁴ If the observed velocity in the region of regular reflection is denoted by V , then the incident shock velocity U is given by $U = V \sin \alpha$, where α is the angle of incidence of the shock. Taking the ambient velocity of sound as 1,140 ft/sec, the relevant quantities are shown in Table 4.6.

The value of 12.6 gives an initial energy ratio of $12.6/21.9 = 0.575$ at high pressures in free air. As may be seen in Sec. 4.2 the corresponding value for Shot Easy at high pressures in free air is 0.33. Similarly, at the 10-psi level the ratios of blast to total tonnage are 0.67 and 0.50 for Shots Able and Easy, respectively. This indicates an increase of 9 per cent of the total energy added to the blast wave on Shot Able by means of the adiabatic wave mechanism discussed in Chap. 5. The initial energy ratio of 0.575 being so much larger than the Easy ratio of 0.33 is an indication that Able was a more efficient blast producer or that the measurements are in error, or both.

The scatter of measurements is great on Able, and their absolute reliability is small. In particular the deduction of tonnage based on free-air measures just given is exceedingly tenuous, depending on differentiation at the end of a series of points. There is a further difficulty that the time scale assigned in Ref. 4 is extremely uncertain. It is concluded that the measurements of blast on Able are too uncertain to permit any serious concern over disagreements between Able and other bombs.

4.2 FREE-AIR-PRESSURE-DISTANCE CURVE FOR SHOT EASY

A free-air pressure vs reduced-distance curve has been drawn in Fig. 4.5, taking the radiochemical kilotonnage for Easy as 47. The curve is fitted approximately by the following relations:

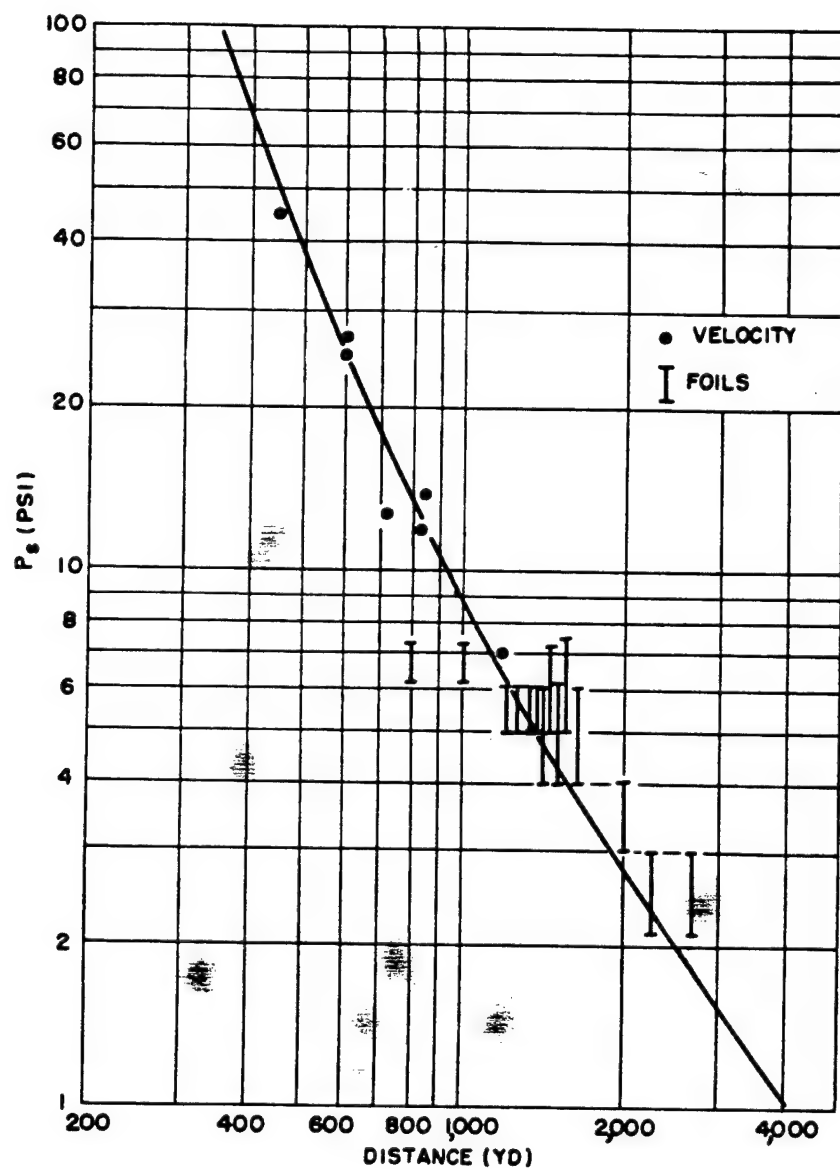


Fig. 4.4 Trinity Data

$P_s = 930\lambda^{-3.16}$ where $10,000 > P_s > 1,500$; $\lambda < 0.905$
 $P_s = 957\lambda^{-2.82}$ where $1,500 \geq P_s \geq 150$; $\lambda > 0.905$

The values of P_s calculated by these formulas are within 1 per cent of the curve throughout the range of validity. The validity of the first formula may extend well beyond pressures of 10^4 .

At 150 psi, before the adiabatic wave has influenced the initial shock wave, $\lambda_{RC} = 1.96$ and $\lambda_{TNT} = 2.65$, from which $W_{TNT} = 0.40W_{RC}$.

If an atomic bomb releases 1 kt of energy (4.20×10^{18} ergs), then to produce the same peak pressure at the same distance, 0.40 kt of TNT would be needed at the 150-psi level and

TABLE 4.6 ANALYSIS OF SHOT ABLE IN THE REGION OF REGULAR REFLECTION

Distance from Bomb								
Foot (ft)	V† (ft/sec)	sin α	U (ft/sec)	U C ₀	P _s ‡ (psi)	TNT§	W _{TNT} (kt)	
400	6,700	0.61	4,090	3.58	206	2.30	11.5	
500	5,620	0.69	3,880	3.40	185	2.41	13.3	
600	4,600	0.76	3,500	3.07	146	2.68	13.1	
						Av.	12.6	

† Taken from Ref. 4.

‡ See Sec. 2.3.

§ See Sec. 2.1.

It will be observed that there is a bulge in the atomic bomb curve starting at about 145 psi and ending at about 40 psi. This is taken to mean that energy in the form of an overtaking adiabatic wave is being added to the shock wave. In the Mach region this transition occurs at a greater distance presumably because, owing to reflection, both waves travel faster. After the point of catch-up, the single coalesced shock behaves like the single detached shock from an ordinary high-explosive source. At 10 psi the value of λ_{RC} , as calculated from radiochemical data (47 kt), is 7.1 and the value of λ_{TNT} is 8.35. Hence $W_{TNT} = 0.61W_{RC}$. This quantity 0.6, the ratio of W_{TNT} to W_{RC} , shall be considered the blast efficiency of an atomic explosion. It is clear that a smaller energy in the form of TNT can be released to produce a pressure of 10 psi at the same distance. Therefore TNT is a more efficient blast producer than nuclear explosives. The reason for this is that the blast wave from TNT starts out at much lower pressures than the blast wave from atomic bombs and therefore is able to propagate outward with smaller dissipation of energy. The entropy increase becomes quite significant for very strong shocks.

0.62 at the 10-psi level. This means that the second wave adds the blast effectiveness of $0.60 - 0.40 = 0.20$ kt of TNT. If it is assumed that all the TNT energy goes into blast (and this is the assumption made by Kirkwood et al. in their calculations) and that the second wave is adiabatic and hence travels without loss of energy, then it can be stated that 20 per cent or approximately one-fifth the total bomb energy goes into the second wave. The amount of energy that goes into the first shock is actually considerably more than 40 per cent since this shock has traveled out with large entropy increase near the bomb.

4.2.1 Comparison of Shots Dog and Easy, Free Air

Three points in the free-air region on Shot Dog were obtained by the balloon-telemetering method. The validity of these points may be checked by comparison with Shot Easy data on a reduced basis. Figure 4.6 shows that there is good agreement between the shots, provided [redacted] is chosen for the yield of Shot Dog and 47 kt for the yield of Shot Easy. These

DNA
(b)(3)

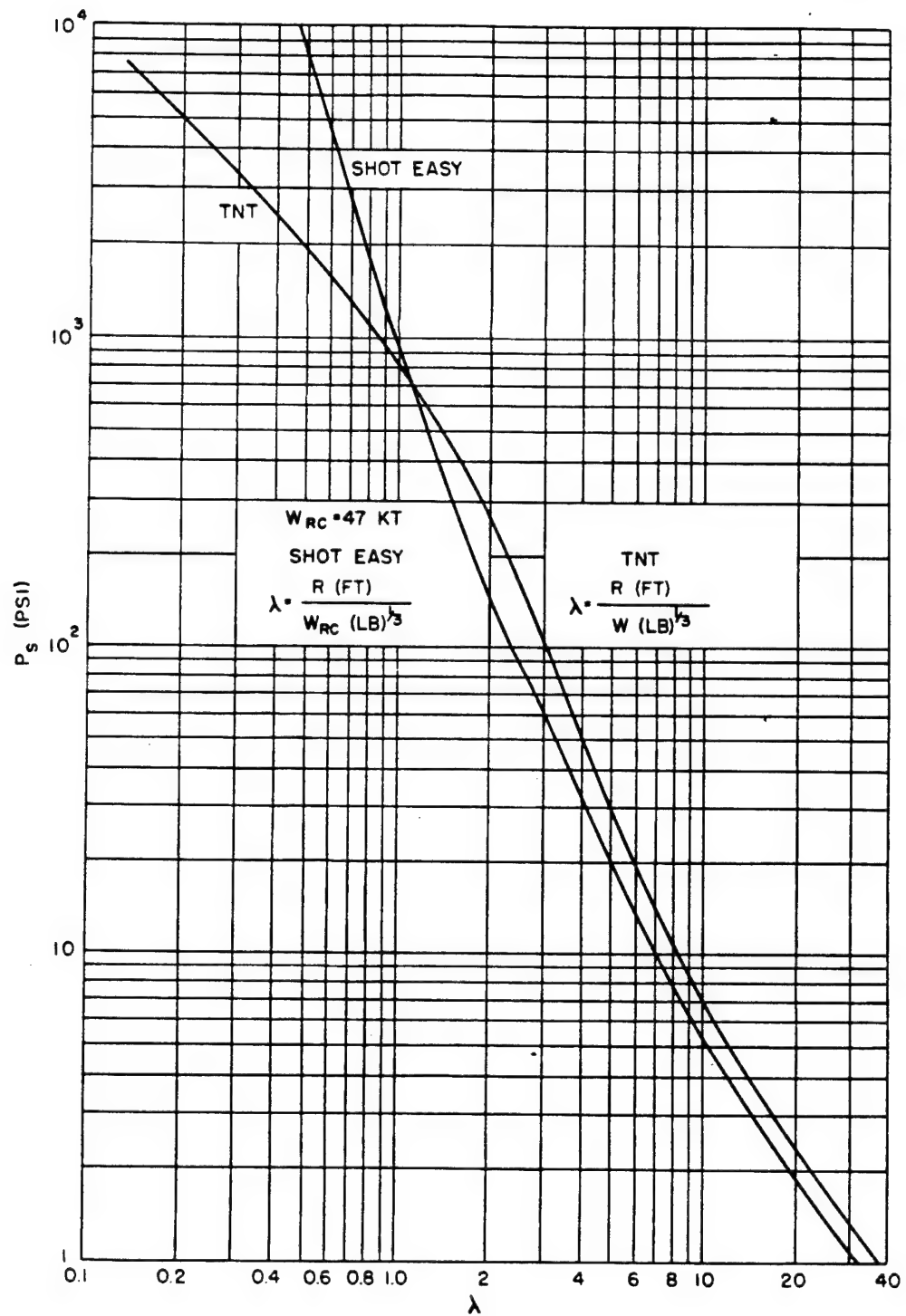


Fig. 4.5 Free-air Pressure vs Reduced Distance; Atomic Bomb and TNT Compared

P_a (PSI)

DNA
(b)(3)

$$\lambda = \frac{R}{W^{\frac{1}{3}}} \left(\frac{FT}{(LB)^{\frac{1}{3}}} \right)$$

Fig. 4.6 Free-air Pressure vs Reduced Distance; Shots Dog and Easy Compared

values were chosen because the preliminary blast measurements along the ground on Dog [REDACTED] and on Shot Easy gave 47 kt. The latter value is identical with the radiochemical value of 47. The radiochemical value [REDACTED] for Shot Dog, on the other hand, does not give so good agreement between the two shots.

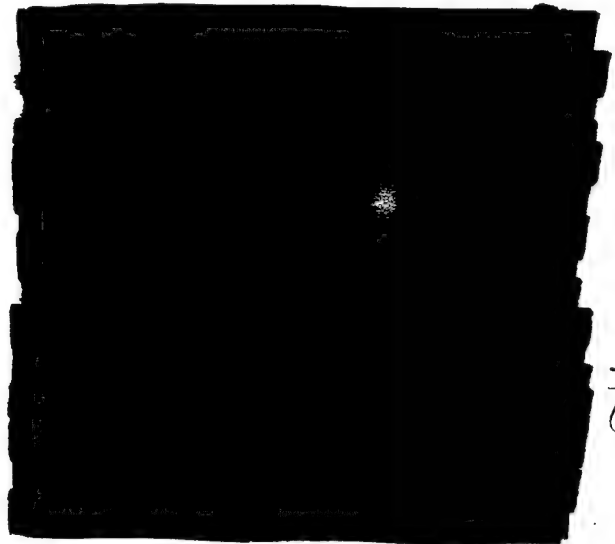
4.3 COMPARISONS AMONG VARIOUS SHOTS

In this section are to be found composite graphs of various measured quantities plotted in reduced coordinate.

4.3.1 Pressure



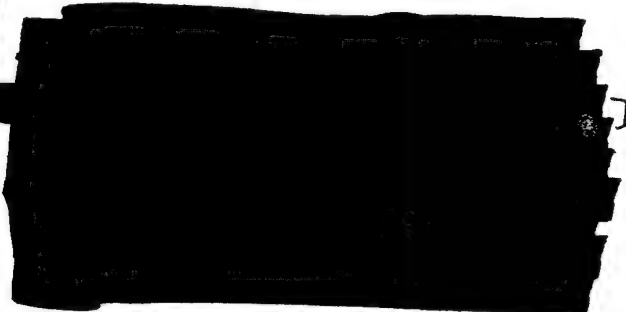
4.3.2 Impulse



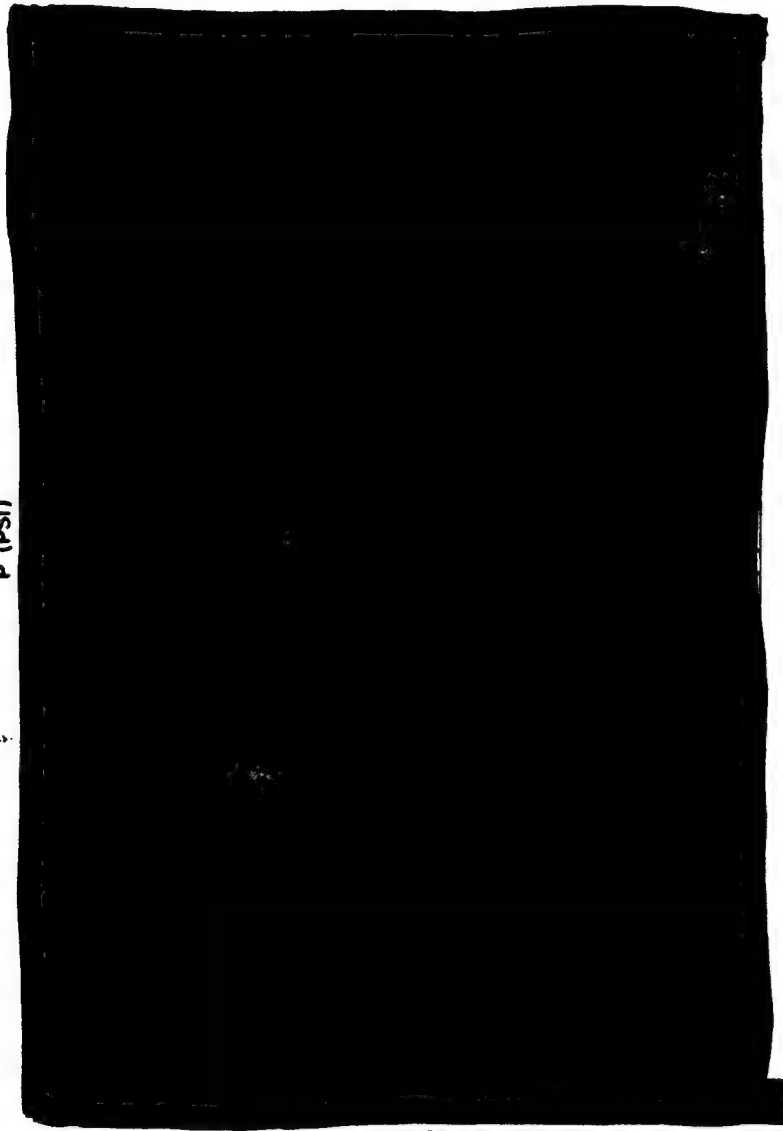
4.3.3 Positive Duration



4.3.4 Reduced Negative Quantities



P (psi)



DNA
(b)(3)

$$\lambda = \frac{R}{(w_{RC})^{\frac{1}{3}}}$$

Fig. 4.7 Peak Pressure by the Velocity Method vs Reduced Distance

DNA
(b)(3)

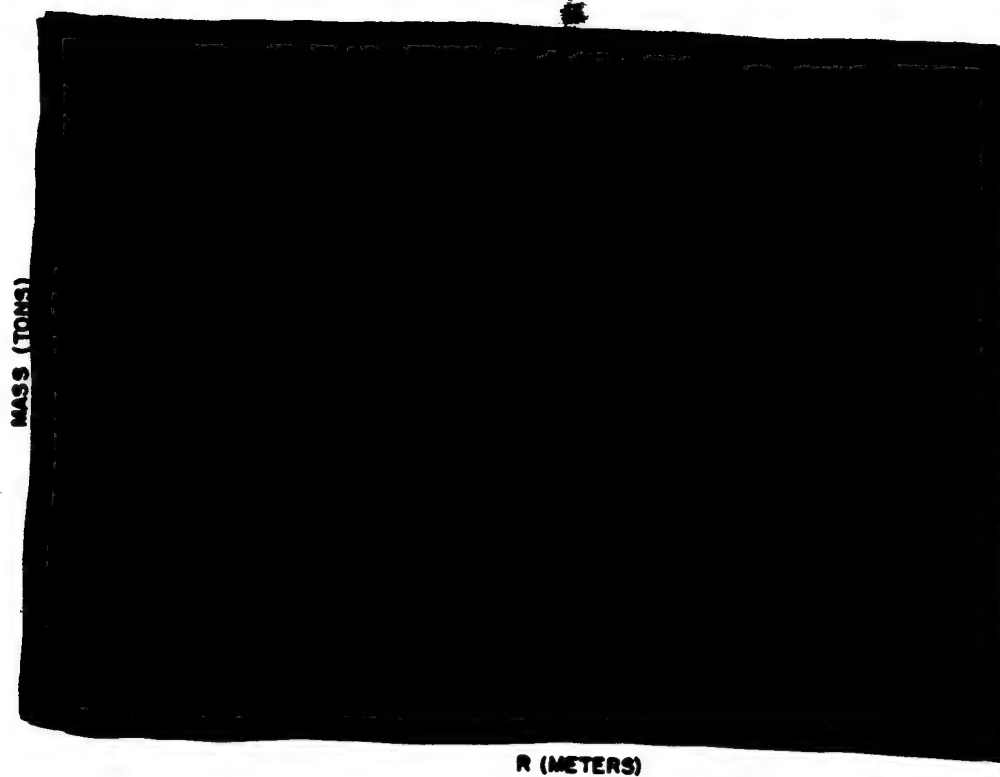
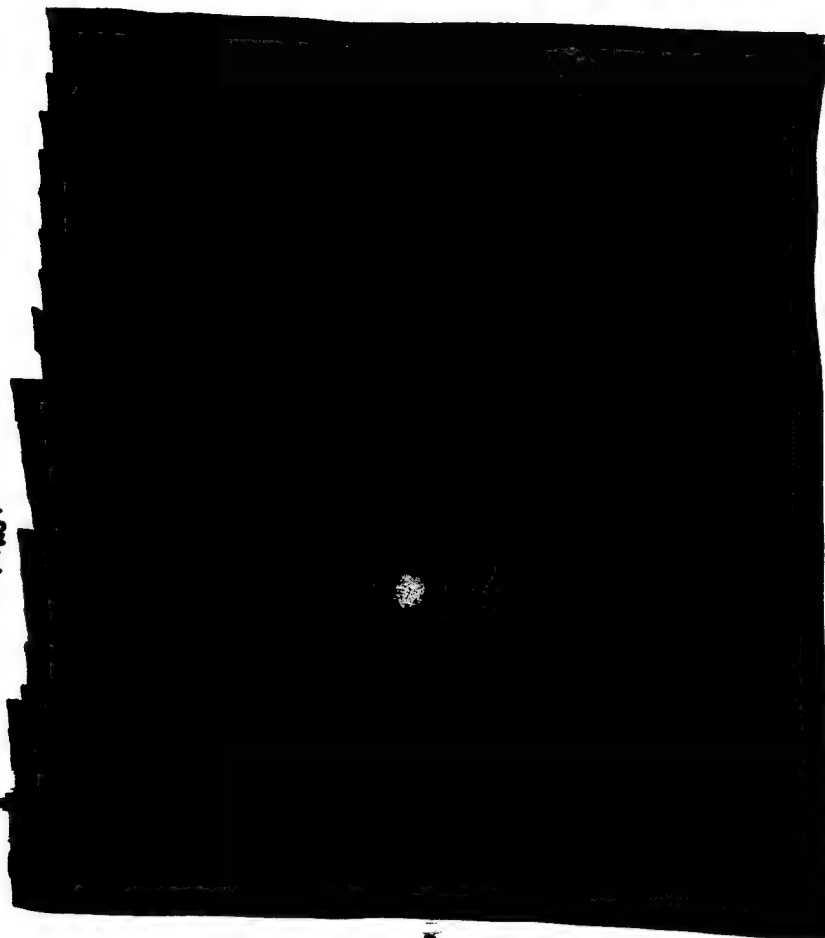


Fig. 4.8 Mass of Fireball vs Radius for Shots George and Easy

$$\frac{I}{(W_{RC})^{\frac{1}{2}}}$$



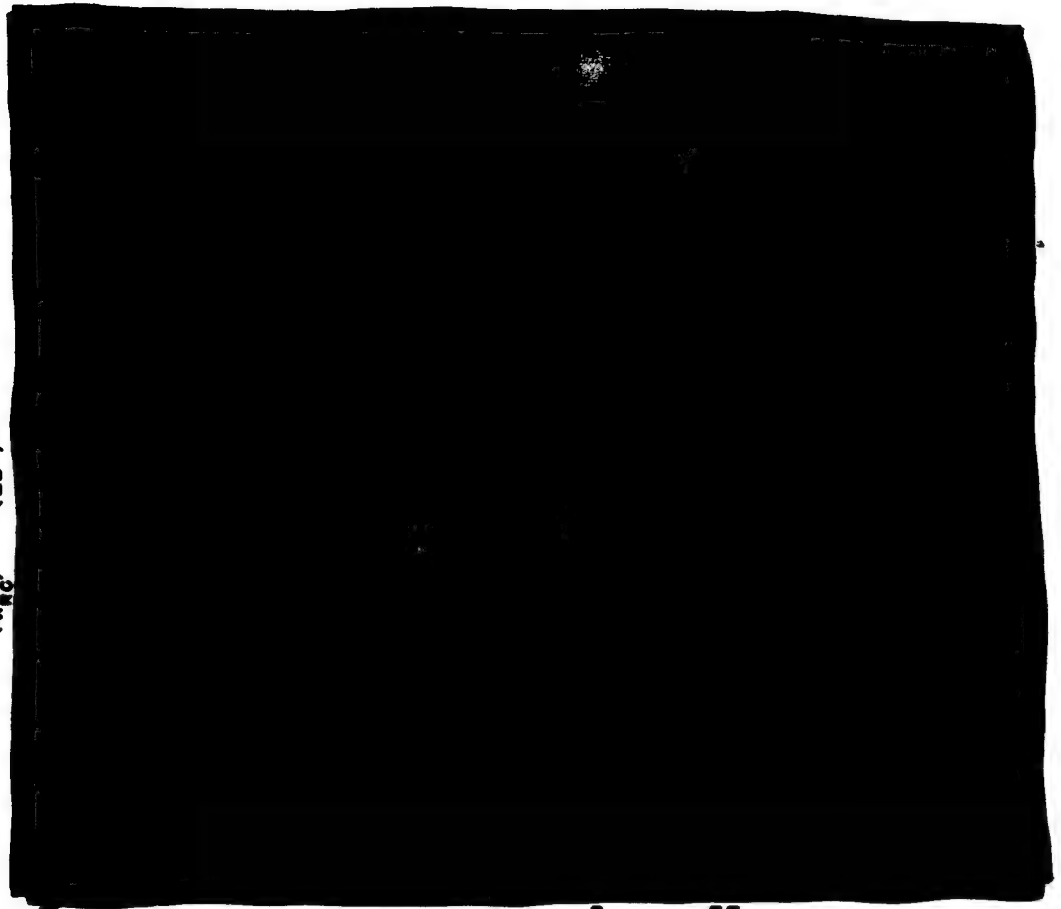
DNA
(b)(3)

$$\lambda = \frac{N}{(W_{RC})^{\frac{1}{2}}}$$

Fig. 4.9 Reduced Positive Impulse vs λ

DNA
(b)(3)

$$\frac{T_0}{(w_{RO})^{\frac{1}{3}}} \left(\frac{SEC}{(LB)^{\frac{1}{3}}} \right)$$



$$\lambda = \frac{R}{(w_{RO})^{\frac{1}{3}}} \left(\frac{FT}{(LB)^{\frac{1}{3}}} \right)$$

Fig. 4.10 Reduced Positive Duration vs λ

P_n (PSI)

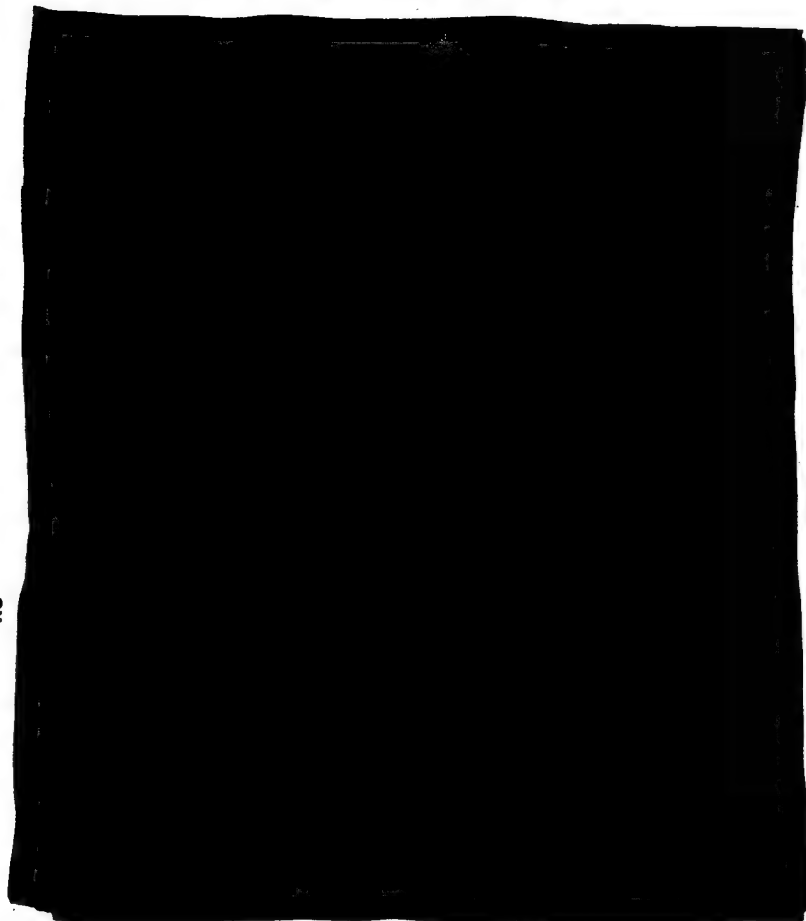
DNA
(b)(3)

$$\lambda = \frac{R}{(W_{RO})^{\frac{1}{3}}} \left(\frac{PT}{(LB)^{\frac{1}{3}}} \right)$$

Fig. 4.11 Reduced Negative Pressure vs λ

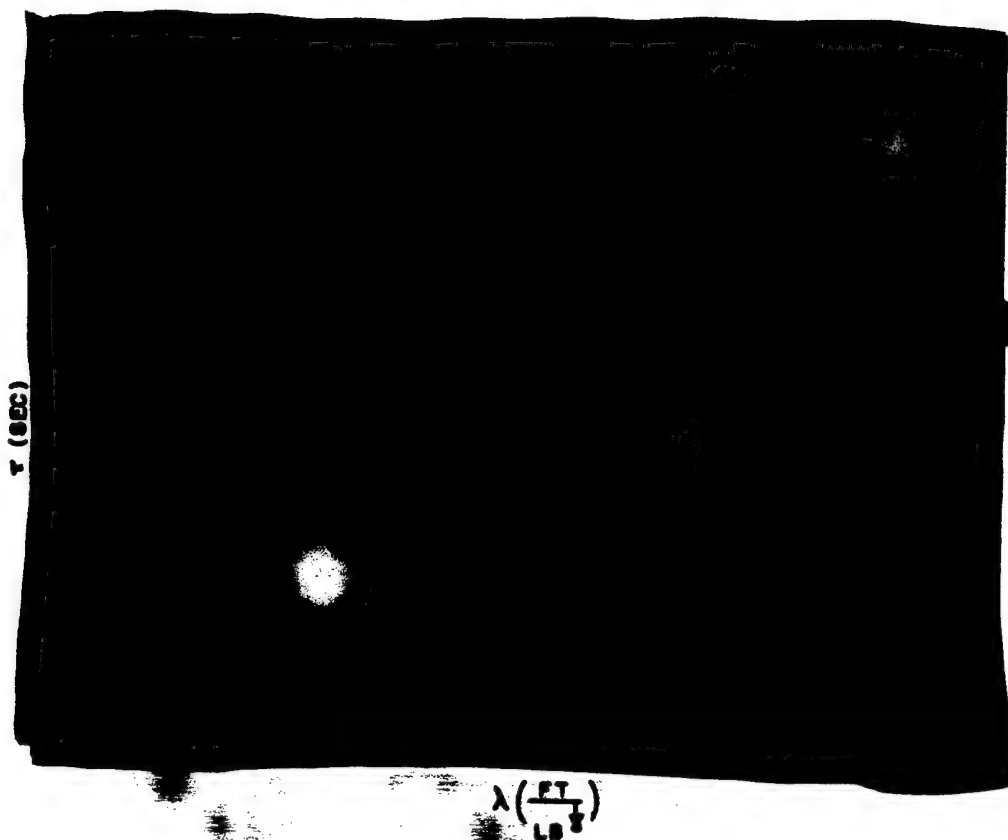
DNA
(b)(3)

$$\frac{I}{(W_{RC})^{\frac{1}{3}}} \left(\frac{PSI SEC}{LB^{\frac{1}{3}}} \right)$$



$$\lambda = \frac{R}{(W_{RC})^{\frac{1}{3}}} \left(\frac{FT}{(LB)^{\frac{1}{3}}} \right)$$

Fig. 4.12 Reduced Negative Impulse vs λ



DNA
(b)(3)

Fig. 4.13 Reduced Negative Duration vs λ

4.3.5 Decay Parameter for Pressure-time Curves

It is well known that conventional blast waves exhibit a rate of decay of pressure at a given distance which can be closely approximated for a short time by an exponential function. If the pressure-time relation of a blast wave has the form

$$P_s = P_{sm} e^{-t/\theta^*},$$

where P_s is excess pressure at time t and P_{sm} is excess pressure at $t = 0$, then

$$\theta^* = \frac{-P_s}{\frac{\partial P_s}{\partial t}},$$

where the quantities P_s and $\partial P_s / \partial t$ are to be evaluated at the peak of the shock, i.e., at $t = 0$. For general, not necessarily exponential, pressure-time relations, the above may be taken as the definition of θ^* . Theilheimer⁶ has shown that

$$\frac{\theta^*}{W^{1/2}} = \frac{\gamma}{\gamma + 1} \frac{1}{C_0 \sqrt{\frac{\gamma}{\gamma + 1} + 1} \left[\frac{-d\gamma}{d\lambda} \frac{1}{\gamma} \left[\frac{11}{2} - \frac{5}{\gamma(\gamma + 1)} - \frac{4\gamma}{3(\gamma + 7)} \right] - \frac{7}{3\lambda} \right]},$$

where γ denotes P_{sm}/P_0 , C_0 is the ambient velocity of sound, and γ is taken as constant and equal to 1.4. This formula relates θ^* to the value of the peak pressure and the value of the rate of change of peak pressure with distance at a point. Using the measured values of Bleakney and Stoner⁷ for $\lambda > 5$, and the theoretical values of Brinkley and Kirkwood⁸ for $\lambda < 5$, the values of $\theta^*/W^{1/2}$ have been computed as a function of λ for the Pentolite free-air blast wave. The values are shown in Fig. 4.14.

4.3.6 Comparison of Measured θ^* with Theory

In order to save the labor of recalculating this curve for an atomic bomb, it may be remembered that, at pressure levels below about 50 psi, $W_{TNT} = 0.61W_{RC}$ in free air and also $W_{TNT} = 1.2W_{Pento}$. Therefore in free air $W_{Pento} = 0.51W_{RC}$. Since the measurements are made along the ground, however, the equation must be written $W_{RC} = 1.8 \times W_{RC(ground)}$

in order to take account of the reflection factor. Then $W_{Pento(ground)} = 0.92W_{RC(ground)}$, and $\lambda_{Pento} = 1/0.97 \lambda_{RC}$ along the ground. Therefore in order to compare the calculated free-air Pentolite values of reduced θ^* with the measured Mach-region (ground) atomic bomb values, all calculated λ and $\theta^*/(W_{Pento})^{1/2}$ values should be multiplied by 0.97 and the term replotted as λ_{RC} and $\theta^*/(W_{RC})^{1/2}$. This has been done in Fig. 4.15, and the various reduced values of θ^* as measured have been plotted on the same graph. The rather good agreement lends credence to the idea that the initial disturbances in the pressure-time curves are not part of the main shock since the decay parameters are measured from the maximum pressure onward, ignoring the initial disturbances.

4.3.7 Calculation of Decay Parameter for Free-air Atomic Blast

The power-law expressions for the pressure-distance curve for free-air atomic blast given in Sec. 4.2 have been used with the θ^* formula of Sec. 4.3.5 in order to deduce the values of $\theta^*/(W_{RC})^{1/2}$ for incident pressures in excess of 156 psi. For pressure below this, the curve of Fig. 4.15 should be satisfactory with suitable modification to take care of the reflection coefficient. The use of this formula restricts one to the case of constant γ . It is believed, however, that this does not introduce a large deviation from the true state of affairs. The reduced time decay parameter is useful in providing a rough estimate of the forcing function determining the response of the ball-crusher gauges placed at high pressure levels. The values calculated are shown in Fig. 4.16. No attempt has been made to smooth in a junction between the two fitting formulas.

It is interesting to learn from this figure, for example, that at the base of the Shot Easy tower, where $P_s = 3,500$ psi (from shock-velocity measurements), $\theta^*/[W_{RC}(\text{lb})]^{1/2} = 0.0027$. Since $[W_{RC}(\text{lb})]^{1/2} = 488$, $\theta^* = 1.32$ msec. A shock of this strength is traveling at $U/C_0 = 15.65$ or $U = 17,900$ ft/sec. Therefore, if the pressure continues to decay exponentially, it reduces to $1/e$ of its value about 22 ft behind the shock front. It could then be concluded that most of the shock energy is carried out at this stage in a narrow band.

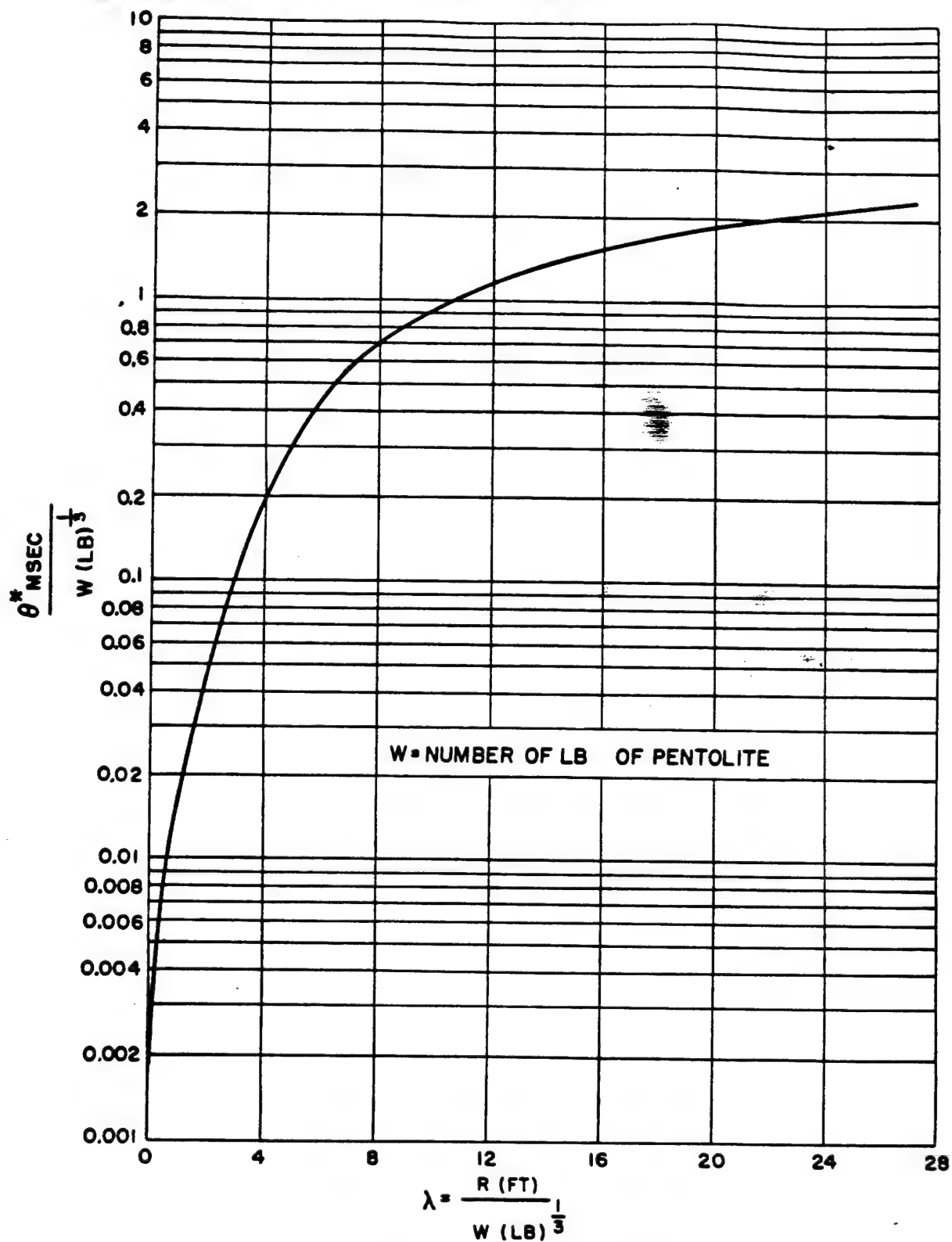


Fig. 4.14 Reduced θ^* vs λ for Free-air Pentolite

DNA
(b)(3)

$\frac{\theta^m \text{ MSEC}}{W_{RC} \text{ LB}} \frac{1}{\lambda}$

$$\lambda = \frac{W \text{ (FT)}}{W_{RC} \text{ (LB)}^{\frac{1}{2}}}$$

Fig. 4.15 Reduced Decay Parameter vs λ ; Theory and Experiment Compared

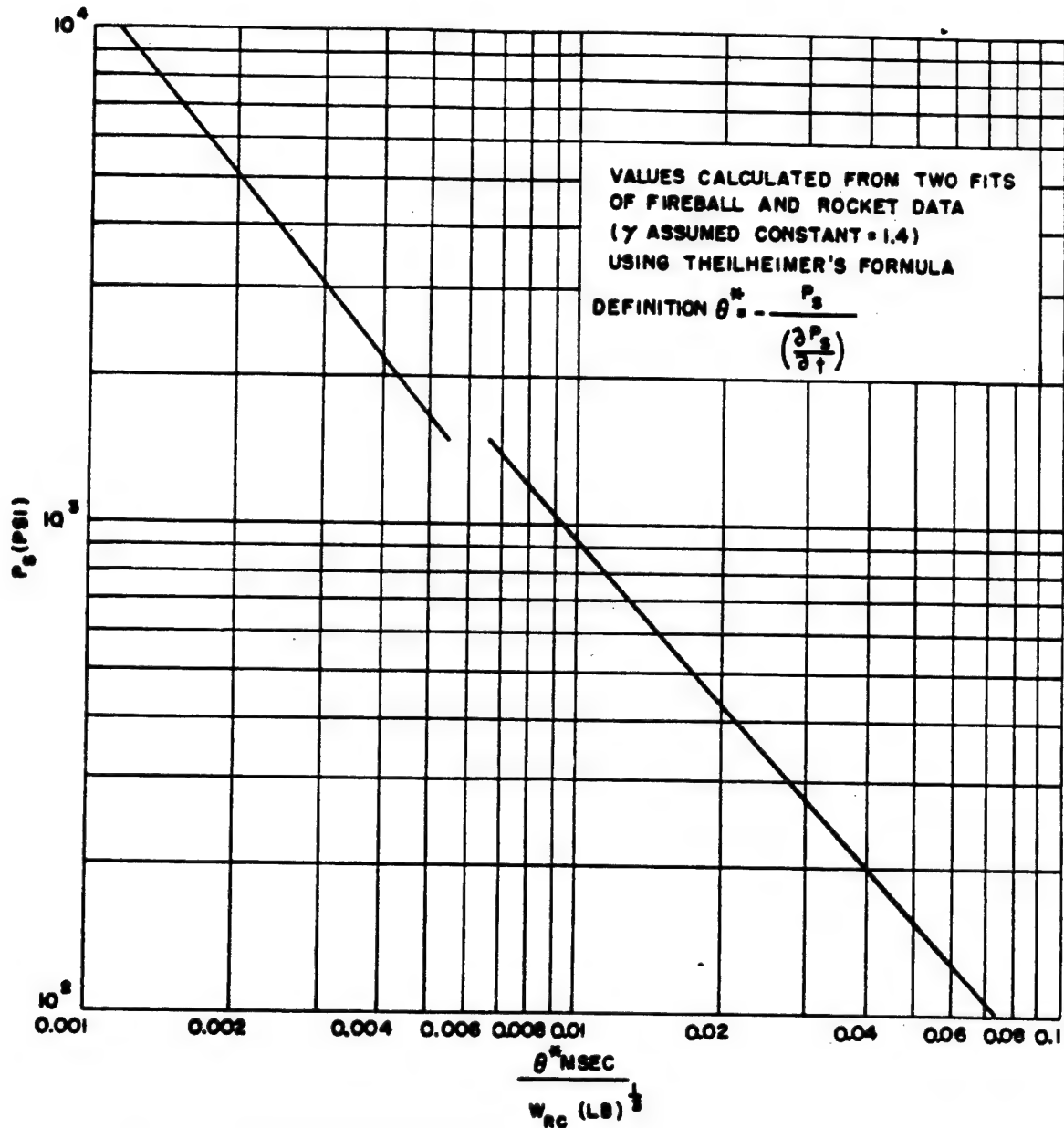


Fig. 4.16 Calculated Values of Decay Parameters vs Free-air Pressure for Atomic Bomb

4.3.8 Reduced Arrival Time

In Fig. 4.17, reduced arrival time τ , defined as actual time in milliseconds divided by $[W_{RC} (lb)]^{1/2}$, is plotted against λ . The three shots show differences at $\lambda < 8$ which are attributed to jets and to the adiabatic wave.

It is suggested that a fairly accurate determination of radiochemical tonnage can be made by means of this curve if, for an unknown explosion, the time of arrival is measured to the nearest millisecond at a distance corresponding to $8 < \lambda < 12$. The ratio of distance to time determines the slope of a straight line drawn from the origin, which intersects the reduced curve at the value of λ or τ which gives the tonnage immediately. If arrival times are measured too close to the bomb, the results are likely to be false because of jets which make the travel time too short or because of the adiabatic wave which alters the times, depending on whether or not it has caught up with the original shock. Measurements of arrival times at too large a distance are essentially sound-velocity measurements, and the variation in size from one bomb to another would act as a small difference difficult to detect. Furthermore at large distances the propagation of sound would be affected by atmospheric conditions.

4.4 DISCUSSION OF BLAST ANOMALIES

In this section, various matters such as asymmetry, jets, rise times, and the adiabatic wave velocity are discussed briefly.

4.4.1 Asymmetry

A great deal has been said about asymmetry in the blast wave. The extraordinary behavior of the blast along the short line E2 on Shot Easy, blowing the first pylon to the right with great violence and the second to the left, is indeed anomalous. One wall was blown over, and several were tilted on the two shots. Pressures measured on opposite sides of a wall were in some cases widely different. However, in spite of these evidences on the ground, aerial photographs have failed to show asymmetries. This is probably largely due to the general lack of suitable photographs taken from the air. Tower photographs, however, show very striking jets travel-

ing down the messenger cables and down the tower guy wires on all shots, although to a lesser extent on Shot George. These jets traveling at roughly twice the speed of the ball of fire cause tremendous local effects which appear to persist for a relatively long distance down a blast line. Examination of the craters after Dog and Easy showed that the jets gouged out the ground and exposed the anchor blocks where the guy wires had been fastened.

Figure 4.18, showing the times of arrival of the initial disturbance along E1 (no guy wire or cable) and E2 (guy wire), indicates clearly that the disturbance traveled more rapidly down E2 and continued to do so right to the end of E2 at 1,200 yd, where the two curves join. This is considered to be strongly indicative evidence that the difference in behavior is due to the guy-wire jet and that its influence persists in the same general direction, a distance out of all proportion to the original length of the wire. On the same figure there is also plotted for comparison the arrival curve for the free-air shock as far out as it was measured by rocket-trail photographs. The free-air shock agrees well with the long line (free of jets) initially but falls behind noticeably beyond about 300 yd. Since it has not been reinforced by reflection from the ground, it is traveling at a reduced speed compared with the Mach stem, and this accounts at least qualitatively for the difference in the two curves.

The rocket-trail photographs show that the incident shock proceeds outward in free air with spherical symmetry. The pressure measurements down the two blast lines show a decided decrease in pressure on the short line. However, the short-line impulse is very nearly the same as the long-line impulse. The short-line positive durations are correspondingly longer than the long-line durations. Whether these differences can all be attributed to the presence of the guy wire remains an open question. There is nothing in the adiabatic wave mechanism discussed in Chap. 5 to produce asymmetry.

4.4.2 Pressure near a Jet

Crusher gauges were placed on both Dog and Easy Shots in order to distinguish between ground pressures near a jet and those unaffected by a jet. The gauges on Shot Easy, nearly all of

λ REDUCED DISTANCE

T REDUCED ARRIVAL TIME

DNA
(b)(3)

Fig. 4.17 Reduced Arrival Time vs Reduced Distance for All Shots

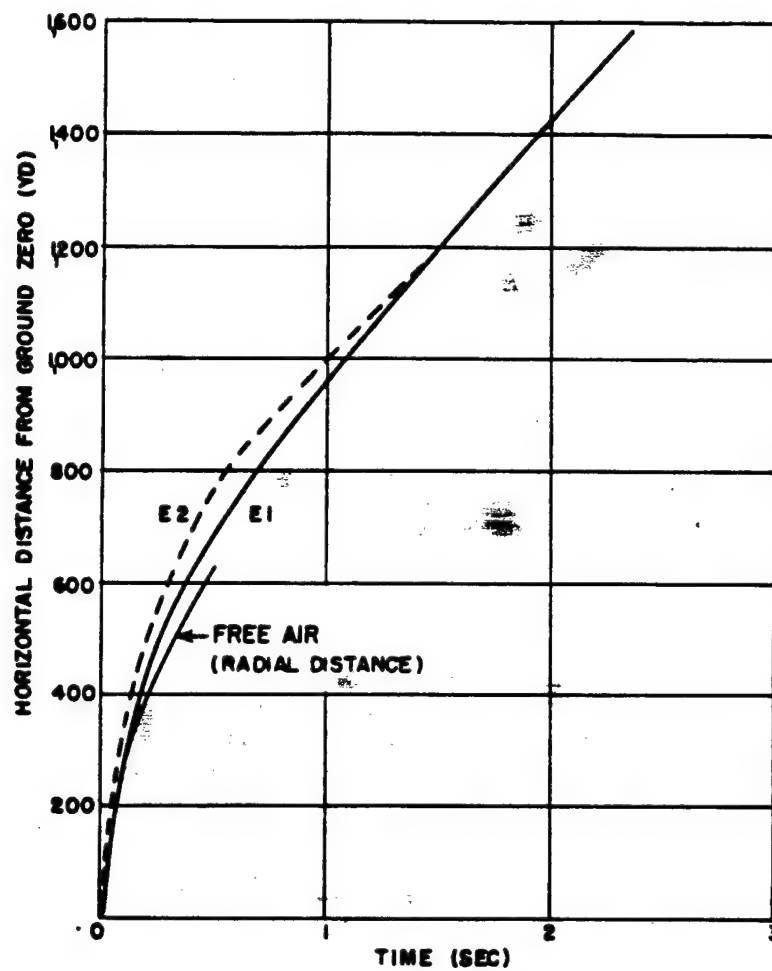


Fig. 4.18 Times of Arrival of Initial Disturbance, Shot Easy

which were recovered, were placed as shown in Fig. 4.19. All deformations obtained are shown in Fig. 4.20. The deformations obtained near and away from the jet are shown in Table 4.7. This table reveals the remarkable fact that the deformations at the base of the jet (Station 34) are roughly half as large as the deformations away from the jet (Station 33) at the same distance and that the assumption of gradual loading gives pressures which are substantially the same at the base of the guy wire as elsewhere. There is no obvious interpretation of these readings to give pressures which are higher. These measurements indicate that the higher jet velocity is associated with the electrical or thermal mechanism of jet formation and is not to be interpreted as characteristic of a shock in air. The analogy may be cited of the bow wave from a bullet or projectile which travels along with it and yet has the shock strength calculated from its velocity only at a point directly in front of the projectile. There is some uncertainty as to the last value since it is impossible to say at what distance the time during which the pressure rises at the gauge becomes short enough so that neither static nor dynamic calibrations are proper and so that the resulting deformation is a function of this time and may be intermediate between static and dynamic.

There is one other curious result from these data, namely, that the deformations immediately under the tower (see Fig. 4.20) are so much lower than the adjacent stations. This may be due in the same way to a relatively gradual build-up of pressure due to precursor wave of increasing intensity reaching the gauge before the main shock. Assuming this to be the case, the application of static loading still will not bring the calculated pressure up to the value obtained from the neighboring stations. The low value in this case is similar to the low value observed in Station 34a nearest the base of the guy wire. These results indicate that the presence of steel leading from the vicinity of the bomb may actually reduce the pressure locally.

4.4.3 Discussion of Rise Times

For values of λ approximately equal to 8 and greater, the multiple structure in the pressure-time curves disappears except for minor fine structure, and the blast wave takes on the con-

ventional shape that occurs for the positive phase of blast waves at all distances from high-explosive charges. The velocity of this wave is such that the pressure computed from it on the assumption that it is a shock agrees with the pressure actually measured by other direct means. If the wave were not a shock but instead still traveled with finite rise time, then the pressure calculated from the adiabatic assumption would be much larger. In other words a shock wave of a given pressure travels more slowly than an adiabatic wave of the same pressure. It is therefore necessary to conclude that at distances greater than λ equal to about 8 along the ground the wave has essentially a discontinuous front and that the rise time should be far less than the resolving power of any instrument employed in the tests. It is interesting to find that the inductance-gauge measurements bear out this conclusion. For certain selected records the frequency-modulated signal from the magnetic tape was played directly into an oscilloscope and photographed on moving film. The wave length of the resulting wave was measured by means of a comparator from cycle to cycle. In this way it was possible to assign a frequency to each cycle, with a time resolution of the order of the carrier period, i.e., about 0.3 msec. Only those records were selected for this analysis which could be compared with interferometer gauges which were adjacent. The inductance gauges used in the low-pressure region are known to have a rise time associated with the gauge diaphragm and the filling time, as determined in the shock tube, which is somewhat in excess of 1 msec. Consequently a measured rise time between 1 and 2 msec is considered to be introduced by the instrument itself. On the other hand, an indicated rise time of 3 msec is to be ascribed to an actual finite rise time in the pressure wave. Table 4.8 shows the result of a few detailed comparisons which have been made in the general region in which $\lambda > 8$. It will be noticed that in all cases where inductance gauges were mounted above the ground in walls or pylons the rise times are not inconsistent with the presence of a true shock front. Comparison of inductance and interferometer gauges at ground level in the same location shows good agreement, both indicating a rise time of about 3 msec. At a height 3.5 ft above this the rise time is cut in

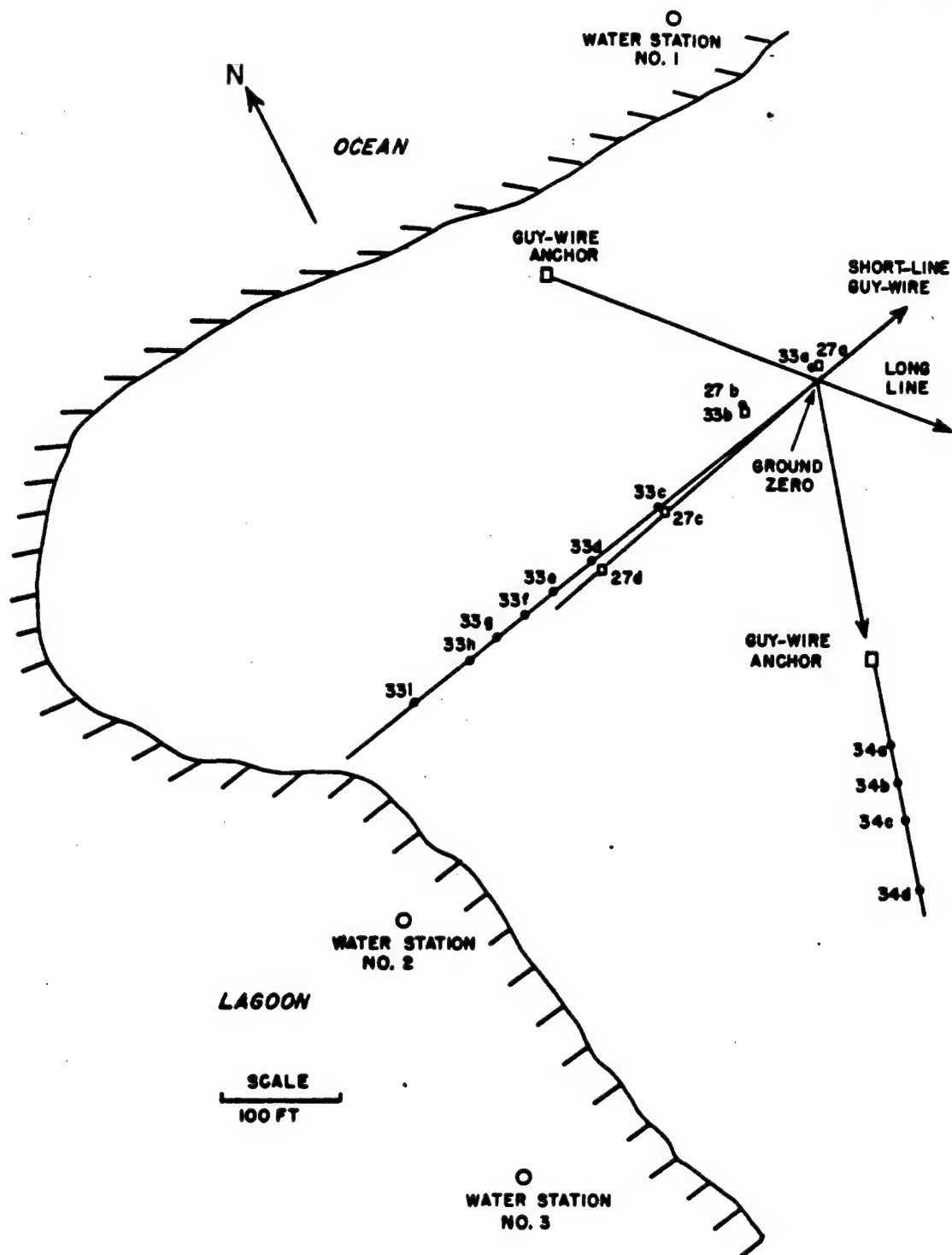


Fig. 4.19 Crusher-gauge Locations, Shot Easy

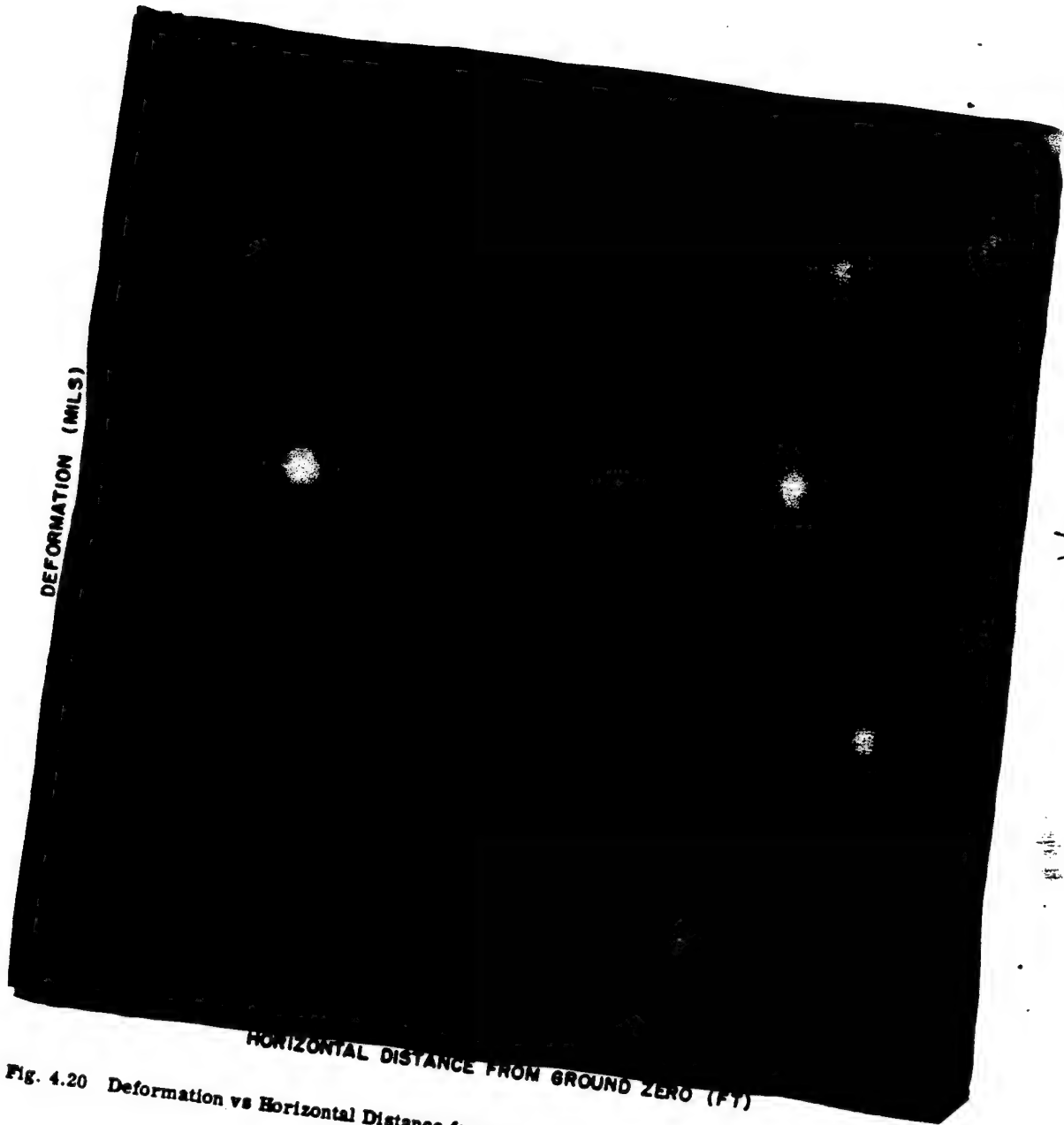


Fig. 4.20 Deformation vs Horizontal Distance for Ball-crusher Gauges on Shots Dog and Er

half, and 14 ft above ground at the same location the indication is that the rise time is still decreasing. The far longer rise times shown by the interferometer gauge at other comparable locations are to be associated either with lin-

rise time observed on and near the ground is in some way connected with the presence of the ground. It may be postulated, for example, that the radiation preceding the blast wave and intercepted by the ground serves to heat the

TABLE 4.7 PRESSURES IN THE VICINITY OF A JET

Away from Jet				Near Jet				
Hor. Dist. (ft)	Sta. No.	Deformation (in.)	Pressure Dynamic Loading (psi)	Sta. No.	Deformation (in.)	Av. Deformation (in.)	Pressure Dynamic Loading (psi)	Pressure Static Loading (psi)
309	33f	0.048	3,550	34a	0.020 0.026	0.020	1,500	3,050†
339	33g	0.042	3,040	34b	0.021 0.022	0.023	1,725	3,450†
369	33h	0.036	2,550	34c	0.018 0.019	0.019	1,425	3,210†
429	33i	0.032	2,360	34d	0.023	0.023	1,850†	3,700

† These quantities are the probable values of the pressure and are the values quoted in Table 3.2a.

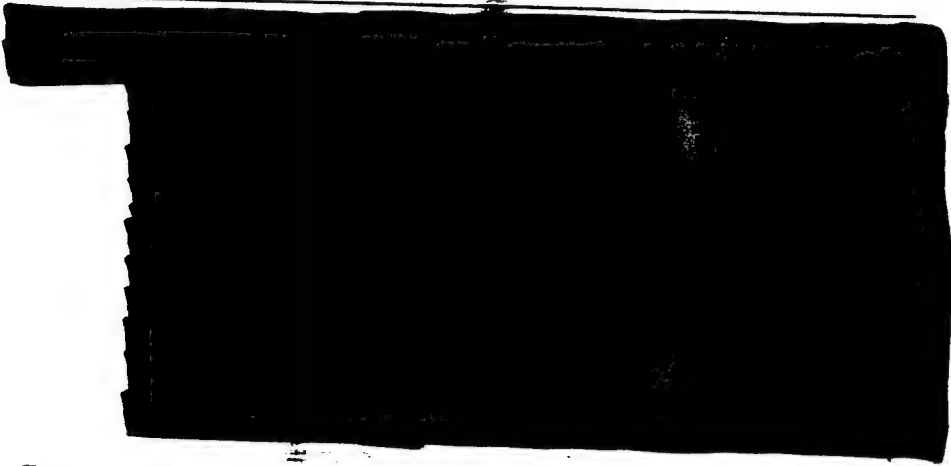
gering diffraction effects from obstacles further up the line (unlikely), or with local diffraction effects produced by the lead shielding bricks or other local obstacles, or with delays introduced by possible obstructions in the pressure inlet tube.

The conclusions to be drawn from the evidence presented are that for λ greater than about 8 the blast-wave front propagates as a shock front except for a thin layer at ground level not more than 3 ft thick where the rise times may be a few milliseconds in duration.

For gauges in walls at closer distances ($\lambda < 8$) the rise times of the first pressure peak increase very definitely to between 20 and 40 msec. Rise times of the same order are observed on the front walls of structures at the same distances. In view of the fact that at still closer distances all the evidence from fireball photography and from the sharpness of the rocket-trail breaks indicates that the pressure wave starts out as a shock and remains a shock in free air, it may be speculated that the slow

ground surface so that the temperature rise of any particular square foot increases according to the inverse-square law with corrections for the interception area and air absorption as this area is taken nearer to the bomb. This heated ground then may transfer some of this heat to the adjacent air, which expands and rises an amount depending on its temperature and the time allowed for this process. By this means an inhomogeneity is introduced into the medium at ground level and slightly above such that the velocity of sound is increased. Therefore a curvature is introduced into the shock front. If this occurs it is certain that a pressure gradient will exist along the curved shock front. This mechanism is suggested as a means of providing a low-amplitude precursor wave which travels along at the same velocity as the pressure pulse behind it. The actual strength of this precursor wave is that associated with the velocity of the wave normal to the wave front. Since on this hypothesis the precursor is moving at an angle with the ground considerably less than a right angle, its normal velocity is

TABLE 4.8 RISE TIMES IN THE LOW-PRESSURE REGION

Shot	Station No.	Gauge	Locations	Rise Time, t (msec)
				
Easy	37f	Inductance	1,430 yd, lagoon (long) line; ground station at pylon	$2.46 < t < 3.15$
	90c	Interferometer	1,430 yd, lagoon side of 37f about 50 ft away	$t \approx 0.77, 2d$ peak at 4, 3d peak at 8
	90d	Interferometer	1,430 yd, land side of 37f about 50 ft away	$t \approx 3.1$
	37c	Inductance	1,430 yd, lagoon (long) line, pylon gauge 3.5 ft above ground (same height as in walls)	$1.6 < t < 2.0$
	37c	Inductance	Same as immediately above, gauge 14 ft above ground	$1.25 < t < 1.6$

DNA.
(b)(3)

actually much less than the velocity of passage along the ground.

It is not possible to state at the present writing how high above the ground it is reasonable to expect this effect to be noticeable. The proposed mechanism has the merit of being able to account for the observed facts on rise times and also provides a possible explanation for the fact that the blast velocity switches, although closing on the arrival of the low-amplitude initial signal, nevertheless indicated a velocity characteristic of the maximum pressure signal which arrived a very appreciable time later.

4.4.4 Effect of Height of Gauge above Ground

Data obtained with the pylons are displayed in Table 4.9 and the pressure time curves are shown in Figs. 4.21, 4.22, and 4.23. The anomalous blast behavior characteristic of the ocean line is also shown in the pylon data, making any generalization concerning rise time as a function of height of dubious value. The maximum pressures obtained at the various heights are shown in Fig. 4.24. The curves indicate no variation of pressure with height at 1,430 yd. At 950 yd and 700 yd, however, the pressure measured on the ground is definitely lower than the pressures measured off the ground. This behavior would be consistent with the hypothesis of pressure weakening associated with a thermal layer which is more pronounced as the distance to the explosion is decreased.

4.4.5 Adiabatic Wave

The observed character of the pressure-time records taken on the ground on Shots Dog and Easy (see Figs. 3.1, 3.2, 3.10, and 3.11) leads to the conclusion that the pressure wave at short distances from the bomb is not a shock wave but is better classified as an adiabatic or isentropic wave. The slow rise of the pressure to a peak plus the presence of large perturbations on the pressure wave are characteristics of these records, which are taken at reduced distance of $\lambda = 7.5$ or less.

on Shot Easy one of the two blast lines seems to be relatively free of jets so that some intrinsic properties of the pressure wave unencumbered

by jet complications should be visible. These records are generally simpler in detail than those taken near jets but show that again the pressure wave is nonshock in character at the short distances.

There is a coalescence of these secondary pulses (see Figs. 3.1, 3.2, 3.10, and 3.11) as the wave progresses until at a reduced distance of approximately 8.4 the wave shape is that of a conventional blast wave from high explosives with one possible exception: there are no secondary shocks in the negative phase which are characteristic of high-explosive charges. The decay with distance beyond this critical distance is regular and similar to the decay rate of a high-explosive charge; in fact, the blast equivalent in terms of high explosives can be assigned at these distances.

The possibility that the presence of a secondary pulse in the pressure-time records is due in some unexplained way to the presence of the ground and to asymmetries introduced by jets could not be discounted until free-air-pressure-vs-distance curves were obtained by measuring the intersection of the pressure-wave front in free air with rocket-smoke trails in a manner described in Annex 1.6, Part II, Sec. 1. These data, when reduced to pressures as a function of distance, show a bump and an apparent displacement of the curve at a reduced distance of $\lambda = 2$ to 3. Data from the shock-velocity measurements made by balloon-supported switches at somewhat larger distances but still in free air confirm this apparent shift in the position of the curve at distances greater than 3. This bump in the pressure-distance curve is probably caused by the coalescence of a secondary pressure pulse with the primary shock front produced by the expanding fireball. This secondary pulse is probably of the same nature and origin as that observed at the ground level, but it coalesces with the pressure front at a much smaller radius because of the more rapid decay of pressure of the primary shock with distance in free air compared to the decay along the ground. This is plausible since the pressure is increased markedly in magnitude by reflection and the formation of a Mach stem near the ground, and therefore the front travels faster, and although the reflection increases the amplitude of the secondary pulse the latter travels more slowly relative to the front at the high pressures than it does at low

pressures. This hydrodynamical phenomenon is illustrated in a graph (Fig. 4.25) showing the velocities relative to sound, of shock and adiabatic waves of various pressure levels. It will be seen that at pressures exceeding 300 psi it is difficult for a secondary pulse to catch a shock front unless its magnitude greatly exceeds the shock-front pressure.

the isothermal sphere and the shock front since the highest temperature in the shock should be immediately at the front. The shock front remains luminous until it reaches a temperature of approximately 2500°K at which time it becomes transparent and the phenomenon called "breakaway" occurs. At some time previous the air at some distance between the shock

TABLE 4.9 PYLON DATA FOR SHOT EASY

Pylon	Distance (yd)	Height above Ground (ft)	Pressure at	
			First Maximum (psi)	Rise Time to First Maximum (msec)
37a	700 on ocean line	0	~10	~ 70
		3.5 to 10	~20	~100
37b	950 on ocean line	0	~ 8	~ 90
		14	~ 8	~130
37c	1,430 on lagoon line	0	~ 8.5	~ 3
		14	~ 8.5	< 1.6

The inference is made then that the free-air-pressure-vs-time curve contains a secondary pulse or pulses which are similar in nature to those directly observed on the ground by pressure gauges. If this inference is accepted, it accordingly remains to explain the origin of this delayed pressure pulse produced by the fireball.

The formation of NO and subsequently NO₂ from the dissociated molecules of nitrogen and oxygen of the atmosphere is a highly exothermic process which releases a very large amount of energy somewhat delayed in time due to the relatively low temperature at which these oxides are formed. This delayed emission of heat energy from the dissociated gas molecules could in principle produce a secondary pressure wave by conversion of this heat energy into kinetic energy of the molecules of nitrogen and nitrogen dioxide.

It is stated in the literature⁸ that when the temperature drops to about 300,000°K at 0.1 to 0.3 msec after detonation, the shock front breaks away from the isothermal sphere and advances at a higher velocity than does the isothermal sphere. Presumably there is then a trough in the temperature distribution between

front and isothermal sphere has dropped to 5000°K, or so, at which time the oxides of nitrogen begin to be formed. This process continues releasing energy until the temperature falls to about 2000°K. This region then provides the source for a new expansion wave which acts as a strong perturbation on the decaying pressure behind the shock. That this perturbation is not negligible is shown by the calculation in Sec. 4.2 on Shot Easy in which the apparent energy in the secondary pulse is computed to be about 20 per cent of the total energy in the bomb. This amount of energy is consistent with that released in the formation of NO₂ if the total amount of NO₂ formed is consistent with the calculation quoted on page 181 of "The Effects of Atomic Weapons," in which it is stated that approximately 100 tons of nitrogen dioxide is formed in the explosion of a nominal atomic bomb.

The heat of formation of NO₂ from N⁺ and O⁻ is computed to be 284.6 kcal/mole, which amounts to 5.6×10^{10} cal/ton. It is stated on page 183 of "The Effects of Atomic Weapons" that 100 tons of NO₂ are formed in the explosion of a nominal atomic bomb. This corresponds to 5.6×10^{12} or 5.6 kt of radiochemical energy,

PRESSURE p (PSI)

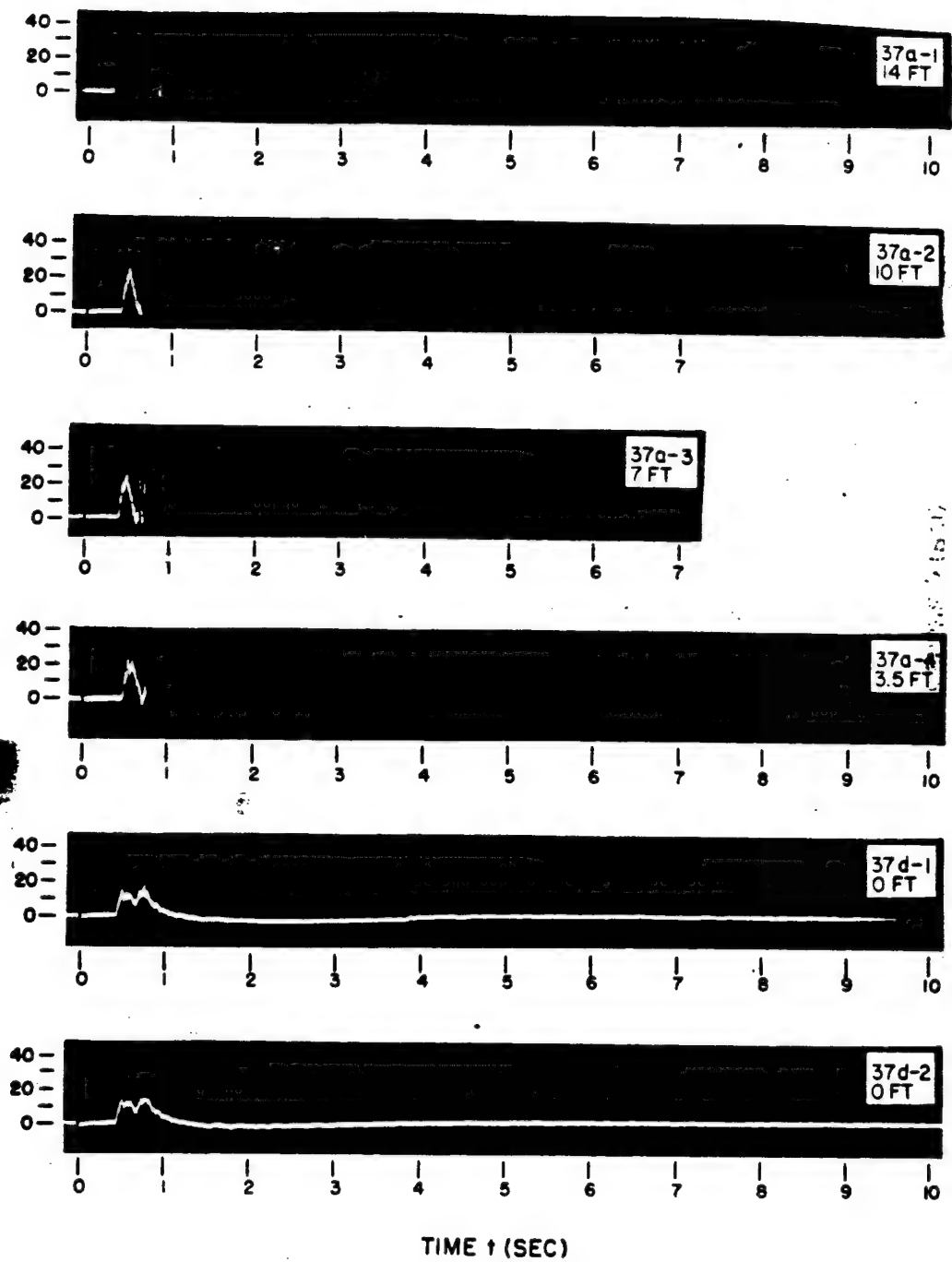


Fig. 4.21 Pressure-time Curves, Shot Easy, Pylon 37a

PRESSURE p (PSI)

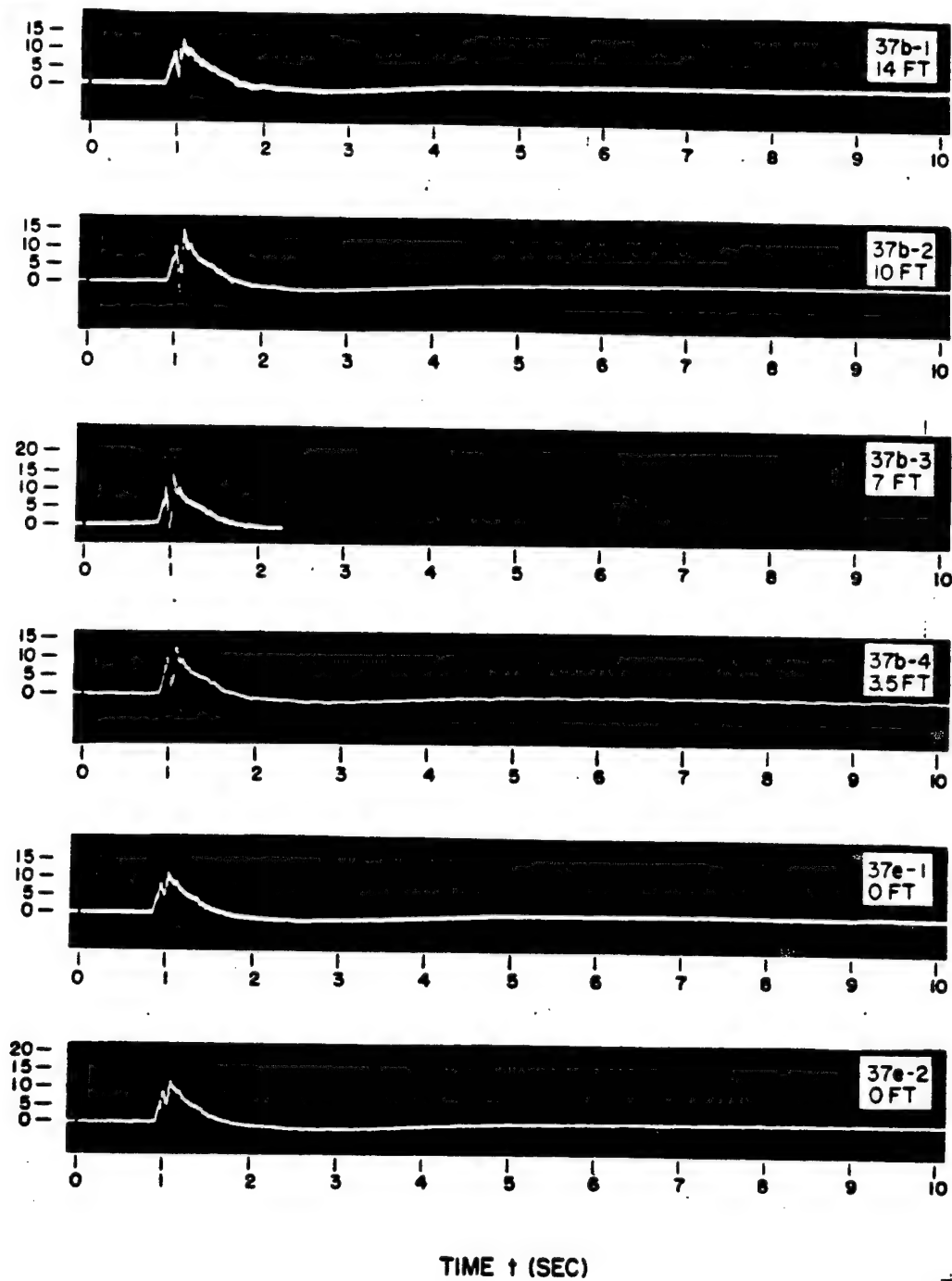


Fig. 4.22 Pressure-time Curves, Shot Easy, Pylon 37b

PRESSURE p (PSI)

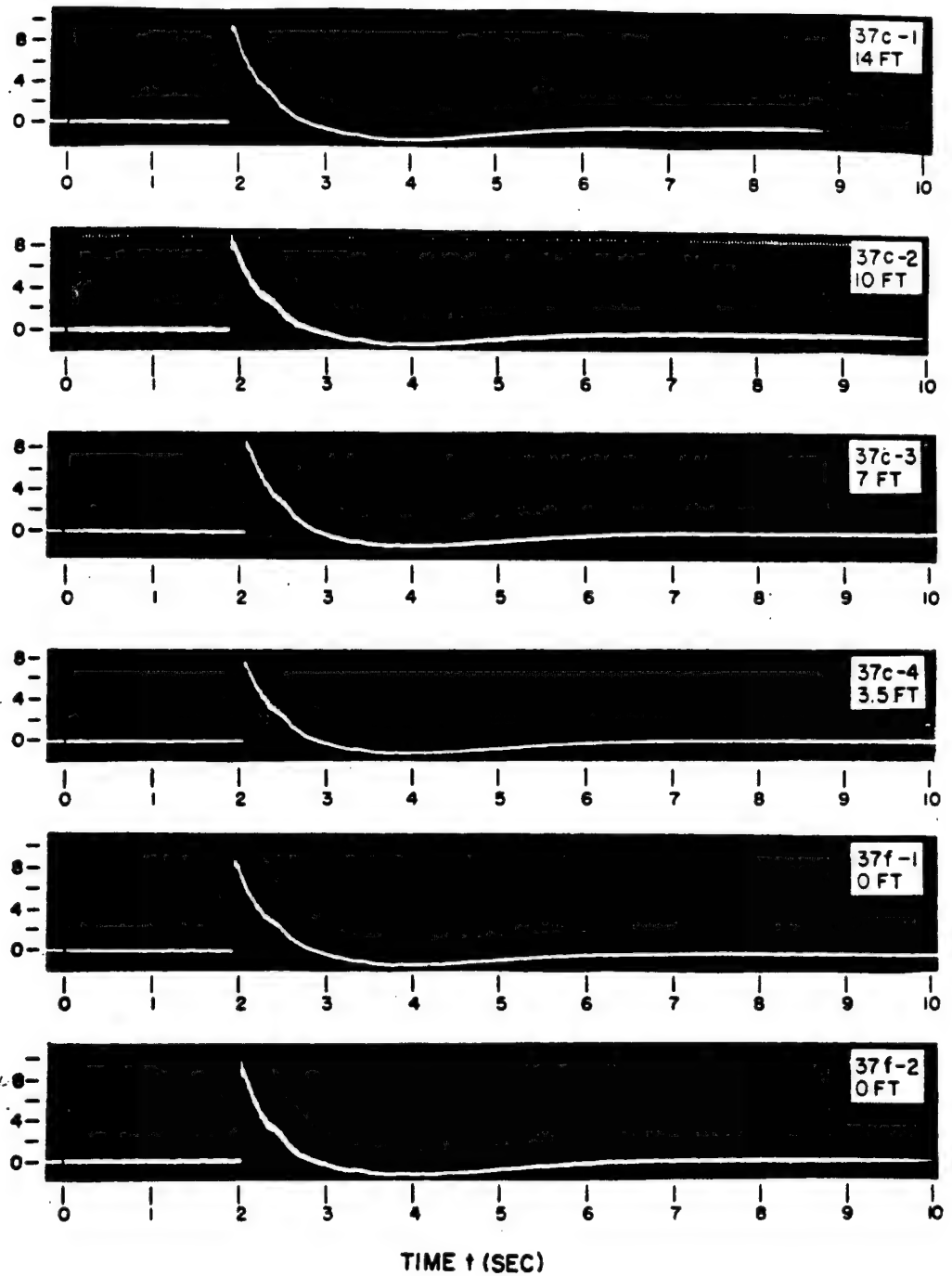


Fig. 4.23 Pressure-time Curves, Shot Easy, Pylon 37c

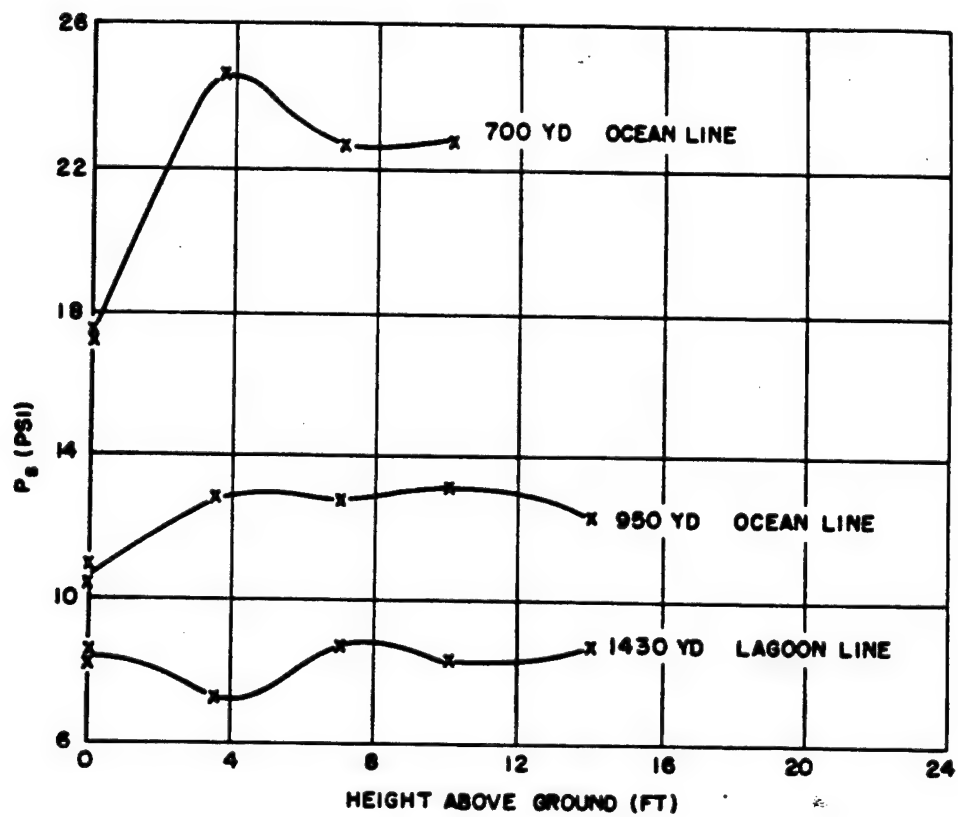


Fig. 4.24 Pylon Data, Shot Easy, Maximum Overpressure vs Height above Ground at Various Distances

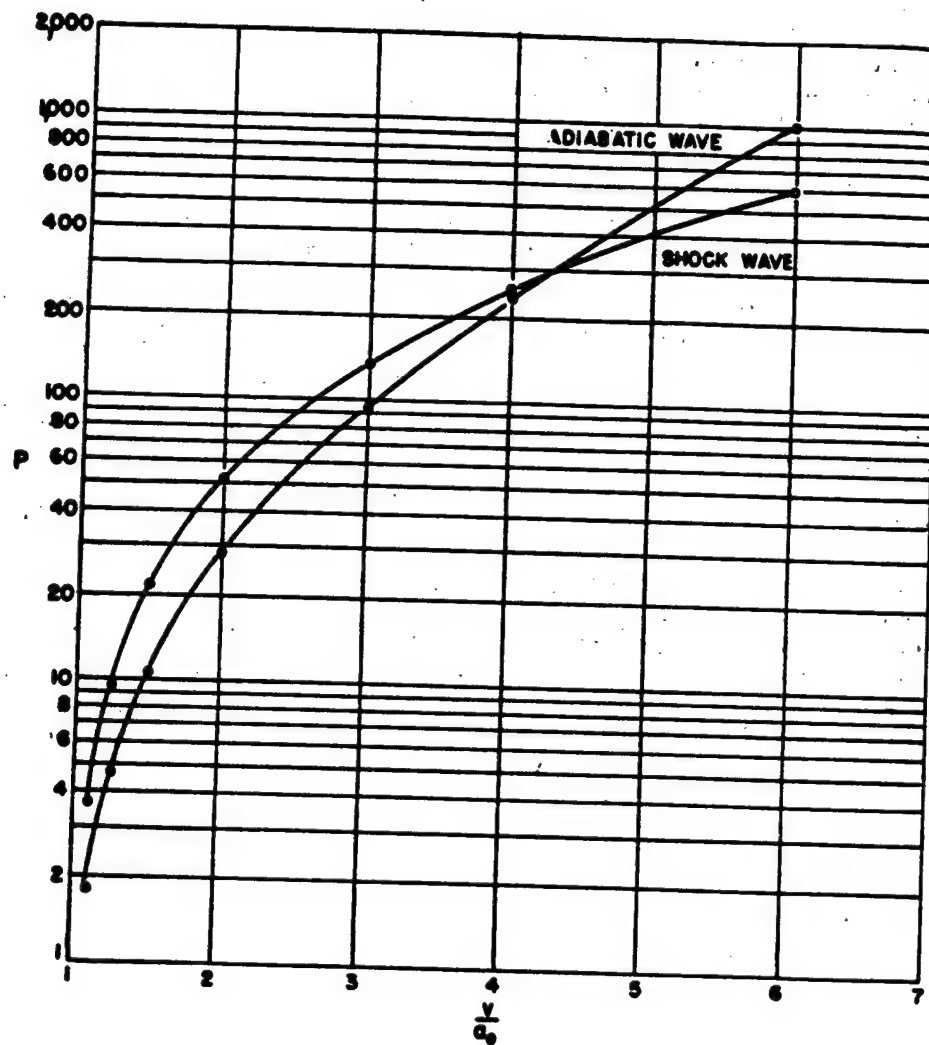


Fig. 4.25 Ratio of the Velocities of the Peak to the Velocity of Sound for Shock and Adiabatic Waves as a Function of Pressure

REFERENCES

1. J. H. Manley, Blast Measurements, vol. 7, Chap. 16, Report LA-1023.
2. Dictionary of Altitudes, U. S. Geodetical Survey, 1906.
3. K. T. Bainbridge, Report LA-1012, May 8, 1947.
4. C. W. Lampson, Peak Air Blast Pressure as a Function of Distance Determined by Photographic Method, JTF 1 Tech. Staff, Bureau of Ordnance, Navy Dept., Washington, D. C., Sept. 30, 1946.
5. Kirkwood and Brinkley, Theoretical Blast-wave Curves for Cast TNT, Report OSRD-5481, August 1945, p. 31.
6. F. Theilheimer, The Determination of the Time Constant of a Blast Wave from the Pressure-Distance Relation, Report NavOrd-1734, December 1950.
7. Bleakney and Stoner, The Attenuation of Spherical Shock Waves in Air, J. Applied Phys., 19: 670-678 (1948).
8. S. Glasstone, J. O. Hirschfelder, A. Kramish, D. B. Parker, and R. C. Smith, eds., "The Effects of Atomic Weapons," U. S. Government Printing Office, Washington, 25, D. C.

Chapter 5

Evaluation and Conclusions Concerning Blast

In this chapter a brief evaluation of the experiments performed and a résumé of the principal results and conclusions are given.

5.1 REMARKS AND RECOMMENDATIONS CONCERNING THE VARIOUS EXPERIMENTS

1. Velocity measurements as a means of calculating the peak shock pressure are valid only if the velocity in the direction of propagation of the shock is determined. The assumption of spherical symmetry must therefore be made, and the evidence of these tests indicates that this is not always true because of the presence of jets or because of the proximity of the ground. The free-air rocket-trail photographs show that spherical symmetry is preserved for the incident shock above the tower. The use of backup switches or transducers to indicate arrival times is recommended. The blast microphones used in the present tests were not successful because they were paralleled in an effort to save wire. Subsequent signals from the forward microphones were therefore superimposed on the signals from the more distant ones. If this measurement is made in the future, separate lines should be used for each switch or microphone, and their signals should be registered on paralleled recorders. The use of magnetic tape is satisfactory. A blue-box device should be used to record the zero of time. The recording system should be designed to reduce the labor of counting the cycles of the 10-kc timing traces. If sound-velocity measurements are made from prefired explosive charges, the charges should be set off not more than 1 sec before the explosion of

the bomb. This experiment would be undertaken principally in order to give the wind component along the line. The sound velocity simultaneously determined should agree with that calculated from the local temperature and humidity.

2. The inductance-gauge system gave satisfactory results. However, the system could be improved probably by the use of twisted Bourdon gauges (Wiancko) instead of diaphragm gauges, and the frequency response could also be improved by direct recording of the modulated carrier on the magnetic tape instead of first heterodyning the signal with a lower frequency wave. The system of downbeating used on these tests was worked out to relieve a stringent specification regarding the wow in the tape recorder. However, it appears probable that harmonics and subharmonics introduced by this practice are more objectionable than the error due to wow, which in any case is small because of the careful design of the recorders used. Considerable simplification in the field electronics would result from elimination of this stage. Another possibility for improvement which would merit investigation lies in multiplexing two or more signals on the same wires, thus resulting in a great saving in wire costs. A zero time common to all records should be introduced by means of a photocell (blue box), rather than relying on electromagnetic pickup at the time of the explosion.

3. The mechanical pressure-time device developed for these tests gave good results on the whole and served its purpose as a backup mechanism and as a means of giving independent confirmation to the pressure-time curves obtained. It is believed that the purpose of developing a simple recording mechanical gauge

[REDACTED] should be pursued, with certain fundamental modifications suggested by the present experience. There should be no sliding members or bearings which are exposed in any way to the air because of the inevitable uncertainties introduced by sand, debris, and salt corrosion. The recording system developed for the spring-piston gauge is capable of such high resolution that it can be used to make records on a very small scale. The slight motion of a suitable diaphragm could therefore be recorded and the diaphragm itself protected against sand and radiation by means of a porous sintered plug. It is believed that a very small, light, and rugged device could be developed having a relatively high frequency response and proper damping which might be used in quantity for free-air measurements at very low cost.

4. The foils used as backup devices, although flush-mounted and streamlined in the present test and hence not subject to the gross errors encountered on Sandstone, nevertheless gave results which were consistently higher than all the other methods and are believed to be unreliable under the circumstances of use, namely, many hours after final mounting and in the presence of sand and salt. It is therefore recommended that their use be abandoned for tests of this sort. Another uncertainty, of course, in their use is their behavior in the presence of waves of various shapes having finite rise times.

5. The indenter gauges used in the present tests were designed and calibrated for use with shocks. The damping was altered sufficiently by the use of heavy greases between Shot Dog and Shot Easy to permit these gauges to respond statically to the loading, and the pressures so calculated from the deformations were in good agreement with the inductance gauges on Shot Easy. The leakage of air past the piston is, however, a difficulty when these gauges are subjected to a wave having a very slow rise to maximum. In view of their cheapness and ease of use it is believed that these gauges can be redesigned in the light of present knowledge to give accurate information on atomic blast. The gauges could be used in sets, mounted in the ground, some members of the set being undamped to take care of those conditions when the blast wave is a shock and others overdamped and adequately sealed to take care of the blast waves exhibiting the long rise to maxi-

mum pressure shown by the secondary pulse. It is believed that the correct interpretation of the resulting sets of deformations can be found from the variation with distance of the calculated pressures.

6. The rocket-trail experiment proved to be extremely fruitful and gave a large amount of information on the free-air curve, the path of the triple point, and the question of symmetry. This experiment should be repeated in the future to gather more data on the free-air curve and to confirm the jog in the pressure-distance curve which is now presumed to indicate the addition of energy from the secondary pulse. It is pointed out that the success or failure of this experiment depends not only on the presence of adequate smoke trails at the right time, but also on the proper photography with proper exposure, rate, timing marks, etc.

7. The balloon-telemetering experiment, although successful, was not able to cover a wide enough range of itself to be more than a confirmation of a part of the rocket-trail experiment. In addition the cost of the experiment, the manpower involved in it, and the generally cumbersome, awkward, and difficult operations required make it appear unnecessary to pursue this method further.

8. The ball-crusher gauges used in the regular and near Mach regions gave results which were surprisingly consistent at any one location. The methods of mounting to ensure more complete recovery can be improved. The stake mounts as used were not good. The results of these measurements are perhaps provocative of further work to ascertain pressures close to the bomb or in the vicinity of jets. If similar measurements are made again, the gauges should be redesigned to use larger copper balls, thus extending the linear region of the gauge operation to higher pressures.

5.2 PRINCIPAL NEW RESULTS AND CONCLUSIONS

The results and analysis of the Greenhouse blast experiments are given in Chaps. 3 and 4. In summary, the principal new observations have been (1) the finite rise time at high pressures on or near the ground, (2) the presence of a secondary maximum in the pressure-time curves on or near the ground at the higher

[REDACTED]

pressures, (3) the confirmation of very striking asymmetry as revealed between the long and short blast lines on Engebi, (4) the determination of the free-air-pressure-distance curve, (5) the confirmation of a plateau in the pressure-distance curve along the ground as observed on Sandstone and the ascribing of this to the secondary pulse mechanism postulated in Sec. 4.4.5, (6) the determination of a considerable part of the path of the triple point, (7) the measurement of pressures in the region of regular reflection and in the presence and absence of jets produced by metallic cables leading from the vicinity of the bomb, and (8) the determination that the free-air incident wave possesses spherical symmetry. A new figure for blast efficiency has been found. It has been postulated that the presumably lower temperature of the fireball on Shot George is responsible for the relative lack of evidence for the existence of a secondary wave on this shot. This hypothesis remains to be substantiated by radiation data.

Certain mechanisms have been suggested to account for some of the observations. For the secondary wave it is supposed that the energy released on recombination of disassociated oxygen and nitrogen is delivered into the pressure wave at a time determined by the mechanical expansion and cooling which occurs after the passage of the shock front. For the finite rise time, the supposition is that the ground, heated by bomb radiation, has transferred some of this heat to the adjacent air layers creating a nonuniform medium which can support the passage of a shock wave having a pressure gradient along its front. Concerning the gross asymmetry observed between the two blast lines along the ground, there is no explanation other than the one obvious asymmetry, namely, that a guy wire pointed down the short line, whereas the long line bisected the angle between guy wires. These asymmetries must therefore be laid to the presence or absence of jets.

There are certain discrepancies in the impulse determinations which should be pointed out. These are not instrumental. The impulses determined for Shot Easy along both lines are too high at the high pressures compared with Shot Dog. It may be that the very large jet down the blast line on Shot Dog is in some way to blame for this discrepancy. Similarly the posi-

tive durations at high pressures on Shot Dog are too short.

One of the objectives of the experiments was to obtain information on whether it is necessary to mount gauges off the ground to avoid flow interference or whether gauges could be mounted at ground level provided adequate precautions to smooth the adjacent areas were taken. Comparisons made at low pressures between interferometer and inductance gauges at ground level and inductance gauges in walls showed essentially no differences except that rise times for ground gauges were a few milliseconds longer. There is no evidence which permits comparison at high pressure where both flow effects and temperature effects are more important. However, in view of the agreement of the ground-mounted ball crushers in the Mach region with other methods, it appears reasonable that gauges may be ground-mounted with no greater disadvantages than wall mounting presents. Ground mounting, although inconvenient and difficult to waterproof, has definite advantages in that the orientation of the bomb need not be known in advance. Furthermore ground-mounted gauges are not subject to local disturbances such as missiles, turbulence, jets, or reflections, which caused the destruction of some of the closest walls.

Tonnages deduced from the blast measurements show a rather wide scatter. Total yields, meaning total energy release in terms of so-called "radiochemical kilotons," of the three shots and blast tonnages (weight in kilotons of TNT to give a blast pressure of 10 psi at the same distance), both deduced from blast measurements, are given in Table 5.1.

[REDACTED]

These impulse tonnages are determined using the theoretical TNT impulse curve arising from the same theory which gives such excellent peak-pressure agreement with experiments. Rather precise impulse measurements¹ on spherical charges show good agreement with the theoretical curve for $\lambda > 10$. The experimental impulses are considerably higher for the higher pressures. In determining the total yield from impulse measurements the weight of TNT necessary to give the same impulse in

DN
(b)X³

TABLE 5.1 TOTAL YIELDS DETERMINED FROM BLAST

Shot	Yield from Press. Measurements (kt) ^a	Yield from Impulse Measurements (kt) ^a	Fireball Data				Radio- chemical Data	W _{TNT} from Press. Measurements (kt TNT)
Dog								
Easy, long line	47.6	78						25
Easy, short line	34	72	50 ^b	46.7 ^c	46.7 ^d	46.7 ^e		
George								

^a1 kt = 4.20×10^{10} ergs.

^bPreliminary data, May 1951, before adjustment to Shot Easy.

^cFireball data from Fussell (EG&G).

^dFireball data from Houghton (LASL).

^eNewest radiochemical figures from Los Alamos, March 1952.

free air is determined at the farther distance where agreement is good. It is then assumed that the same reflection factor holds for impulse as for peak pressure and that the same blast efficiency holds. Since one or both of these assumptions may be false, the assignment of yield tonnage from impulse measurements is meant to be strictly tentative.

The yields assigned from the peak-pressure measurements are independent of assumptions about blast efficiency or reflection coefficients, being based solely on the correlation between total yields determined prior to Greenhouse

and the experimentally determined distances at which the 10- μ level was found. Consequently discrepancies between these are far more difficult to explain. It is believed proper to allow some of the various figures to stabilize themselves before serious thought is given to explanation of discrepancies.

REFERENCE

E. M. Fisher, Spherical Cast TNT Charges; Air Blast Measurements on, Report NOLM-10780, NOL, January 1950.

Chapter 6

Ground-shock Measurements

6.1 INTRODUCTION

A rather limited program of measurement of ground shock was undertaken in order to obtain some information concerning the motion of the ground and the effect that it might have on the performance of certain instrumentation during the course of the explosion. These instruments were primarily those having collimation equipment that was sensitive to slight variations of alignment to the bomb center. In addition the structures program of the various Services imposed, at a later date, the requirement that some information be available relating to the motion of structure footings during the time of passage of the blast wave.

From a fundamental point of view there seemed to be a relatively small probability of correlation of the ground motions in this rather special case to those derived by scaling of explosive tests or to the motions caused by the detonation of atomic weapons over continental sites, since the geography of the site and the probable motion of the subsurface structures were so markedly different from that of any other underground explosion test site. From this viewpoint a limited effort which would yield the information specifically desired from these tests seemed to be in order.

6.2 SCOPE OF THE MEASUREMENTS

The decision to instrument the last two shots rather than all three was based largely on the availability of manpower and recording instruments which could be applied to this project. The major emphasis was on Easy Shot since in this test two blast lines required instrumenta-

tion and, also, since the structures program had its tests on this site.

The major effort in instrumentation was on the measurement of accelerations since this appeared to be the only quantity that could be measured over a wide range of amplitude with commercially available instruments. In principle, if this quantity is measured accurately, it is possible by integration of the record to derive successfully the particle velocity and displacement as a function of time.

Two kinds of instruments were used, namely, a vacuum-tube accelerometer recording remotely on a pen recorder (Brush) and a self-recording instrument, recording on a magnetic tape which could be recovered at leisure and played back (ERA). A direct-reading self-recording displacement gauge utilizing the principle of a free piston was used as an auxiliary instrument for horizontal displacement readings.

These instruments were disposed as shown in Figs. 6.1 and 6.2 for Shots Easy and George.

The range of accelerations expected from scaling high-explosive tests was approximately 2 to 0.02 g measured from the edge of the expected crater to the end of the island. Associated with these accelerations it was expected that there would be motions ranging from 10 ft to 4 in. at the extreme of the instrumentation line. The instrumentation was accordingly planned to cover these ranges. Attempts were made to fasten the instruments to the compressed coral-rock strata which underlay the island at depths of 2 to 10 ft, but in certain cases the water level from seepage was above the rock layer, and the instrument had to be tamped in coral sand. Such cases are indicated in the data.

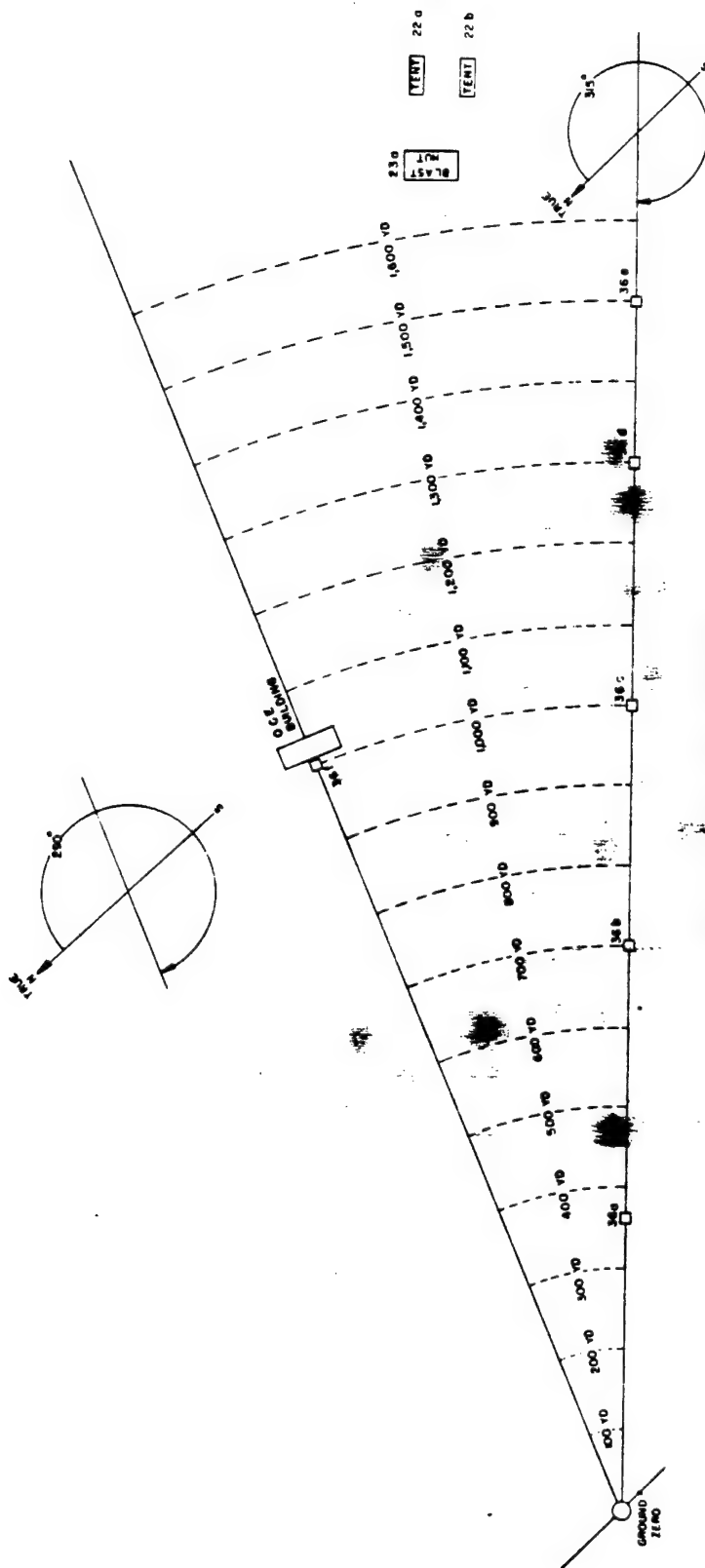
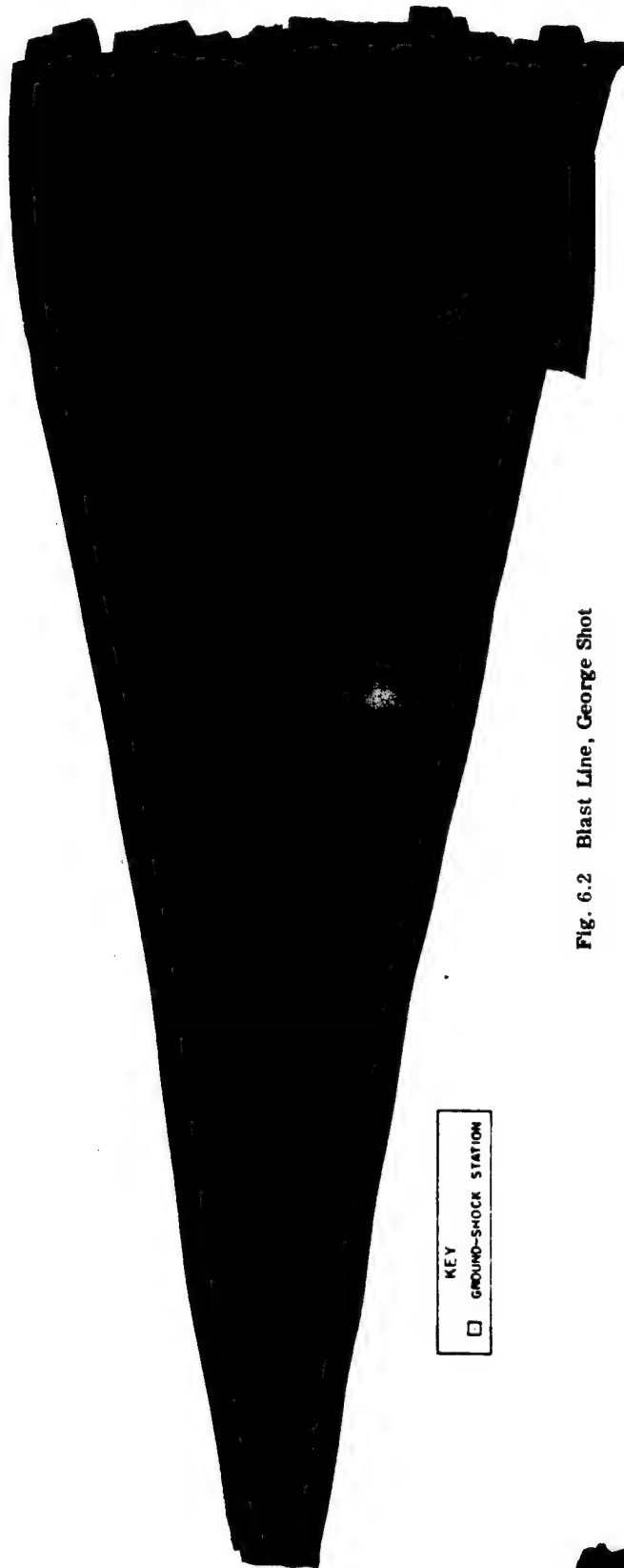


Fig. 6.1 Blast Line, Easy Shot



DNA
(b)(3)

Fig. 6.2 Blast Line, George Shot

KEY
□ GROUND-SHOCK STATION

6.3 TERRAIN PROBLEMS

The problem of the coral atoll from a measurement standpoint is that primarily it is a peak, extending above the ocean floor, with rather sharply sloping sides whose characteristic structures are not well understood, chiefly because the method of formation of coral atolls is obscure. The peripheral islands of the atoll are naturally rather close to the sloping edge with whatever complications this may cause in any study of underground-explosion pressure waves.

The greatest contribution to a knowledge of the structures of atolls as far as the authors are aware is the work reported by Dobrin et al.¹ in measuring refraction profiles during the Crossroads tests at Bikini. Later on, during the resurvey, test borings were made, but the information from these had not been made available to us at time of writing.

The borings made during the construction program on the site of Shot Easy were incomplete in that drilling difficulties made it impossible to attain the depth desired, but the results obtained indicate that the peripheral islands are built up as a long succession of beaches with layers of compressed coral alternated with patches of porous sand in a random manner. It was shown in these borings that the "bedrock" to which we fastened the majority of the accelerometers was in reality a comparatively thin slab of coral which was underlain by various strata of sand and coral whose continuity of disposition in a horizontal plane is doubtful, and whose seismic velocities are probably variable over a large range. Under these conditions the scale predictions based on a reasonably uniform medium went rather wide of the mark, giving expected values of accelerations and displacements that were approximately a factor of 10 too low and too high, respectively, compared to the measured values. This effect is consistent with the difference between observed and expected periods of the seismic waves in that the predicted periods were about ten times as long as were observed. Whether or not this would have been the case had the substrata of coral been more massive, it is difficult to say, but it is possible that more or less current tests under way at Dugway, Utah, will shed light on this matter.

6.4 RESULTS OF THE MEASUREMENTS

Figures 6.3 and 6.4 show the peak values of the ground-propagated accelerations in the horizontal and vertical planes. These are labeled "first peak accelerations" since on one or two records taken at distant stations the effect of the air-blast waves passing over the station gave another peak reading of acceleration which was slightly higher than the primary peak. The dotted lines are the predicted values based on scaled high-explosive charges in soil. It will be seen that the recorded values of acceleration are about a factor of 10 larger than predicted. Fortunately, these larger values were anticipated by the accidental discovery of an Air Force Office for Atomic Energy (AFOAT) seismograph record of the previous shot (Dog) in which values of period and displacement could be obtained. The derived accelerations were hurriedly compared with the predicted settings of the instrument ranges and found to be about ten times higher. The instrument settings were accordingly revised and hit very near the center of the necessary scale on each position with gratifying results as far as measurability of records was concerned.

On Figs. 6.3 and 6.4 are placed the preliminary values from the AFOAT project, who kindly supplied this information in advance of their report. The slope of the line on the log-log coordinate paper is slightly less than would be predicted by the inverse fourth-power law, but the scatter of points is insufficient to allow a firm conclusion to be drawn.

Figures 6.5 and 6.6 show the peak particle velocities derived from a single integration of the records of accelerations as a function of time. It will be seen that these bracket the predicted values, being slightly lower for one component and appreciably higher for the other component, although the discrepancy is of the order of a factor of 2 or less rather than a factor of 10 as in the accelerations. Strangely the slope of the line as drawn on the graph is somewhat greater than predicted, which is inconsistent with the slopes of the stress-strain curves which these and allied material are thought to have. However, again the paucity of data prevents a conclusive result.

Figure 6.7 shows the data obtained by a double integration of the accelerometer records

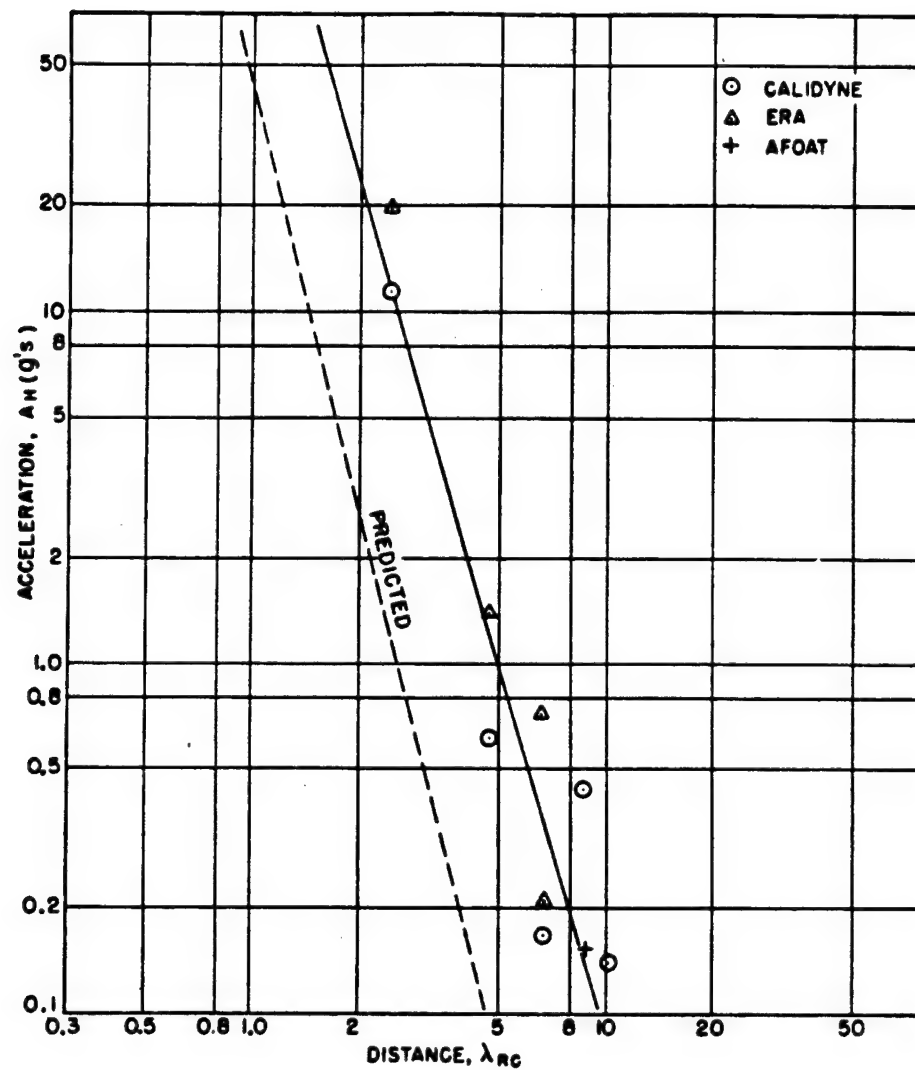


Fig. 6.3 First Peak Horizontal Acceleration as a Function of λ_{RC} , Easy Shot

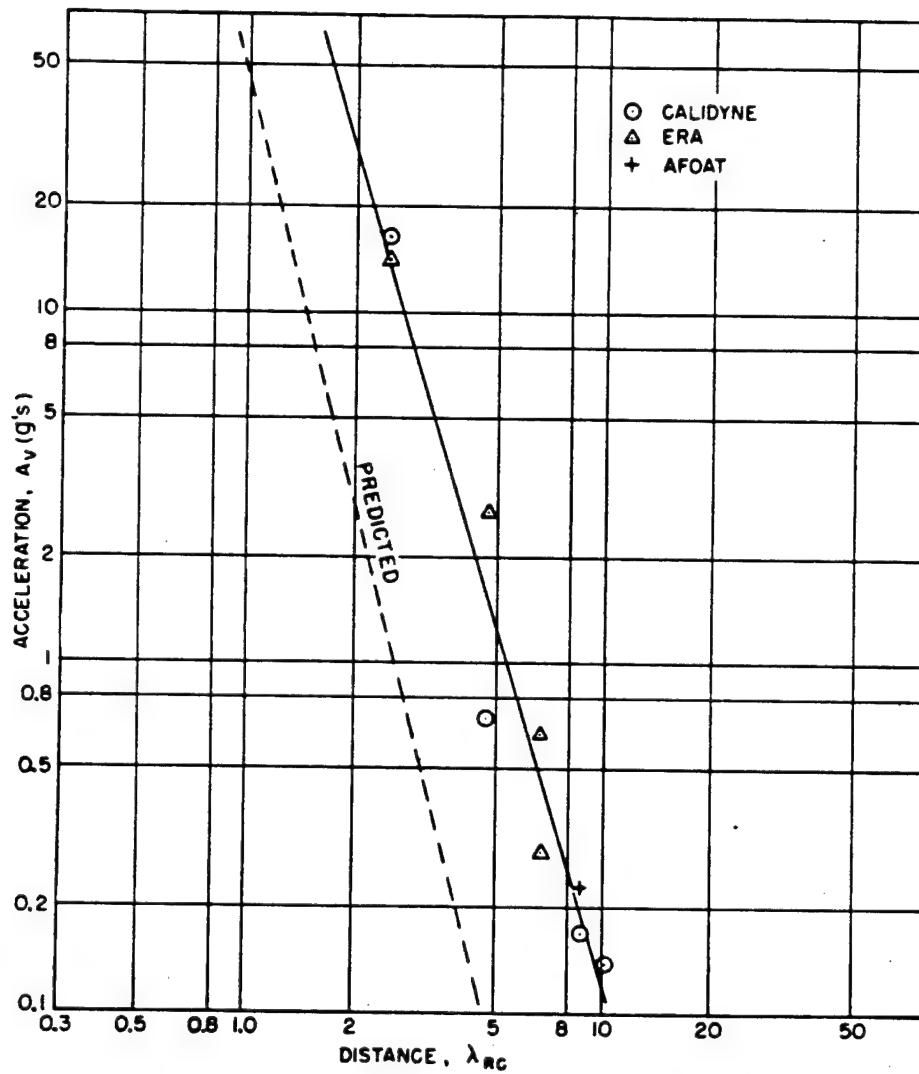


Fig. 6.4 First Peak Vertical Acceleration as a Function of λ_{RC} , Easy Shot

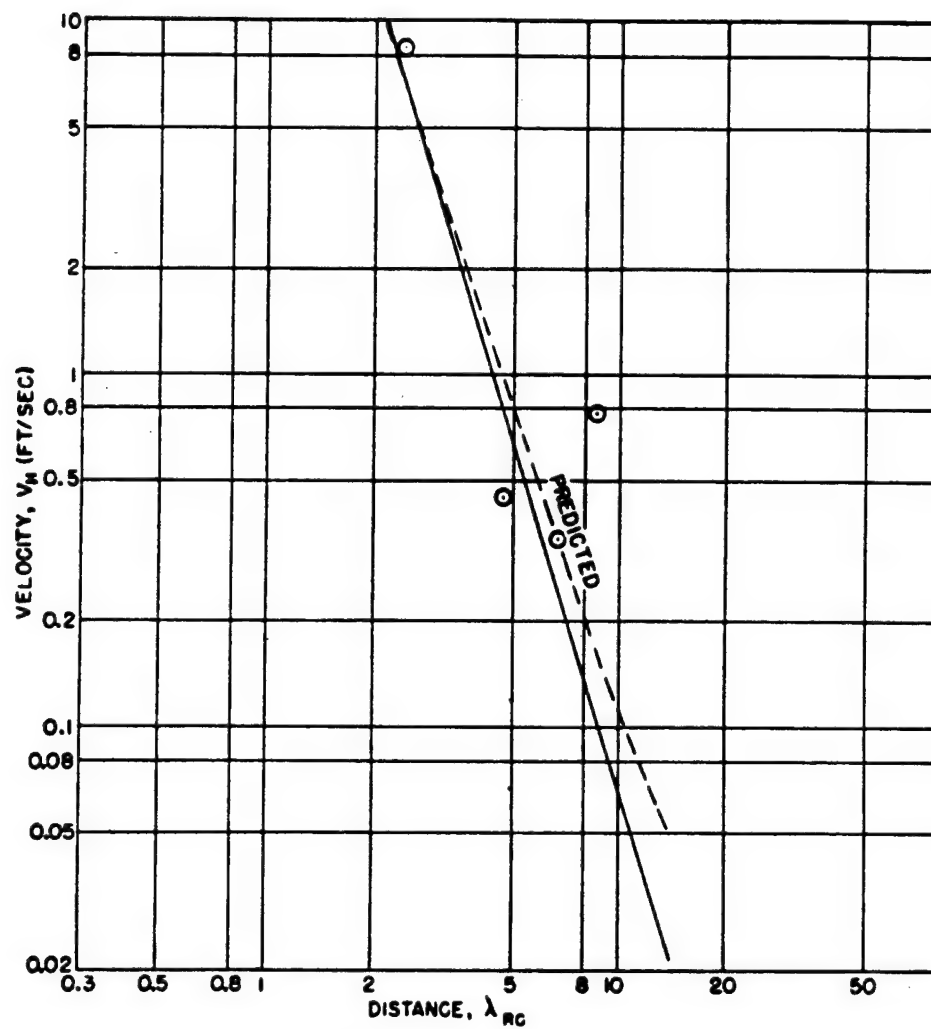


Fig. 6.5 Maximum Horizontal Velocity as a Function of λ_{RC} , Easy Shot

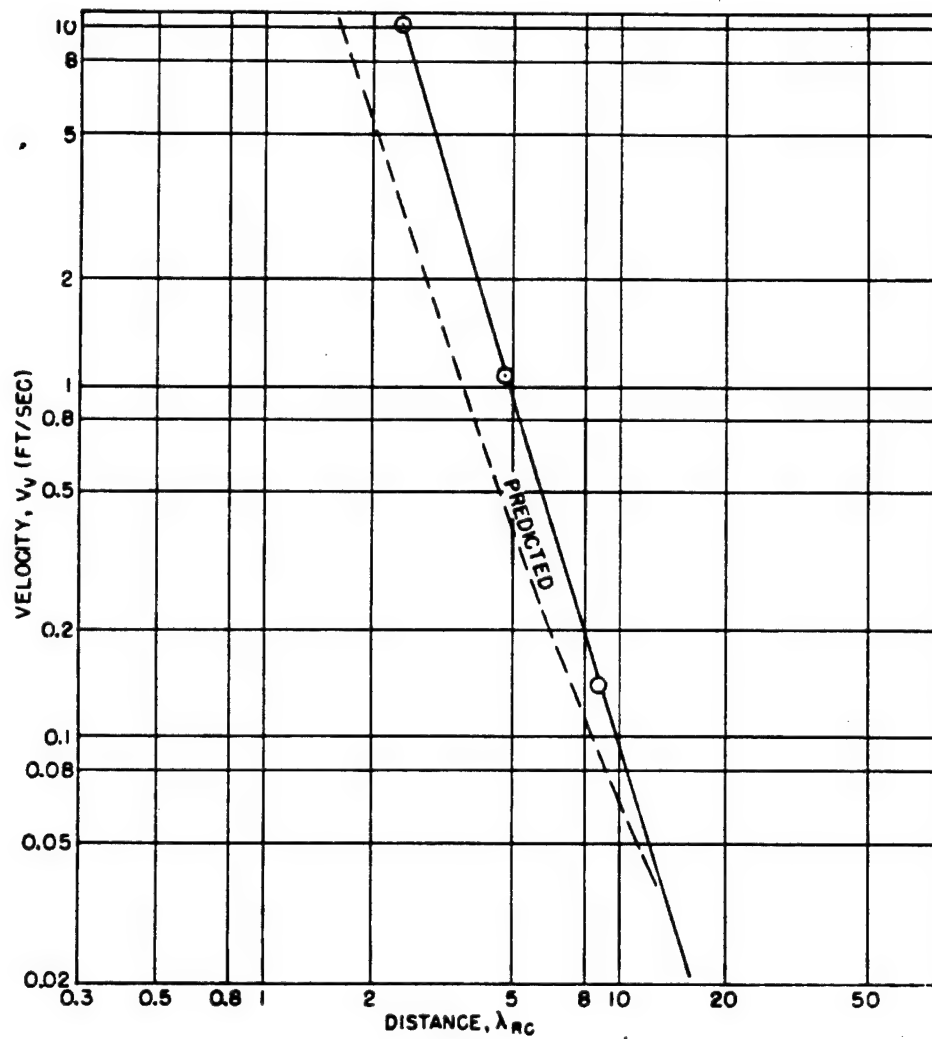


Fig. 6.6 Maximum Vertical Velocity as a Function of λ_{RC} , Easy Shot

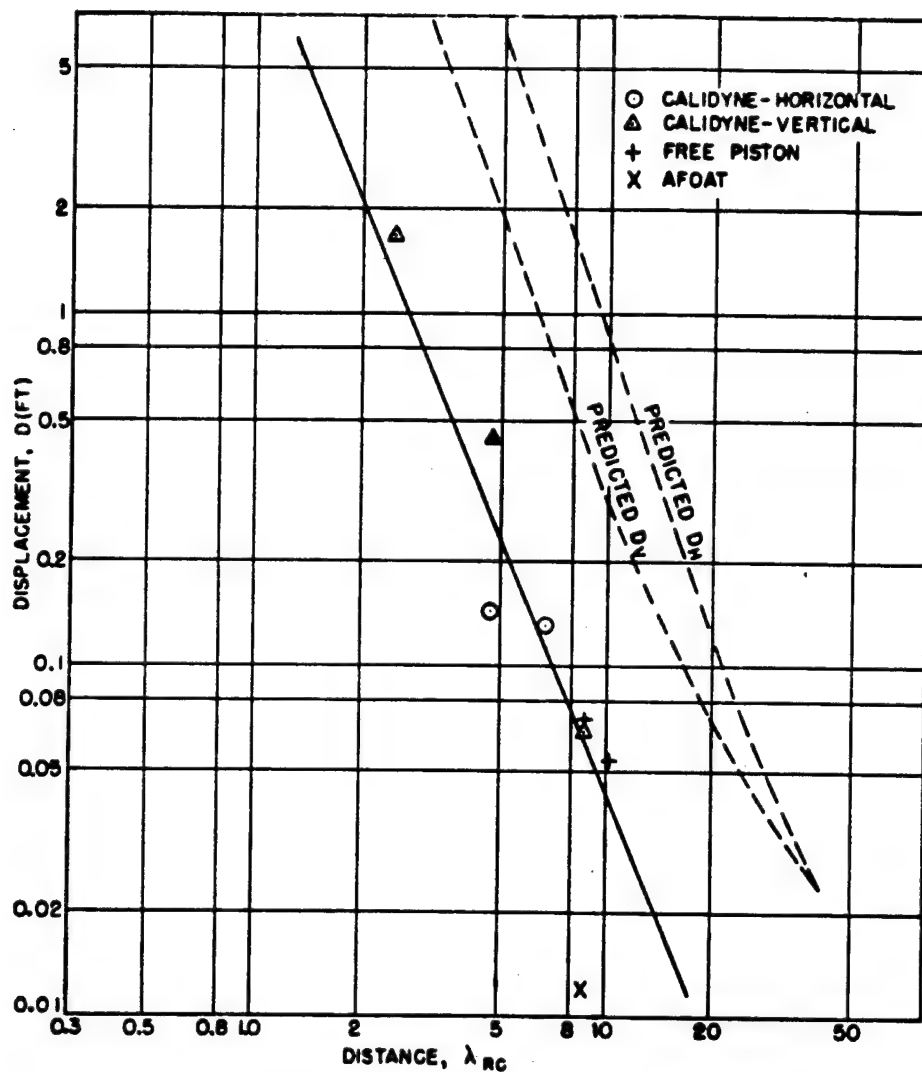


Fig. 6.7 Maximum Displacement as a Function of λ_{RC} , Easy Shot

and should in principle be representative of the maximum value of transient displacement of the instruments during the blast. The values of displacement are lower by a factor of 10 or more than would be predicted by scaling of high-explosive results. This, of course, is consistent with the smaller period or higher frequency of the disturbance, which resulted in an excess of acceleration and deficit in motion over that expected.

The performance of the instrumentation on George Shot was extremely poor due partly to the rain and poor weather preceding the shot, which filled up instrumentation holes with water, and partly to recording failures due to the deterioration of equipment in the tropics. Acceleration readings over the range of distances were obtained, however, from the backup instrumentation, which was self-recording, but the records were not in a form to lend them-

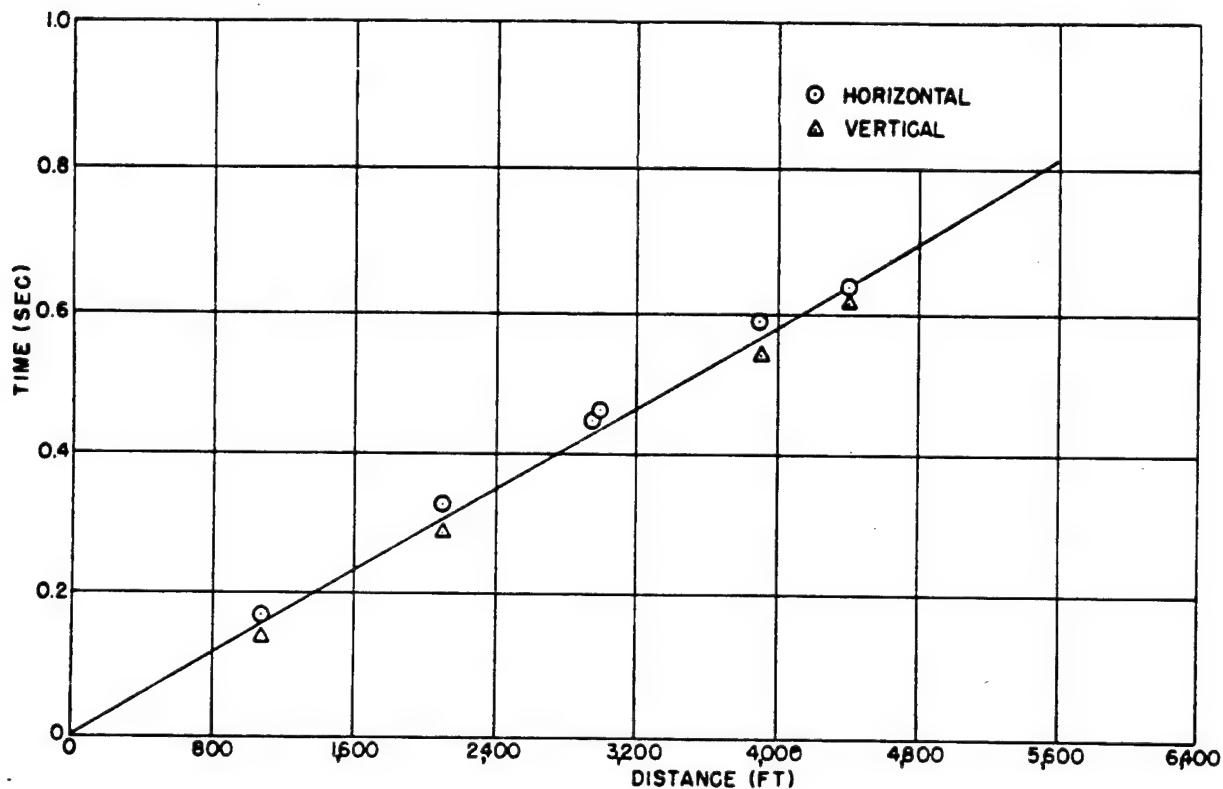


Fig. 6.8 Time-travel Curves for First Ground Motion, Easy Shot

Figure 6.8 shows the times of arrival of the first discernible disturbance on the record as a function of distance from ground zero. The slope of this curve indicates a seismic velocity of 6,900 ft/sec for the upper layers through which the signal first arrived. There is a slight indication that the remote distances are beginning to receive the signal from a deeper high-velocity layer but the departure from the general slope is too small to be significant.

selves easily to integration because the information appears as modulation on a wave envelope and requires transcribing. This has not been done to date.

Figure 6.9 shows the combined curve of the horizontal and vertical accelerations observed on this shot.

DNA
(6)(3)

DNA
(b)(3)

ACCELERATION, A (g's)

DISTANCE, λ_{RC}

Fig. 6.9 First Peak Acceleration as a Function of λ_{RC} , George Shot

DNA
(b)(3)

6.5 SUMMARY

The results presented in this chapter, which are a condensation of the detailed report² on the experiment, indicate that the frequency of the seismic disturbance did not decrease proportionally to the scale, a result that had been observed at the Trinity experiments also. Whether this effect is a general result or not cannot be determined at this time, but reference made only to the two instruments shots (Trinity and Greenhouse) which occurred under radically different terrain conditions would indicate that a large explosion over the surface excites characteristic oscillations of the earth's surface which do not scale in the same manner

as small-scale underground charges. The consequences of the higher excited frequency of earth motion is that the accelerations are higher whereas the actual displacements are lower in about the same proportions. Current large-scale explosive tests should cast some light on this problem and probably indicate whether the same increase of frequency over scaled value will hold for underground explosions. Another question of interest, of course, is the effect of this possible change in character of the oscillations on the damage inflicted to structures.

Regardless of the generality of the results obtained in this experiment, it should be possible for the interested agencies to obtain from these measurements the general order of magnitude of the ground motion at selected parts of this island, which was the principal objective of the measurement program.

REFERENCES

1. M. B. Dobrin et al., Subsurface Constitution of Bikini Atoll as Indicated by a Seismic Refraction Survey, Bull. Geol. Soc. Am., 62: 807 (1951).
2. Greenhouse Report, Annex 1.6, Part VI, Sec. 1.

Chapter 7

Administrative and General Technical Details

7.1 SCOPE

This chapter contains brief summaries of the administrative arrangements that were used by the Blast Measurements Group on Operation Greenhouse and of technical details of general interest, not separately discussed in the individual instrumentation reports.

7.1.1 Authorization

The problem of making air-blast and ground-shock measurements for the 1951 atomic weapons tests was assigned jointly to the Naval Ordnance Laboratory (NOL), White Oak, Silver Spring, Md., and the Ballistic Research Laboratories (BRL), Aberdeen Proving Ground, Md., by official correspondence in the winter of 1948-1949. Shortly thereafter one measurement, that of free-air peak pressures as measured by telemetering blast-arrival times from transmitters hung along a balloon cable, was taken over by the Armed Forces Special Weapons Project (AFSWP) under the technical direction of NOBL, as the combined NOL, BRL, and AFSWP group was designated.

7.1.2 Chronological Summary

A few highlights of the Blast-measurements Program are listed below to indicate the time scale of the project.

December 1948	First major planning conference at Los Alamos
28 March 1949	First funds assigned to NOBL
20 May 1949	First progress report of NOBL
8 August 1949	AFSWP program under way

8 September 1949	Major instrumentation decided upon
October 1949	Personnel recruiting essentially completed
15 February 1950	Building 336 completed at NOL for blast-measurements works
November 1950	Overseas packing started
20 December 1950	Last major shipment leaves East Coast
3 February 1951	Advance (cable-laying) party arrives at Eniwetok Atoll (See Appendix A for details)
8 March 1951	Main party arrives at Eniwetok Atoll
8 April 1951	First shot instrumented by NOBL
21 April 1951	Second shot instrumented by NOBL
9 May 1951	Third and last shot instrumented by NOBL
24 May 1951	Roll-up completed; bulk of data analyzed
28 May 1951	Last personnel leave Eniwetok Atoll

7.2 ADMINISTRATIVE DATA

7.2.1 Division of Responsibilities

The various blast-measurements programs were divided among the NOL, BRL, and AFSWP groups as follows:

1. Free-air pressures by blast-velocity-switch telemetering from balloons—AFSWP [and Edgerton, Germeshausen, & Grier (EG&G)]
2. Pressures by photography of shock waves and rocket trails—NOL (and EG&G)

3. Mach-region peak pressures by blast-velocity switches—BRL

4. Mach-region peak pressures by indenter gauges—NOL

5. Mach-region peak pressures by foil meters—BRL

6. Mach-region pressure-time (inductance and spring-piston gauges)—NOL

7. Regular region reflected pressures—NOL

8. Ground-shock measurements—BRL

7.2.2 Personnel

The personnel who participated in the field program, together with their primary assignments and laboratory affiliations, are listed in the accompanying table. Most of these men are pictured in Fig. 7.1.

Name	Assignment	Laboratory
G. K. Hartmann	Program Director	NOL
C. W. Lampson	Associate Program Director	
	Director	BRL
S. N. Anastasian (LCDR, USN)	Inductance gauges	NOL
C. J. Aronson	Technical Assistant to Program Director	NOL
J. E. Berry	Inductance gauges	NOL
E. J. Bryant	Velocity switches	BRL
M. F. Clarke	Velocity switches	BRL
W. E. Curtis	Velocity switches (in charge)	BRL
G. B. Eggenberger (RELE, USN)	Telemetry	AFSWP
R. T. Ellis	Telemetry	APL/JHU (AFSWP)
A. J. Frolich (Lt Col, USA)	Telemetry (in charge)	AFSWP
J. O. Green (Maj, USA)	Telemetry	AFSWP
F. L. Hafer (LT, USN)	Telemetry	AFSWP
C. L. Karmel	Shock-wave photography	NOL
R. L. Knodle	Inductance gauges	NOL
R. P. Long	Velocity switches	BRL
N. M. Masich (Lt Col, USAF)	Velocity switches	BRL
J. J. Meszaros	Foil meters (in charge)	BRL
J. R. Mitchell	Logistics (in charge)	NOL
W. H. Moore (Maj, USAF)	Cable laying (in charge)	NOL
J. F. Moulton, Jr.	Shock-wave photography (in charge)	NOL
J. J. O'Connor	Ground shock	BRL
F. J. Oliver	Regular region pressures (in charge)	NOL
D. R. Powers (1st Lt, USA)	Ground shock (in charge)	BRL
J. F. Price	Inductance gauges (in charge)	NOL
G. D. Robertson (LT, USN)	Telemetry	AFSWP
J. D. Rowe	Inductance gauges	NOL
P. E. Shafer	Indenter gauges (in charge)	NOL
J. V. Shepherd (M/Sgt, USA)	Telemetry	AFSWP
B. T. Simonds (CDR, USN)	Shock-wave photography	NOL
J. T. Smith (LT, USN)	Telemetry	AFSWP
G. M. Sokol	Inductance gauges	NOL

Name	Assignment	Laboratory
J. F. Steelman (Capt, USA)	Telemetry	AFSWP
Garth Stevens (Maj, USA)	Telemetry	AFSWP
W. J. Taylor	Velocity switches	BRL
R. L. Vader (LT-JG, USN)	Spring-piston gauge (in charge)	NOL
E. R. Walthall	Spring-piston gauge	NOL
W. S. Winn (Capt, USAF)	Telemetry	AFSWP
Seymour Yalen (LT, USN)	Telemetry	AFSWP
C. G. Young (Maj, USAF)	Telemetry	AFSWP



Fig. 7.1 Main Group of NOBL Personnel

7.3 COSTS

Approximate costs of the Blast-measurements Program are listed below for the NOL, BRL, and AFSWP groups to show the program's magnitude. A coarse breakdown of the NOL costs is also listed to provide a guide for future estimating and to show in a rough way how costs were distributed.

7.3.1 Total Costs (Approximate) (Exclusive of Holmes and Narver (H&N) charges for construction and support in the field and of salaries for military personnel)

NOL	\$742,836
BRL	260,000
AFSWP	180,000
Total	\$1,182,836

7.3.2 NOL Cost Breakdown (Including estimated costs for last half of Fiscal Year 1951 and for Fiscal Year 1952)

Operations

Salaries and Wages	\$162,914
Supplies and Materials	232,749
Travel	25,028
Communications	900
Fixed Charges	147,733
Services of Other Naval Estabs.	7,912

(Subtotal) Operating Expense \$577,236

Equipment

Purchased and Fabricated	\$64,000
Building 336 at NOL	101,600

(Subtotal) Equipment \$165,600

Total Expenditures \$742,836

7.4 SUPPLIES AND SHIPPING

7.4.1 Supply Arrangements at the NOL

Of the three groups (NOL, BRL, AFSWP), NOL had the largest supply problem, largely because it made some purchases for the other two groups in addition to its own purchases. Therefore a few remarks on the NOL supply procedures seem warranted. The initiation and follow-up of nearly all NOL orders was the responsibility of one man (J. R. Mitchell) assigned from the NOL Supply Department to the Explosives Research Department for this program. In other words, there was a single individual who could be consulted and counted upon to act as a link between the technical personnel and the regular supply channels at the Laboratory. Because of the experience gained on Operation Sandstone and the fact that about 18 months of preparation time was available, no serious supply problems were encountered which were not satisfactorily overcome. In a few instances the Los Alamos Scientific Laboratory was asked to supply items directly to the proving ground (such as battery acid, small high-explosive charges, and gasoline motor generators) to ease the NOL supply and shipping facilities. Among the general (i.e., not associated with any single blast-measurements program) supplies which the NOL took direct responsibility for obtaining were tool kits, stationery and drafting supplies, calculators,

reference books, heavy tools, batteries, cable, chargers, power tools, and racks. As a rule the supply requirements listed in Table 19 of Sandstone Report, Annex 5, Vol. 20, Blast Measurement Summary Report, were followed, with a few additions worthy of special comment below.

7.4.2 Special Supplies

It was found that powder-actuated tools such as are marketed under the trade names "Ram-set Guns" and "Drive-It" were invaluable for mounting equipment on the concrete walls of blast huts. These devices enabled the technical workers to do this job themselves with a minimum of time and effort and greatly speeded the work. The blast-velocity group found that one of their most useful supplies was a number of aluminum ladders, which were easy to handle and hence to transport from one gauge position to another. A small Multi-Stamp outfit for making multiple copies of lists and notices also proved to be a good investment. Among the useful items brought along for personal use of the field party were field shoes, ponchos, sun helmets, sun glasses, sweep-second watches, and water bags.

7.4.3 Shipping Arrangements

A successful attempt was made to organize the shipping at NOL so that a minimum of time of the technical workers would be required by this problem. The procedure was for the technical group to tag items with the group name, name of item, and destination of item. The shipping group of the project would have these items picked up and taken to an assembly building where they would be grouped for packing, invoicing, and having shipping lists made up. When a fairly large amount of material was accumulated it was taken to the main Laboratory shipping room for waterproofing, tropicalization, and boxing. From this point boxes were shipped to the West Coast, in most cases by motor van.

7.4.4 Return Shipping

Return shipping was taken care of by the BRL, NOL, and AFSWP groups in the field with the aid of H&N labor, in accordance with procedures set up by Los Alamos Scientific Laboratory.

7.4.5 Amount of Shipping

Laboratory	Pieces	Tons	Cu Ft
From USA to Forward Area			
NOL	1,200†	136	10,368.4†
BRL	227	17	1,384.6
AFSWP	201	18	4,058.2
Total	1,628	171	15,811.2

Return from Forward Area to USA

NOL	241‡	34.0	2,467.7
BRL	95	7.0	800.0
AFSWP	93	11.3	3,287.5
Total	429	52.3	6,555.2

†Includes an estimated 500 reels of cable for all groups.

‡Includes an estimated 4,000 cu ft of cable for all groups.

§Includes 101 reels of cable for all groups returned to AEC.

7.5 CONSTRUCTION DETAILS

A number of construction problems common to more than one technical group will be briefly discussed in this paragraph. Engineering design and construction of field installations (see Table 7.1) were performed by H&N, all work being based on preliminary NOBL designs, and with few exceptions these were entirely satisfactory. The two most important constructions of interest to more than one NOBL measurement group were four blast huts (Stations 23 and 25) and fifteen instrument walls (Stations 20 and 21), which will be discussed in Secs. 7.5.1 to 7.5.3. Besides these there were three facilities of interest to several groups which are mentioned solely to remind planners for subsequent tests of their value. These were an air-conditioned photographic darkroom, a small dehumidified laboratory, and a number of 14-by 20-ft tents located near each blast hut for storage of unpacked apparatus and for final assembling and check outs of instruments. Finally there were a few facilities which will be briefly mentioned here to supplement details furnished in specific technical reports; these

include (1) pylons (for the inductance gauges), (2) velocity-gauge posts, (3) ground-shock stations, (4) explosives storage huts, and (5) crusher-gauge mounts.

7.5.1 Blast Huts

On each shot site there was one blast hut [inside dimensions 10 by 15 by 7 ft (high)] left over from Operation Sandstone (Station 23a). These were modified and reused by the blast-measurements groups as follows: On Runit and Biihiri no additional space was provided, but forced ventilation was installed and additional T slots were fixed to the walls. On Engebi, in addition to this, the existing blast hut had a new door cut out of one wall, and an extra chamber (Station 23b) for batteries and converters was added. This had dimensions 8 by 15 by 7 ft (high). Figure 7.2 shows the structural plans and details for Stations 23a and 23b. The only entirely new blast hut was Station 25, located at the end of the short blast line on Engebi. It had inside dimensions of 14 by 15 by 7 ft (high) and was by far the best design (Fig. 7.3). The conclusions drawn from the use of these huts were that the open area of Station 25 was better than the divided area of Stations 23a and 23b and that, in general, the forced-ventilation system provided was inadequate and unsatisfactory. The system provided had long ducts with small openings running across the back of the huts. A better system would have had only flush wall openings on each side of the hut, remote from the door. The ventilating motors provided were designed to move 400 cfm of air on Runit and Biihiri and 600 cfm on Engebi long line (Stations 23a plus 23b). Station 25 was provided with a 750-cfm system. All systems were inadequate, perhaps because the design did not adequately anticipate the fumes emitted by batteries under charge. Figures 7.4 to 7.8 illustrate the appearance of the blast huts.

7.5.2 Instrument Walls

As was discussed in Chap. 2 it seemed desirable to reduce flow effects on the pressure-time gauges by mounting them in streamlined housings. It also seemed desirable to reduce the effects of ground unevenness by mounting all gauges at least a few feet above the general level of the terrain. The resulting design of instrument wall was made up of a welded-steel-

plate field panel 5 by 8 by 1 ft (thick), Fig. 7.9, to hold the gauges; this was mounted integrally within a concrete wall, Stations 20 and 21, which had rounded ends and extended 10½ ft on each end of the panel, Fig. 7.10. The mechanical design of the blast wall is illustrated by Fig. 7.11. The hollow portion of the field panel, not occupied by gauge chambers or bracing, was filled with concrete. The sand surfaces of the blast

shots where walls were used and might have been prevented with more reinforcing rods between the walls and their foundations, as illustrated by Figs. 7.13 (Runit Station 20b) and 7.14 (Engebi Station 20b). On the other hand, at least one wall tilted with its foundation, so that perhaps heavier and deeper foundations were also needed on close-in walls, Figs. 7.15 and 7.16 (Runit Station 20c).

TABLE 7.1 HOLMES AND NARVER DRAWINGS PREPARED FOR THE BLAST-MEASUREMENTS PROGRAM

Item	Station	Site	Drawing Numbers		
			Structural Dwgs.	Mechanical Dwgs.	Electrical Dwgs.
Wall	20, 21	C, E	3E-5614.1 17G-801	17G-802 — 17G-805 17G-807 — 17G-809	
Tent	22	C, V, E			3G-082.1 — 3G-082.3
Blast hut (old)	23	C, V, E	3G-698.1	3G-5425	3G-073
Tent	24	E			3G-082.1
Blast hut (new)	25	E	3E-689	3E-5420	3E-074
Balloon anchor	26	C, E	3G-627.2		
Crusher mount (concrete)	27	C, E	17G-811		
Velocity post	28, 29	C, V, E	17G-812	17G-809	
Explosive storage.	30	C, V, E	3G-5644.1		
Crusher mount (stake)	33, 34	C, E		17G-810	
Charge rig for tower	35	C, E		3G-5658.2	
Ground shock	36	E, V	17G-813		
Pylon	37a,b,c	E	17G-815	17G-818	
Pylon (aux.)	37d,e,f	E	17G-816		
Tent	38	C, E	2H-5115		
Balloon bed	39	C, E	3E-691.3		

lines were stabilized with oil for their entire length for about 10 ft on each side of the walls. In the immediate vicinity of each wall an area was paved with asphalt 10 ft on each side of the wall and from 20 ft ahead of the wall to the trailing edge of the wall. As can be seen from Fig. 7.12, the oil stabilization was only moderately successful in obtaining a smooth surface on sand.

7.5.3 Results of Use of Walls

Use of the walls as a gauge-mounting system seems to have been successful except as discussed below. The exception to satisfactory performance of the walls occurred on both

7.5.4 Pylons and Pylon Ground Auxiliary

The pylons, Stations 37a, b, and c on Engebi, which are also discussed in earlier chapters of this report and in the Inductance Gauge Report, are essentially high walls erected to determine whether there is any effective change in the blast wave as measured at different heights above ground. As an auxiliary to each pylon there was a ground mount to hold two inductance gauges flush with the ground (Stations 37d, e, f). The pylon itself held four inductance gauges, one each of the following heights: 14, 10, 7, and 3½ ft (as shown in Figs. 7.17 to 7.20). The pylons were 15 ft by 6½ in. by 15 ft (high), which made them quite tall and thin (see Fig.

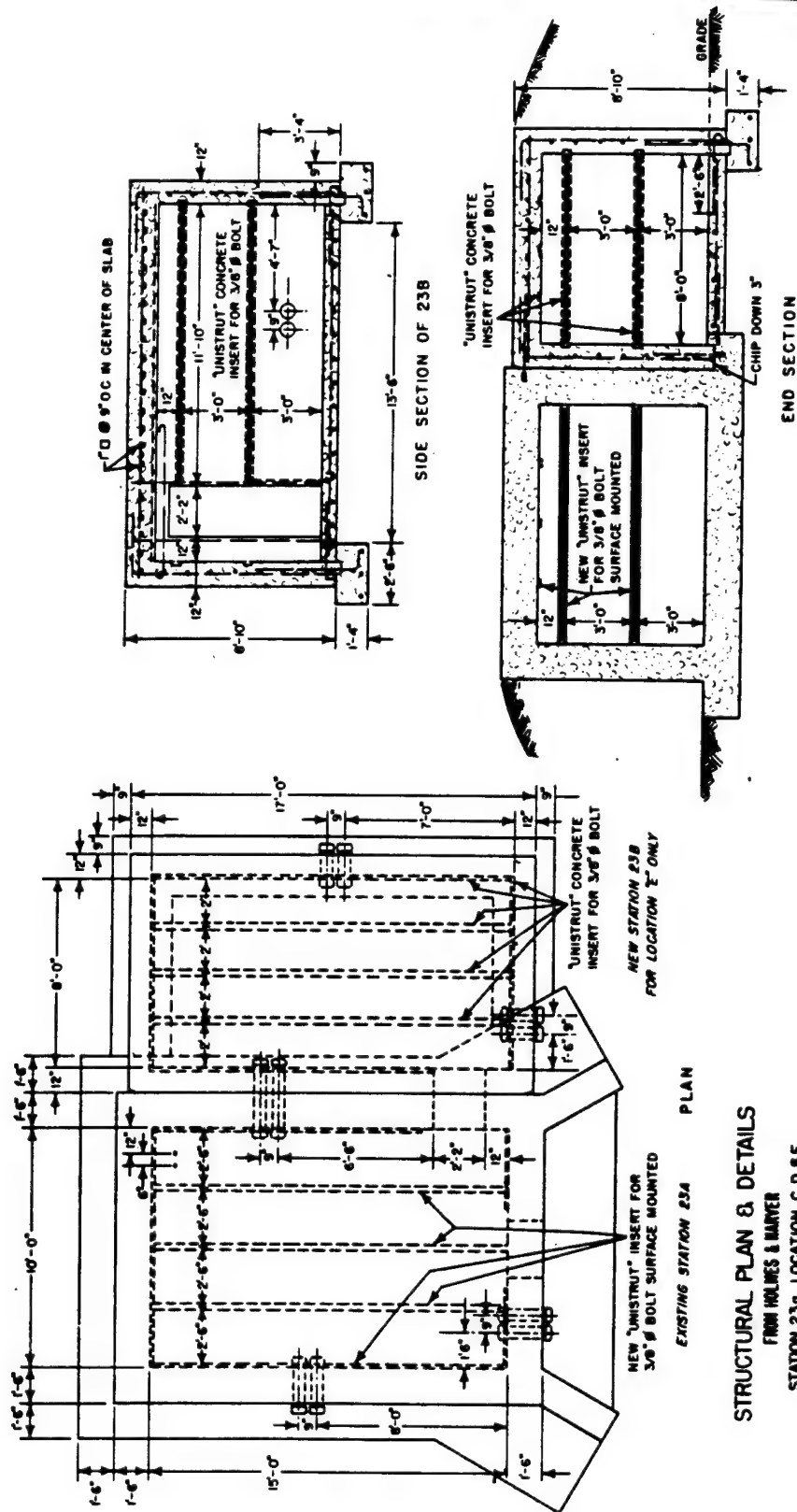


Fig. 7.2 Blast-hut Structures (Stations 23a, 23b)

Fig. 7.3 Blast-hut Structures (Station 25)

7.21). Two of the three pylons were destroyed by the blast. As shown in Fig. 7.22, pylon 37b was tipped over, together with its foundation, and Figs. 7.23 and 7.24 show that pylon 37a was uprooted and blown at least 120 ft. The man in the background of Fig. 7.24 is standing in the hole left by the foundation of pylon 37a, the remains of which are shown in the foreground.

However, it is then difficult to explain the fact that, although the H&N survey indicates that the misalignment has the leading edge of the wall to the right of the radial line as the observer faces zero, this pylon was blown away from zero and about 45° to the left of the original radius. Similarly, 37b was misaligned so that its leading edge was to the left of a radial

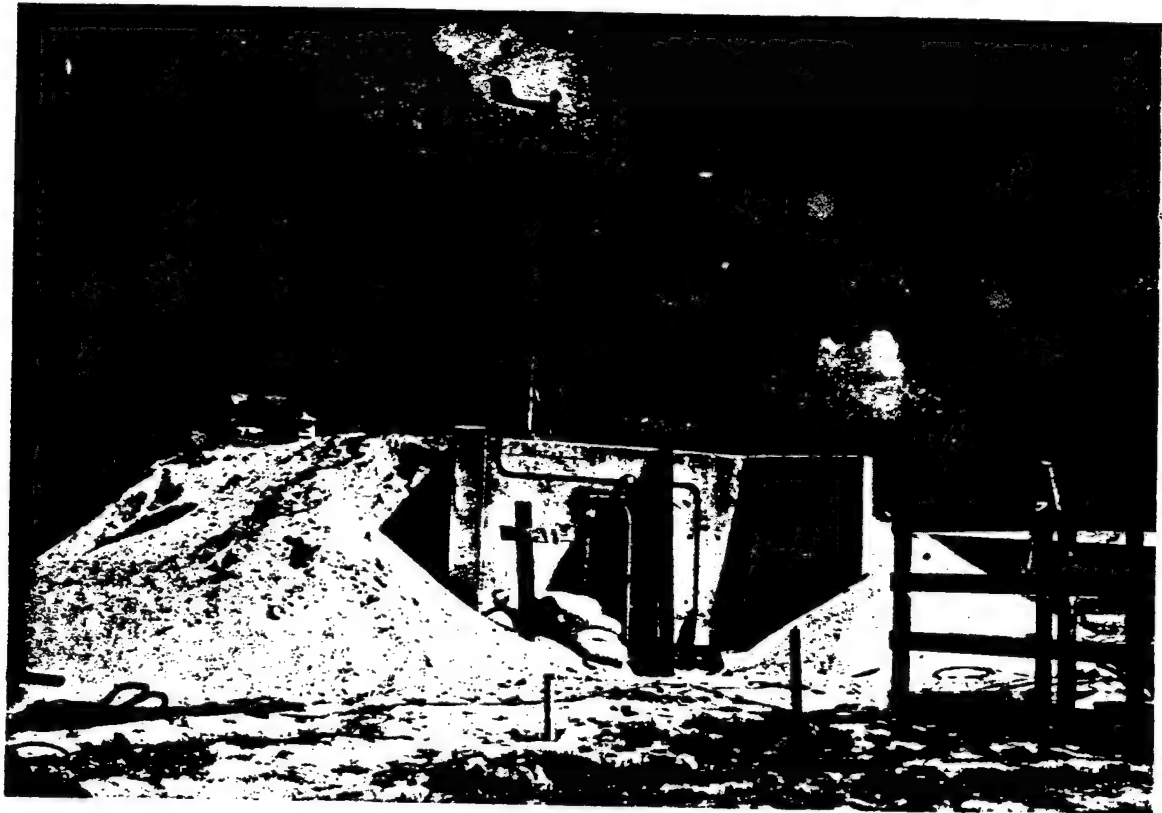


Fig. 7.4 Exterior of Station 23a, Runit

The pylons, like the wall field panels, were steel shells filled with concrete. Because of their large surface area it is not surprising that they were blown over. An attempt was made to align them to within 3' of arc with the radius from zero, but this proved to be impossible, and 37a was aligned to within 00°30'50'', 37b to within 00°04'38'', and 37c to within 00°00'06''. This, combined with the fact that the pressure level was greatest on 37a and least on 37c, is consistent with the result that 37a was uprooted and blown away, 37b was tipped over, and 37c was essentially undamaged.

line, and it was flopped over on its right side (see Fig. 7.25).

The basic design of the pylon assumed perfect radial alignment, and the calculations which were done to predict the size and weight of the pylon footing are given in Appendix B.

7.5.5 Other Instrument Stations

The velocity switches were mounted at the tops of 10-ft-long 3-in.-diameter pipes. Where there were walls, the pipe stood at the rear of the field-panel section and extended 5 ft above

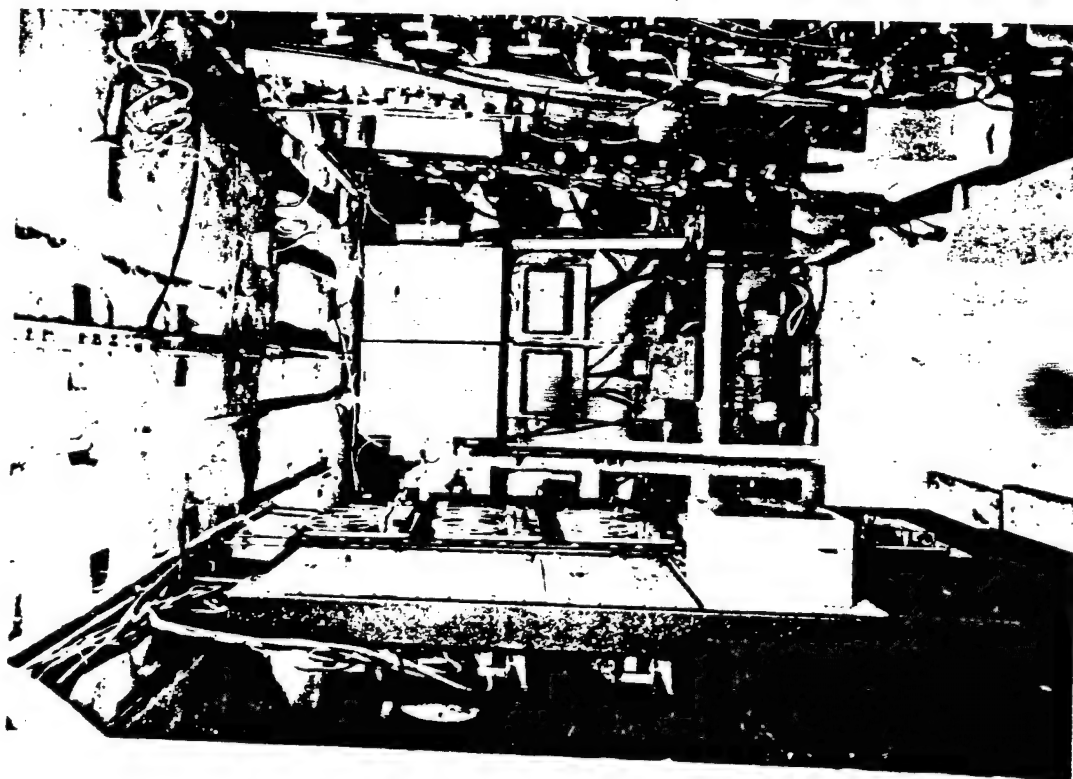


Fig. 7.5 Interior of Station 23a, Runit

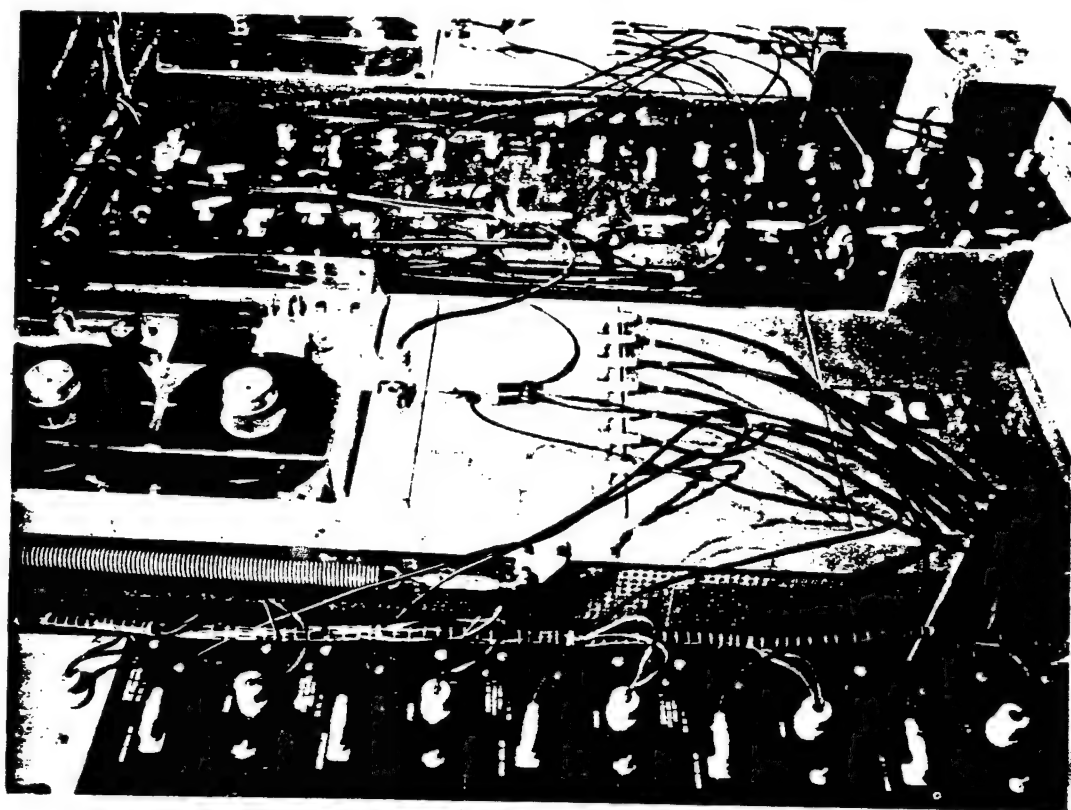


Fig. 7.6 Interior of Station 23a, Runit



Fig. 7.7 Interior of Station 23a, Engebi

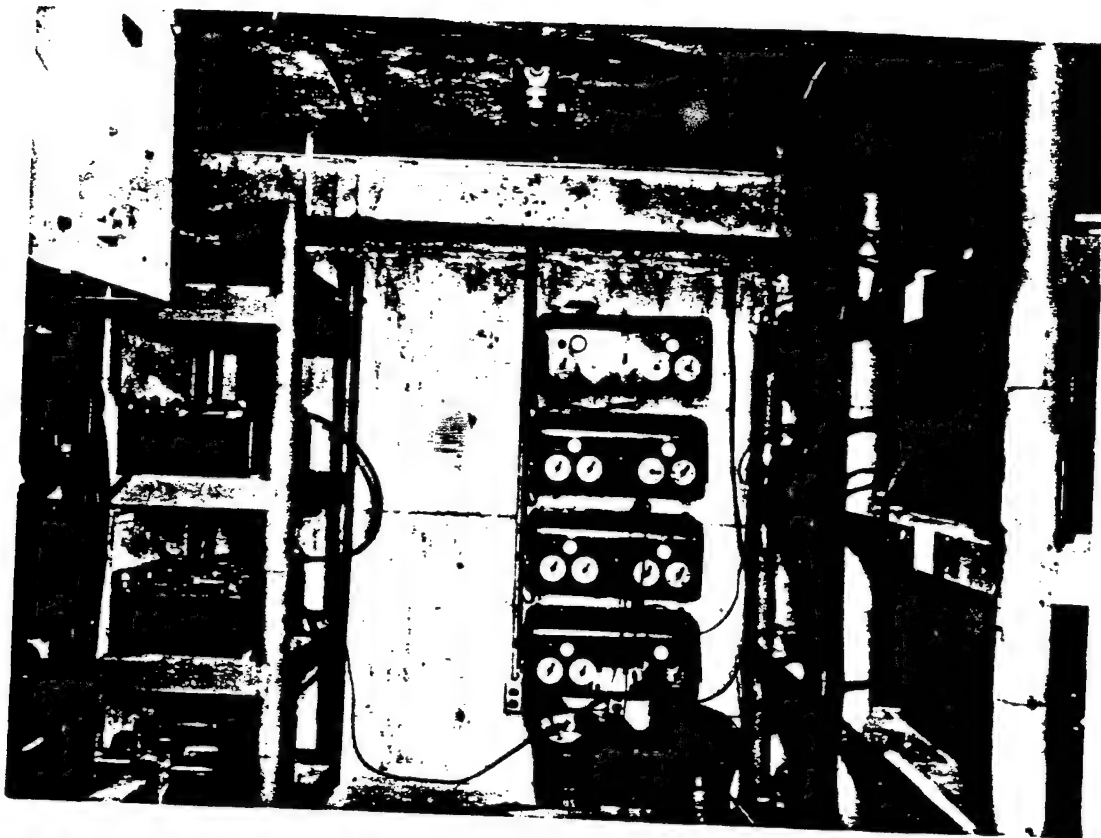


Fig. 7.8 Interior of Station 23b, Engebi

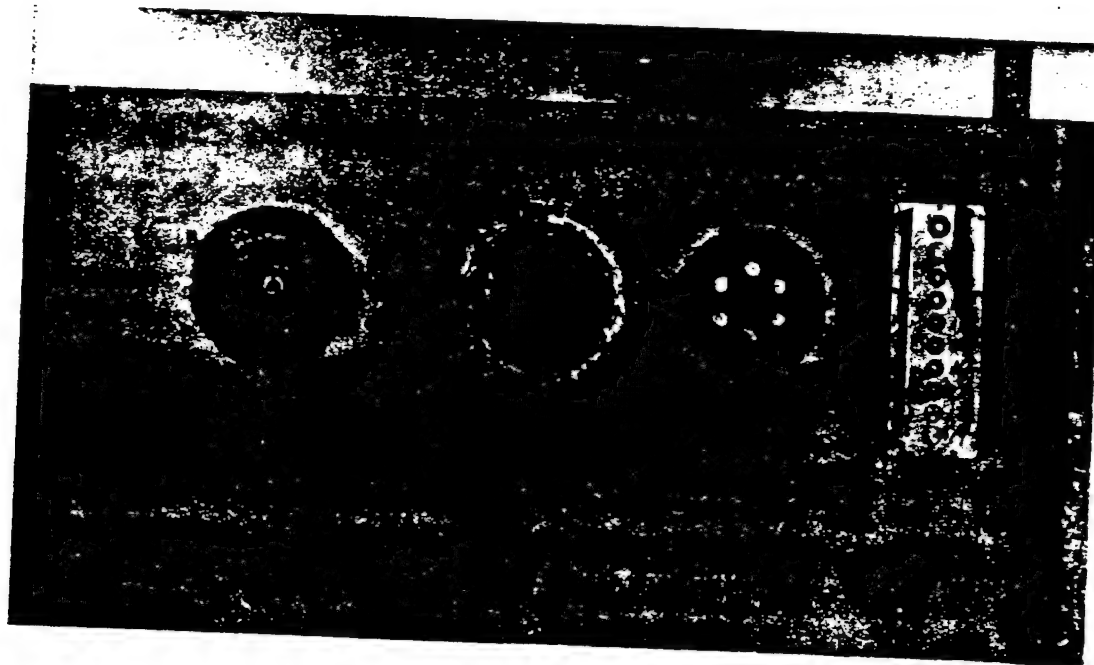


Fig. 7.9 Field Panel for Wall

the general wall height. Where there were no walls, the 10-ft length of pipe was mounted in a concrete block (Stations 28 and 29), Figs. 7.26 and 7.27.

Ground-shock stations were sunk into the ground and fastened when possible to bed coral. Sand was prevented from sliding into the hole by a lining of corrugated steel pipe. Before the shot the hole containing the instruments was filled with sand. The bolts holding the instru-

rear view of six of these relays, and Fig. 7.34 shows the front view of the same installation plus the spring-piston timing clock and the tape recorders for shock-velocity measurements.

7.7 GENERAL CONDITIONS ON BLAST ISLANDS

Figures 7.35 to 7.42 give a general impression of the appearance of the shot islands and

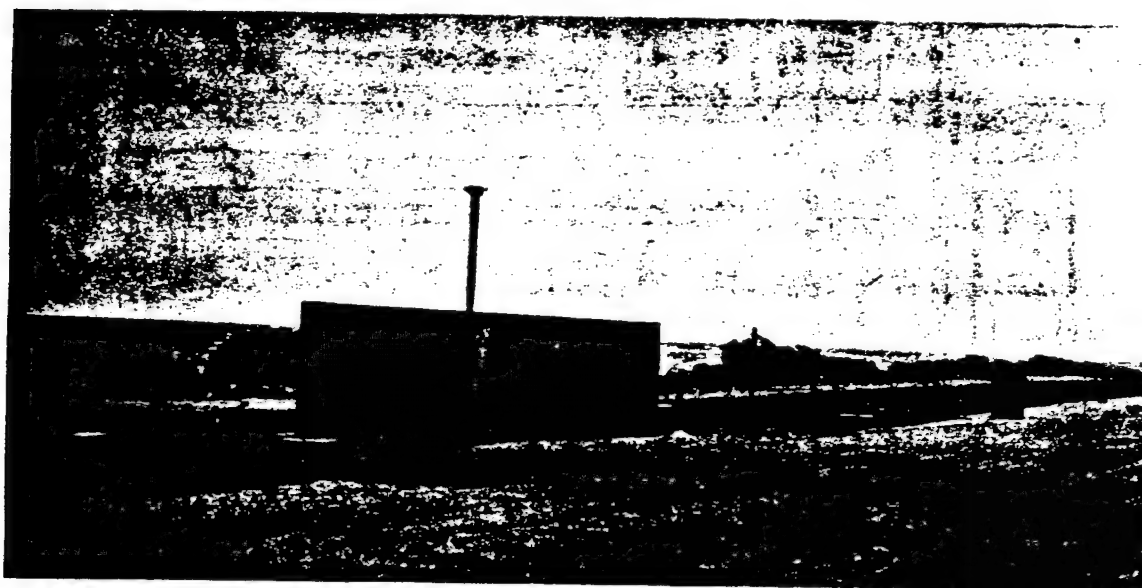


Fig. 7.10 Wall (Stations 20 and 21)

ment to the base extended to the surface as did cables fastened to the instrument. Hence recovery of gauges necessitated only loosening the long bolts and hauling out the instrument by hooking the cable over an A frame to a winch. This meant that very little hand shoveling was necessary during recovery (see Figs. 7.28 and 7.29).

Ball-crusher gauges, which were located close to ground zero, were mounted in two styles of mounts: steel plates in concrete bases holding four gauges (Figs. 7.30 and 7.31) and steel stakes holding a single gauge (Figs. 7.31 and 7.32).

7.6 TIMING SIGNALS

Timing signals and suitable timing relays were provided by EG&G. Figure 7.33 shows a

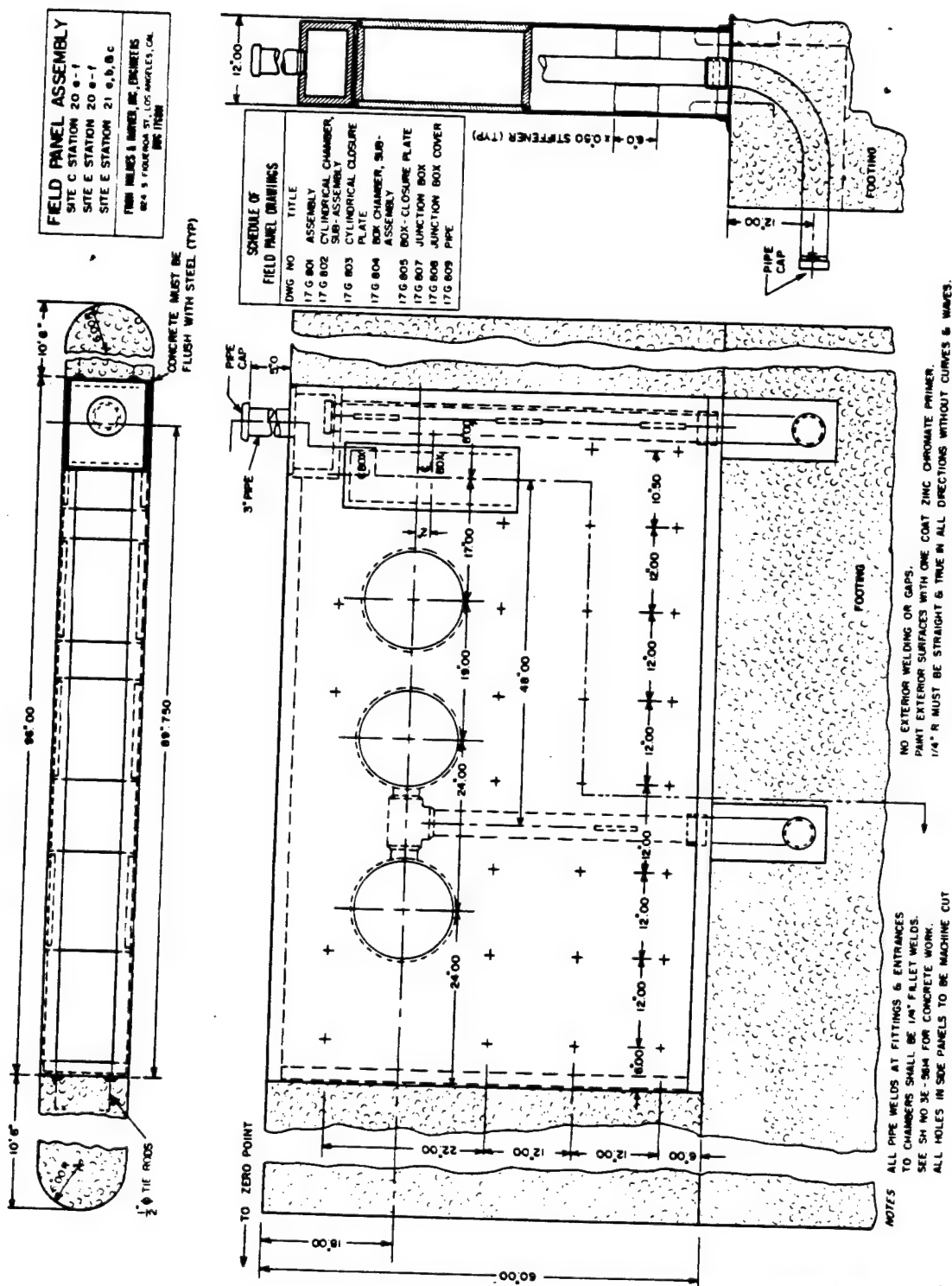
point out conditions which may have substantially affected the blast measurements.

7.8 RECOMMENDATIONS

It is appropriate to make a few recommendations, based on the experience gained during this operation, concerning items of general interest not discussed elsewhere.

1. It is advisable to bring along laboratory and shop trucks or trailers so that final adjustments in the field can be conducted under relatively dust-free conditions. These can be used up to the last minute and then driven or transported to a safe location. This gives more working time and eliminates quite a bit of packing and repacking.

2. It is advisable to bring along a special vehicle equipped with winch, A frame, and



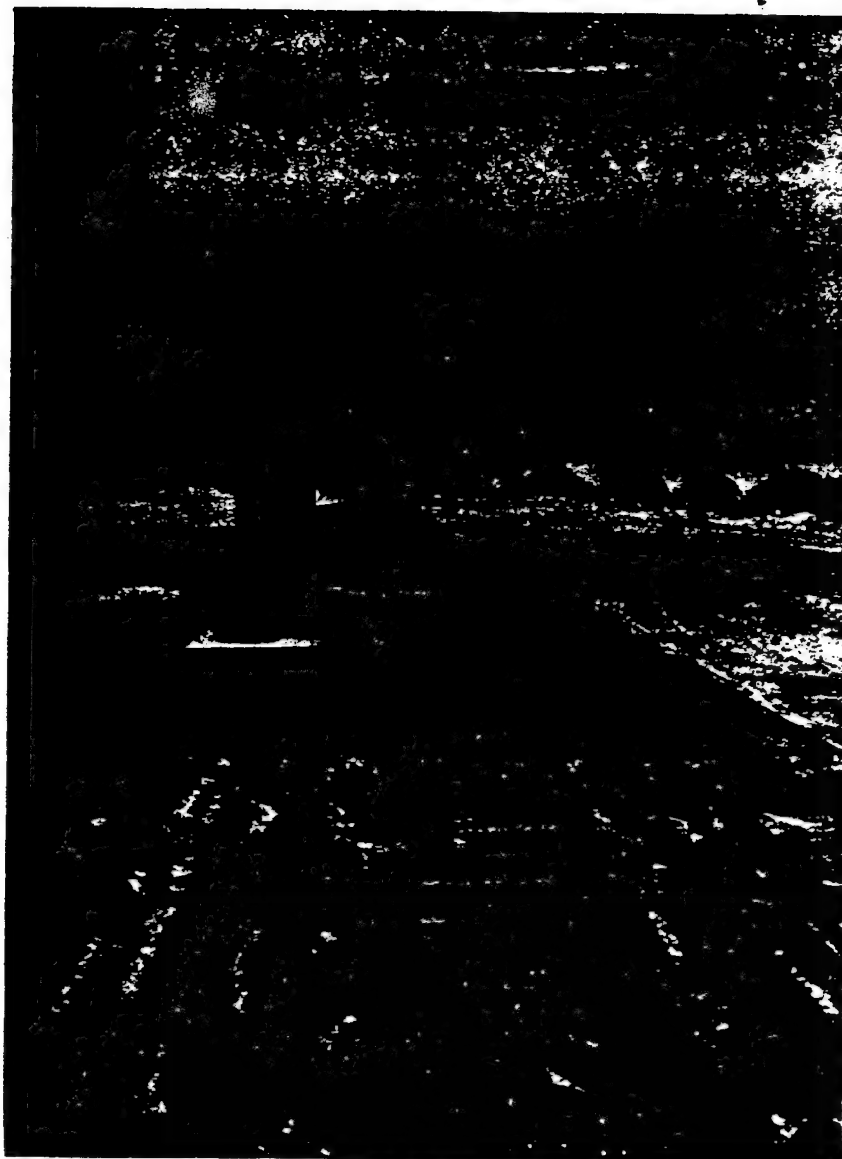


Fig. 7.12 Looking South along Blast Line near Station 20c (Runit)

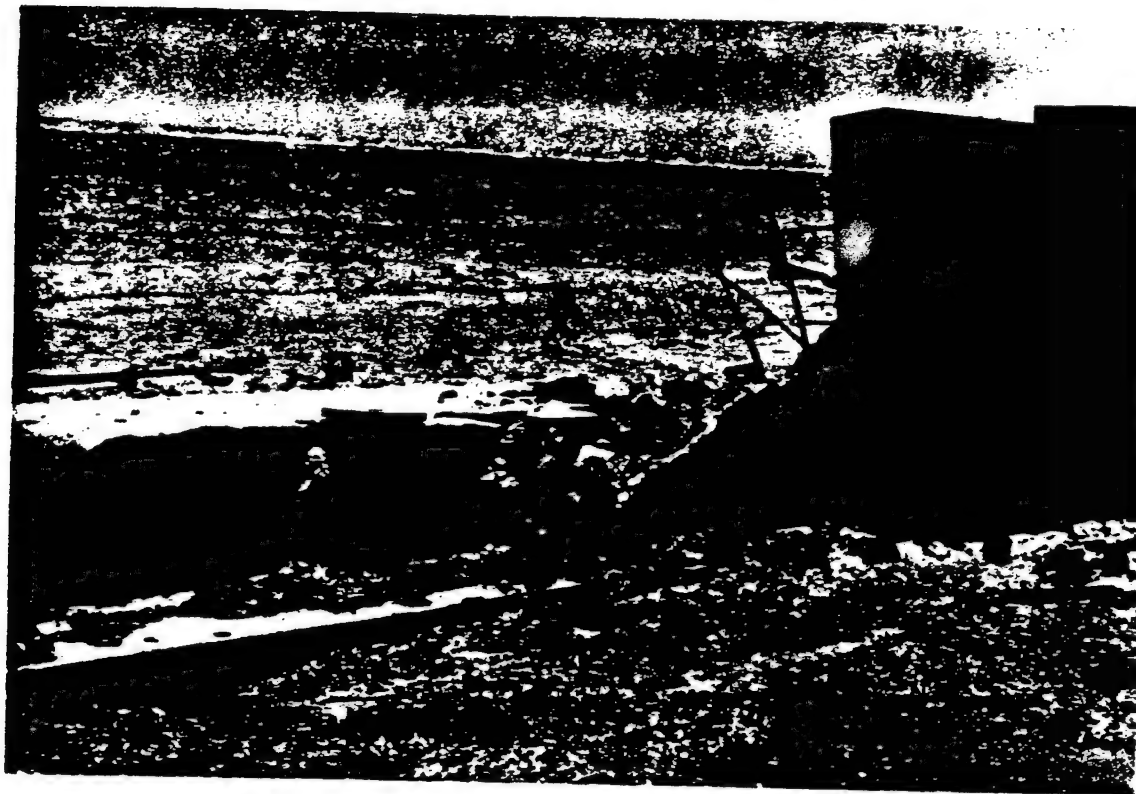


Fig. 7.13 Tipped-over Wall, Runit (Station 20b)



Fig. 7.14 Tipped-over Wall, Engebi (Station 20b)



Fig. 7.15 Inclined Wall and Foundation, Runit (Station 20c)

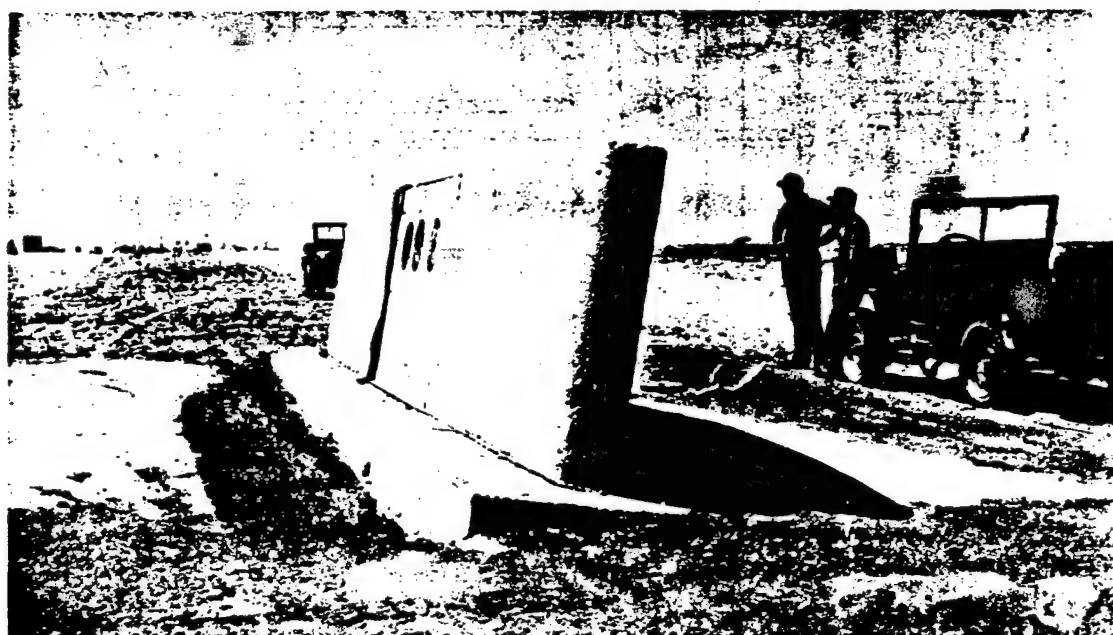


Fig. 7.16 Inclined Wall and Foundation, Runit (Station 20c)

FUNCTIONAL END
ELEVATION

190

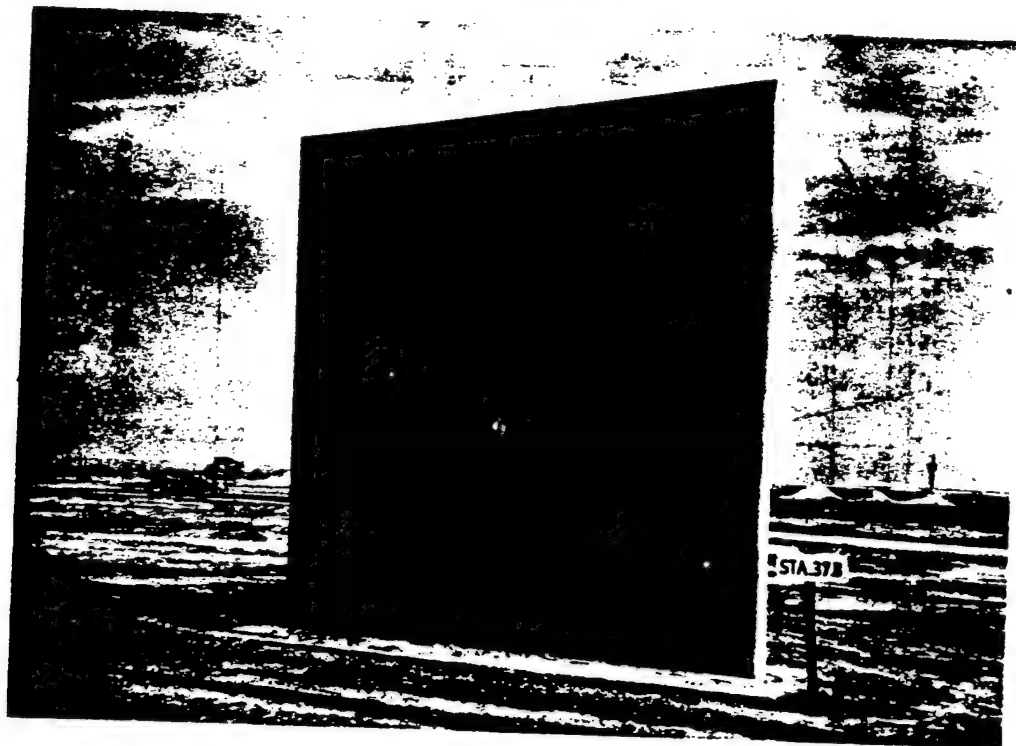


Fig. 7.19 Pylon (Station 37b)

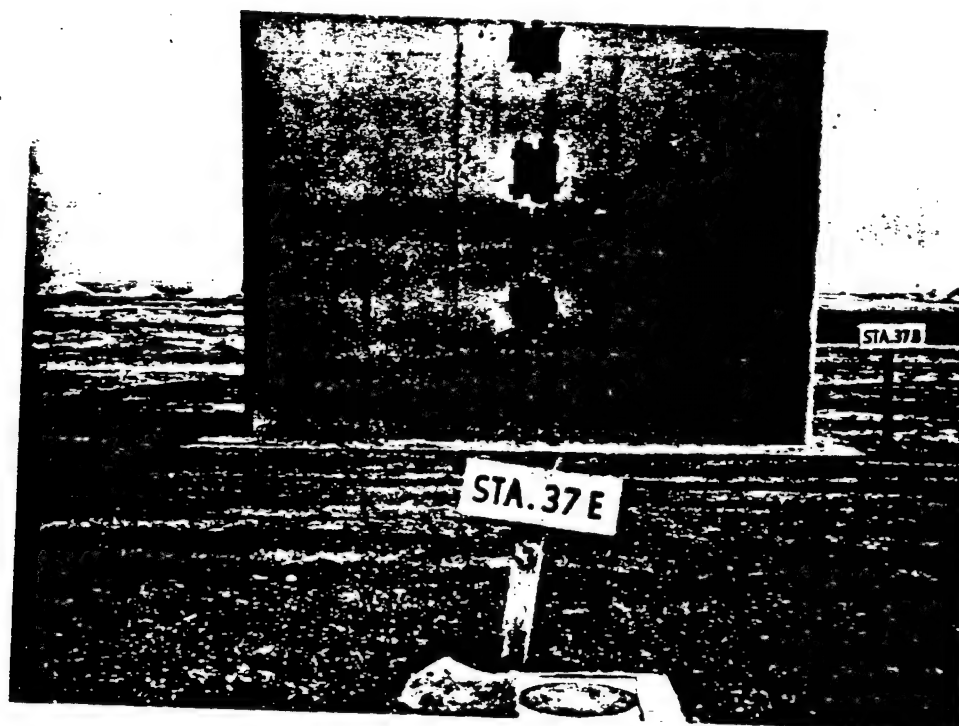


Fig. 7.20 Pylon (Station 37b) and Ground Auxiliary (Station 37e)

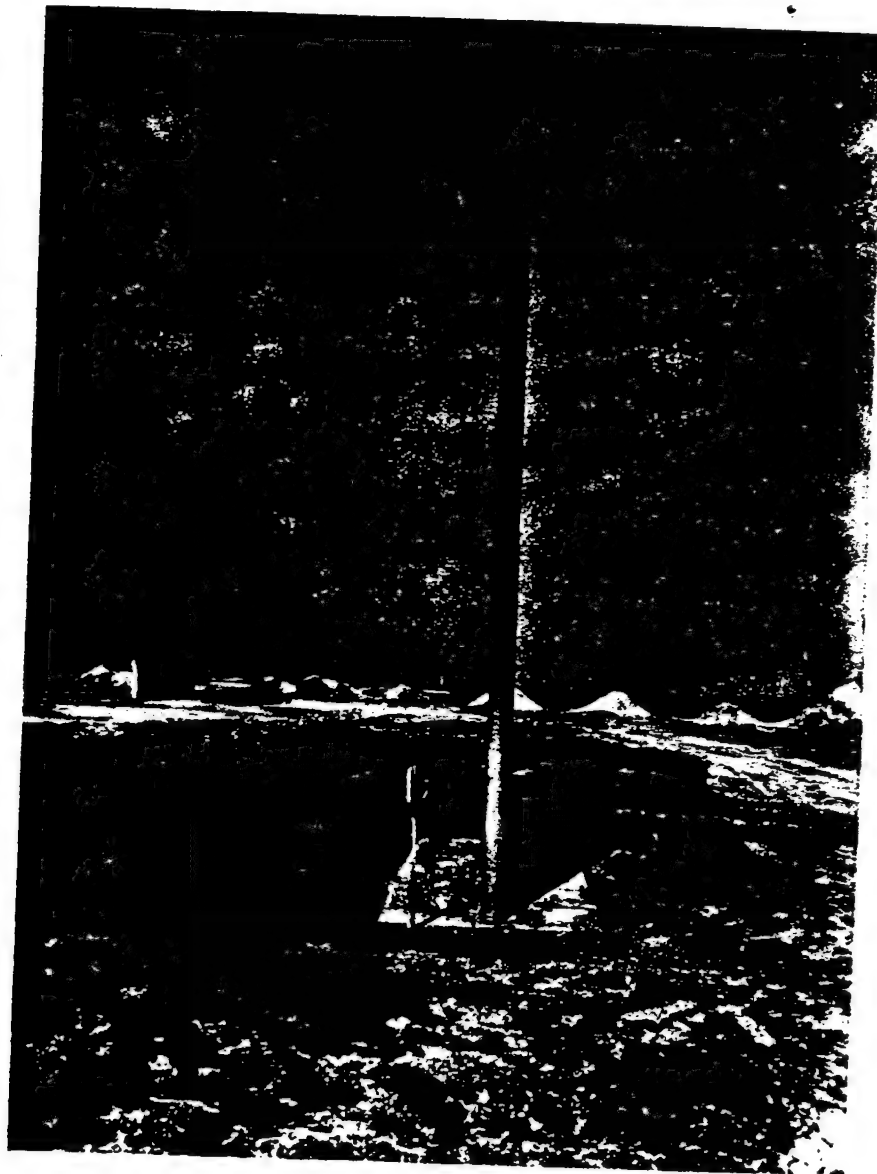


Fig. 7.21 End View of Pylon (Station 37b)



Fig. 7.22 Tipped Pylon and Foundation (Station 37b)



Fig. 7.23 Pylon Which Was Blown Away (Station 37a)

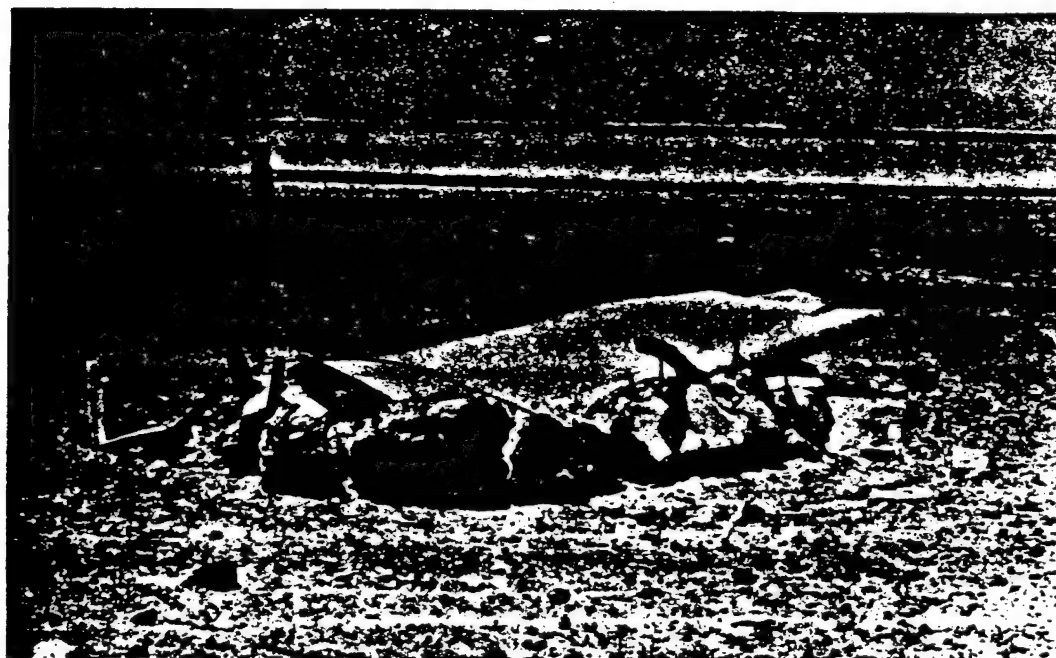


Fig. 7.24 Pylon (Blown Away) Showing Original Location (Station 37a)

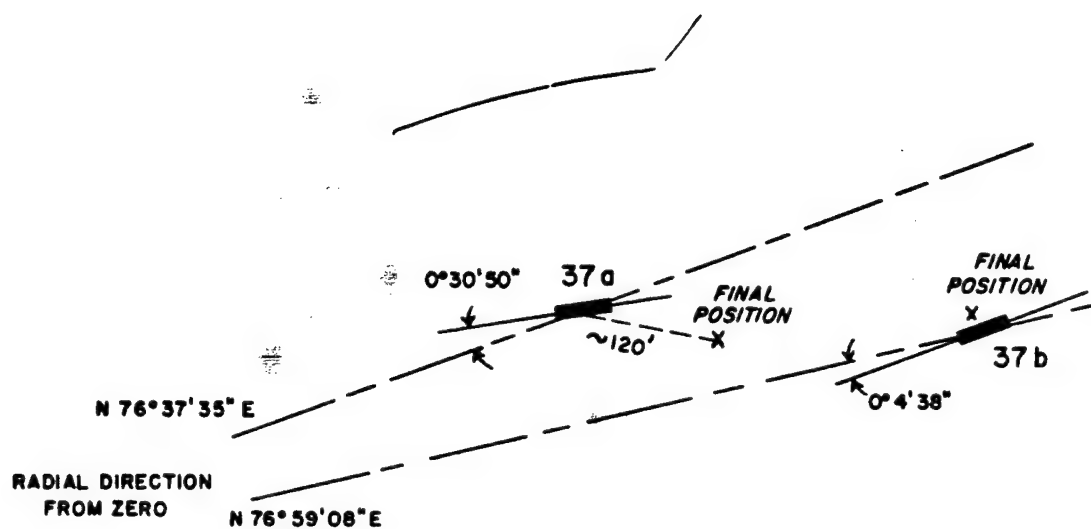


Fig. 7.25 Sketch of Pylon Misalignments

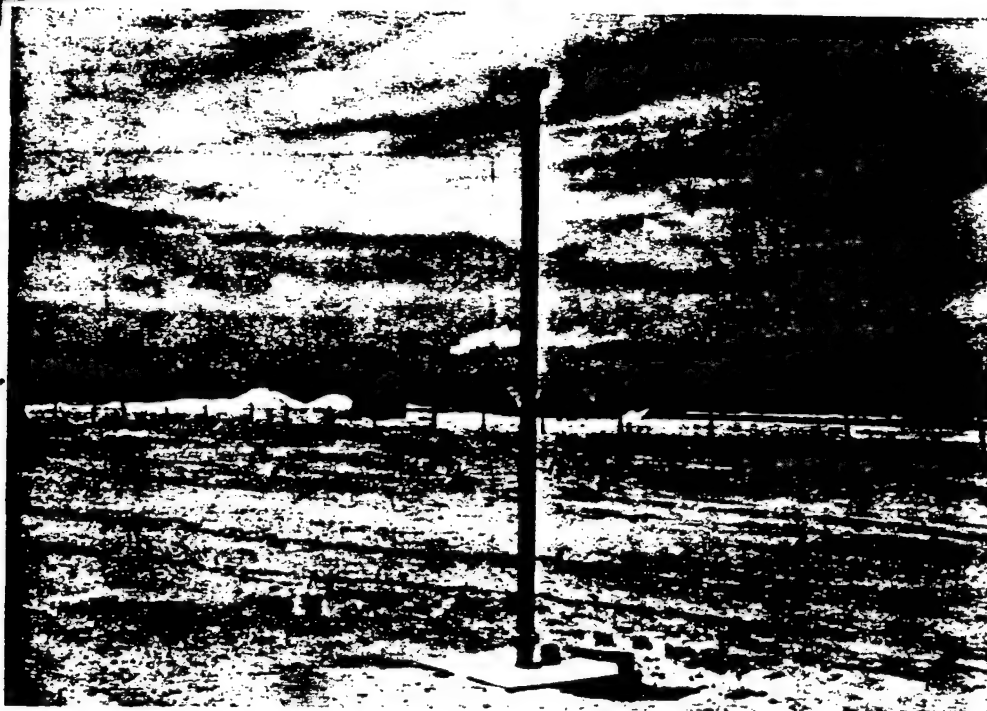


Fig. 7.27 Blast-velocity Post (Station 28b), Runit

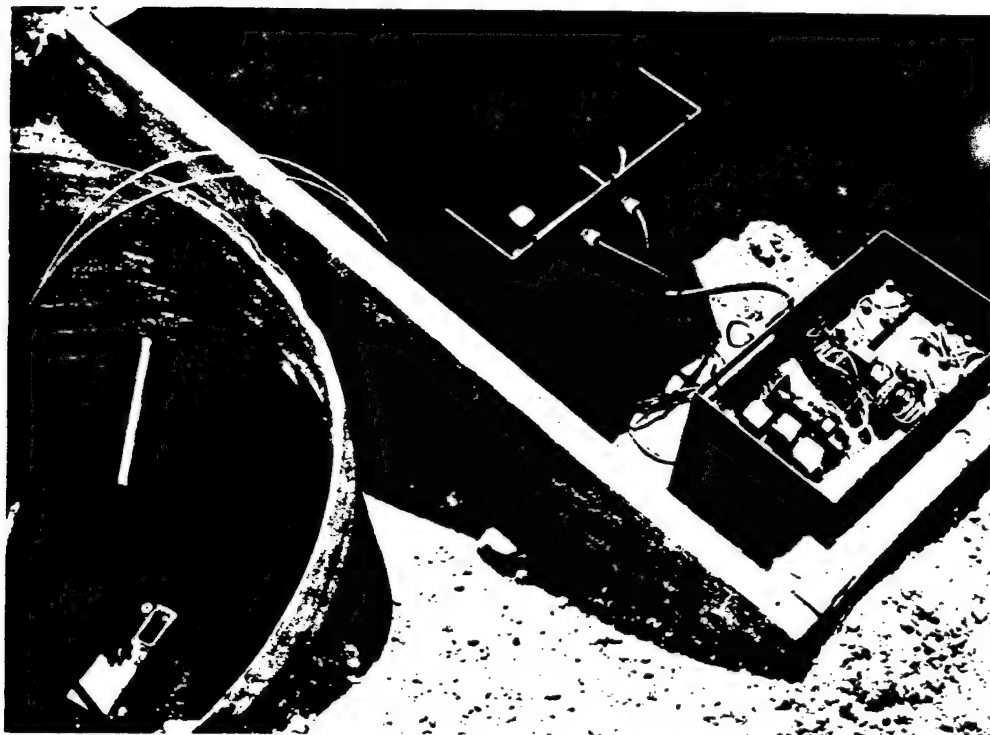


Fig. 7.28 Ground-shock Station, Engebi (Station 36c)

INSTALLATION DETAIL
FROM HOLMES & MARVER
SITE E-STATIONS 360-f
SITE D-STATIONS 360-e
DWG. 176813

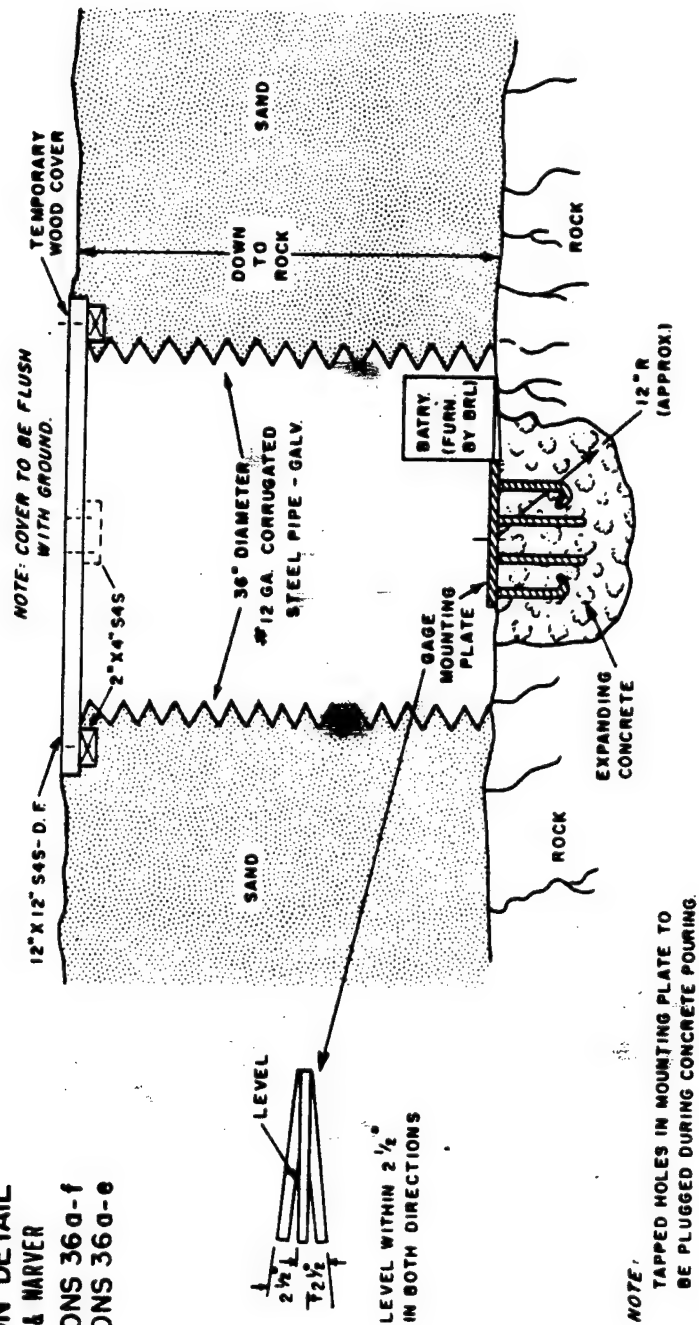


Fig. 7.29 Ground-shock Station (Structure)

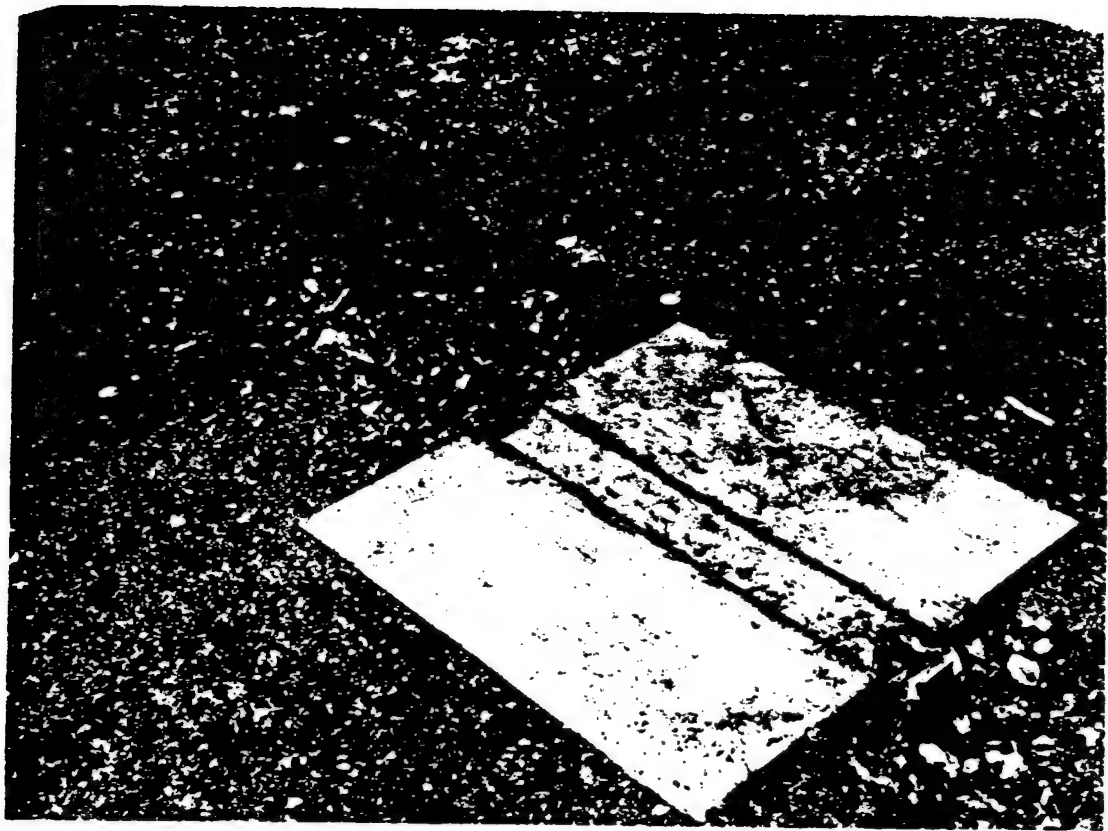


Fig. 7.31 Concrete and Stake Crusher Gauges, Runit (Stations 33, 34)

**NOTE: STEEL CAP TO BE REMOVED IN FIELD, USING TWO SPANNER WRENCHES.
ALL TOLERANCES $\pm 1/32"$ UNLESS OTHERWISE NOTED.
MATERIAL: STAKE AND CAP - A.I.S.I. B1113 COLD FINISHED STEEL SCREW STOCK.**

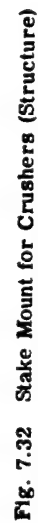




Fig. 7.34 Timing Relay Rack (Front)

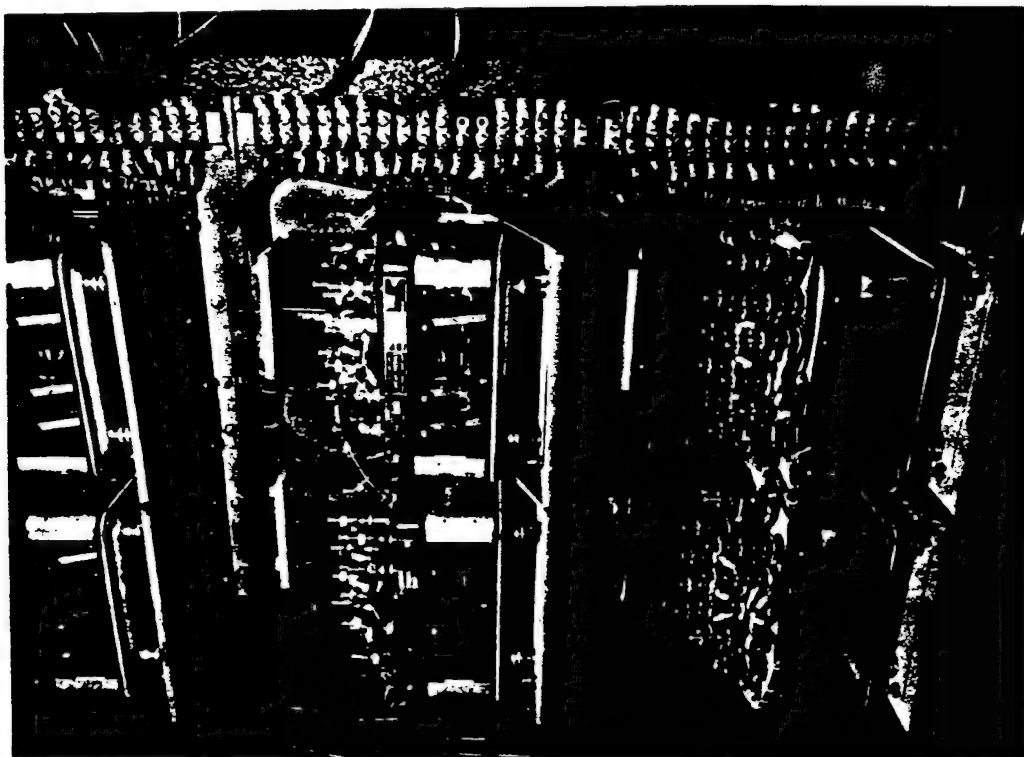


Fig. 7.33 Timing Relay Rack (Rear)

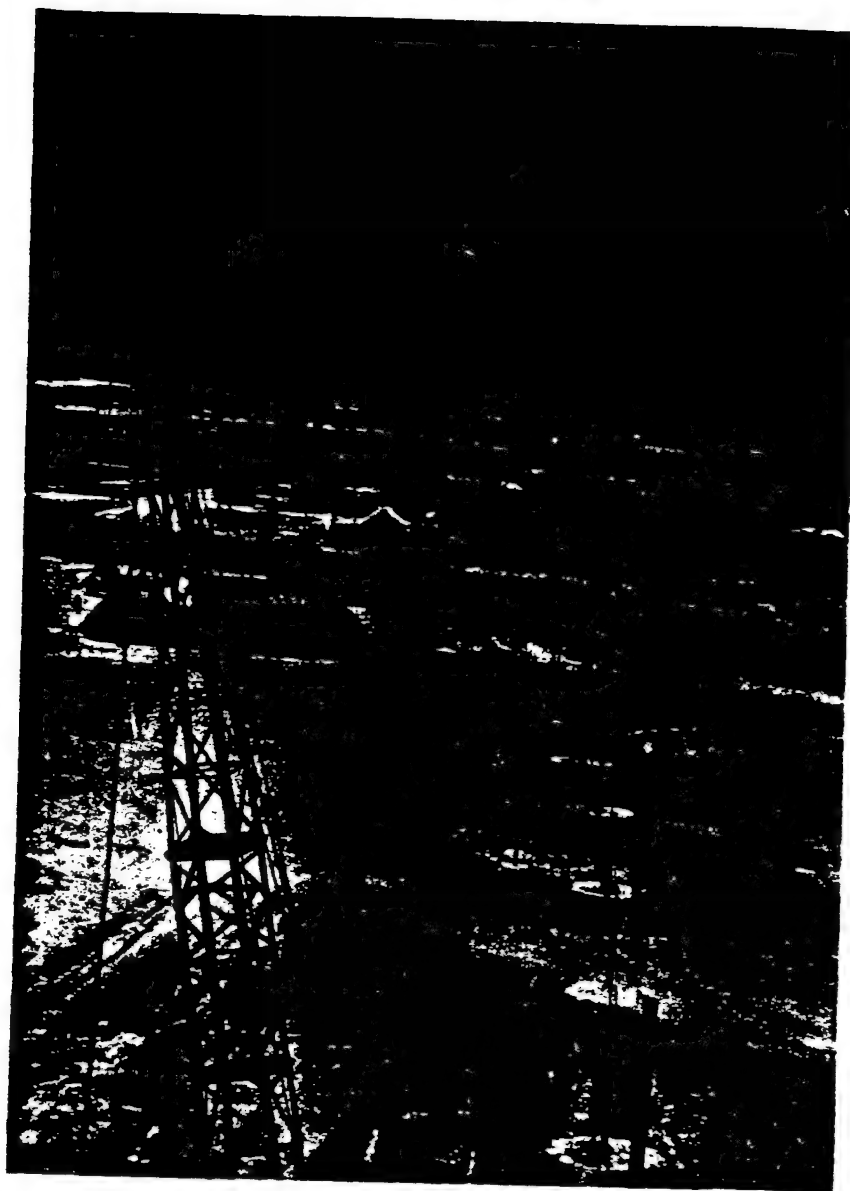


Fig. 7.35 Engel Long Line from Zero Tower Showing Mound of Earth Crossing Blast Line between Stations 28b and 28c

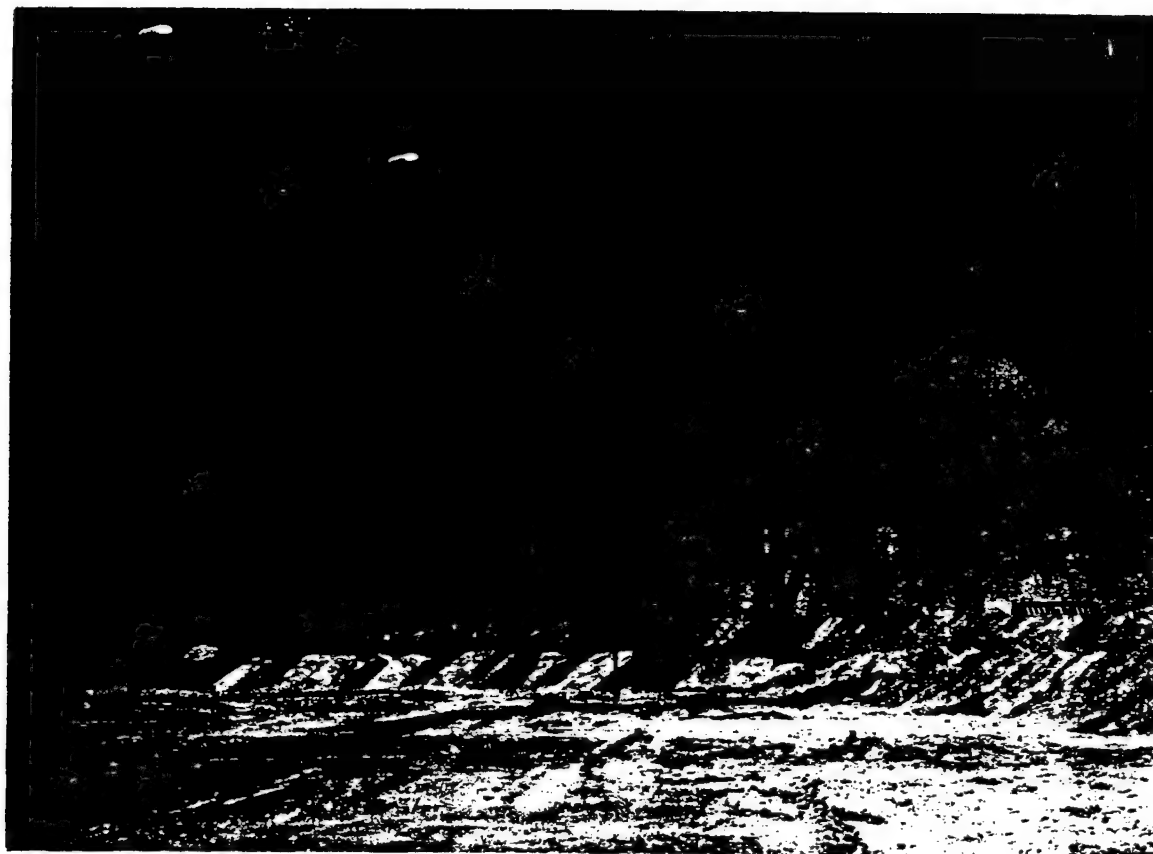


Fig. 7.36 Engebi Long-line Station 28c (See also 7.35)



Fig. 7.37 Engebi Short Line from Zero Tower, Showing Guy Wire



Fig. 7.38 Engebi Long-line Station 20c, Showing Piles of Dirt near Wall

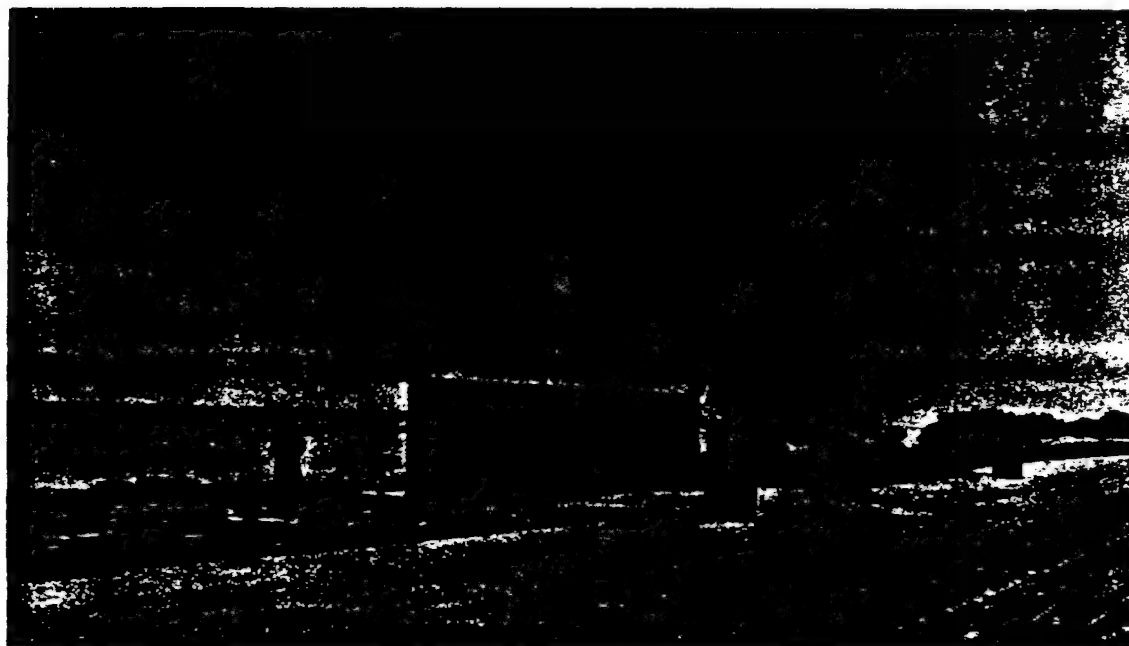


Fig. 7.39 Runit, Station 20d, Showing How Close Wall Was to Drop-off of Island toward the Beach



Fig. 7.40 Runit, Stations 20a and 20b, Showing Blast Line, Zero Tower, and Telemetering Balloon. Note that balloon is not in operating position.



Fig. 7.41 Runit Blast Hut (Station 23a) after Shot, Showing Sand Forced through Cable Inlet by Blast. Note inlet had been buried under a large sand pile as shown in Fig. 7.4.



Fig. 7.42 Engebi (Concrete and Stake Gauges) after the Shot (Stations 27b and 33b)

[REDACTED]

chain fall for cable laying, gauge recovery, and moving of heavy gear.

3. It is advisable to have a portable motor-generator set mounted on a truck or jeep.

4. It is desirable to have at least one survey (radiological contamination) meter and a few dosimeters so that it will not be necessary to rely completely on the Radiological Survey Group.

5. It is advisable that each member of the field party carry with him a Government Trans-

[REDACTED]

portation Request (T.R.) or an airline ticket for the return trip.

6. It is essential to work as nearly directly as possible with the actual construction and service people instead of dealing with intermediaries, even though this may mean some additional travel during the preparation period.

7. It is advisable for a group to be self-sufficient in regard to supplies, manpower, power, and transportation in so far as possible.

Appendix A

Activities of the NOBL Advance Party

By William H. Moore, Major, USAF

A.1 INTRODUCTION

A.1.1 Objectives

The primary objective was the laying of all NOBL instrumentation cable at each of the test sites. Over half a million feet of instrumentation cable was laid by the NOBL advance party during the period 13 February to 17 March 1951. This aggregate length comprised 229 individual cables and required over 600 splices.

Secondary objectives were to serve as advance representatives for NOBL at the forward area, to set up a NOBL laboratory, and to make proper disposition of all NOBL equipment.

A.1.2 Personnel

The advance party—William H. Moore, Major, USAF, Naval Ordnance Laboratory (NOL); Julius J. Meszaros, Ballistic Research Laboratories (BRL); John D. Rowe, NOL; and William J. Taylor, BRL—left San Francisco on 29 January and arrived at the forward area on 2 February, five weeks ahead of the main group.

Assisting the advance party was a crew of four Holmes and Narver (H&N) workers with Berl Kruger as foreman. This group was assigned to NOBL on 23 February for the duration of the program to assist in cable laying, transshipment of equipment, installation of instrumentation, and final roll-up.

A.1.3 Preparation and Planning

Complete cable-laying schedules were prepared during the months of September and October 1950. Requirements were obtained

from each group and consolidated into one overall cable-laying plan. A coding system was devised whereby each cable could be readily identified as to its instrumentation function. Each cable was to be tagged with a number corresponding to its coded designation at all terminals and junction points and each side of every splice. A master schedule was prepared for each test site, treating each cable individually as to type, length, function, and station to be served. Cable requirements were determined for each type, as indicated in Tables A.1 to A.5.

The requirements thus determined included estimated overages for cable loops, laterals to the stations, and connections at the blast huts.

A.2 OPERATIONS AT TEST SITE

A.2.1 Preparation for Cable Laying

Preliminary arrangements for cable laying were begun on 3 February and continued for 10 days. Cable on hand at Site B was inventoried and transshipped to the test sites. Blast lines on all sites were inspected and arrangements were made to have cable ditches surveyed and dug by H&N. These ditches extended the entire length of the blast line, with laterals serving each of the 20, 21, 28, 29, 35, 36, and 37 series stations.

A.2.2 Cable-laying Procedure

Cable was laid from a heavy truck which had been modified to dispense cable from coils and reels, as shown in Figs. A.1 and A.2.

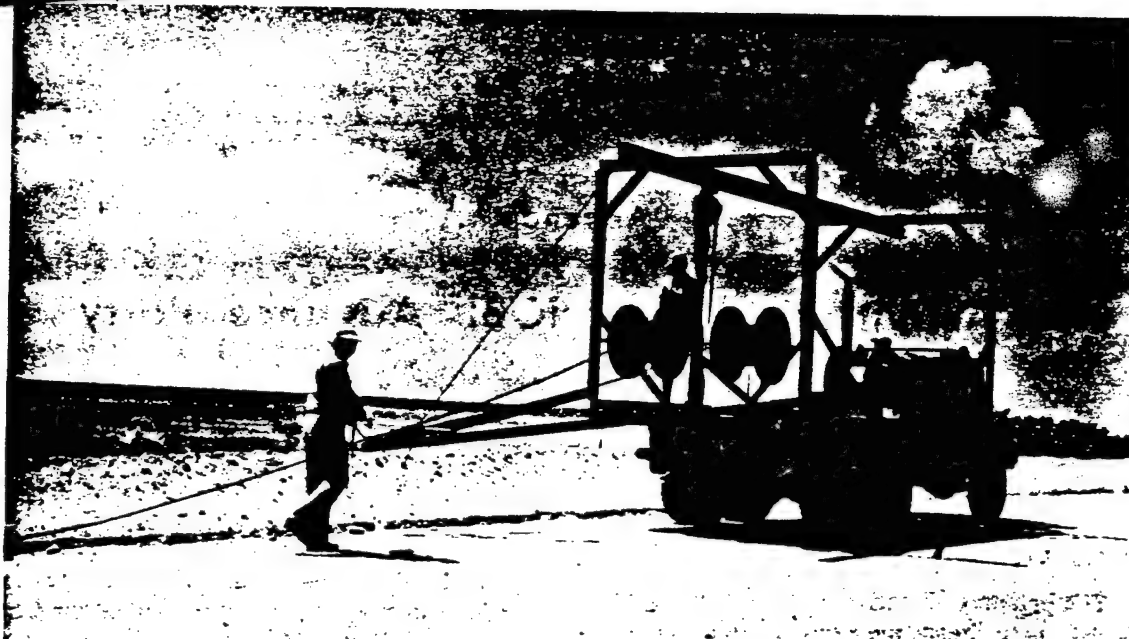


Fig. A.1 Cable Laying

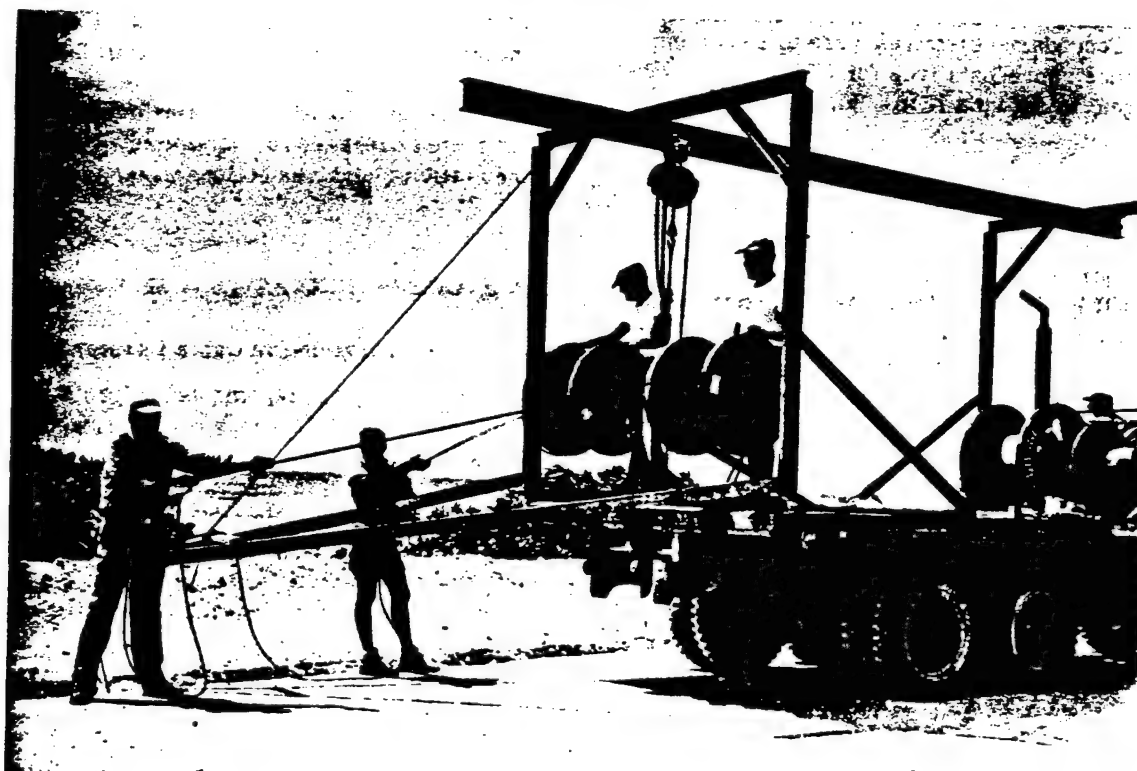


Fig. A.2 Cable Laying (Close-up)

TABLE A.1 CABLE SCHEDULE, E1, LONG LINE
(Letters in Parentheses Refer to Footnotes)

[illegible]

213

(b) Road to be shortened between 1,550 and 1,595 yd.

(4) BS, blast switch; BV, sound-velocity signal; SVS,

(e) Estimated cable lengths computed as follows: for BRL, map distance + 200 yd per cable for terrain contour + 10 yd per joint; for NOL, map distance +

(e) Estimated cable lengths computed as follows: for PRL, map distance + 200 yd per cable for terrain contour + 10 yd per joint; for NOL, map distance + 10 yd per joint + 30 yd at blast

(7) Removed 50 ft from blast line.

(g) Long joint.

UNIT 10 (2)

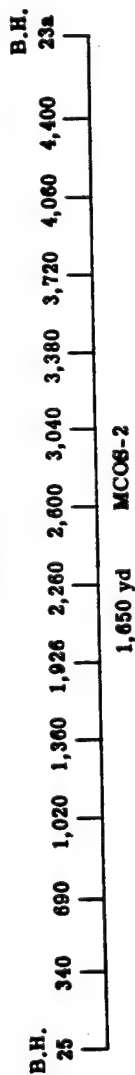
TABLE A.2 CABLE SCHEDULE, E2, SHORT LINE

Distance (yd)	0	100	180	260	360	460	560	620	700	800	900	950	1,000	1,100	1,200	1,250	B.H.†	Cable Codes	Map Distance (yd)	Estimated Cable Required
Velocity-gauge pipes	29a	29b	29c	29d	29e	29f	29g	29h	29i					29j	29k					
Pylons‡								37a				37b								
Walls											21a		21b			21c				
																		21c-IW-1		50
																		21c-IW-2		50
																		21c-8P		50
																		21c-B8-1		210
																		21c-B8-2		210
																		29k-B8-1	50	260
																		29k-B8-2	50	260
																		29j-B8-1	150	360
																		29j-B8-2	150	360
																		21b-IW-1	250	
																		21b-IW-2	250	
																		21b-8P	250	
																		21b-B8-1	250	
																		21b-B8-2	250	
																		37b-IG-1	300	400
																		37b-IG-2	300	400
																		37b-IP-1	300	400
																		37b-IP-2	300	400
																		37b-IP-3	300	400
																		37b-IP-4	300	400
																		37b-IS	300	400
																		21a-IS	350	460
																		21a-IW-1	350	440
																		21a-IW-2	350	440
																		21a-8P	350	440
																		21a-B8-1	350	560
																		21a-B8-2	350	560
																		29l-B8-1	450	660
																		29l-B8-2	450	660
																		37a-IG-1	550	
																		37a-IG-2	550	680
																		37a-IP-1	550	680
																		37a-IP-2	550	680
																		37a-IP-3	550	680
																		37a-IP-4	550	680
																		37a-IS	550	680
																		29h-B8-1	550	760
																		29h-B8-2	550	760
																		29g-B8-1	630	840
																		29g-B8-2	630	840
																		29f-B8-1	690	900
																		29f-B8-2	690	900
																		29e-B8-1	790	1,000
																		29e-B8-2	790	1,000

Rocket Launchers		Distance (ft)										Total		Weight	
		340	690	1,020	1,360	1,926	2,260	2,600	3,040	3,380	3,720	4,060	4,400	4,740	5,080
291-B8-2	450														690
37a-IG-1	550														690
37a-IG-2	550														690
37a-IP-1	550														690
37a-IP-2	550														690
37a-IP-3	550														690
37a-IP-4	550														690
37a-IG	550														690
29h-B8-1	760														760
29h-B8-2	760														760
29g-B8-1	630														840
29g-B8-2	630														840
29f-B8-1	690														900
29f-B8-2	690														900
29e-B8-1	790														1,000
29e-B8-2	790														1,000
29d-B8-1	890														1,100
29d-B8-2	890														1,100
29c-B8-1	990														1,200
29c-B8-2	990														1,200
29b-B8-1	1,070														1,280
29b-B8-2	1,070														1,280
29a-B8-1	1,150														1,360
29a-B8-2	1,150														1,360
29a-SV	1,150														1,400
29a-SV	1,150														1,400
29a-SVS	1,150														1,410
29a-VP	1,150														1,410
35-FL	1,250														1,490
Total														26,110	13,500

Rocket Launchers

Distance (ft)



†Road must be provided to blast hut.

‡Removed 50 ft from blast line between 360 and 460 yd.

IBS, blast switch; SV, sound-velocity signal; SVS, sound-velocity starting; FL, firing line; VP, velocity phone; GS, ground shock; GSS, ground-shock starting; IS, inductance spare; IW, inductance wall; IG, pylon ground station; IP, pylon; SP, spring piston. Cable identification tabs: 20a-B8-1 (Station 20a, Blast Switch, No. 1 of 2 cables).



CABLE SCHEDULE, SITE D-V
 Parentheses Refer to Footnotes)

1,750	1,850(a)	1,950	2,150	2,158	B.H.(b)	2,600(c)	2,700(c)			Estimated Cable Required		
28k	28l	28m	28n			28o	28p	Cable Code(d)	Map Distance (yd)	MCOS		
				36e						2	3	4
								28o-BS-1	420	930		
								28o-BS-2	420	930		
								28p-BS-1	520	1,030		
								28p-BS-2	520	1,030		
								36e-GS	22			232
								28n-BS-1	30	240		
								28n-BS-2	30	240		
								28m-BS-1	230	440		
								28m-BS-2	230	440		
								28l-BS-1	330	540		
								28l-BS-2	330	540		
								28k-BS-1	430	740		
								28k-BS-2	430	740		
								28j-BS-1	530	840		
								28j-BS-2	530	840		
								28i-BS-1	780	1,090		
								28i-BS-2	780	1,090		
								28h-BS-1	880	1,190		
								28h-BS-2	880	1,190		
								36d-GS	880			1,190
								28g-BS-1	980	1,290		
								28g-BS-2	980	1,290		
								28f-BS-1	1,080	1,390		
								28f-BS-2	1,080	1,390		
								28e-BS-1	1,180	1,490		
								28e-BS-2	1,180	1,490		
								36c-GS	1,180			1,490
								28d-BS-1	1,280	1,590		
								28d-BS-2	1,280	1,590		
								28c-BS-1	1,380	1,690		
								28c-BS-2	1,380	1,690		
								28b-BS-1	1,480	1,790		
								28b-BS-2	1,480	1,790		
								36b-GS	1,480			1,790
								28a-BS-1	1,560	1,870		
								28a-BS-2	1,560	1,870		
								36a-GS	1,560			1,870
								36a-GSS	1,560			
								28a-SV-1	1,560	1,910		
								28a-SV-2	1,560	1,910		
								28a-SVS	1,560	1,910		
								28a-FL	1,560			1,880
								28a-VP	1,560			2,000
Total										42,030	1,920	10,452

g 32h

— B.H.

FL, firing line; VP, velocity phone; GS, ground shock; GSS, ground-shock starting; IS, inductance
 n. Cable identification tabs: 20a-BS-1 (Station 20a, Blast Switch, No. 1 of 2 cables).
 shore line. Launchers to be spaced 300 ft apart.

[illegible]

32a 32b 32c 32d 32e 32f

1,000 yd MCOS-2

- (a) At 1,850 yd, add 100 yd per line to by-pass airstrip.
(b) Blast hut.
(c) Cross causeway. Add 300 yd per line.
(d) BS, blast switch; SV, sound-velocity signal; SVS, sound-velocity start spare; IW, inductance wall; IG, pylion ground station; IP, pylion; SP, spring p
(e) Eastern shore of Biihiri Island from northern end to causeway, follow:

A complete record of each cable was maintained as it was laid. Identification tags were placed at cable ends, loops, each side of all splices, and one common identification point about midway along the blast line. At road crossings the cable was placed in a channel-iron conduit for protection from heavy vehicles.

TABLE A.5 TOTAL CABLE REQUIREMENTS

Line or Site	MCOS-2 (yd)	MCOS-3 (yd)	MCOS-4 (yd)
E1	37,950	1,900	28,755
E2	26,110		13,500
Rockets	1,650		
C	29,785		21,410
Rockets	1,000		
D-V	42,030	1,920	10,452
Rockets	1,000		
Total	139,525	3,820	74,117

All cables were threaded into the proper stations and checked for continuity and resistance. About 6 in. of fine sand was poured over the cables, and the remainder of the ditch was covered with fill dirt.

(a) *Site C.* Fifty-eight cables were laid, requiring 150 splices. Total length was approximately 155,000 ft.

With the exception of ditches dug by H&N, the entire cable-laying operation was accomplished by the advance party. The cable truck was the only vehicle available during this operation.

(b) *Site E.* Seventy-one cables were laid on Site E1 and fifty-seven on E2. Total length was approximately 325,000 ft, requiring 310 splices.

In addition to the cable truck, one jeep was made available. The crew of four H&N workers assisted in cable laying and dug all laterals from the main ditch to the individual stations.

(c) *Site D-V.* Forty-three cables were laid; the total length was approximately 165,000 ft, requiring 165 splices. The work was done by members of the advance party and the four H&N workers.

After all cables were laid and the ditches were covered, 26 cables were cut at one point by a ditching machine, and at another point 12 cables were cut by a grader. Repair of this

damage required about 12 additional man-days of labor.

A.2.3 Disposition of Equipment

All NOBL cable and boxes were received at Site B. There were approximately 375 reels, 700 boxes weighing 70 tons from NOL, 225 boxes weighing 18 tons from BRL, and 167 boxes weighing 16 tons from Armed Forces Special Weapons Project (AFSWP). These reels and boxes were inventoried and segregated for transshipment to the appropriate sites. Port authorities were instructed as to the disposition of all reels and boxes and in the care of equipment requiring special handling. Explosives were stored in magazines, and certain batteries were placed under refrigeration for AFSWP.

A.2.4 Miscellaneous

A laboratory was set up within the administrative area and used as headquarters by the advance party.

All installations on the blast lines were inspected for conformity with NOBL specifications. It was found necessary to make some changes in the instrument stations and to relocate certain other stations owing to the shifting shore line. Arrangements were made for construction of work tents at the test sites and for removal of various obstructions from the blast lines. These activities were coordinated with H&N and AEC representatives. Necessary work orders were submitted, and the work was supervised by members of the advance party.

Excellent cooperation was received throughout the operation from H&N personnel and AEC representatives.

A.3 COMMENTS AND RECOMMENDATIONS

A.3.1 Comments

Transportation available to the advance party for cable laying was inadequate and not as requested by NOBL. The truck used for laying cable was borrowed from another group. It was a 2½-ton truck with an overhead chain hoist and trolley specially designed for use in the biomedical program. For this reason, modifications for cable-laying purposes were kept at a

[REDACTED]

minimum, consisting only of horizontal supports for cable reels and vertical turntable mounts for coils.

A.3.2 Recommendations

The following recommendations are submitted for consideration in planning future operations:

1. An advance party should be made an integral part of any similar future operations. The work accomplished by such a group makes it possible for the main body of personnel to arrive at the forward area at a later date and for the technical groups to proceed immediately with their instrumentation work.

2. Cable laying should be done by the contractors in accordance with rigid specifications to be furnished by the technical groups. This would allow the contractors to better fit the operation into their own work schedule and would enable members of the advance party to exercise closer supervision of the entire project.

3. Special-purpose vehicles and equipment should be furnished by the technical groups. Such items are not always available at the forward area. Advance planning and procurement should include at least the minimum requirements to accomplish the mission in the field.

Appendix B

Determination of Design Criteria for Construction of a Pylon for Blast Instrumentation

By H. P. Feldman, G. K. Hartmann, and C. J. Aronson

B.1 PROBLEM

To establish the design criteria for the erection of a stable pylon for blast instrumentation (assuming there are no components of force normal to the sides of the pylon).

B.2 METHOD

To solve this problem an estimate was made of the turning moment which would be caused by a 40-psi blast against the leading face of the pylon, and this was then compared with the counter turning moment caused by the weight of the pylon and its base. To estimate the former, Table 6 of the Sandstone blast-measurement report¹ was used to give values of P_d/C_d and Mach numbers for various shock overpressures as follows:

P_s (psi)	P_d/C_d (psi)	M	C_d	P_d (psi)
3	0.213	0.131	1.20	0.26
6	0.827	0.238	1.20	0.99
10	2.22	0.356	1.21	2.69
15	4.77	0.478	1.30	6.20
20	8.15	0.577	1.50	12.2
30	16.95	0.735	1.80	30.5
40	28.0	0.851	2.50	70.0

where P_s = shock overpressure
 C_d = drag coefficient

M = Mach number, i.e., V/V_c = ratio of particle velocity to (local) sound velocity

P_d = drag pressure

The values of C_d were read off or estimated from Fig. 18 of National Advisory Committee for Aeronautics (NACA) study² on the drag of circular cylinders. The C_d values for circular cylinders were used rather than the values for elliptical cylinders to introduce a safety factor of about 10. P_d was calculated by multiplying P_d/C_d by C_d . P_d vs P_s is plotted in Fig. B.1.

B.3 CALCULATIONS

It was first assumed that the required structure could be designed on the basis of total impulse. To find this total impulse, the area under the curve of P_d (drag pressure) vs t (time) or $\int_0^t P_d dt$ was obtained.

However, it was first necessary to obtain the pressure-time curve in the 40-psi peak pressure zone for an explosion of the size expected to be instrumented. This curve may be plotted using the form

$$p = P(1 - at)e^{-bt}, \quad (B.1)$$

where p is pressure in psi at time t in seconds, P is maximum pressure at $t = 0$, and a and b are constants.

Values of a and b are obtained from the

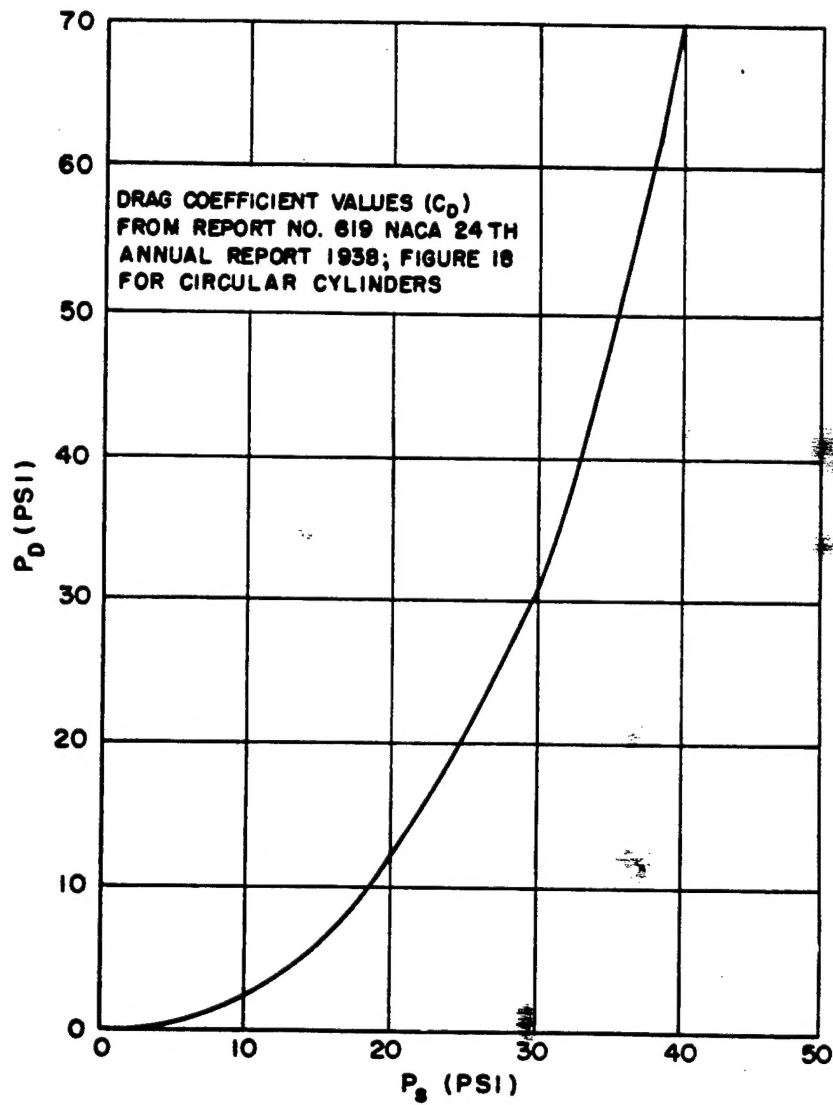


Fig. B.1 Overpressure vs Drag Pressure

Sandstone report¹ as follows: From Fig. 2 of this reference

$$\lambda = \frac{r \text{ ft}}{W^{1/2} \text{ lb}} = 5 \text{ for } P = 40 \text{ psi.}$$

If a blast tonnage of 32.1 kt is assumed, then

$$\lambda = 5 = \frac{r \text{ ft}}{(64.2 \times 10^6 \text{ lb})^{1/2}} = \frac{r}{400}$$

or

$$r = 2,000 \text{ ft,}$$

and from Fig. 18 of the same reference,¹ $T_0 = 0.44 \text{ sec}$ for the positive duration of the blast. It can be seen that $a = 1/T_0 = 2.27$, since, when $t = T_0$, $p = 0$. If $p = P(1 - at)e^{-bt}$ is differentiated with respect to t

$$\frac{\partial p}{\partial t} = -P(1 - at)be^{-bt} - P_{ae}^{-bt},$$

and

$$-\frac{\partial p}{\partial t} = [(1 - at)b + a]e^{-bt}.$$

From Theilheimer³

$$\theta = -\left(\frac{P}{\partial p}{\partial t}\right)_{t=0},$$

and hence

$$\frac{1}{\theta} = b +$$

Also from Theilheimer³ it can be seen that for

$$\lambda = 5, \frac{\theta}{W^{1/2}} \approx 0.3 \text{ msec/lb}^{1/2}.$$

Hence

$$\theta = 400 \times 0.3 = 120.0 \text{ msec} = 0.120 \text{ sec.}$$

Since

$$\frac{1}{\theta} = b + a,$$

then

$$\frac{1}{0.12} = b + 2.27,$$

and

$$b = 6.06.$$

Hence the equation in its final form is

$$p = P(1 - 2.27t)e^{-6.06t} \quad (\text{B.2})$$

as shown in Fig. B.2. By use of the curve of Fig. B.1 the corresponding curve for the drag pressure P (psi) vs t (time in sec) was plotted on Fig. B.2, and it was then possible to obtain the value for the total impulse for the $\int_0^t P_d dt$.

B.4 STABILITY

To determine the stability of the structure, use was made of the following equation:

$$\int_0^t P_d dt AL_1 - WL_2 t = I\omega, \quad (\text{B.3})$$

where A = front area presented to the blast, in.²

L_1 = moment arm acted on by blast, in.

W = weight of structure, lb

L_2 = distance horizontally from center of gravity of structure to assumed point of rotation, in.

I = moment of inertia of the structure, in.-lb sec²

ω = angular velocity attained at the end of time t , radians/sec

The outline above gives structural design figures which will result in small enough values of ω so that on the basis of total impulse it is indicated that the disturbance or rise of the structure would be negligible.

However, if these design figures are used with the value of $\int_0^t P_d dt$ for the impulse, the structure is unstable. New design figures have to be established to meet this condition.

Repetitions of the above procedure using lesser and lesser values of t in the determination of $\int_0^t P_d dt$ will finally indicate that values near

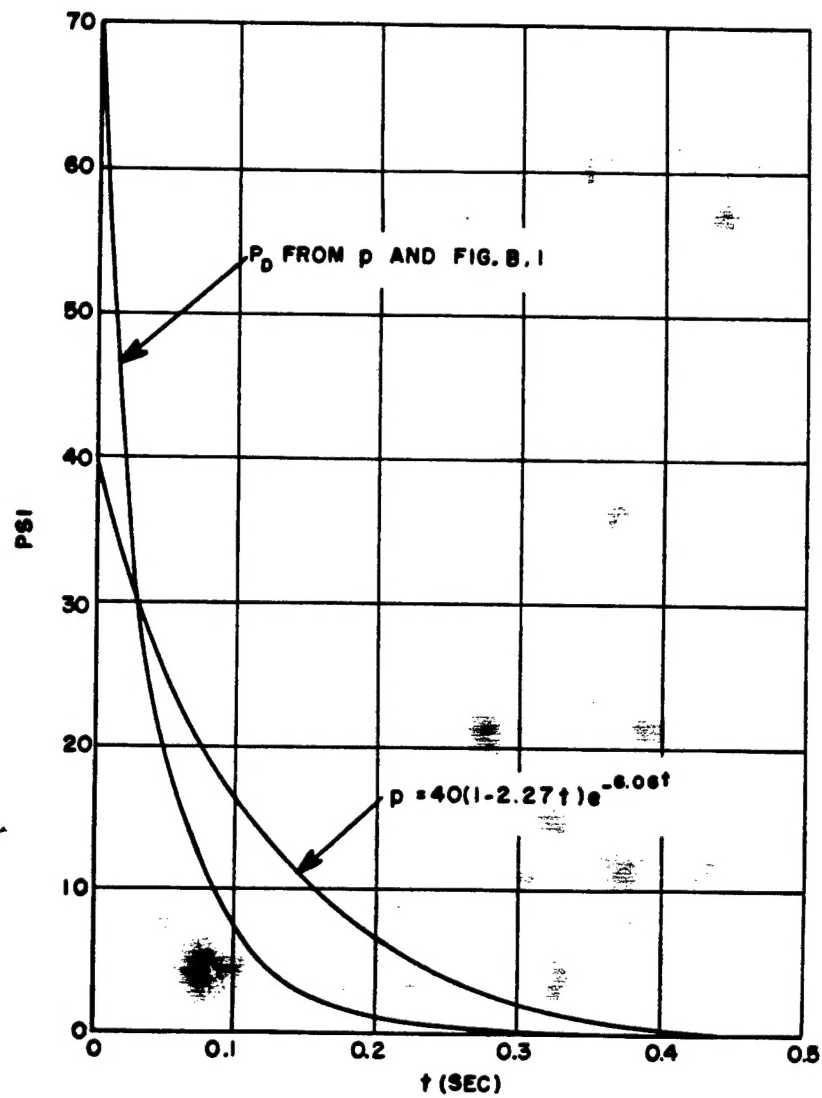


Fig. B.2 Overpressure and Drag Pressure vs Time

the peak drag pressure must be used as the basis of design criteria.

The design of the pylon as shown in the Holmes and Narver drawing 17-G-815 (Fig. 7.17) was based on the above considerations, and calculations for $t = 0.01$ sec follow.

B.5 EXAMPLE

Substitute in Eq. B.3 to obtain the following:

$$I\omega = \int_0^{0.01} P_d dt \times 6.5 \times 15 \times 12 \times 7.5 \times 12 \\ - 38,700 \times 8.5 \times 12 \times 0.01.$$

Now the expression

$$\int_0^{0.01} P_d dt = 0.60$$

can be obtained from Fig. B.2.

Therefore

$$I\omega = 23,600 \text{ lb sec in.}$$

and I is calculated from the equation

$$I_1 = \frac{M(a^2 + b^2)}{12} + Md^2, \quad (\text{B.4})$$

where I_1 is the moment of inertia around an axis perpendicular to a face of dimensions $a \times b$ and at a distance d from a parallel axis through the center of gravity. The first term of B.4 is the moment of inertia around the axis through the center of gravity, and the second term transposes the axis of rotation the distance d . Also

$$I = I_1 + I_2 + I_3, \quad (\text{B.5})$$

where $I_{1,2,3}$ = the individual I 's for three components of the total mass.

$$I_1 = 4.57 \times 10^5 \text{ lb sec}^2 \text{ in.}, \\ I_2 = 1.54 \times 10^5 \text{ lb sec}^2 \text{ in.}, \\ I_3 = 13.1 \times 10^5 \text{ lb sec}^2 \text{ in.};$$

therefore

$$I = 19.2 \times 10^5 \text{ lb sec}^2 \text{ in.},$$

and

$$\omega = \frac{23,600}{19.2 \times 10^5} = 0.0123 \frac{\text{lb sec in.}}{\text{lb sec in.}}$$

Now to calculate the rise distance of the front of the pylon, use the equation

$$D = \frac{\omega}{2} \times t \times l, \quad (\text{B.6})$$

where D = rise distance, in.

ω = angular velocity, radian/sec = 0.012

t = time, sec = 0.01

l = distance from assumed axis of rotation to front of concrete base = 204 in.

Thus

$$D = \frac{0.012 \times 0.01}{2} \times 204; \\ D = 0.0122 \text{ in.}$$

This rise seems negligible, and it may then be concluded that the structure will be stable when all the force is applied to the leading face and is parallel to the sides of the pylon.

REFERENCES

1. Sandstone Report, Annex 5, Vol. 20, Blast Measurement Summary Report.
2. National Advisory Committee for Aeronautics, Twenty-fourth Annual Report (1938), Technical Report 619.
3. F. Thellheimer, The Determination of the Time Constant of a Blast Wave from the Pressure-Distance Relation, Naval Ordnance Laboratory Report NavOrd-1734, Dec. 8, 1950.